



University
of Glasgow

Rezig, Imane Nour El-Houda (2019) *Investigating the regulation of fission yeast cytokinesis by the anillin mid1, the ESCRT regulator vps4 and the Aurora kinase ark1*. PhD thesis.

<http://theses.gla.ac.uk/76725/>

Copyright and moral rights for this work are retained by the author

A copy can be downloaded for personal non-commercial research or study, without prior permission or charge

This work cannot be reproduced or quoted extensively from without first obtaining permission in writing from the author

The content must not be changed in any way or sold commercially in any format or medium without the formal permission of the author

When referring to this work, full bibliographic details including the author, title, awarding institution and date of the thesis must be given

Enlighten: Theses

<https://theses.gla.ac.uk/>
research-enlighten@glasgow.ac.uk



University
of Glasgow | College of Medical,
Veterinary & Life Sciences

Investigating the regulation of fission yeast cytokinesis by the anillin *mid1*, the ESCRT regulator *vps4* and the Aurora kinase *ark1*

Imane Nour El-Houda Moussa Rezig

BSc MSc

Thesis submitted in fulfilment of the requirements for the Degree of
Doctor of Philosophy

November 2019

Institute of Molecular, Cell and Systems Biology

College of Medical, Veterinary and Life Sciences

University of Glasgow

Abstract

Mammalian and fission yeast cells determine the site of division by the medial placement of an actomyosin contractile ring. Contraction of this ring then leads to cytokinesis and the final separation of the equal-size daughter cells. In the fission yeast *Schizosaccharomyces pombe* (*S. pombe*) the anillin Mid1p, aurora Ark1p and the ESCRT family of proteins are involved in regulating specification of division site, mitotic entry and establishment of the final separation, respectively.

In this Thesis, for the first time, we provide evidence of genetic interactions between both the *vps4⁺* and *ark1⁺* genes with the *mid1⁺* gene. Combinatorial mutants revealed a synthetic growth phenotype indicating their requirement for *S. pombe* survival. Therefore, this research investigated Mid1p potential regulation by the ESCRT regulator Vps4p (Chapters 3 and 4). Initially, a physical interaction between Vps4p and Mid1p recombinant proteins was detected and mapped to the "C-term" domain of Mid1p.

Next, the effects of absence of this interaction on the cellular localization of Mid1p were determined; this analysis revealed mis-localization of Mid1p and suggested a potential mechanism whereby Vps4p interacts with Mid1p through the PH domain to regulate Mid1p localization to cortical nodes. This hypothetical mechanism was investigated by determining the effects of Mid1p PH domain absence on its localization in *S. pombe*. Such analysis revealed mis-localization of Mid1p, but it was inconclusive in confirming the interaction between Mid1p-PH domain and Vps4p. Interestingly, the absence of the PH domain caused a Mid1p nuclear exclusion phenotype, suggesting that Mid1p PH domain is involved not only in its known role in Mid1p cortical anchorage but also in Mid1p nuclear localization. Therefore, it is possible that Mid1p nuclear localization regulates its interaction with Vps4p. To test this hypothesis, the well-characterized NLS regions in Mid1p were utilized, and their requirement for the interaction with Vps4p was tested. Such analysis revealed that the interaction between Vps4p and Mid1p does not depend on Mid1p nuclear localization.

Mid1p potential regulation by the aurora kinase Ark1p was also tested (Chapters 5 and 6). Initially, *in vitro* phosphorylation of recombinant Mid1p by mammalian

recombinant aurora A and plk1 kinases was tested; such analysis confirmed this interaction and mapped it to the "N-term" and "Middle" domains of Mid1p.

Next, Mid1p "N-term" and "Middle" domains were mapped to yield six potential phospho-sites (S167, S328, S331, S332, S523 and S531), which were utilized to confirm the *in vitro* phosphorylation by the aurora kinase Ark1p. The results were inconclusive, so an *in vivo* integration *S. pombe* approach was utilized to analyze the phospho-sites. This approach involved the production of several versions of the *mid1* gene, each bearing a single or multiple phospho-mimetic or phospho-resistant mutation/s. These *mid1* gene versions were integrated into the chromosomal DNA of wild-type (W-T) or an *ark1-T11* *S. pombe* strain at the endogenous *mid1*⁺ locus. Cell morphology phenotypes were then characterized for two selected Mid1p potential phospho-sites, S523 and S531. Defects in cell morphology were observed in the case of all phospho-resistant mutants but were not observed in the case of all phospho-mimetic mutants. Therefore, we concluded that the two Mid1p sites, S523 and S531, are important for its function.

Overall, the work reported in this thesis provides insights into *S. pombe* cell cycle regulation. Using *in vivo* *S. pombe* genetic and microscopic approaches in addition to *in vitro* pull-down and phosphorylation experiments, we discovered novel Mid1p-dependent pathways for *S. pombe* cell cycle regulation.

Table of Contents

Abstract.....	2
Table of Contents.....	4
List of Tables	12
List of Figures	13
Acknowledgement.....	17
Author's Declaration	18
Definitions/Abbreviations.....	19
Chapter 1 Introduction.....	22
1.1 A historical overview of the cell cycle	22
1.2 How do eukaryotic cells divide?	23
1.2.1 A contractile ring is positioned at the site of division	23
1.2.1.1 Formation of the acto-myosin contractile ring	23
1.2.1.2 Anillin-based contractile ring drives cytokinesis in mammalian cells	25
1.2.1.3 Mid1p-based contractile ring drives cytokinesis in <i>S. pombe</i> cells	28
1.2.2 Cytokinesis leads to the final separation	29
1.2.2.1 The ESCRT family of proteins drives abscission in mammalian cells	29
1.2.2.2 <i>S. pombe</i> septation is equivalent to mammalian cytokinesis	33
1.3 Regulation of eukaryotic cell cycle.....	35
1.3.1 Spindle assembly checkpoint	35
1.3.2 Exit from mitosis	38

1.4	Cytokinesis dysregulation and cancer	40
1.5	The use of fission yeast as a model organism to study eukaryotic cell cycle	41
1.6	General Aims of this thesis	42
Chapter 2 Materials and Methods		43
2.1	Materials	43
2.1.1	Media and strains	43
2.1.1.1	<i>S. pombe</i> media	43
2.1.1.2	<i>S. pombe</i> strains	44
2.1.1.3	<i>E. coli</i> media.....	47
2.1.1.4	<i>E. coli</i> strains	47
2.1.2	Standard solutions and reagents	49
2.1.2.1	List of standard solutions	49
2.1.2.2	List of reagents and kits.....	50
2.2	Methods	51
2.2.1	<i>S. pombe</i> methods	51
2.2.1.1	General methods	51
2.2.1.2	Mating and tetrad analysis.....	52
2.2.1.3	Mating type determination	52
2.2.1.4	Genotype screening	52
2.2.1.5	Septation analysis	53
2.2.1.6	Confocal microscopy	53
2.2.1.7	<i>In vivo S. pombe</i> integration.....	54
2.2.2	<i>E. coli</i> methods	55
2.2.2.1	General methods	55
2.2.2.2	DNA constructs design for recombinant protein expression	55

2.2.2.3	Plasmid DNA extraction for bacterial transformation	56
2.2.2.4	Competent cells	56
2.2.2.5	DNA transformation	57
2.2.2.6	Recombinant protein expression	57
2.2.3	<i>In vitro</i> biochemical methods	58
2.2.3.1	Recombinant protein purification	58
2.2.3.2	DNA sequencing	58
2.2.3.3	Pull-down	59
2.2.3.4	Gel electrophoresis	59
2.2.3.5	<i>In vitro</i> phosphorylation	60
2.2.3.6	<i>In vitro</i> phosphorylation stoichiometric analysis	60
2.2.3.7	ATPase assay	61

Chapter 3 Interactions between the *mid1*⁺ and *vps4*⁺ genes and their encoded proteins (Mid1p and Vps4p) suggest they coordinate to regulate *S. pombe* cytokinesis..... 62

3.1	Introduction	62
3.1.1	Mammalian cytokinesis	62
3.1.2	Mid1p and ESCRT proteins are involved in <i>S. pombe</i> cell cycle regulation.....	62
3.1.3	Could Mid1p and Vps4p coordinate to regulate <i>S. pombe</i> septation?	63
3.2	Aims.....	64
3.3	Results	65
3.3.1	Chromosomal deletions of the <i>mid1</i> ⁺ or <i>vps4</i> ⁺ genes	65
3.3.2	Septation analysis of wild-type, <i>mid1</i> Δ and <i>vps4</i> Δ <i>S. pombe</i>	66
3.3.3	A genetic interaction between the <i>mid1</i> ⁺ and <i>vps4</i> ⁺ genes	69

3.3.3.1	<i>S. pombe</i> tetrad analysis provides a powerful tool to study genetic interactions	69
3.3.3.2	The <i>mid1Δ vps4Δ</i> double mutant growth phenotype suggests a genetic interaction between the <i>mid1⁺</i> and <i>vps4⁺</i> genes	69
3.3.4	A physical interaction between Mid1p and Vps4p proteins	71
3.3.4.1	Design of pull-down experiments	71
3.3.4.2	Purification of prey proteins for the pull-down experiments	72
3.3.4.3	Purification of bait proteins for the pull-down experiments	75
3.3.4.4	Pull-down experiments reveal a physical interaction between Vps4p and the "C-term" domain of Mid1p	76
3.3.5	Localization analysis of GFP-Mid1p in wild-type, <i>vps4Δ</i> and PHΔ <i>mid1 S. pombe</i>	79
3.3.5.1	Investigating the localization of Mid1p in wild-type and <i>vps4Δ S. pombe</i>	79
3.3.5.2	<i>S. pombe</i> Mid1p shares structural homology with mammalian anillin	82
3.3.5.3	Investigating the localization of Mid1p in PHΔ <i>mid1 S. pombe</i> ..	83
3.4	Conclusions	87
Chapter 4 Investigation into the role of nuclear localization of Mid1p in regulating <i>S. pombe</i> septation		88
4.1	Introduction	88
4.1.1	Mid1p localization phenotypes regulate its function during <i>S. pombe</i> cell cycle	88
4.2	Aims	89
4.3	Results	90
4.3.1	Does the genetic interaction between the <i>mid1⁺</i> and <i>vps4⁺</i> genes require Mid1p nuclear shuttling?	90
4.3.1.1	The use of Mid1p nuclear localization sequence mutant strains	90

4.3.1.2	Generation of <i>mid1</i> NLS <i>vps4</i> Δ double mutants	92
4.3.2	Septation analysis of <i>mid1</i> NLS <i>vps4</i> Δ double mutants	93
4.3.3	Localization of GFP-Mid1p in <i>mid1</i> NLS* cells	96
4.4	Conclusions	99
 Chapter 5 Genetic interactions between the <i>mid1</i>⁺ and <i>ark1</i>⁺ genes, and physical interactions between the Mid1p and aurora A kinase suggest Mid1p regulation by Ark1p in <i>S. pombe</i>.		
5.1	Introduction	100
5.1.1	Could Plo1p and Ark1p coordinate with Mid1p to regulate <i>S. pombe</i> cell cycle?	101
5.2	Aims.....	102
5.3	Results	102
5.3.1	<i>ark1</i> ⁺ <i>S. pombe</i> temperature sensitive mutants.....	102
5.3.2	A strong genetic interaction between the <i>mid1</i> ⁺ and <i>ark1</i> ⁺ genes 103	
5.3.3	A physical interaction between Mid1p and plk1 and aurora A kinases.....	105
5.3.3.1	Design of Mid1p <i>in vitro</i> phosphorylation experiments.....	105
5.3.3.2	<i>In vitro</i> phosphorylation of the "N-term" and "Middle" domains of Mid1p by plk1 and aurora A kinases	106
5.3.3.3	Mid1p "N-term" and "Middle" domains <i>in vitro</i> phosphorylation stoichiometric analysis	109
5.3.3.4	Mid1p "N-term" and "Middle" domains phospho-sites determination	112
5.3.4	Mid1p "N-term" domain phospho-sites confirmation.....	116
5.3.4.1	Design of Mid1p "N-term" domain phospho-resistant mutants .	116
5.3.4.2	Purification of Mid1p "N-term" domain phospho-resistant mutants 117	

5.3.4.3	<i>In vitro</i> phosphorylation of Mid1p "N-term" domain phospho-resistant mutants by plk1 and aurora A kinases.....	118
5.3.5	Mid1p "Middle" domain phospho-sites confirmation.....	120
5.3.5.1	Design of Mid1p "Middle" domain phospho-resistant mutants..	120
5.3.5.2	Purification of Mid1p "Middle" domain phospho-resistant mutants	121
5.3.5.3	<i>In vitro</i> phosphorylation of Mid1p "Middle" domain phospho-resistant mutants	122
5.4	Conclusions	124
Chapter 6	Investigation into Mid1p regulation by Ark1p through <i>in vivo</i> <i>S. pombe</i> analyses.....	125
6.1	Introduction	125
6.1.1	Aurora kinases play important roles in mammalian cell cycle regulation.....	125
6.2	Aims.....	126
6.3	Results	127
6.3.1	<i>In vitro</i> phosphorylation experiments of Mid1p by plk1 and aurora kinases yielded six potential Mid1p phospho-sites	127
6.3.2	Investigating the functional relevance of the Mid1p S523 and S531 potential phospho-sites	129
6.3.2.1	An <i>in vivo</i> <i>S. pombe</i> integration approach.....	129
6.3.2.2	Integration of <i>mid1</i> phospho-mimetic/resistant genes into the <i>mid1</i> Δ <i>S. pombe</i> strain.....	132
6.3.2.3	<i>In vivo</i> integration of <i>mid1</i> phospho-mimetic/resistant genes into the <i>mid1</i> Δ <i>ark1</i> -T11 <i>S. pombe</i> strain.....	135
6.3.3	<i>In vivo</i> analysis of the role of S167, S328, S331 and S332 phospho-sites for the function of Mid1p during <i>S. pombe</i> cell cycle ..	139

6.3.4	Potential coordination between Mid1p, Ark1p and Vps4p to regulate <i>S. pombe</i> cell cycle	141
6.3.5	Investigation of the localization of GFP-Mid1p in <i>ark1</i> -TS cells	142
6.3.5.1	Generation of GFP-Mid1p <i>ark1</i> -TS <i>S. pombe</i> strains	142
6.3.5.2	Ark1p is required for the localization of GFP-Mid1p in <i>S. pombe</i>	143
6.4	Conclusions	149
Chapter 7	Discussion	150
7.1	Control of the anillin Mid1p by the ESCRT regulator Vps4p in <i>S. pombe</i> cell cycle.	150
7.1.1	The <i>mid1</i> ⁺ and <i>vps4</i> ⁺ genes are involved in <i>S. pombe</i> cell cycle regulation.....	150
7.1.2	A model for the interaction between Mid1p and Vps4p to regulate <i>S. pombe</i> cortical nodes localization	151
7.2	Regulation of anillin/Mid1p by the aurora kinase Ark1p in <i>S. pombe</i> cell cycle.	154
7.2.1	<i>mid1</i> ⁺ genetic interaction with the <i>ark1</i> ⁺ gene suggests the phosphorylation of Mid1p by Ark1p to regulate <i>S. pombe</i> cell cycle ..	154
7.2.1.1	Investigation of Mid1p potential plk1 and aurora A phospho-sites (S167, S328, S331, S332, S523 and S531)	156
7.2.2	<i>In vivo</i> analysis of the role of S523 and S531 phospho-sites for the function of Mid1p during <i>S. pombe</i> cell cycle	157
7.3	Overall conclusions	159
7.4	Future directions	160
Chapter 8	Appendices	165
8.1	Appendix 1: <i>S. pombe</i> characterized phenotypes.....	165
8.1.1	A summary of <i>S. pombe</i> septation phenotypes	165

8.1.2	A summary of <i>S. pombe</i> GFP-Mid1p localization phenotypes.	166
8.1.3	A summary of <i>S. pombe</i> cell morphology phenotypes.....	168
8.1.4	Classification and quantification of cell morphology phenotypes in <i>mid1</i> phospho-mimetic/resistant mutant <i>S. pombe</i> strains.....	169
8.1.5	Classification and quantification of cell morphology phenotypes in <i>mid1</i> phospho-mimetic/resistant mutant <i>S. pombe</i> strains.....	170
List of References		171

List of Tables

Table 2-1 List of <i>S. pombe</i> strains used in this study. The "GG" number refers to the laboratory reference collection	44
Table 2-2 List of plasmid vector DNA constructs used in this study. The "GB" number refers to the laboratory reference collection	48
Table 3-1 Description and localization of Mid1p putative domains in <i>S. pombe</i> cells	72
Table 4-1 Mid1p nuclear localization sequences mutations	91
Table 5-1 Quantification and optimization of Mid1p <i>in vitro</i> phosphorylation experiments using Mid1p "N-term", "Middle" and "C-term" recombinant proteins and plk1, aurora A and aurora B kinases	107
Table 5-2 Mid1p "N-term", "Middle" and MBP <i>in vitro</i> phosphorylation stoichiometric analysis	111
Table 6-1 A summary of Mid1p phospho-sites for potential <i>in vitro</i> phosphorylation by plk1 and/or aurora A kinases	128
Table 6-2 A summary of the phospho-mimetic/resistant mutant versions of the <i>mid1</i> gene integrated into <i>mid1</i> Δ <i>S. pombe</i> for the <i>in vivo</i> microscopy analysis	130
Table 6-3 A summary of the phospho-mimetic/resistant mutant versions of the <i>mid1</i> gene integrated into <i>ark1</i> -T11 <i>S. pombe</i> for the <i>in vivo</i> microscopy analysis	136
Table 8-1 <i>S. pombe</i> septation phenotypes characterized in this study	165
Table 8-2 <i>S. pombe</i> GFP-Mid1p localization phenotypes characterized in this study	166
Table 8-3 <i>S. pombe</i> cell morphology phenotypes characterized in this study....	168

List of Figures

Figure 1-1 Anillin-related proteins in different systems show structural homology	26
Figure 1-2 Cleavage furrow formation and ingression during cytokinesis in animal cells.....	27
Figure 1-3 Cytokinesis is mediated by the assembly of nodes and the contractile ring in fission yeast	29
Figure 1-4 ESCRT proteins mediate abscission during cytokinesis in mammalian cells.....	31
Figure 1-5 The sequential function of ESCRT proteins mediates the MVB biogenesis in yeast	32
Figure 1-6 A schematic representation of <i>S. pombe</i> septation stages	34
Figure 1-7 Regulation of the metaphase/anaphase transition in mammalian cells	36
Figure 1-8 The localization of Ark1p throughout <i>S. pombe</i> cell cycle.....	38
Figure 3-1 Generation of <i>mid1Δ</i> and <i>vps4Δ</i> <i>S. pombe</i> strains and their growth phenotype	66
Figure 3-2 Classification and quantification of septation phenotypes in wild-type, <i>mid1Δ</i> and <i>vps4Δ</i> <i>S. pombe</i>	67
Figure 3-3 Meiotic nuclear division produces four haploid spores in <i>S. pombe</i> ..	69
Figure 3-4 A schematic representation of <i>S. pombe</i> spore's micro-manipulation	70
Figure 3-5 A synthetic lethal growth phenotype in the <i>mid1Δ vps4Δ</i> <i>S. pombe</i> double mutant indicates a genetic interaction between the <i>mid1⁺</i> and <i>vps4⁺</i> genes	71
Figure 3-6 Design of <i>in vitro</i> pull-down experiments to test for the physical interaction of Mid1p and Vps4p proteins.....	72
Figure 3-7 Design of Mid1p "N-term", "Middle" and "C-term" domain constructs to test for their physical interaction with Vps4p	73
Figure 3-8 Purification of GST-tagged "N-term, "Middle" and "C-term" domains of Mid1p	74
Figure 3-9 Elution of GST-tagged "N-term", "Middle" and "C-term" domains of Mid1p	75

Figure 3-10 Purification of 6His-tagged Vps4p and "C-term" Myo2p proteins.....	76
Figure 3-11 Quantification of 6His-tagged: Vps4p, "C-term" Myo2p and GST-tagged: Mid1p "N-term", "Middle" and "C-term" proteins.....	77
Figure 3-12 A physical interaction between Vps4p and the "C-term" domain of Mid1p	78
Figure 3-13 Design of GFP-Mid1p wild-type and <i>vps4Δ</i> strains	79
Figure 3-14 Classification and quantification of GFP-Mid1p localization phenotypes in wild-type and <i>vps4Δ S. pombe</i>	80
Figure 3-15 Structural lipid-binding domain similarities between anillin and Mid1p	82
Figure 3-16 Design of the PHΔ <i>mid1</i> strain and its growth phenotype	84
Figure 3-17 Classification and quantification of GFP-Mid1p localization phenotypes in wild-type and PHΔ <i>mid1 S. pombe</i>	85
Figure 4-1 The localization of Mid1p throughout <i>S. pombe</i> cell cycle	89
Figure 4-2 Mid1p NLS signals (aa 691-695 and aa 450-506) are not required for the genetic interaction between the <i>mid1</i> ⁺ and <i>vps4</i> ⁺ genes.....	92
Figure 4-3 Classification and quantification of septation phenotypes in wild-type and NLS* <i>mid1 S. pombe</i>	94
Figure 4-4 Classification and quantification of GFP-Mid1p localization phenotypes in wild-type and <i>mid1</i> NLS* <i>S. pombe</i>	97
Figure 5-1 Colony growth test of <i>ark1-TS</i> mutant strains at permissive and restrictive temperatures	103
Figure 5-2 A synthetic lethal growth phenotype in the <i>mid1Δ ark1-T11 S. pombe</i> double mutant indicates a potential genetic interaction between the <i>mid1</i> ⁺ and <i>ark1</i> ⁺ genes.....	104
Figure 5-3 Design of <i>in vitro</i> phosphorylation experiments to test for interactions between the Mid1p domains with aurora A and B or plk1 kinases	106
Figure 5-4 <i>In vitro</i> phosphorylation of Mid1p "N-term" and "Middle" domains by plk1 and aurora A kinases	108
Figure 5-5 Stoichiometric analysis of Mid1p <i>in vitro</i> phosphorylation by plk1 and aurora A kinases	110
Figure 5-6 Mid1p "N-term" and "Middle" domains have potential plk1 and aurora A kinases phospho-sites	114

Figure 5-7 Comparison of Mid1p potential phospho-sites from published studies and mass-spectrometry analysis presented in this Thesis	115
Figure 5-8 Design of Mid1p "N-term" domain phospho-resistant mutants to confirm its <i>in vitro</i> phosphorylation	117
Figure 5-9 Purification of the GST-tagged Mid1p "N-term" domain phospho-resistant mutants.....	118
Figure 5-10 <i>In vitro</i> phosphorylation of Mid1p "N-term" phospho-resistant mutants by plk1 and aurora A kinases.....	119
Figure 5-11 Design of Mid1p "Middle" domain phospho-resistant mutants to confirm its <i>in vitro</i> phosphorylation.....	121
Figure 5-12 Purification of GST-tagged Mid1p "Middle" domain phospho-resistant mutants	122
Figure 5-13 <i>In vitro</i> phosphorylation of Mid1p "Middle" phospho-resistant mutants by plk1 and aurora A kinases.....	123
Figure 6-1 An integrative vector is used to replace the endogenous <i>mid1</i> ⁺ gene with phospho-resistant/mimetic mutant versions of the gene.....	131
Figure 6-2 Microscopic analysis of <i>mid1</i> phospho-resistant/mimetic mutant <i>mid1</i> Δ <i>S. pombe</i>	133
Figure 6-3 Microscopic analysis of <i>mid1</i> phospho-resistant/mimetic mutant <i>mid1</i> Δ <i>ark1</i> -T11 <i>S. pombe</i>	137
Figure 6-4 Mid1p S332 potential phospho-site is important for its function during <i>S. pombe</i> cell cycle	140
Figure 6-5 Mid1p S523 and S531 potential phospho-sites might regulate its interaction with Vps4p during <i>S. pombe</i> cell cycle	142
Figure 6-6 Classification and quantification of GFP-Mid1p localization phenotypes in W-T and <i>ark1</i> -T11 <i>S. pombe</i>	145
Figure 6-7 Classification and quantification of GFP-Mid1p localization phenotypes in W-T and <i>ark1</i> -T8 <i>S. pombe</i>	147
Figure 7-1 A model for the interaction between Mid1p and Vps4p to regulate <i>S. pombe</i> septation	153
Figure 7-2 Sequence homology between <i>S. pombe</i> Ark1p and human aurora kinases.....	155
Figure 8-1 Classification and quantification of cell morphology phenotypes in <i>mid1</i> phospho-resistant/mimetic mutant <i>mid1</i> Δ <i>S. pombe</i>	169

Figure 8-2 Classification and quantification of cell morphology phenotypes in <i>mid1</i> phospho-resistant/mimetic mutant <i>mid1</i> Δ <i>ark1</i> -T11 <i>S. pombe</i>	170
---	-----

Acknowledgement

I am grateful to God Almighty for giving me the strength, knowledge and opportunity to undertake this wonderful experience. Without his blessings, this achievement would not have been possible.

I wish to express my sincere thanks to my great supervisors, Dr. Christopher McInerny and Professor Gwyn Gould for their aspiring guidance, constructive criticism, valuable comments on my thesis and moral support throughout the period of my PhD. I also thank Dr. Ian Salt for his help with the radiation-based lab experiments.

Profound gratitude must go to my beloved parents, Souad and Moussa, and my sisters Amina, Asma, Mimo and Nina, for their unconditional love, continues encouragement and support. I also thank my dear friends Zaaz, Muna, Rawan and Samia for their inspirational sparkly conversations. Salam, despite the long distance between us, I owe you a huge thank you.

I am using this opportunity to express my gratitude to everyone who supported me in Lab 241, staff and students, past and present. In particular I would like to thank the lab technicians, Alexandra Kaupisch and Laura Stirrat, for introducing me to the lab work in the early days.

Finally, I thank Anne Paoletti, Tomoko Iwaki and Silke Hauf for their generosity in sending us fission yeast strains.

لکم جزیل الشکر.

Thank you so much.

Author's Declaration

I declare that the work presented in this Thesis is my own, unless otherwise cited or acknowledged. It is entirely of my own composition and has not, in whole or in part, been submitted for any other degree.

Imane Nour El-Houda Moussa Rezig

November 2019

Definitions/Abbreviations

~	Approximately
°C	Degrees Celsius
μ	Micro-prefix
6His	Six histidine residue tag
aa	Amino acid
AAA-ATPase	ATPase associated with diverse cellular activities
ADP	Adenosine diphosphate
ALIX	Apoptosis-linked gene 2-interacting protein
Amp	Ampicillin
APC	Anaphase promoting complex
APS	Ammonium persulphate
Ark1p	Aurora-related kinase (fission yeast protein)
ATP	Adenosine 5'-triphosphate
bp	DNA base pair(s)
BSA	Bovine serum albumin
C-terminal	Carboxy terminal
Cdc	Cell division cycle
Cdk	Cyclin-dependent kinase
CEP55	Centrosomal protein of 55 kDa
CHMP	Charged multivesicular body protein
CaCl ₂	Calcium chloride
DAPI	4'6-diamidino-2-phenylindole, dihydrochloride
dH ₂ O	Distilled water
DNA	Deoxyribonucleic acid
DTT	Dithiothreitol

EDTA	Ethylenediaminetetraacetic acid
EMM	Edinburgh minimal medium
ESCRT	Endosomal sorting complex required for transport
g	Gramme
<i>g</i>	Relative centrifugation force
GDP	Guanosine-5'-diphosphate
GFP	Green fluorescent protein
GST	Glutathione S transferase
GTP	Guanosine-5'-triphosphate
h	Hour
HCl	Hydrochloric acid
HEPES	2-[4-(2-Hydroxyethyl)-1-piperazine] ethanesulfonic acid
HIV	Human immunodeficiency virus
ILV	Intralumenal vesicle
IPTG	Isopropyl- β -D-thiogalactopyranoside
Kan	Kanamycin
k	Kilo-prefix
kb	Kilobases
kDa	Kilo daltons
L	Litre
LSB	Laemmli's sample buffer
m	Milli-prefix
M	Molar
ME	Malt extract
min	Minute
ml	Millilitre

MVB	Multivesicular body
n	Nano-prefix
N-terminal	Amino terminal
Ni-NTA	Nickel-nitrilotriacetic acid
nmt	not-made-in-thiamine
OD	Optical density
PAGE	Polyacrylamide gel electrophoresis
PBS	Phosphate buffered saline
PCR	Polymerase chain reaction
p	Pico-prefix
Plk1	Polo-like kinase (mammalian protein)
Plo1p	Polo-like kinase (fission yeast protein)
RNA	Ribonucleic acid
rpm	Rotations per minute
SDS	Sodium dodecyl sulfate
SIN	Septation initiation network
TB	Terrific broth
TEMED	N, N, N', N' - tetramethylenediamine
Tris	2-Amino-2-(hydroxymethyl)-1,3-propanediol
TSG101	Tumour susceptibility gene 101
Vps	Vacuolar protein sorting
(v/v)	Units volume per unit volume
W-T	Wild-type
(w/v)	Units weight per unit volume
YE	Yeast extract

Chapter 1 Introduction

1.1 A historical overview of the cell cycle

There is an internal clock inside every cell, according to which parent cells proceed through several phases to divide into two identical daughter cells. Each newly divided cell passes again through the same phases, hence the name "cell cycle" (Hunt, Nasmyth, and Novák, 2011).

The fundamental principles leading to the discovery of the cellular theory were reviewed by Turner (1890) and were summarized as follows:

- 1831, Robert Brown first discovered the nucleus in plant cells.
- 1839, Theodore Schwann explained that cells are the building blocks of animal and plant tissues.
- 1841, Martin Barry discussed the concept of nuclear division.
- 1842, John Goodsir described the nucleus as the "reproductive organ" within cells.
- 1843, Albert Von Kolliker observed nuclear division of fertilized ova of parasitic worms. He classified cell nuclei into several groups, including elongated nuclei, nuclei constricted to the cell centre, or two nuclei in a single cell with each smaller in size than the single nucleus of the mother cell. The simple explanation to these observations was that nuclei of parent cells divide to yield daughter cells each originated from a new nucleus.

Following the discovery of the cellular theory, subsequent work by Walther Flemming and Eduard Strasburger led to the structural characterization of the nucleus. It was thought to be composed of a membrane encapsulating the nucleolus, threads of fibers arranged in a network called nuclein or chromatin fibers, and the nuclear fluid called nucleoplasm (Turner, 1890).

In 1850s, after the structural characterization of the nucleus, Robert Remark described cell division as a process that initiates from the cell centre towards the periphery, meaning that cellular division begins with nuclear division followed by division of the cell body and membrane. In 1880s, Walther Flemming was the first to introduce the term mitosis (thread in Greek) to describe cell division (Wilson, 1900).

The term "cytokinesis" was then introduced to describe cytoplasmic division, after which a landmark study by Thomas Schroeder described the role of the contractile ring in this process; he observed that the contractile ring consists of filaments similar to actin filaments present in muscles (Schroeder, 1972). One year later, Schroeder confirmed that actin was indeed a component of the contractile ring and described the ring as the "mechanochemical" organelle that drives cell division (Schroeder, 1973).

By 1974, the distinct stages of a typical eukaryotic cell cycle were well demonstrated starting with the G1-phase, defined as the time interval separating a previous division from a newly initiated division. This is followed by chromosomal replication or the DNA synthesis phase, called the S-phase. Then, a second time interval called the G2-phase separates chromosomal DNA replication from mitosis. Finally, dramatic alterations in chromosome segregation and structure occur in mitosis, the M-phase, which ends with cytokinesis, where the final separation of the two daughter cells occurs (Hartwell et al., 1974).

In 1976, Fujiwara and Pollard demonstrated that myosin is also a component of the contractile ring; they investigated its subcellular distribution in human cells, where it localized in the mitotic spindle suggesting that a contractile mechanism is involved in chromosome separation (Fujiwara and Pollard, 1976). In 1977, Mabuchi and Okuno demonstrated the interaction between myosin and actin filaments in the contractile ring during cytokinesis (Mabuchi and Okuno, 1977).

1.2 How do eukaryotic cells divide?

1.2.1 A contractile ring is positioned at the site of division

1.2.1.1 Formation of the acto-myosin contractile ring

The actin cytoskeleton has well established roles in controlling several important cell cycle processes, such as cytokinesis, motility and endocytosis (Pollard, Blanchoin and Mullins, 2000). Actin exists in globular (G-actin) and filamentous (F-actin) forms, where the polar F-actin form results from the assembly of the monomeric G-actin form. In *S. pombe* genome, a single gene called *act⁺* encodes for actin (Mertins and Gallwitz, 1987), which polymerizes into filaments that, in

turn, bundle to form actin cables. These cables, in addition to cortical patches and an actomyosin contractile ring (ACR), constitute the actin cytoskeleton during cytokinesis (Marks J, Hyams, 1985). Structurally, the binding of myosin to F-actin creates an arrowhead pattern with a rapidly-growing and a slowly-growing end of the filament (Pantaloni, Le Clainche and Carlier 2001; Paavilainen et al., 2004), but for this structure to translate into a functional network of actin filaments, several actin-binding proteins are essential to regulate the assembly and dis-assembly of the filaments (Pollard, Blanchoin and Mullins, 2000).

Important actin regulators were originally identified in experiments screening for cell cycle division mutants (Nurse, Thuriaux and Nasmyth, 1976). To date, a large number of actin-monomer binding proteins were identified in yeast and mammalian cells; these include the profilin and actin-depolymerizing factor (ADF)/cofilin and Srv2/cyclase-associated protein (CAP) classes of proteins (Hussey, Allwood and Smertenko, 2002). For example, profilin is known to play a key role in actin dynamics as its absence in flies, yeast and mammalian cells resulted in failure of actin-dependent processes, including cytokinesis (Schlüter, Jockusch and Rothkegel, 1997).

The term "myosin" refers to "within muscle" and is used to describe ATPase activity-dependent proteins located within muscle cells (Pollard and Korn, 1973). The myosin superfamily, which is composed of conventional-type II myosins and unconventional myosins, is essential for actin-dependent processes in all eukaryotes (Anderson et al., 1998). On the one hand, Myo1 is an unconventional *S. pombe* myosin composed of a motor domain with ATP and actin binding sites (head region), a variable number of isoleucine- and glutamine-rich motifs (neck region) in addition to other functional domains (tail region) (Anderson et al., 1998). On the other hand, *S. pombe* possess two types of conventional-type II myosins called Myo2p and My2p.

Two mechanisms are proposed to explain ACR formation in *S. pombe*. In the first mechanism "leading cable", an aster structure branches out from actin cables at the cell equator (Arai and Mabuchi, 2002). As the aster structure expands, it forms a primary ring leading to bundling of the accumulated actin filaments (Pelham and Chang, 2002); this results in the formation of a ring composed of two species of parallel filaments with opposite directions (Kamasaki, Osumi and Mabuchi, 2007).

In the second mechanism "search and capture", actin filaments extend from node structures containing Myo2p. The filaments are then captured by Myo2p in neighboring nodes pulling the nodes together and forming actin cables. This process results in the coalescing of actin cables and nodes into an ACR (Coffman et al., 2009).

1.2.1.2 Anillin-based contractile ring drives cytokinesis in mammalian cells

Since actin filaments and myosin motors are essential building blocks of the ACR, their assembly in an organized manner is required. Therefore, a scaffold composed of several cytoskeletal proteins is assembled at the cleavage site to connect these filaments to the plasma membrane. Anillin, alongside other proteins, is an important organizer of this scaffold (D'Avino, 2009).

Anillin was first identified in the fruit fly *Drosophila melanogaster* (*D. melanogaster*) in 1989 as an F-actin-binding protein (Miller et al., 1989); homologues of this protein were then characterized in all eukaryotes including the nematode worm *Caenorhabditis elegans* (*C. elegans*) ANL1, ANL2 and ANL3 (Maddox et al., 2005), the fission yeast Mid1p (Sohrmann et al., 1996), and the human anillin (Oegema et al., 2000). The anillin-related proteins share a general structure that is conserved in metazoans, where myosin- and actin- binding domains are located within the N-terminal domain, while an anillin homology region (AHR) and a PH domain are located within the C-terminal domain of these proteins (D'Avino, 2009) (Figure 1-1).

Human anillin binds actin and myosin through its N-terminal domain to regulate cytokinesis (Straight, Field and Mitchison, 2005). Similarly, *S. pombe* Mid1p binds Myo2p to promote ACR assembly (Motegi et al., 2004); however, the specific binding region is not confirmed. In this study, we detected a physical interaction between 6His-tagged Myo2p C-terminal region (aa 1394-1526) and the N-terminal region (aa 1-578) of GST-tagged Mid1p, named in this Thesis "N-term" and "Middle" domains (Section 3.3.4.4).

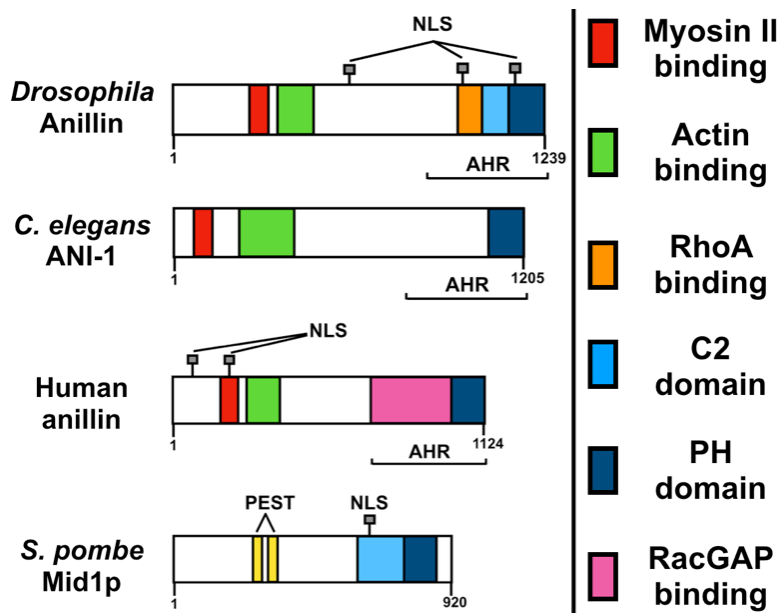


Figure 1-1 Anillin-related proteins in different systems show structural homology. *C. elegans* has three anillin-like proteins, but only one protein called ANI-1 shows sequence similarity to actin- and myosin-binding domains found in humans and vertebrates (Maddox et al., 2005). The different characterized or putative domains are colour coded. C2: cryptic domain (Sun et al., 2015), PH: Pleckstrin homology domain. Note that the RacGAP region binds the RacGAP20C protein of the centralspindlin complex (see text below), and the sequence rich in proline (P), glutamic acid (E), serine (S) and threonine (T) (PEST) (Rechsteiner and Rogers, 1996) targets Mid1p for degradation (Sohrmann et al., 1996). Anillin homology region (AHR) and nuclear localization signals (NLS) are indicated. Figure derived from D'Avino et al. (2009).

Anillin has a direct role in connecting the ACR to the spindle microtubules via the small GTPase RhoA signaling pathway (D'Avino, 2008). In *D. melanogaster*, RhoA is activated by the centralspindlin complex. This complex is a heterotetramer composed of two dimers of: the Pavarotti pulse-end directed kinesin-like protein (Pav-KLP/mammalian MLKP1) (Mishima, Kaitna and Glotzer, 2002) and a Rho-GTPase protein (RacGAP506C/mammalian male germ cell RacGAP (MgcRacGAP)) (Touré et al., 1998). In this pathway, RacGAP506C binds the Rho guanine nucleotide exchange factor (Pbl/mammalian ECT2), which promotes the activity of RhoA to initiate formation of the cleavage furrow and assembly of the ACR. RacGAP506C and RhoA then interact with anillin to recruit it to the cell equator; this connects the actomyosin filaments in the ACR to the spindle microtubules (Figure 1-2) (D'Avino, 2009).

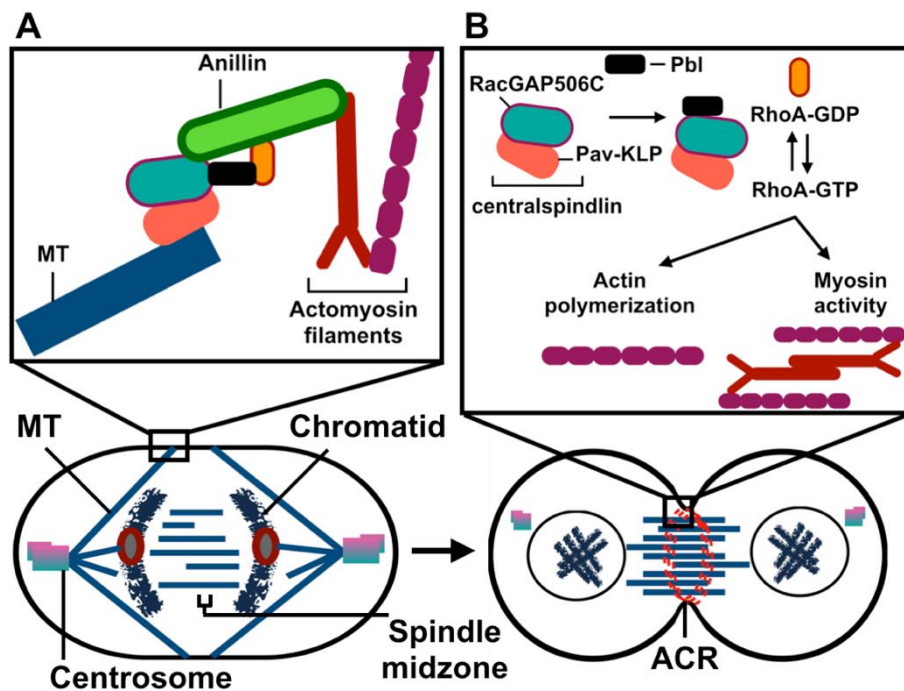


Figure 1-2 Cleavage furrow formation and ingression during cytokinesis in animal cells. Schematic representation of cells in anaphase (left) and telophase (right). (A) Anillin functions in connecting the spindle MT with the ACR through interactions with RacGAP and other proteins (see (B) for labels). (B) RhoA GTP-dependent activity is induced by interactions with the RacGAP506c component of the centralspindlin complex and Pbl1, after which two events are induced: first, the polymerization of actin filaments, and second induction of the phosphorylation-dependent activity of myosin; these events lead to the formation and ingression of the cleavage furrow through interactions between myosin heads and actin filaments. Figure adapted from D'Avino (2009).

Kim and colleagues demonstrated that human anillin phosphorylation during mitosis is required for proper cytokinesis (Kim et al., 2017). In particular, phosphorylation of the S635 residue was found to be essential for the localization and function of anillin. It regulates anillin recruitment to the equatorial plasma membrane and mediates stabilization of the cleavage furrow. Hickson and O'Farrell (2008) used a high-resolution microscopic approach to analyze the localization of anillin in *D. melanogaster*. Anillin was localized to the nucleus throughout interphase, and upon mitotic entry its concentration shifted uniformly to the cell cortex. During anaphase prior to the onset of cytokinesis, anillin disappeared from the opposite poles and localized to the equatorial zone. This localization pattern confirms the role of anillin in linking the ACR to the equatorial membrane.

1.2.1.3 Mid1p-based contractile ring drives cytokinesis in *S. pombe* cells

Although *S. pombe* cell cycle highly represents a typical eukaryotic cell cycle, disassembly of the nuclear envelope does not occur during M phase. Instead, microtubules from the mitotic spindle form within the nucleus (Grallert et al., 1998), and an ACR is then assembled surrounding the cell equator. To evaluate how *S. pombe* divides medially, it is important to understand the composition and contraction dynamics of the ACR. The basic precursors of this ring are described as punctuate structures called nodes that are associated with the plasma membrane around the medial region of the cell (Vavylonis et al., 2008).

Studies by Wu et al. (2003) and Wu and Pollard (2005) aimed to measure the kinetics of nodes appearance and their constituent proteins. Such studies suggested that approximately 65 nodes assemble into the contractile ring through interactions with myosins, which then interact with actin filaments originating from a different type of nodes (Wu et al., 2006). Studies by Laporte et al., (2011) and Laplante et al., (2016) showed that the nodes are organized such that the myosin-II tails are anchored to a base composed of anillin Mid1p near the plasma membrane, while the heads of myosin-II project into the cytoplasm (Figure 1-3).

Akamatsu and colleagues investigated the assembly of the contractile ring from interphase cortical nodes in *S. pombe* (Akamatsu et al., 2014). They grouped these interphase nodes into Type 1 nodes, composed of Cdr1p and Cdr2p cell cycle kinases and the anillin Mid1p, in addition to Type 2 nodes, composed of Blt1p, Gef2p, and Klp8p.

The mechanism by which the two immature node types fuse to form mature cytokinesis nodes is thought to begin when Type 2 nodes diffuse into the cell cortex, after which they are captured by Type 1 nodes present around the cell equator. Both types of interphase nodes are known to associate with the plasma membrane by different mechanisms. The interaction between Type 1 and Type 2 nodes to form cytokinesis nodes is thought to be mediated through a diffuse-and-capture mechanism (Akamatsu et al., 2014). Type 1 nodes interact with the cell membrane through the PH and C2 domains of Mid1p (Sun et al., 2015), while Type 2 nodes interact through the phospholipid binding protein Blt1p (Guzman-Vendrell et al., 2013). Other proteins are then recruited to the cytokinesis nodes to form the ACR (Laporte et al., 2011) (Figure 1-3).

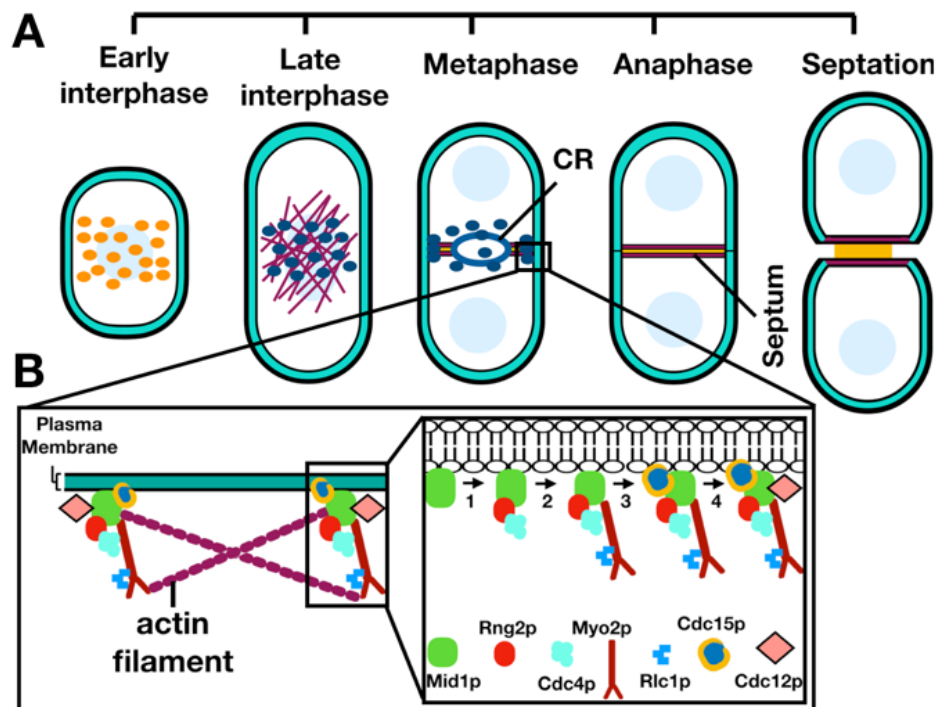


Figure 1-3 Cytokinesis is mediated by the assembly of nodes and the contractile ring in fission yeast. (A) *S. pombe* cell cycle stages showing the nuclei (light blue), immature interphase nodes (Type 1 and Type 2) (orange), mature cytokinesis nodes (navy blue) and actin filaments (purple). Cytokinesis nodes are formed by the fusion of Type 1 and 2 interphase nodes. (B) The Mid1-dependent assembly of nodes is initiated by the binding of Mid1p to the plasma membrane; sequential recruitment of cytokinesis proteins then leads to the formation of cytokinesis nodes. The final recruitment of the formin Cdc12 leads to the nucleation (polymerization) of actin filaments. Myo2p heads, which point towards the cell interior, capture actin filaments then cause the condensation of nodes to the contractile ring. Figure adapted from Laporte et al. (2011).

1.2.2 Cytokinesis leads to the final separation

1.2.2.1 The ESCRT family of proteins drives abscission in mammalian cells

After the completion of furrowing, the two daughter cells remain connected via an intercellular bridge. At the centre of this bridge lies the midbody, which is believed to anchor the cleavage furrow to the plasma membrane serving as a platform for the components of the abscission machinery. During abscission, the endosomal sorting complex required for transport (ESCRT) machinery is assembled to catalyze membrane remodeling events allowing for the final separation of the daughter cells (Elia et al., 2011). The ESCRT family of proteins is divided into

different classes: ESCRT-0, I, II and III in addition to the ATPase associated with different activities (AAA-type) family ATPase vacuolar protein sorting 4 (VPS4) (for review of the ESCRT role in cytokinesis see Wollert and Hurley, 2010 and references therein). In mammalian cells, absence of the ESCRT proteins leads to inhibition of cytokinesis (Morita et al., 2010), which indicates their vital role to establish the final abscission event.

Elia and colleagues summarized the role of ESCRT-mediated abscission in two steps. First, a platform to initiate abscission is formed by CEP55, TSG101 and ESCRT-III at the midbody. Second, upon abscission initiation, the CHMP4B subunit of ESCRT-III re-localizes at a distance $\sim 1 \mu\text{m}$ away from the midbody centre (called the narrow constriction site) through the formation of spiral ESCRT-III polymers. This re-localization or elongation of ESCRT III is thought to mediate constriction of the cleavage furrow followed by disruption of the intercellular bridge and the complete separation of the two daughter cells (Elia et al., 2011).

Furthermore, Goliand and colleagues indicated that completion of the abscission event requires continuous breakage and depolymerization of the ESCRT-III subunits, which is mediated by the catalytic activity of VPS4 (Goliand et al., 2018 & Ghazi-Tabatabai et al., 2008). In fact, VPS4 cleaves the ESCRT-III filaments prior to their complete disassembly (Maity et al., 2019). The C-terminal domain of some ESCRT-III proteins contains microtubule interacting and transport (MIT) interacting motifs (MIMs) (Obita et al., 2007); Vps4 interacts with ESCRT-III through MIM-binding motifs located at its N-terminal domain (Stuchell-Brereton et al., 2007).

At least two findings support the previously illustrated model. In terms of ESCRT-III structure, they exist as monomers or dimers in solution, but their active form is defined as membrane-bound oligomeric assemblies that can have different forms including spirals, filaments or helical tubes (Yang et al., 2015). This confirms the need of polymerization for the activity of ESCRT-III subunits. Moreover, Morita and colleagues demonstrated that the subunits of the ESCRT-III complex localized to the midbody, whereas VPS4 was detected only in thin midbodies indicating that it is recruited only during the late stages of cytokinesis (Morita et al., 2007). This later observation is consistent with VPS4 function in re-cycling ESCRT-III subunits to promote cleavage of the midbody (Figure 1-4).

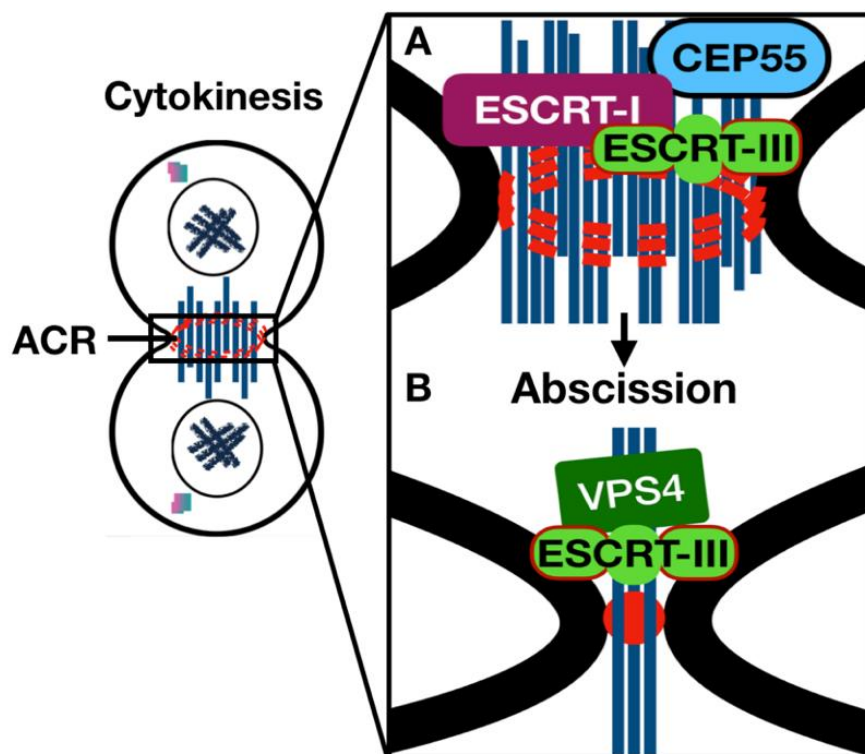


Figure 1-4 ESCRT proteins mediate abscission during cytokinesis in mammalian cells. During late cytokinesis, CEP55 is first localized to the midbody, after which it recruits ESCRT-I/TSG101; this, in turn, results in the recruitment of ESCRT-III components to the centre of the midbody. Prior to abscission, ESCRT-III polymerization into a spiral on the MT bridge leads to the constriction of the intercellular bridge. Following polymerization, spiral ESCRT-III rearrangement is mediated by VPS4. Daughter cell separation is then mediated by the dome-like end-cap of the ESCRT-III fission complex. Figure adapted from Elia et al. (2012).

Previous work examined the formation of a medial single septum in *S. pombe* cells with single chromosomal ESCRT gene deletion mutations. The different classes of the ESCRT genes, including the ESCRT-III regulator *vps4⁺*, were found to be required for correct septation, suggesting that they have a role in fission yeast cytokinesis (Bhutta et al., 2014).

The different classes of ESCRT proteins carry out important roles in different membrane remodeling pathways including HIV budding (reviewed by Hurley & Hanson, 2010), multivesicular bodies (MVB) biogenesis (reviewed by Hanson & Cashikar, 2012) and in cytokinesis.

The role of ESCRTs in membrane remodeling is well understood through MVB biogenesis (reviewed by Babst *et al.*, 2011). For example, in budding yeast, the protein cargo that is targeted for inclusion in endosomes is ubiquitinated; the ubiquitin-cargo protein is then identified by ubiquitin-binding domains in ESCRT-0, I and II, which promotes sequestration of the ESCRT-cargo complex into endosomal vesicles budding into the intraluminal vesicles (ILVs). In this process, the ESCRT-III subunits, Vps20, Snf7, Vps24 and Vps2, assemble (in that order) to form a polymer, and Vps4 is required for their disassembly (Figure 1-5) (Babst *et al.*, 2002).

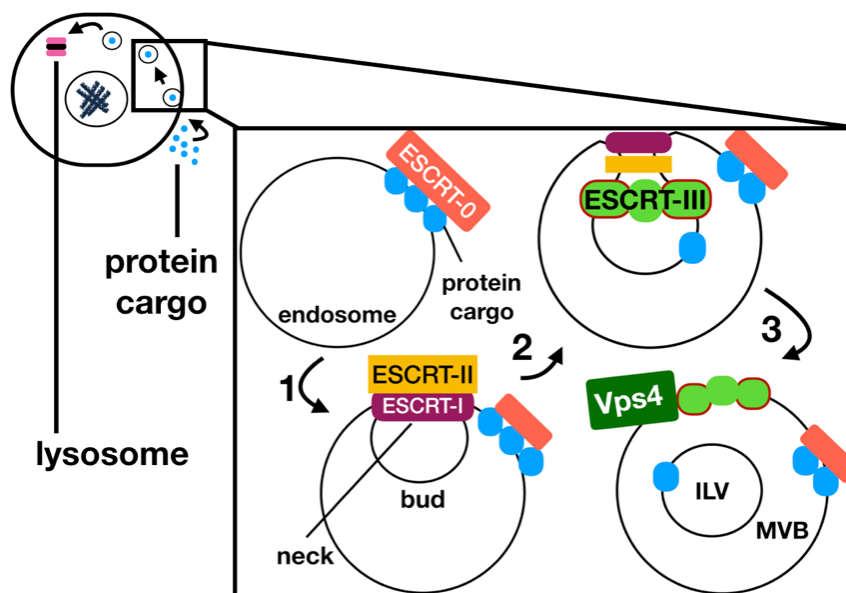


Figure 1-5 The sequential function of ESCRT proteins mediates the MVB biogenesis in yeast. (1) The ubiquitinated cargo protein is sequestered by ESCRT-0 to the endosomal membranes targeted for degradation in the lysosome; rigid stalks are then formed by ESCRT-I and ESCRT-II to deform the peripheral membrane and produce an inward bud. (2) ESCRT-III polymerization leads to the constriction of bud neck. (3) this induces protein cargo internalization and the formation of an intraluminal vesicle (ILV) inside MVBs; degradation (re-cycling) of ESCRT-III subunits is then mediated by Vps4. Figure adapted from Wollert and Hurley (2010).

In vitro analysis using giant unilamellar vesicles (GUV) and purified recombinant ESCRT-III subunits revealed that ESCRT-III facilitates the formation of vesicles inside GUVs lumen (Yang *et al.*, 2015), which further confirms the role of ESCRT-III proteins in the ILVs formation.

In yeast, the role of ESCRT proteins in membrane fission events such as endocytic trafficking is well demonstrated; however, further investigations are required to understand their role in cytokinesis and how these different activities and complexes are controlled (Schuh and Audhya, 2014).

Previous work examined the formation of a medial single septum in *S. pombe* cells with single chromosomal ESCRT gene deletion mutations. The different classes of the ESCRT genes, including the ESCRT-III regulator *vps4⁺*, were found to be required for correct septation suggesting that they have a role in fission yeast cytokinesis (Bhutta et al., 2014).

1.2.2.2 *S. pombe* septation is equivalent to mammalian cytokinesis

Septation in *S. pombe* is equivalent to mammalian cytokinesis (Wolfe and Gould, 2005), where the contractile ring placement at the cell equator, and thus the division site, is determined by the position of the nucleus and the recruitment of the scaffold protein anillin-like Mid1p (Daga and Chang, 2005). Unlike in mammalian cells, the contractile ring is assembled in the early stages of the cell cycle in *S. pombe*. This assembly initiates with the formation of precursors called “nodes” that are attached to the cell membrane (Vavylonis et al., 2008). These nodes fuse together to form the contractile ring, after which a cell wall-like structure called the septum is deposited behind the constricted ring forming the new edges of daughter cells (Figure 1-6) (Willet, McDonald and Gould, 2015).

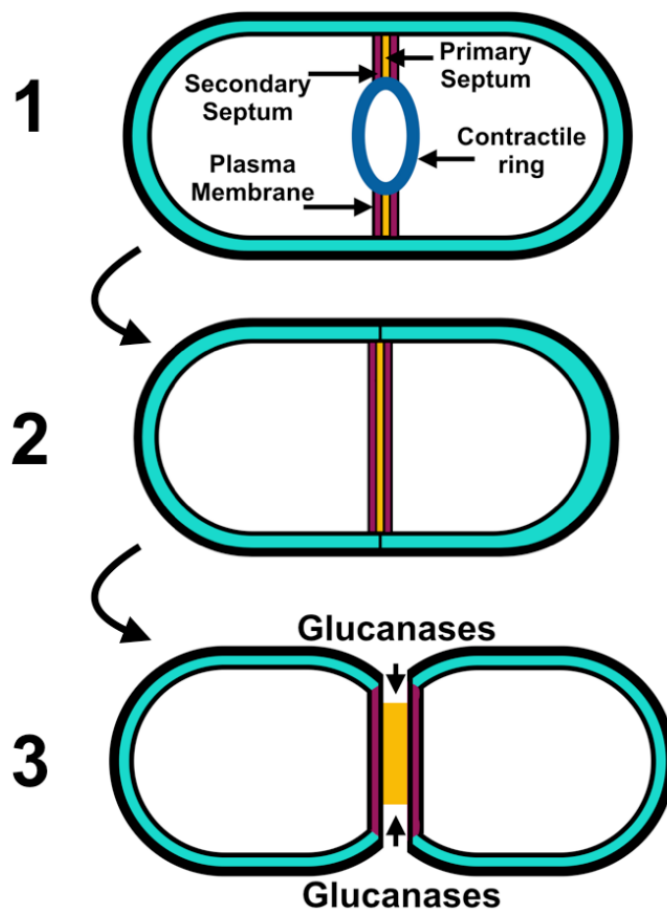


Figure 1-6 A schematic representation of *S. pombe* septation stages. *S. pombe* divides by medial fission into two equal-size daughter cells. (1) Following placement of the contractile ring, simultaneous formation of primary and secondary septa occurs as the ring constricts. (2) After completion of ring constriction, the septum matures. (3) The primary septum is then degraded by secreted Glucanases leading to the final separation of the daughter cells. Figure adapted from Willet, McDonald and Gould (2015).

Wu and colleagues determined the time-course of *S. pombe* cytokinesis (Wu et al., 2003). They marked the moment of spindle pole separation as the zero-time point and defined it as an internal clock. The beginning of anaphase was observed after ~9 min and completed after ~20 min. After ~7 min, contraction of the acto-myosin ring was observed in addition to the initial appearance of the septum, and finally after ~66 min, separation of the two daughter cells was observed. The total recorded time to accomplish cytokinesis was ~102 min.

1.3 Regulation of eukaryotic cell cycle

1.3.1 Spindle assembly checkpoint

In mammalian cells, chromosome replication (DNA synthesis, S phase) and segregation (mitosis, M phase) are not coupled. Consequently, to ensure faithful genome transmission, each daughter cell must receive one copy of each chromosome by the end of the M phase (Lara-Gonzalez, Westhorpe and Taylor, 2012). Thus, a quality control mechanism named the spindle assembly checkpoint (SAC) is responsible for blocking anaphase until the correct attachment of all chromosomes to the spindle is completed (Nezi and Musacchio, 2009).

Attachment of chromosomes to microtubules takes place in kinetochores, which are structures that provide a platform for spindle microtubules. The SAC proteins begin to be recruited by unattached kinetochores during prophase (Johnson et al., 2004), and during prometaphase, an anaphase inhibitor named the mitotic checkpoint complex (MCC) is activated as a result of SAC signaling; this complex inhibits the anaphase promoting complex (APC), which further enforces a faithful cell division (Musacchio and Salmon, 2007)

The highly regulated kinase family (cyclin dependent kinases CDK proteins) promotes cell cycle progression through a cascade of protein phosphorylation events; the enzymatic activity of CDKs requires their binding to cyclins (Morgan, 1995), which were identified in sea urchin eggs, with their synthesis and degradation oscillating throughout the cell cycle (Evans et al., 1983). For example, mitotic entry is regulated by CDK1/cyclin B activity, where cytokinesis is suppressed until anaphase (Niiya et al., 2005). The APC, which is activated by CDK1, is involved in metaphase/anaphase transition through proteolysis of certain proteins, such as the anaphase inhibitor securin (Castro et al., 2005). The degradation of securin is required for sister chromatid separation (Figure 1-7) (Hagting et al., 2002), and expression of the non-degradable form of securin prevents sister chromatid separation in flies (Nasmyth, 2001).

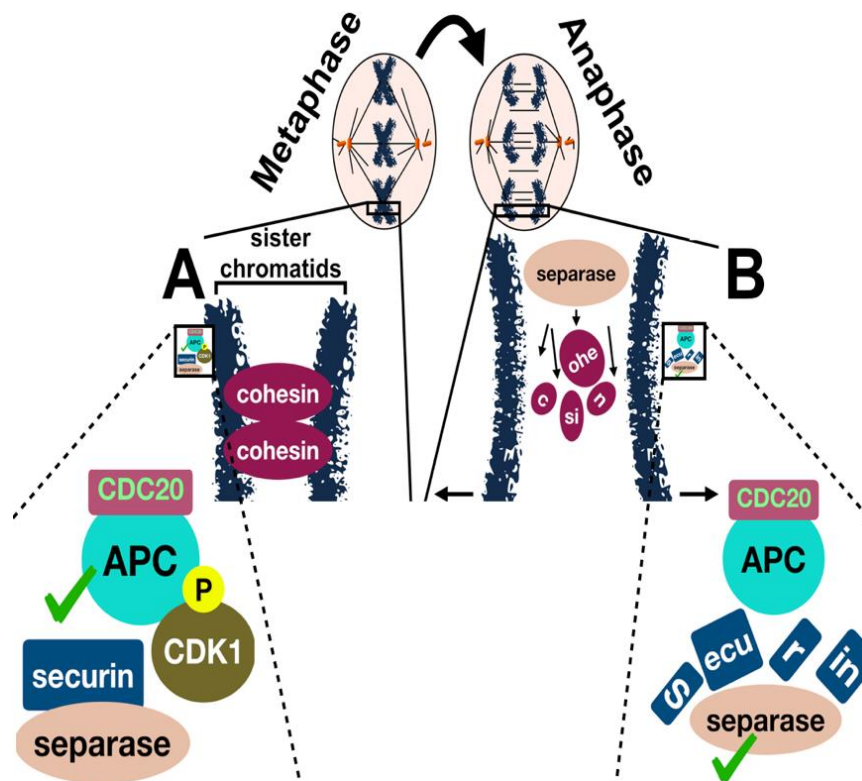


Figure 1-7 Regulation of the metaphase/anaphase transition in mammalian cells. A: during metaphase, the two sister chromatids are held together by the cohesin protein complex. Phosphorylation of the APC by CDK1 leads to its activation. B: the securin protein is degraded by the APC/CDC20; this leads to separase activation allowing for sister chromatids separation and the onset of anaphase. Green ticks = active proteins. Figure adapted from Castro et al. (2005).

The aurora family of kinases has well-established roles in cell cycle regulation. Mammalian cells have three different classes of aurora kinases: aurora-A, B and C. These kinases were initially discovered in *D. melanogaster* in a screen of mutants defective in spindle-pole behavior, which resulted in mis-localized DNA distribution. The mutants were given the name "aurora" as the DNA distribution resembled the *aurora borealis* (the Northern Lights) natural phenomenon in the polar regions observed in the night sky (Glover Goliand et al., 1995).

Aurora B kinase was discovered in *Saccharomyces cerevisiae* as a protein essential for ploidy maintenance and was initially named increase in ploidy 1 (*IPL1*) (Chan and Botstein, 1993). Later, it was found to regulate different important aspects of chromosome segregation in eukaryotes (Glover et al., 1995; Gopalan, Chan and Donovan 1997).

Aurora B is one component of the chromosome passenger complex (CPC), with three additional components being the inner centromeric protein (INCENP) (Adams et al., 2001), survivin and borealin (Gassmann et al., 2004). Recruitment of the CPC to the inner centromere is achieved by survivin and borealin, where both proteins interact with the N-terminal domain of INCENP to achieve its centromeric recruitment; aurora B, however, is not required for this centromeric localization (Kelin, Nigg and Gruneberg 2006). Instead, the role of aurora B is clearly demonstrated during metaphase in attaching the chromosomes to the mitotic spindle and during anaphase in the formation of the central spindle (Vagnarelli and Earnshaw, 2004). Briefly, during metaphase, chromosomes are aligned on the metaphase plate followed by the onset of anaphase, when the aligned chromosomes are segregated; however, this process is subject to errors from improper attachment of microtubules to kinetochores, and the kinase activity of aurora B is required for the correction of these attachment errors (Hauf et al., 2003). Furthermore, in mammalian cells, cleavage-furrow formation is disrupted when a catalytic inactive form of aurora B is overexpressed leading to cytokinesis failure; this indicates a role for aurora B in cytokinesis regulation (Terada et al., 1998).

Ark1p is the sole aurora-related kinase in *S. pombe*. Petersen and colleagues described the localization of Ark1p during *S. pombe* cell cycle as follows: in mitosis, it localizes to the kinetochores/centromeres, and following anaphase-A, the localization shifts from the kinetochores/centromeres to the spindle. Furthermore, they indicated that *S. pombe* cells with a defective *ark1⁺* gene showed reduced kinetochore activity and defective spindle formation, confirming *ark1⁺* requirement in *S. pombe* chromosome segregation (Petersen et al., 2001). A study then revealed that Ark1p is required for the attachment response generated during SAC signaling. During this checkpoint, the onset of anaphase is delayed until chromosomal bipolar attachment is completed, whereby the absence of MT activity triggers the attachment response (Petersen and Hagan, 2003). The localization of Ark1p in *S. pombe* is represented in (Figure 1-8).

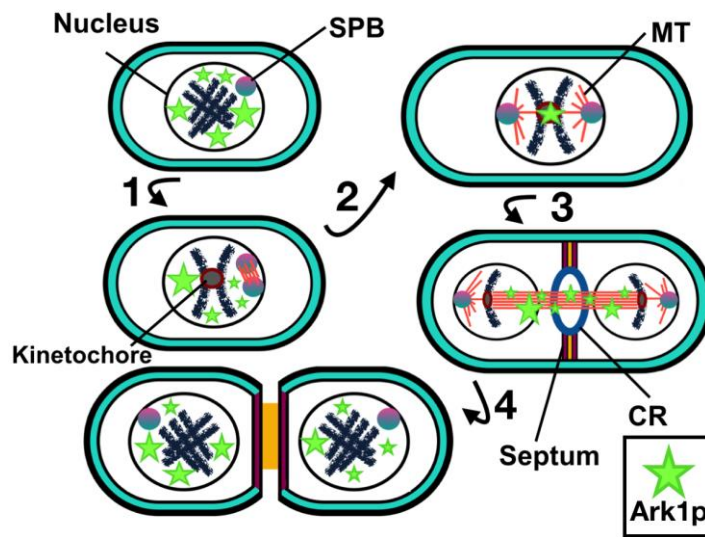


Figure 1-8 The localization of Ark1p throughout *S. pombe* cell cycle. During (1) prophase, Ark1p localizes to the nucleus, and during (2) late mitosis, its concentration shifts to the kinetochores, after that during (3) anaphase, it is detected along the spindle, and at the end of the cell cycle after (4) cytokinesis, it re-localizes to the nucleus. SPB: spindle pole bodies. Figure adapted from Petersen et al. (2001).

1.3.2 Exit from mitosis

In eukaryotic cells, inactivation of CDKs is required for mitosis exit (Morgan, 1999). For example, the phosphatase Cdc14p inactivates CDKs in budding yeast by inducing B-type mitotic cyclin degradation (Visintin et al., 1998). Sequence similarity search of budding yeast Cdc14p identified orthologs in many species including fission yeast (Cueille et al., 2001) and *C. elegans* (Gruneberg et al., 2002). In *S. pombe*, the Cdc14p homologue Clp1p is not essential for mitotic exit as *clp1Δ* mutants are viable but have defected septation (Cueille et al., 2001).

In both fission and budding yeast analogous mechanisms regulate the timing of mitotic septation and kinase inactivation, respectively, which in turn negatively regulate mitotic CDKs leading to the positive regulation of cytokinesis (McCollum and Gould, 2001). In budding yeast, the mitotic exit network (MEN) orchestrated by the phosphatase Cdc14p leads to the inactivation of CDKs by inducing B-type mitotic cyclin degradation (Visintin et al., 1998). In fission yeast, the septation initiation network (SIN) is not required for Cdk1p inactivation but plays important roles during late mitosis to induce ACR constriction (Le Goff, Utzig and Simanis, 1999).

The SIN pathway facilitates contractile ring constriction and promotes the formation of a cell wall-like structure between the two daughter cells, called the septum. Thus, SIN components associate with the spindle pole bodies (SPB) and couple mitotic exit with cytokinesis. Sid2p is one important regulator of the SIN-pathway (Akamatsu et al., 2014). It terminates the signaling cascade leading to the transition from the SPB to the cell division site promoting the onset of cytokinesis (Sparks, Morpew and McCollum, 1999). A recent study identified Mid1p as a substrate for Sid1p and indicated that phosphorylation of Mid1p facilitates its removal from the cell cortex during the ACR constriction (Willet et al., 2019).

Two phenotypes are generated by SIN mutants in *S. pombe*: either cells with multiple nuclei due SIN inactivation or cells with multiple septa due to SIN hyper-activation. The fact that mutants of either the *mid1* gene (Sohrmann et al., 1996) or the SIN components (Balasubramanian et al., 1998) retain the ability to assemble contractile rings suggests that the Mid1p and SIN pathways are independent.

In *mid1* Δ cells, a mis-shaped contractile ring is assembled during anaphase (at this point the SIN pathway becomes active); this confirms the important role of Mid1p in directing contractile ring assembly to the proper location (Chang, Woollard and Nurse, 1996). In SIN mutants, a contractile ring is assembled during mitosis but dissolves in anaphase, which implicates a role of SIN signaling in ring assembly and maintenance at the end of mitosis (Balasubramanian et al., 1998). Upon the disruption of both the *mid1* gene and the SIN components, ring assembly is blocked; this suggests that each of the two pathways contributes significantly towards ring assembly (Johnson, McCollum and Gould, 2012).

Tanaka and colleagues proposed that Plo1p activates the SIN pathway to regulate septation (Tanaka et al., 2001). Plo1p was then found to act upstream of the SIN component septum-promoting GTPase (Spg1p) to induce ACR formation (Hachet and Simanis, 2008). Using yeast two-hybrid analysis, Bhutta and colleagues (2014) detected interactions between ESCRT family proteins, including Sst4p, Vps28p, Vps25p, Vps20p and Vps32p, with Plo1p in *S. pombe* (Bhutta et al., 2014).

1.4 Cytokinesis dysregulation and cancer

Cytokinesis failure can occur due to multiple mechanisms, including the presence of physical barriers that obstruct the cleavage furrow, which prevents ingression, and altered expression of proteins that regulate cytokinesis initiation or progression (Lens and Medema, 2019). For example, mutations in RhoA pathway have been reported to prevent furrowing initiation; in particular, the gene encoding the GEF for RhoA is found to be amplified in several solid cancers including non-small-cell-lung cancer (NSCLC), head and neck squamous cell carcinoma, and cervical squamous cell carcinoma (Fields and Justilien, 2010).

When cytokinesis fails, aneuploid cells are generated. Aneuploid cells refer to highly precancerous cells that have either gains/losses of whole chromosomes or a segment of a chromosome. The functional impact of these alterations translates into chromosome segregation errors, called chromosomal instability, and DNA repair errors both of which are common occurrences in cancers. In fact, approximately 80% of human cancers (Duijf, Schultz and Benezra, 2012) are identified as aneuploid making it increasingly necessary to understand the mechanisms behind this genetic phenotype.

As an essential component of the ACR, anillin was found to be overexpressed in hepatocellular carcinoma (HCC) cells (Lian et al., 2018), and its knockdown by small interference RNA (siRNA) inhibited both cytokinesis and the development of liver tumour in mice (Zhang et al., 2018).

Furthermore, the cell cycle regulating kinase plk1 was found to be overexpressed in a variety of solid tumour including melanoma, colorectal cancer and NSCLC (Gutteridge et al., 2016). This high expression was also associated with poor patient prognosis (Bhola et al., 2015) and therapy resistance in a number of cancers (Zhang et al., 2014). Moreover, aurora A/B (Anand et al., 2003; Tuncel et al., 2012) are both known to be overexpressed in different cancers and their overexpression associate Guzman et al. with poor prognosis (Chieffi et al., 2006; Sorrentino et al., 2005).

Thus, plk inhibitors and aurora A/B inhibitors (Melichar et al., 2015) are already in clinical trials, but currently their use seems rationale only in the context of combination therapy. This could be due to functional redundancy of cell cycle

regulation proteins or evasion mechanisms developed by tumors. Since anillin is indispensable for ACR formation and was also associated with cancer progression in preclinical studies, it is important to comprehensively understand the functional regulation of this protein as it could constitute a promising target for anticancer drug development.

1.5 The use of fission yeast as a model organism to study eukaryotic cell cycle

S. pombe shares various fundamental cellular activities with higher multicellular organisms. Due to its short doubling time, it can be easily manipulated in the laboratory. Another feature of *S. pombe* is the small genome size of approximately 1.5×10^7 base pairs (Bostock, 1970). Additionally, it exists as a haploid yeast, which allows the creation and identification of mutants; using this feature, strains with specific genetic backgrounds could be constructed by mating haploid *S. pombe* cells (Zhao and Lieberman, 1995).

The budding yeast *Saccharomyces cerevisiae* (*S. cerevisiae*) and *S. pombe* vastly differ in certain cell cycle features, the most obvious of which is the division mechanism as *S. pombe* divides by medial fission resembling mammalian cells, while *S. cerevisiae* divides by budding. In fact, *S. pombe* cell cycle events represent a typical eukaryotic cell cycle with distinct phases and its three chromosomes being visibly condensed during mitosis. Furthermore, it is shown that the *S. pombe* chromatin is compacted to 2000-folds (2000X), which is only five-folds (5X) less than the compaction of mammalian chromosomes during metaphase (Umesono et al., 1983).

In contrast to *S. pombe*, the mitotic spindle is present throughout most of *S. cerevisiae* cell cycle due to the budding event, and mitosis initiation is established early in the cell cycle since initiation of the bud occurs during the S phase. Remarkably, the cell cycle lacks the G2 phase, which translates into absence of condensation of the seventeen chromosomes of *S. cerevisiae* (Russell and Nurse, 1986).

As the above lines of evidence suggest, fission yeast forms an ideal model organism to study eukaryotic cell cycle. Therefore, the Chapters of this Thesis will

focus on aspects of fission yeast cell cycle regulation, specifically, the potential interactions between the anillin Mid1p with the ESCRT-regulator Vps4p and the aurora kinase Ark1p.

1.6 General Aims of this thesis

In mammalian cells, tumorigenesis is the main consequence of a mis-regulated cell cycle. Therefore, understanding the mechanisms underlying cell cycle regulation can improve our understanding of cancer. The major aims of this Thesis were to investigate the regulation of eukaryotic cell cycle using *S. pombe* as a model organism. The anillin Mid1p, the ESCRT-regulator Vps4p and the aurora kinase Ark1p are important regulatory components of *S. pombe* cell cycle, yet coordination between these proteins to regulate *S. pombe* cell cycle has not been investigated. Therefore, we hypothesized that Mid1p genetically and physically interacts with Vps4p and Ark1p to regulate *S. pombe* cell cycle and described a series of experiments to test this hypothesis.

Overall, the work reported in this Thesis provides insights into *S. pombe* cell cycle regulation. Using *in vivo* *S. pombe* genetic and microscopic approaches, in addition to *in vitro* pull-down and phosphorylation experiments, we discovered novel Mid1p-dependent pathways for *S. pombe* cell cycle regulation.

Chapter 2 Materials and Methods

2.1 Materials

2.1.1 Media and strains

All *S. pombe* and *Escherichia coli* (*E. coli*) growth media were prepared in one litre of distilled water and autoclaved before use. Solid media were produced by adding 20 g Bacto agar to one litre of medium (*S. pombe* YE, ME or EMM or *E. coli* 2YT) prior to autoclaving; they were then poured into 90 mm Petri dishes and allowed to set. For standard solid medium, ~20 ml per Petri dish was poured, whereas for "thin" solid YE medium for micro-manipulation of tetrads (Section 2.2.1.2), ~10 ml per Petri dish was poured.

2.1.1.1 *S. pombe* media

S. pombe cells were cultured and maintained as described in Moreno et al. (1991) and Rezig et al. (2019).

Complete medium. Yeast Extract (YE): 30 g D-glucose, 5 g Bacto yeast extract, 225 mg adenine and 255 mg uracil.

Mating medium (limiting for nitrogen). Malt Extract (ME): 30 g Bacto malt extract.

Selective medium. Edinburgh Minimal Medium (EMM): 20 g D-glucose, 5 g NH₄Cl, 0.1 g Na₂SO₄, 0.1 g MgCl₂, 15 mg CaCl₂, 3 g C₈H₅KO₄ (potassium hydrogen phthalate), 1.8 g Na₂HPO₄, 1 ml vitamins (per litre of distilled H₂O: 10 g inositol, 10 g nicotinic acid, 1 g calcium pantothenate and 10 mg biotin) and 0.1 ml trace minerals (per litre of distilled H₂O: 5 g boric acid, 5.2 g MnSO₄, 4 g ZnSO₄, 2 g FeCl₃, 1.44 g molybdic acid, 0.4 g CuSO₄, 10 g citric acid and 0.1 g KI).

Supplements for EMM, per litre of yeast medium: 375 mg adenine, 375 mg uracil and 187.5 mg leucine. G418 (Geneticin) was added to solid YE medium to a final concentration of 100 µg ml⁻¹.

2.1.1.2 *S. pombe* strains

Each fission yeast strain was given a laboratory reference "GG" annotation number and stored long-term in 30% glycerol at -70°C (Table 2-1).

Table 2-1 List of *S. pombe* strains used in this study. The "GG" number refers to the laboratory reference collection.

GG No.	Genotype
397	h ⁺ <i>ade6-210 leu1-32 ura4-D18</i>
400	h ⁻ <i>ade6-216 leu1-32 ura4-D18</i>
1129	h ⁻ <i>mid1::ura4⁺ ade6-216 ura4-D18 leu1-32</i>
1347	<i>pmid-mid1-4GFP (integrated;pAP221; leu⁺)</i> h ⁻ <i>dmf1::ura4⁺ ura4-D18 leu1-32 ade6-M216</i>
1349	<i>pmid-NLS*-mid1-GFP (integrated; pAP167#2; leu⁺)</i> h ⁻ <i>dmf1::ura4⁺ ura4-D18 leu1-32 ade6-M216</i>
1384	<i>pAM19(D450-506 mid1:12myc:leu1⁺) integrated clone1</i> h ⁻ <i>dmf1::ura4⁺ ura4-D18 ade6-M216 leu1-32</i>
1388	<i>pAM23(NLS*mid1:12myc:leu1⁺) integrated clone1</i> h ⁻ <i>dmf1::ura4⁺ ura4-D18 ade6-M216 leu1-32</i>
1554	h ⁺ <i>dmf1::kanMX4 ura4-D18 leu1-32 ade6-216</i>
1622	h ⁻ <i>vps4::ura4⁺ leu1-32 ura4-D18</i>
2417	h ⁺ <i>ark1-T11<<kanR leu1-32</i>
2673	h ⁺ <i>vps4::ura4⁺ leu1-32 ura4-D18</i>
2886	<i>pmid-mid1-4GFP (integrated;pAP221; leu⁺)</i> h ⁻ <i>dmf1::ura4⁺ ura4-D18? leu1-32 ade6-M216 ark1-T11<<kanR</i>
2922	<i>pmid-mid1-4GFP (integrated;pAP221; leu⁺)</i> h ⁺ <i>dmf1::ura4⁺ ura4-D18 leu1-32 ade6-M216 ark1-T8<<kanR</i>
3100	<i>NLS* mid1:12myc:leu1⁺</i> h ⁻ <i>dmf1::ura4⁺ vps4::ura4⁺ ura4-D18 leu1-32 ade6-M216</i>
3107	<i>D450-506 mid1:12myc:leu1⁺</i>

	<i>h⁻ dmf1::ura4⁺ vps4::ura4⁺ ura4-D18 leu1-32 ade6-M216</i>
3181	pJK148 : <i>mid1</i> ⁺ (wild-type) <i>h⁻ mid1::ura4⁺ ade6-216 ura4-D18 leu1-32</i>
3185	pJK148 : <i>mid1</i> S523 to A523 <i>h⁻ mid1::ura4⁺ ade6-216 ura4-D18 leu1-32</i>
3189	pJK148 : <i>mid1</i> S523 to D523 <i>h⁻ mid1::ura4⁺ ade6-216 ura4-D18 leu1-32</i>
3193	pJK148 : <i>mid1</i> S531 to A531 <i>h⁻ mid1::ura4⁺ ade6-216 ura4-D18 leu1-32</i>
3197	pJK148 : <i>mid1</i> S531 to D531 <i>h⁻ mid1::ura4⁺ ade6-216 ura4-D18 leu1-32</i>
3201	pJK148 : <i>mid1</i> S523 to A523 + S531 to A531 <i>h⁻ mid1::ura4⁺ ade6-216 ura4-D18 leu1-32</i>
3205	pJK148 : <i>mid1</i> S523 to D523 + S531 to D531 <i>h⁻ mid1::ura4⁺ ade6-216 ura4-D18 leu1-32</i>
3218	pJK148 : <i>mid1</i> S523 to A523 <i>h[?] mid1::ura4⁺ ark1-T11<<kanR</i>
3230	pJK148 : <i>mid1</i> S523 to D523 <i>h[?] mid1::ura4⁺ ark1-T11<<kanR ura4-C190T leu1-32 ade6-216</i>
3235	pJK148 : <i>mid1</i> S531 to A531 <i>h[?] mid1::ura4⁺ ark1-T11<<kanR ura4-C190T leu1-32 ade6-216</i>
3239	pJK148 : <i>mid1</i> S531 to D531 <i>h[?] mid1::ura4⁺ ark1-T11<<kanR ura4-C190T leu1-32 ade6-216</i>
3242	pJK148 : <i>mid1</i> S523 to A523 + S531 to A531 <i>h[?] mid1::ura4⁺ ark1-T11<<kanR ura4-C190T leu1-32 ade6-216</i>
3246	pJK148 : <i>mid1</i> S523 to D523 + S531 to D531 <i>h[?] mid1::ura4⁺ ark1-T11<<kanR ura4-C190T leu1-32 ade6-216</i>
3250	pJK148 : <i>mid1</i> (wild-type) <i>h[?] mid1::ura4⁺ ark1-T11<<kanR ura4-C190T leu1-32 ade6-216</i>
3267	pJK148 : <i>mid1</i> S167 to A167 <i>h⁻ mid1::ura4⁺ ade6-216 ura4-D18 leu1-32</i>
3271	pJK148 : <i>mid1</i> S167 to D167 <i>h⁻ mid1::ura4⁺ ade6-216 ura4-D18 leu1-32</i>

3275	pJK148 : <i>mid1</i> S328 to A328 <i>h⁻ mid1::ura4⁺ ade6-216 ura4-D18 leu1-32</i>
3279	pJK148 : <i>mid1</i> S328 to D328 <i>h⁻ mid1::ura4⁺ ade6-216 ura4-D18 leu1-32</i>
3283	pJK148 : <i>mid1</i> S331 to A331 <i>h⁻ mid1::ura4⁺ ade6-216 ura4-D18 leu1-32</i>
3287	pJK148 : <i>mid1</i> S331 to D331 <i>h⁻ mid1::ura4⁺ ade6-216 ura4-D18 leu1-32</i>
3291	pJK148 : <i>mid1</i> S332 to A332 <i>h⁻ mid1::ura4⁺ ade6-216 ura4-D18 leu1-32</i>
3295	pJK148 : <i>mid1</i> S332 to D332 <i>h⁻ mid1::ura4⁺ ade6-216 ura4-D18 leu1-32</i>
3299	pJK148 : <i>mid1</i> S167+S328+S331+S332 to A167+A328+A331+A332 <i>h⁻ mid1::ura4⁺ ade6-216 ura4-D18 leu1-32</i>
3303	pJK148 : <i>mid1</i> S167+S328+S331+S332 to D167+D328+D331+D332 <i>h⁻ mid1::ura4⁺ ade6-216 ura4-D18 leu1-32</i>
3307	pJK148 : <i>mid1</i> S167+S328+S331+S332+S523+S531 to A167+A328+A331+A332+A523+A531 <i>h⁻ mid1::ura4⁺ ade6-216 ura4-D18 leu1-32</i>
3311	pJK148 : <i>mid1</i> S167+S328+S331+S332+S523+S531 to D167+D328+D331+D332+D523+D531 <i>h⁻ mid1::ura4⁺ ade6-216 ura4-D18 leu1-32</i>
3321	pJK148 : <i>mid1</i> S167 to A167 <i>h[?] mid1::ura4⁺ ark1-T11<<kanR ura4-C190T leu1-32 ade6?</i>
3324	JK148 : <i>mid1</i> S167 to D167 <i>h[?] mid1::ura4⁺ ark1-T11<<kanR ura4-C190T leu1-32 ade6?</i>
3327	pJK148 : <i>mid1</i> S328 to A328 <i>h[?] mid1::ura4⁺ ark1-T11<<kanR ura4-C190T leu1-32 ade6?</i>
3330	pJK148 : <i>mid1</i> S328 to D328 <i>h[?] mid1::ura4⁺ ark1-T11<<kanR ura4-C190T leu1-32 ade6?</i>
3333	pJK148 : <i>mid1</i> S331 to A331 <i>h[?] mid1::ura4⁺ ark1-T11<<kanR ura4-C190T leu1-32 ade6?</i>
3336	pJK148 : <i>mid1</i> S331 to D331 <i>h[?] mid1::ura4⁺ ark1-T11<<kanR ura4-C190T leu1-32 ade6?</i>

3339	pJK148 : <i>mid1</i> S332 to A332 <i>h[?] mid1::ura4⁺ ark1-T11<<kanR ura4-C190T leu1-32 ade6?</i>
3342	pJK148 : <i>mid1</i> S332 to D332 <i>h[?] mid1::ura4⁺ ark1-T11<<kanR ura4-C190T leu1-32 ade6?</i>
3345	pJK148 : <i>mid1</i> S167+S328+S331+S332 to A167+A328+A331+A332 <i>h[?] mid1::ura4⁺ ark1-T11<<kanR ura4-C190T leu1-32 ade6?</i>
3349	pJK148 : <i>mid1</i> S167+S328+S331+S332 to D167+D328+D331+D332 <i>h[?] mid1::ura4⁺ ark1-T11<<kanR ura4-C190T leu1-32 ade6?</i>
3352	pJK148 : <i>mid1</i> S167+S328+S331+S332+S523+S531 to A167+A328+A331+A332+A523+A531 <i>h[?] mid1::ura4⁺ ark1-T11<<kanR ura4-C190T leu1-32 ade6?</i>
3355	pJK148 : <i>mid1</i> S167+S328+S331+S332+S523+S531 to D167+D328+D331+D332+D523+D531 <i>h[?] mid1::ura4⁺ ark1-T11<<kanR ura4-C190T leu1-32 ade6?</i>

2.1.1.3 *E. coli* media

E. coli cells were cultured and maintained as described in Sambrook and Green (2012).

Complete medium. Yeast Extract Tryptone (2YT): 15 g tryptone, 5 g NaCl, 10 g yeast extract.

Protein expression medium. Terrific broth (TB): 47.6 g Terrific broth, modified and 4 ml glycerol. Isopropyl β -D-1-thiogalactopyranoside (IPTG) was added at a final concentration of 1 mM to induce protein expression.

Bacterial antibiotics: Ampicillin was added to solid 2TY medium to a final concentration of 100 μ g ml⁻¹.

2.1.1.4 *E. coli* strains

Plasmid vector DNA constructs maintained in *E. coli* (Table 2-2).

Each plasmid vector DNA construct was transformed into *E. coli*, given a Glasgow laboratory reference "GB" number and stored long-term in 30% glycerol at -70°C.

Table 2-2 List of plasmid vector DNA constructs used in this study. The "GB" number refers to the laboratory reference collection.

GB No.	Abbreviated plasmid vector description
824	pGEX-4T-1 - GST tagged + ampicillin, Mid1p N terminus 1-422 amino acids, cloned with <i>Sma</i> I/ <i>Sa</i> I transformed into <i>E. coli</i> BL21. Hart Lab - J00039-p4015- Almonacid et al. 2009 <i>Current Biology</i> 19: 961-966 (same for GB 825 and 826)
825	pGEX-4T-1 - GST tagged + ampicillin, Mid1p middle 331-534 amino acids, cloned with <i>Sma</i> I/ <i>Sa</i> I transformed into <i>E. coli</i> BL21.
826	pGEX-4T-1 - GST tagged + ampicillin, Mid1p C terminus 433-end amino acids, cloned with <i>Sma</i> I/ <i>Sa</i> I transformed into <i>E. coli</i> BL21.
880	pET-14b – His tagged + ampicillin, Vps4p, Cloned with <i>Nde</i> I/ <i>Bam</i> HI transformed into <i>E. coli</i> BL21. Invitrogen - 13AB6ZFP
881	pGEX4T1 - GST tagged + ampicillin, Mid1p amino acids 1-453, cloned with <i>Bam</i> HI/ <i>Xho</i> I GeneScript order number U2640BJ110 - Transformed into BL21 (same for GB 882-884)
882	pGEX4T1 - GST tagged + ampicillin, Mid1p amino acids 452-579, cloned with <i>Bam</i> HI/ <i>Xho</i> I transformed into <i>E. coli</i> BL21.
883	pGEX4T1 - GST tagged + ampicillin, Mid1p amino acids 478-799, cloned with <i>Bam</i> HI/ <i>Xho</i> I transformed into <i>E. coli</i> BL21.
884	pGEX4T1 - GST tagged + ampicillin, Mid1p amino acids 798-920, cloned with <i>Bam</i> HI/ <i>Xho</i> I transformed into <i>E. coli</i> BL21.
889	pET-14b – His tagged + ampicillin, Myo2p C-terminus aa1394-1526, cloned with <i>Nde</i> I/ <i>Bam</i> HI Genescript order number U9540CD270_2 - Transformed into BL21
923	<i>mid1</i> mutant gene full length + 1 kb upstream of ORF - 3,853 bp in total Polo sites S167 to A167 pJK148 - Transformed into XL1-Blue. <i>Kpn</i> I/ <i>Sac</i> I fragment from cloned into same sites of PJK148 by GeneScript order number U894VEB050. To linearise for yeast integration use <i>Nde</i> I to cut in <i>leu1+</i> (same for GB 924-934).
924	<i>mid1</i> mutant gene full length + 1 kb upstream of ORF - 3,853 bp in total Polo sites S167 to D167 Transformed into XL1-Blue
925	<i>mid1</i> mutant gene full length + 1 kb upstream of ORF - 3,853 bp in total Aurora/Polo sites S328 to A328 Transformed into XL1-Blue

926	<i>mid1</i> mutant gene full length + 1 kb upstream of ORF - 3,853 bp in total Aurora/Polo sites S328 to D328 Transformed into XL1-Blue
927	<i>mid1</i> mutant gene full length + 1 kb upstream of ORF - 3,853 bp in total Polo sites S331 to A331 Transformed into XL1-Blue
928	<i>mid1</i> mutant gene full length + 1 kb upstream of ORF - 3,853 bp in total Polo sites S331 to D331 Transformed into XL1-Blue
929	<i>mid1</i> mutant gene full length + 1 kb upstream of ORF - 3,853 bp in total Polo sites S332 to A332 Transformed into XL1-Blue
930	<i>mid1</i> mutant gene full length + 1 kb upstream of ORF - 3,853 bp in total Polo sites S332 to D332 Transformed into XL1-Blue
931	<i>mid1</i> quadruple (4) mutant gene full length + 1 kb upstream of ORF - 3,853 bp in total Aurora/Polo sites S167 to A167 + S328 to A328 + S331 to A331+ S332 to A332 Transformed into XL1-Blue
932	<i>mid1</i> quadruple (4) mutant gene full length + 1 kb upstream of ORF - 3,853 bp in total Aurora/Polo sites S167 to D167 + S328 to D328 + S331 to D331+ S332 to D332 Transformed into XL1-Blue
933	<i>mid1</i> hexa (6) mutant gene full length + 1 kb upstream of ORF - 3,853 bp in total Aurora/Polo sites S167 to A167 + S328 to A328 + S331 to A331+ S332 to A332 + S523 to A523 + S531 to A531 Transformed into XL1-Blue
934	<i>mid1</i> hexa (6) mutant gene full length + 1 kb upstream of ORF - 3,853 bp in total Aurora/Polo sites S167 to D167 + S328 to D328 + S331 to D331+ S332 to D332 + S523 to D523 + S531 to D531 Transformed into XL1-Blue

2.1.2 Standard solutions and reagents

2.1.2.1 List of standard solutions

Phosphate buffer saline (PBS): 137 mM NaCl, 2.7 mM KCl, 10 mM Na₂HPO₄ and 1.8 mM KH₂PO₄, pH 7.4.

Calcofluor-white: 1 g l⁻¹ distilled H₂O.

HEPES buffer: 25 mM HEPES, 400 mM KCl and 10% (v/v) glycerol, pH 7.4.

Glutathione beads elution buffer 1: 1 mM reduced-GST in PBS, pH 8.

Glutathione beads elution buffer 2: 20 mM reduced-GST in PBS, pH 8.

Glutathione beads elution buffer 3: 20 mM reduced-GST and 1% (w/v) octylglucoside in PBS, pH 8.

Ni-NTA beads washing buffer: 25 mM imidazole in HEPES buffer, pH 6.5.

Ni-NTA beads elution buffer 1: 250 mM imidazole in HEPES buffer, pH 4.5.

Ni-NTA beads elution buffer 2: 500 mM imidazole in HEPES buffer, pH 4.5.

Laemmli sample buffer (LSB) 6X: 375 mM Tris pH 6.8, 12% (w/v) SDS, 60% (v/v) glycerol, 600 mM DTT and 0.6% (w/v) Bromophenol Blue.

SDS-PAGE running buffer: 25 mM Tris-HCl, 250 mM glycine and 0.1% (w/v) SDS.

P1 solution: 50 mM Tris, 10 mM EDTA and 100 $\mu\text{g}.\text{ml}^{-1}$ RNase A, pH 8.

P2 solution: 0.2 M NaOH and 1% (w/v) SDS.

P3 solution: 2.55 M KOAc, pH 4.8.

Tris-acetate-EDTA (TAE) buffer: 40 mM Tris, 20 mM acetic Acid, and 1 mM EDTA, pH 8.5.

DNA loading dye 6X: 0.25% (w/v) Bromophenol Blue, 0.25% (w/v) xylene cyanol FF and 30% (v/v) glycerol.

Kinase assay buffer: 25 mM MOPS, 25 mM MgCl_2 , 1 mM EDTA and 0.25 mM DTT, pH 7.2.

ATP- ^{32}P cocktail: 2 μl [γ - ^{32}P] ATP, 1 μl of 10 mM ATP and 37 μl kinase assay buffer

2.1.2.2 List of reagents and kits

Adenosine 5'-triphosphate magnesium salt (ATP): SIGMA-ALDRICH

Acrylamide: Severn Biotech

Ampicillin: SIGMA-ALDRICH

Bacto agar: BD Biosciences

EDTA free protease inhibitors: Complete protease inhibitor, ROCHE

Geneticin: Promega

Glutathione sepharose beads: GE Healthcare Bio-Sciences

Isopropyl β -D-1-thiogalactopyranoside (IPTG): SIGMA-ALDRICH

Malachite Green Assay kit: SIGMA-ALDRICH

Nickel-nitroacetic (Ni-NTA) beads: SIGMA-ALDRICH

Octylglucoside: SIGMA-ALDRICH

Precision Plus Protein Standards All Blue: Bio-Rad

Recombinant aurora kinase A: SIGMA-ALDRICH

Recombinant aurora kinase A: Biaffin GmbH.

Recombinant aurora kinase B: SIGMA-ALDRICH

Recombinant polo-like kinase: SIGMA-ALDRICH

Recombinant polo-like kinase: Merck Chemicals Ltd.

Terrific broth (TB), modified: SIGMA-ALDRICH

Tetramethylethylenediamine (TEMED): SIGMA-ALDRICH

TrackIt 1 kb DNA Ladder: Invitrogen

Triton X-100: SIGMA-ALDRICH

Ultrapure water: SIGMA-ALDRICH

Wizard Plus SV Minipreps DNA purification kit: Promega

[γ -³²P] ATP 6000 Ci mmol⁻¹, 10 mCi ml⁻¹: EasyTide, Perkin Elmer

2.2 Methods

2.2.1 *S. pombe* methods

S. pombe methods were as described in Moreno et al. (1991) and Rezig et al. (2019).

2.2.1.1 General methods

For long-term storage of fission yeast strains, 30% glycerol stocks were generated of cells and kept at -70°C. Cells were recovered from glycerol stock by streaking on solid YE medium and incubating at 28°C for 2-3 days. Fission yeast cells were grown on yeast extract (YE) solid medium, mated with malt extract (ME) solid medium, and screened genotypically on Edinburgh minimal medium (EMM). A

laboratory reference number was given to all fission yeast strains preceded by the annotation "GG" (Table 2-1).

2.2.1.2 Mating and tetrad analysis

Opposite mating type h^+ and h^- parent strains were freshly grown at 28°C for three days. On solid ME medium, approximately equal amounts of each of the parent strains were mixed with 30 μ l sterile distilled H₂O in an area of about 1 cm². The mating mixture was allowed to air dry for 5-10 minutes and was incubated at 25°C for up to three days. Growth was monitored on days 2 and 3 for the formation of four ascospores using light microscopy.

After the formation of asci tetrads, a small amount of the mating mixture was transferred to solid "thin" YE medium along one side of the Petri dish (Rezig et al., 2019). The Petri dish was inverted and placed on a Singer MSM Ascus Dissector stage. Intact asci were identified and selected using the micro-manipulator needle; up to eight asci were placed in an adjacent vertical line on the same solid "thin" YE medium Petri dish. Asci were incubated at 37°C for 3-5 h to induce tetrad membrane dissolution.

The four spores were separated using a micro-manipulator needle with each spore placed horizontally; spores were then incubated at 28°C for 3-5 days until they formed colonies, 1-2 mm in size.

2.2.1.3 Mating type determination

The mating type of new double mutant strains was determined by re-plating the strains onto solid ME and mating them with standard h^+ and h^- strains. After incubating for two days at 25°C, the formation of tetrads was scored microscopically.

2.2.1.4 Genotype screening

After colonies formation, replica plating onto selective media was used for genetic screening of colonies (described in Section 2.1.1.1) . A sterile scalpel was used to remove the solid YE medium area containing the grown mating mixture, and a

sterile velvet material was assembled over the replica-plating device. The YE medium Petri dish was inverted with its lid removed, then it was placed on the sterile velvet and the colonies were transferred. The Petri dish was removed, and Petri dishes containing selective solid medium were placed instead; were incubated at 28°C for 1-2 days.

2.2.1.5 Septation analysis

Septation studies were carried out by visualizing *S. pombe* septa using calcofluor-white stain and fluorescence microscopy. 50 ml YE cultures were incubated overnight in a soaking water bath at 25°C. Cells were examined for septa formation using light microscopy. 1 ml of the culture was transferred to a micro-centrifuge tube and the cells were pelleted at 17,530 *g* for 30 seconds. The pellet was re-suspended in 1 ml PBS, and 30 µl of calcofluor-white stain was added; the tube was incubated in the dark for 5 minutes. The cells were then centrifuged at 17,530 *g* for 30 seconds and the pellet was re-suspended in 20 µl PBS; cells were then visualized using the bright field and DAPI filters of a Zeiss Axiovert 135 fluorescent microscope equipped with a Zeiss 63X Plan-APOCHROMAT oil-immersion objective lens. Images were processed using ImageJ, Microsoft PowerPoint and Keynote software.

2.2.1.6 Confocal microscopy

GFP-tagged *mid1*⁺ and different *mid1*⁺ mutants were integrated into the *S. pombe* genome under the control of *nmt1* promoter, as described (Bähler et al., 1998). Confocal microscopy analysis was used in two separate experiments: (1) Fission yeast strains containing a GFP tag on the *mid1*⁺ gene were used to study GFP-Mid1p localization, or (2) Fission yeast strains containing phospho-mimetic/resistant mutations on the *mid1* gene were used to study cell morphology. (Section 2.1.1.2, Table 2-1)

In both experiments, *S. pombe* cells were cultured in 50 ml YE in a water bath shaker at 28°C (or at 25°C for *ark1*-TS strains) overnight. Septa were viewed under a light microscope, with 10 µl samples used for examination by a He/Ne and Ag laser system of Zeiss LSM microscope using 63X high NA objective lens. cell

images were collected using Zeiss Pascal software and processed using ImageJ, Microsoft PowerPoint and Keynote software.

2.2.1.7 *In vivo S. pombe* integration

Phospho-mimetic/resistant mutant versions of the *mid1*⁺ gene were designed to test for their functional relevance. Nineteen different versions of *mid1* with different phospho-mimetic/resistant mutations were created (Table 2-2). These *mid1* gene versions were designed to have the wild-type *mid1*⁺ endogenous promoter and 1 kbp upstream of *mid1*⁺ reading frame, were all synthesized by GenScript, and cloned into the pJK148 integrative vector. Integration of *mid1* genes (1-19) into *mid1*Δ *S. pombe* (GG 1129) was performed via homologous recombination. The pJK148 integrative vector has a *leu*⁺ selective marker that includes a *Nde* I restriction site. The plasmid was digested with *Nde* I to linearize in *leu*⁺; then it was transformed into a *mid1*Δ *S. pombe* strain (GG 1129) with a *leu*1-32-point mutation, where it integrates at the *leu*⁺ locus. The resulting *S. pombe* strain is subjected to cell morphology analysis through confocal microscopy as described in Section 2.2.1.6.

Following the successful integration of all the 19 *mid1* mutant genes into *S. pombe* - summarized in Table 2-1 and Table 6-2 – some of the strains were subjected to an *in vivo* microscopy analysis (Chapter 6 and Chapter 7).

To test the involvement of Mid1p phospho-sites with the interaction of Ark1p, experiments were designed to test the effect of Mid1p phospho-mimetic/resistant mutations on the cell morphology of *ark1*-T11 *S. pombe*. The individual 19 phospho-mimetic/resistant strains (Table 6-2) were each crossed with an *ark1*-T11 *S. pombe* strain (GG 2417) and tetrad analysis used to identify triple mutants. This yielded 19 new *mid1*Δ *ark1*-T11 *S. pombe* triple mutant strains - summarized in Table 2-1 and Table 6-2- which were subjected to *in vivo* microscopic analysis (Chapter 6).

2.2.2 *E. coli* methods

2.2.2.1 General methods

For long-term storage of *E. coli*, 30% glycerol stocks were generated and kept at -70°C. Cells were recovered from glycerol stock by streaking on solid 2YT medium and incubating at 37°C overnight. *E. coli* cells were grown on 2YT solid medium and cultured on 2YT liquid medium, and protein expression was carried out in TB liquid 2YT medium. A laboratory reference number was given to all *E. coli* strains using the annotation "GB".

2.2.2.2 DNA constructs design for recombinant protein expression

The DNA constructs used in this study were synthesized by GenScript or Invitrogen, transformed into *E. coli*, given a laboratory GB number and stored at -70°C (Section 2.1.1.4, Table 2-1).

Two approaches to design *mid1*⁺ DNA constructs for bacterial expression were carried out.

The first approach used three domains of the *mid1*⁺ gene cloned into *Sma* I and *Sal* I restriction sites of the pGEX-4T-1 vector with an N-terminal glutathione S-transferase (GST) tag to express the corresponding Mid1p domains. The plasmid encoding Mid1p N terminus 1-422 amino acids was designated GB 824, Mid1p middle 331-534 amino acids designated GB 825, and Mid1p C terminus 433-end amino acids designated GB 826 (Section 2.1.1.4, Table 2-1).

The second approach used four domains of the *mid1*⁺ gene (Saha and Pollard, 2012b) cloned into *Bam* HI and *Xho* I restriction sites of the pGEX-4T-1 vector with an N-terminal GST tag to express the corresponding four Mid1p domains. The plasmid encoding Mid1p amino acids 1-453 was designated GB 881, Mid1p amino acids 452-579 designated GB 882, Mid1p amino acids 478-799 designated GB 883, and Mid1p amino acids 798-920 designated GB 884 (Section 2.1.1.4, Table 2-1).

Full-length *vps4*⁺ gene was cloned into *Nde* I and *Bam* HI restriction sites of the pET-14b vector with a 6His tag to express Vps4p, and designated GB 880 (Section 2.1.1.4, Table 2-1).

The C-terminal domain of the *myo2⁺* gene was cloned into *Nde* I and *Bam* HI restriction sites of the pET-14b vector with a 6His tag to express the C-terminal domain of Myo2p, and designated GB 889 (Section 2.1.1.4, Table 2-1).

2.2.2.3 Plasmid DNA extraction for bacterial transformation

Plasmid DNA was extracted using the Wizard Plus SV Minipreps DNA purification kit according to manufacturer's protocol or using a chemical method, where *E. coli* XL1-blue cells were cultured in 10 ml 2YT medium (100 µg.ml⁻¹ ampicillin; shaking; 37°C; overnight). 1.5 ml of the bacterial culture was centrifuged at 12000 *g* for 1 minute and the bacterial pellet was resuspended in 150 µl P1 solution. Then, 150 µl of P2 solution was added followed by a 5 minutes incubation at room temperature. After that, 150 µl of P3 solution was added and the mixture was centrifuged at 12000 *g* for 5 min, after which the supernatant was transferred into a new microfuge tube followed by the addition of 1 ml ethanol. Finally, the mixture was centrifuged at 12000 *g* for 5 minutes and the pellet was dissolved in 40 µl RNase-free water.

2.2.2.4 Competent cells

Freshly streaked *E. coli* BL21 or XL1-blue cells were cultured in 10 ml 2YT medium (shaking; 37°C; overnight). The 10 ml starter cultures were diluted in 1L TB culture (shaking; 37 °C) and the optical density (OD) was measured every hour; when the OD reached above 0.2, repeated measures were obtained every 15-20 minutes. At OD 0.35-0.4, cells were transferred to ice and incubated for 30 minutes. Cells were then centrifuged at 3000 *g* for 15 minutes at 4°C, and the pellet was re-suspended in 400 ml of ice cold 100 mM MgCl₂. Cells were centrifuged at 2000 *g* for 15 minutes at 4 °C, re-suspended in 200 ml of ice cold 100 mM CaCl₂ and incubated on ice for 20 minutes. After that, cells were centrifuged at 2000 *g* for 15 minutes at 4°C and re-suspended in 50 ml of ice cold 85 mM CaCl₂, 15% glycerol. Suspensions were transferred into 50 ml conical tubes. Then, cells were centrifuged at 1000 *g* for 15 minutes at 4°C and finally re-suspended in 2 ml of ice cold 85 mM CaCl₂, 15% glycerol. 50 µl of cells were

aliquoted into 1.5 ml microfuge tubes, snap frozen with liquid nitrogen, and stored at -70°C freezer.

2.2.2.5 DNA transformation

1 µl of DNA was mixed with 50 µl BL21 or XL1-blue competent cells (prepared as described in Section 2.2.2.4), and the mixture was incubated on ice for 30 minutes. The cells were then transferred to a heat block at 42°C for 40 seconds then placed back on ice for 2 minutes. 300 µl warm 2YT medium were added and cells were incubated at 37°C for 1 h. The cells were then streaked onto 2YT plates with ampicillin 100 µg ml⁻¹ at 37°C overnight.

2.2.2.6 Recombinant protein expression

Expression test (small scale)

After DNA transformation, different colonies were tested for expression of recombinant proteins. From the transformation plate, six random colonies were picked, streaked into a 2YT plate, and incubated at 37°C overnight. 5 ml 2YT cultures of each of the six colonies were incubated at 37°C overnight with shaking. The cultures were then diluted into 50 ml 2YT culture and incubated at 37°C with shaking until OD reached 0.6-0.8; after that, 500 µl of the culture were centrifuged at 12000 *g* for 5 minutes (sample 1: -IPTG). 1mM ml⁻¹ IPTG was added to the cultures, which were incubated at 37°C with shaking for 2 h. 500 µl of the culture were centrifuged at 12000 *g* for 5 minutes (sample 2: +IPTG). Protein expression was compared in samples 1 and 2 using SDS-PAGE.

Large scale expression

E. coli BL21 cells were cultured in 10 ml 2YT medium (100 µg ml⁻¹ ampicillin; shaking; 37°C; overnight). GST-Mid1p, 6His-Vps4p or 6His-C-term myo2p recombinant proteins were expressed in 1L Terrific broth (TB) cultures supplied with 100 µg.ml⁻¹ ampicillin (shaking; 37°C; overnight) until the optical density reached 0.6-0.8; then, protein production was induced by adding 1 mM IPTG, and the cultures were incubated with shaking (210 rpm for 2 h at 37°C).

2.2.3 *In vitro* biochemical methods

2.2.3.1 Recombinant protein purification

Bacterial pellets were produced by centrifugation (3750 rpm at 4°C for 30 min). The pellets were then re-suspended in 20 ml re-suspension buffer with EDTA free protease inhibitors; For GST-Mid1p fusion protein, PBS was used, whereas for 6His-Vps4p protein, HEPES buffer was used. The cells were then lysed using either sonication, where a final concentration of 1 mg ml⁻¹ lysozyme was added for cell wall digestion followed by sonication 4 x 30 sec using a Sanyo Soniprep 150 sonicator (with an amplitude of 15 microns) with a 30 second pause between sonications, or via the micro fluid machine “bug buster”, where 0.1 % (v/v) Triton X-100 was added to the cells prior to lysis. A clear lysate was produced by centrifugation (20000 rpm; 4°C; 1 h) of the lysed cells. GST-tagged fusion proteins were purified using 1ml L⁻¹ Glutathione beads in PBS buffer, while 6His-tagged Vps4p or C-term myo2p were purified using 500 µl L⁻¹ Ni-NTA beads in HEPES buffer either for 2 h or overnight at 4°C using a rotating platform. Mid1p was eluted from glutathione beads using three conditions (Section 2.1.2.1: glutathione beads elution buffers 1-3). Vps4p or C-term myo2p were washed and eluted from Ni-NTA beads using washing (Section 2.1.2.1: Ni-NTA beads washing buffer) and elution buffers (Section 2.1.2.1: Ni-NTA beads elution buffers 1-2). Elution was carried out for 2 h at 4°C using a rotating platform. Three samples (B+: protein bound to glutathione or Ni-NTA beads, E: eluted protein and B-: glutathione or Ni-NTA beads after protein is eluted) were subjected to SDS-PAGE to determine elution efficiency.

2.2.3.2 DNA sequencing

The concentration of DNA was measured using NanoDrop spectrophotometer, and 100 ng µl⁻¹ of DNA samples were sequenced by the University of Dundee sequencing service; reverse complement sequence was obtained using Sequence Alignment Tool (<http://tandem.bu.edu/align.tool.html>); forward and reverse sequences were aligned using Microsoft Word.

2.2.3.3 Pull-down

Pull-down experiments utilized Ni-NTA beads-immobilized bait proteins (6His-Vps4p or Myo2p) and prey eluted proteins (Mid1p: N-terminus, middle or C-terminus, or GST) to investigate protein-protein interactions. Bait proteins were loaded onto Ni-NTA beads by incubation in PBS containing 0.01% (v/v) Triton X-100 for 1 h (4°C) on a rotating wheel. After loading, the mixture was washed with PBS containing 0.01% (v/v) Triton X-100, and beads were blocked for non-specific binding by incubation in PBS containing 0.2% fish-skin gelatin on a rotating wheel (4°C) for 1 h. Then, the beads mixture was incubated with the prey protein in PBS with 0.01% (v/v) Triton X-100 on a rotating wheel (4°C) for 2 h. Subsequently, beads were washed with PBS containing 0.01% (v/v) Triton X-100 three times, 0.5% (v/v) glycerol and 0.2% (w/v) fish skin gelatin three times and with PBS alone four times. After that, 4X Laemmli Sample Buffer (LSB) was added to elute the proteins from beads, and the samples were subjected to sodium dodecyl sulphate polyacrylamide gel electrophoresis (SDS-PAGE).

2.2.3.4 Gel electrophoresis

SDS-PAGE

To resolve the size and identify proteins, they were subjected to SDS-PAGE. 2X Laemmli sample buffer (LSB) was added to protein samples in a ratio of 1:1; the samples were heated to 95°C for 5 minutes and loaded on a 12-15% 1 mm Tris-HCl SDS gel composed of 30% (w/v) acrylamide, 10% SDS, 10% ammonium persulphate and tetramethylethylenediamine (TEMED). Bio-Rad gel casting units were used. A Precision Plus Protein Standards All Blue protein marker was run alongside the proteins to determine molecular weights. SDS-PAGE running buffer was used to run the gels at 90 V initially followed by 120 V using the Bio-Rad Protean III system.

Agarose gel electrophoresis

To confirm the presence of plasmid DNA, samples were subjected to agarose gel electrophoresis. 1% agarose gel was prepared in TAE buffer by dissolving 0.8 g agarose in 80 ml TAE buffer with heating. Once cooled, but still liquid, 8 µl

ethidium bromide was added before pouring in Bio-Rad gel casting units. DNA samples were mixed with 6X DNA loading dye in a ratio of 6:1, and the gel was run in TAE buffer at 80 V for 1 h. TrackIt 1 kb DNA Ladder was run alongside the DNA samples to determine molecular weights.

2.2.3.5 *In vitro* phosphorylation

To determine if Mid1p is phosphorylated by plk1, aurora A and B (AurA and AurB) kinases, *in vitro* phosphorylation experiments implying the different eluted Mid1p domains were carried out using recombinant plk1, AurA and AurB. Each reaction combined either plk1, AurA or AurB (here we refer to as kinase) with Myelin basic protein (MBP) or one of the three Mid1p domains ("N-term", "Middle" or "C-term") (here we refer to as substrate). In pre-cooled microfuge tubes containing the kinase and substrate proteins, 1 μ Ci [γ - 32 P] ATP, 10 mM ATP and kinase assay buffer were added. The reaction was initiated by adding 5 μ l ATP cocktail, carried out at 30°C for 1 h and terminated by the addition of 6X LSB; samples were then subjected to SDS-PAGE followed by autoradiography or phosphor-imaging. Following detection of *in vitro* phosphorylation signals, stoichiometric and mass spectrometric analysis were carried out as described in Sections 5.3.3.3 and 5.3.3.4, respectively. The detailed quantification and optimization of the *in vitro* phosphorylation experiments are shown Table 5-1.

2.2.3.6 *In vitro* phosphorylation stoichiometric analysis

The *in vitro* phosphorylation stoichiometric analysis described in (Figure 5-5, Panel B) (for details please see Section 5.3.3.3) was carried out using Image J software as follows: First, from each reaction in **Exp. A** and **Exp. B**, a fixed area of pixel intensity was measured representing the phosphorylation signal detected by the phospho-imager. In this Section, we will refer to this measured value as the **original pixel intensity**. Second, in all cases, the same measurement was determined for the surrounding background. This value was always subtracted from the **original pixel intensity**. Third, the known concentrations (in μ g) of the substrate proteins were used to determine the number of pmoles of each substrate. This was carried out using the Promega Biomath Calculator

(www.promega.com/a/apps/biomath/). Fourth, the ratio of (the number of moles of ^{32}P incorporated: the number of moles of substrate protein) was determined (Table 5-2).

2.2.3.7 ATPase assay

Malachite Green Assay Kit was used to measure ATPase activity according to the manufacturer's protocol. All reactions were performed at room temperature in a 96 well plate. A standard curve of absorbance and phosphate concentrations was generated using the samples provided by the kit (known phosphate concentrations), which was then used to calculate the rate of ATPase activity of Vps4p. Activity of Vps4p was measured over time by adding 80, 40, 10 or 0 μl of Vps4p into each well to complete a final volume of 100 μl with HEPES buffer. Reactions were initiated by adding 20 μl of the kit working reagent and absorbance was measured at 600 nm after 30, 60 or 90 minutes (Section 7.4).

Chapter 3 Interactions between the *mid1*⁺ and *vps4*⁺ genes and their encoded proteins (Mid1p and Vps4p) suggest they coordinate to regulate *S. pombe* cytokinesis

3.1 Introduction

3.1.1 Mammalian cytokinesis

During mammalian cell division, correct placement and attachment of the actomyosin contractile ring to the plasma membrane mediate division at the cell equator (Bathe and Chang, 2010). The ring position is mainly determined by the mitotic spindle and the scaffold protein anillin (*S. pombe* Mid1p), which is thought to play a major role in coupling the actin/myosin filaments. Interactions between these filaments are known to drive constriction of the ring during cytokinesis (Straight et al., 2005). Following constriction of the ring, the abscission machinery is assembled within the thin bridge connecting the two daughter cells "the midbody" where its cleavage is regulated by the ESCRT family of proteins including the ATPase VPS4 (*S. pombe* Vps4p) (Caballe and Martin-Serrano, 2011).

3.1.2 Mid1p and ESCRT proteins are involved in *S. pombe* cell cycle regulation

The *S. pombe mid1*⁺ gene was found to be required for correct septation as a deletion in the *mid1*⁺ chromosomal gene caused defects in contractile ring positioning and overall septation (Sohrmann et al., 1996). During the final stage of mammalian cytokinesis called abscission, coordinated actions of different classes of the ESCRT family of proteins orchestrate membrane scission events leading to the final separation of daughter cells. (Guizetti et al., 2011). In yeast, the role of ESCRT proteins in membrane fission events such as endocytic trafficking is well demonstrated; however, further investigations are required to understand their role in cytokinesis and how these different activities and complexes are controlled

(Schuh and Audhya, 2014). Previous work in *S. pombe* examined the formation of a medial single septum in cells with single chromosomal ESCRT gene deletion mutations. The different classes of the ESCRT genes, including the ESCRT-III regulator *vps4⁺*, were found to be required for correct septation (Bhutta et al., 2014). In a similar approach, by examining chromosomal deletion mutations of the *mid1⁺* and *vps4⁺* genes, we show that the *mid1⁺* gene is required for the formation of a single medial septum and the *vps4⁺* gene is important for the correct timing of *S. pombe* septation (Section 3.3.2).

3.1.3 Could Mid1p and Vps4p coordinate to regulate *S. pombe* septation?

Previous work revealed that the ESCRT genes (**ESCRT-0**: *sst4⁺*; **ESCRT-I**: *sst6⁺*, *vps28⁺*; **ESCRT-II**: *vps36⁺*, *vps25⁺* and **ESCRT-III**: *vps20⁺*, *vps32⁺*, *vps2⁺* and *vps24⁺*; and *vps4⁺*) are all required for septation in *S. pombe* (Bhutta et al., 2014). Subsequently, these ESCRT genes were tested for genetic interactions with the *mid1⁺* gene. No synthetic growth phenotype was detected in the *sst6Δ mid1Δ*, *vps28Δ mid1Δ*, *vps36Δ mid1Δ*, *vps25Δ mid1Δ*, and *vps20Δ mid1Δ* double mutants (Chris McNerny, pers. comm.).

Here, we investigated *S. pombe* septation in *mid1Δ* and *vps4Δ* strains in comparison with the wild-type strain. As previously published, we found that the *mid1⁺* gene is required for the formation of a medial single septum (Chang and Nurse, 1996). Additionally, although the ESCRT regulator *vps4⁺* gene is not essential for medial formation of the septum, we found that a deletion of the *vps4⁺* gene causes delay in separation after septation (Bhutta et al., 2014; Section 3.3.2). Therefore, we hypothesize that the *mid1⁺* and *vps4⁺* genes might interact to regulate *S. pombe* septation. We used tetrad analysis to test for the genetic interaction between the *mid1⁺* and *vps4⁺* genes. Such analysis revealed a striking genetic interaction as double chromosomal *mid1⁺* and *vps4⁺* gene deletions showed a synthetic lethal phenotype (Section 3.3.3.2).

The genetic interaction observed between the *mid1⁺* and *vps4⁺* genes encouraged us to investigate the physical interaction between the encoded Mid1p and Vps4p proteins. Such an investigation revealed that Vps4p physically interacts with the

"C-term" domain of Mid1p (Section 3.3.4). To further investigate the physical interaction between the two proteins, we used confocal microscopy to determine the localization pattern of GFP-tagged Mid1p in wild-type *S. pombe* and to determine the effect of *vps4* deletion on this localization pattern. We found that the localization of Mid1p is affected by absence of the *vps4⁺* gene, which was mainly manifested in node-membrane attachment defects (Section 3.3.5.1).

Since the interaction between Mid1p and Vps4p is involved in node attachment to the membrane and Mid1p has a PH domain that could be involved in Mid1p attachment to membranes, we sought to investigate the localization of GFP-Mid1p in PHΔ *mid1* cells. Such analysis revealed a novel role of this domain in the nuclear localization of Mid1p (Section 3.3.5.3). Combined, these data suggest a novel interaction between Mid1p (an anillin analogue) and Vps4p (an ESCRT protein regulator) to control septation in *S. pombe*, the first time that this has been shown in any organism.

3.2 Aims

The role of Mid1p in fission yeast septation regulation has been extensively investigated. Similarly, a role of the ESCRT regulator Vps4p is well demonstrated in yeast membrane scission events and cytokinesis. However, a coordination or interaction of both proteins to regulate *S. pombe* septation has not been investigated.

The major aim of this Chapter is to investigate the interaction between the *mid1⁺* and *vps4⁺* genes and the Mid1p and Vps4p proteins, respectively, in an attempt to uncover a novel regulatory pathway of *S. pombe* septation regulation. The following specific aims were therefore addressed:

- Characterization of septation in wild-type, *mid1*Δ and *vps4*Δ *S. pombe* cells
- Investigation of genetic interactions between the *mid1⁺* and *vps4⁺* genes using an *in vivo* *S. pombe* genetic approach
- Identification of physical interactions between Mid1p and Vps4p proteins using an *in vitro* biochemical approach
- Determination of the cellular localization of Mid1p in wild-type, *vps4*Δ and PHΔ *mid1* *S. pombe* cells using an *in vivo* microscopic approach.

3.3 Results

3.3.1 Chromosomal deletions of the *mid1*⁺ or *vps4*⁺ genes

We hypothesize that *mid1*⁺ and *vps4*⁺ genes interact to regulate *S. pombe* septation. To test for this interaction, *S. pombe* strains with chromosomal deletion mutations of either the *mid1*⁺ or *vps4*⁺ genes were utilized in two separate experiments. **First**, a septation analysis experiment was designed to characterize and confirm the individual roles of the *mid1*⁺ and *vps4*⁺ genes during *S. pombe* septation. **Second**, a double mutant strain with deletions in both the *mid1*⁺ and *vps4*⁺ genes was generated to detect synthetic phenotypes including cell growth and morphology.

To study the role of the *mid1*⁺ (named *dmf1*⁺ in the paper below) gene in division plane placement in *S. pombe*, Sohrmann et al. (1996) disrupted the chromosomal copy of *mid1*⁺ gene by replacing it with a fragment of the *ura4*⁺ gene to produce *mid1*⁺::*ura4*⁺ strain (*mid1*Δ), in which the Mid1p protein was absent (Figure 3-1, Top Panel A).

In the *mid1*Δ strain, Sohrmann et al. (1996) reported that cells successfully formed viable colonies, but they were smaller than wild-type colonies. In addition, they reported an increased number of dead cells by observing staining of cells grown in media containing Phloxin B. Furthermore, microscopic analysis of septation in *mid1*Δ cells revealed defective septation with the appearance of branched cells.

To re-examine the growth phenotypes of the *mid1*Δ strain for this project, the strain was grown on solid rich complete medium alongside with the wild-type *S. pombe* strain to compare colony formation and growth (Figure 3-1, Panel B). As reported, the *mid1*Δ strain was able to form viable colonies similar to the wild-type strain (Paoletti and Chang, 2000). However, examining the cells by light microscopy did not show wild-type septation, manifested as a medial single septum, but instead cells appeared branched with mis-aligned septa as reported (Paoletti and Chang, 2000). These observations indicate that the *mid1*⁺ gene is not required for proliferation *per se* but is required for *S. pombe* division and specifically has a role in positioning the division plane. This strain was kindly gifted by Anne Paoletti.

In a separate *S. pombe* study, Iwaki et al. (2007) investigated the roles of class E vacuolar sorting proteins (Vps) in multivesicular body (MVB) sorting pathway, where they disrupted the *vps4⁺* gene by replacing it with the *ura4⁺* gene to produce a *vps4⁺::ura4⁺* strain (*vps4Δ*) (Iwaki et al., 2007) (Figure 3-1, Lower Panel A). This strain was kindly gifted by Tomoko Iwaki.

Here, *vps4Δ* strain was grown on solid rich medium alongside with the wild-type *S. pombe* cells to compare colony formation and growth (Figure 3-1, Panel B). The strain was able to form viable colonies as in the wild-type strain. However, examining cells by light microscopy did not reveal the branched septation phenotype observed in the *mid1Δ* strain. Instead, cells appeared round in shape and smaller in size with septa unaffected. This indicates that the *vps4⁺* gene is not required for proliferation.

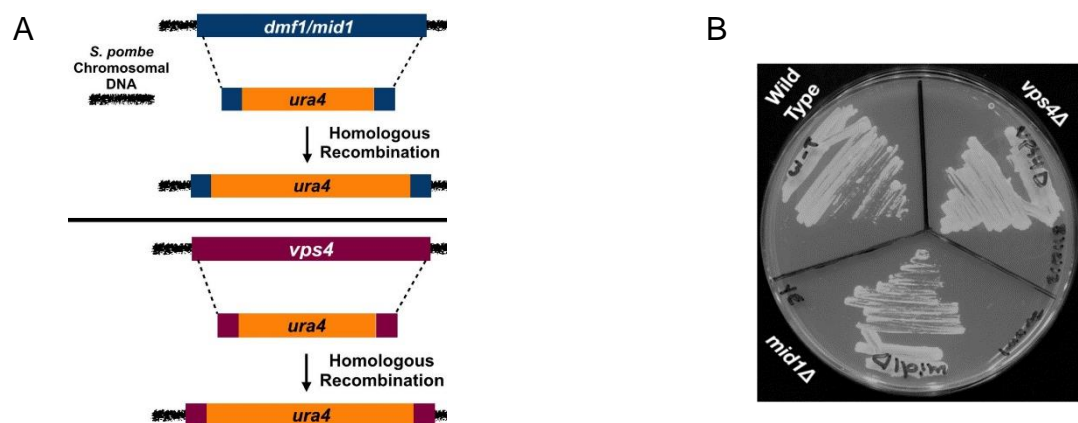
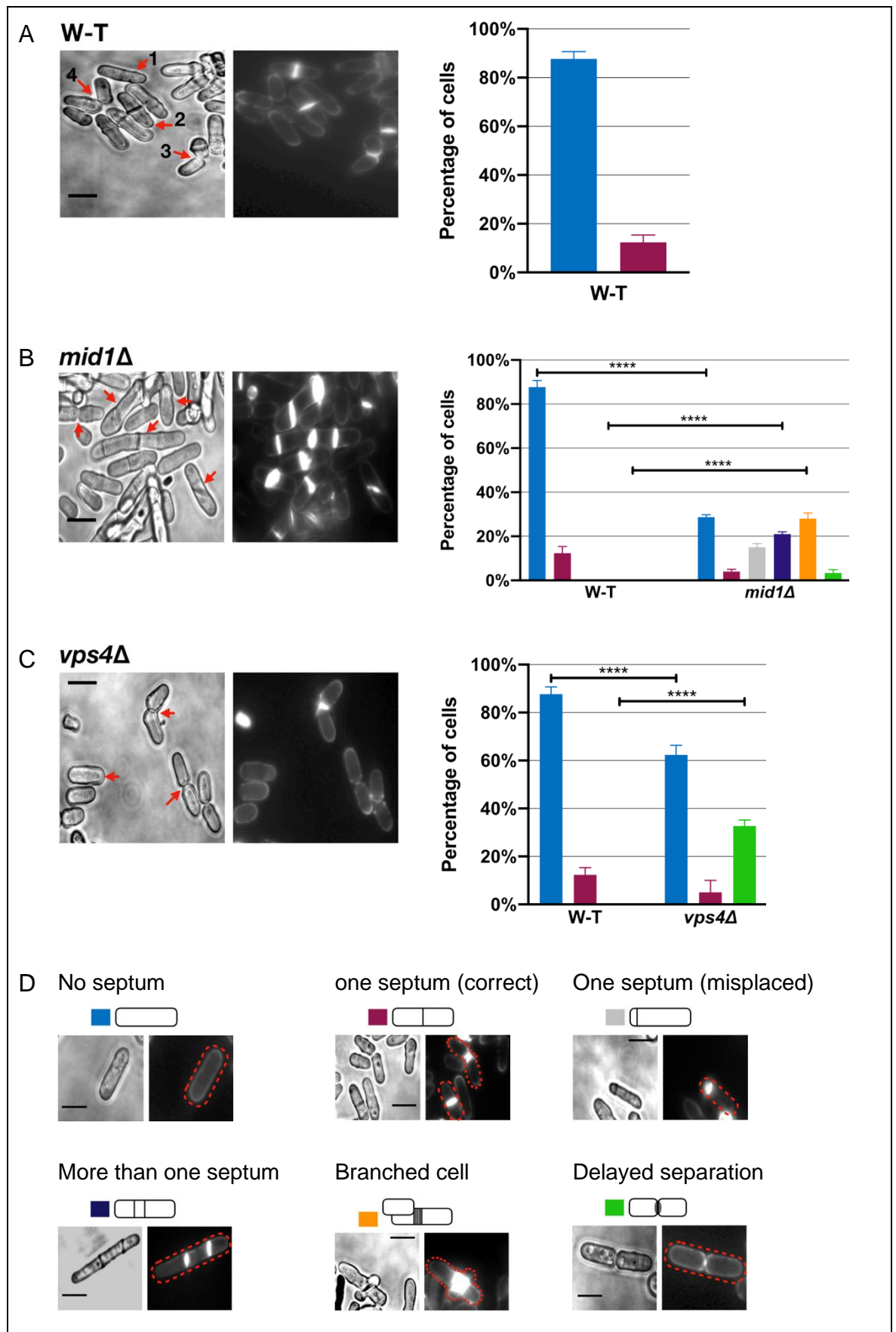


Figure 3-1 Generation of *mid1Δ* and *vps4Δ* *S. pombe* strains and their growth phenotype. Chromosomal deletions of either (A, Top Panel) the *mid1⁺* or (A, Lower Panel) the *vps4⁺* genes were created by replacing the endogenous genes with an *S. pombe ura4⁺* gene (Sohrmann et al., 1996; Iwaki et al., 2007). (B) The *mid1Δ* and *vps4Δ* strains were grown on solid rich YE medium alongside a wild-type *S. pombe* strain at 28°C for two days to show their growth phenotypes.

3.3.2 Septation analysis of wild-type, *mid1Δ* and *vps4Δ* *S. pombe*

Calcofluor staining was applied to *S. pombe* cells grown in liquid rich medium to visualise newly deposited septa by fluorescence microscopy. Septation phenotypes of wild-type, *mid1Δ* and *vps4Δ* cells were characterized and the frequency of each septation phenotype was quantified for each strain. The phenotype frequencies of *mid1Δ* and *vps4Δ* strains were then compared to frequencies of the wild-type strain (Figure 3-2).



In (Figure 3-2, Panel A), a cell population sample represents the different stages of **wild-type** *S. pombe* septation. In cell (1) a septum begins to form by the assembly and attachment of nodes to the plasma membrane. Next, in cell (2), the nodes fuse and form the contractile ring, which starts to constrict. Then, in cells (3 and 4) the ring has completed constriction and a septum is deposited between the two daughter cells, and finally the septum is degraded allowing the final separation of the two daughter cells. Two main septation phenotypes were observed in wild-type cells, cells with no septa and cells with a single -correctly placed- septum. Overall, 88% of wild-type cells had no septa, while 12% of cells showed a single medial septum that is perpendicular to the growth axis.

In (Figure 3-2, Panel B), a cell population sample represents the different stages of ***mid1*Δ** *S. pombe* septation. In this mutant strain, 29% of cells had no septa and only 4% of cells showed a single medial septum that is perpendicular to the growth axis. However, as expected, a total percentage of 67% of cells showed various defective septation phenotypes. These defects were categorized into four classes: 15% of cells had misplaced septa. 21% of cells had more than one septum, 28% of cells were branched and 3% of cells showed delayed separation after septation. Overall, the striking septation defects observed in *mid1*Δ cells confirm the importance of the *mid1*⁺ gene in *S. pombe* division plane placement (Chang and Nurse, 1996).

In (Figure 3-2, Panel C), a cell population sample represents the different stages of ***vps4*Δ** *S. pombe* septation. In this mutant strain, 62% of cells had no septa and only 5% of cells showed a single medial septum that is perpendicular to the growth axis. However, 33% of cells showed delayed separation after septation. This can be explained by the important role of Vps4p in recycling ESCRT-III components to allow for further fission events causing final separation of daughter cells. The increasing percentage of cells showing this septation defect suggests a role of the *vps4*⁺ gene in *S. pombe* late cytokinesis regulation, as previously reported (Bhutta et al., 2014).

3.3.3 A genetic interaction between the *mid1*⁺ and *vps4*⁺ genes

3.3.3.1 *S. pombe* tetrad analysis provides a powerful tool to study genetic interactions

Upon nutrient abundance, *S. pombe* undergoes division, but upon starvation, opposite mating type cells fuse together to form a diploid zygote, which undergoes meiosis and forms four spores encapsulated in the form of a tetrad (Figure 3-3) (Krapp et al., 2006). Tetrad analysis is a technique used for analyzing the phenotypes of meiotic products to identify genetic interactions (Moreno et al., 1991; Rezig et al., 2019).

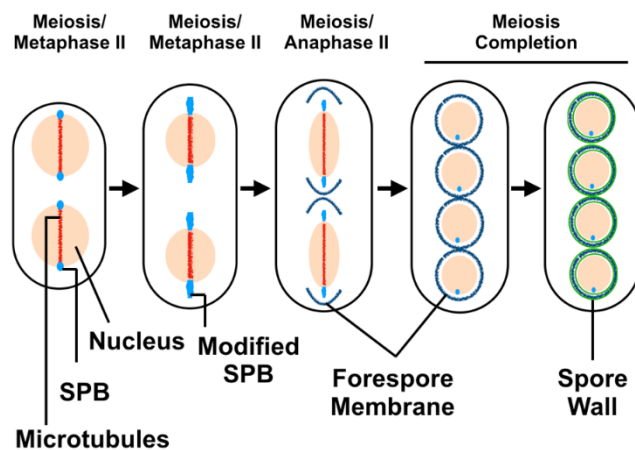


Figure 3-3 Meiotic nuclear division produces four haploid spores in *S. pombe*.

Sporulation of *S. pombe* generates four nuclei each packaged into a spore structure.

During metaphase II, the spindle pole bodies (SPB) undergo morphological modifications resulting in recruitment of the forespore membrane vesicles in anaphase II; then, the nuclei divide and the forespore membranes encapsulate the four nuclei forming the pre-spores with the spore walls. Figure adapted from Shimoda (2004).

3.3.3.2 The *mid1*Δ *vps4*Δ double mutant growth phenotype suggests a genetic interaction between the *mid1*⁺ and *vps4*⁺ genes

To explore the role of Mid1p and Vps4p proteins in *S. pombe* cytokinesis, we first applied a genetic approach aiming to identify the presence of a genetic interaction between the encoding *mid1*⁺ and *vps4*⁺ genes. Thus, we designed *mid1*Δ *vps4*Δ double mutants by mating of two single chromosomal deletion mutation strains, a deletion of the *mid1*⁺ gene and a deletion of the *vps4*⁺ gene (as described in Section 3.3.1). Double mutants were then identified by tetrad analysis using an ascus dissector microscope and selective media (Figure 3-4).

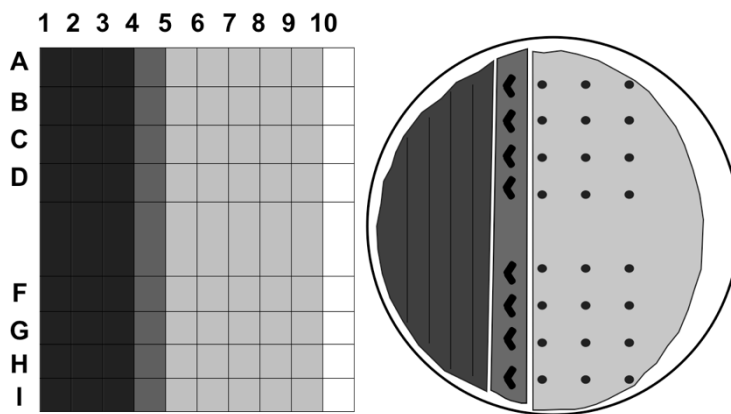


Figure 3-4 A schematic representation of *S. pombe* spore's micro-manipulation. The grid-based stage of the Singer MSM Ascus Dissector (left), and its transfer to cells on solid medium in a 90 mm petri dish (right) are described. The dark grey area represents the area on the solid "thin" YE medium in a petri dish where the mating mixture is spread. The mid-grey area represents the locations of the eight complete tetrads placed in a vertical line at positions A4, B4, C4 to I4. The pale grey area represents the location of three spores separated from each tetrad and placed at horizontal positions A5-7, B5-7 etc., with one spore left at position A4 etc. (Rezig et al., 2019).

Following mating of strains, four spores were separated from each tetrad using the ascus dissector microscope and allowed to grow to form colonies. Genotype screening was then applied to the four yeast colonies using selective solid media (YE+G418 to identify the *mid1* Δ mutant, and EMM -ura to identify the *vps4* Δ mutant) (Rezig et al., 2019). Such analysis allowed for the identification of *mid1* Δ *vps4* Δ double mutants as follows (Figure 3-5):

Colonies with the **wild-type** genotype showed no growth on YE+G418 or EMM -ura; those with the **single *mid1* Δ mutant** genotype showed growth only on YE+G418; those with the **single *vps4* Δ mutant** genotype showed growth only on EMM -ura. Finally, colonies with the **double *mid1* Δ *vps4* Δ mutant** genotype were predicted to show growth on both YE+G418 and EMM -ura.

In all cases, the wild-type and single mutants successfully formed viable colonies (Figure 3-5). However, the double mutant spores identified from the tetrad analysis failed to form colonies. In this Chapter, we refer to such a phenotype as synthetic lethal/impaired growth phenotype.

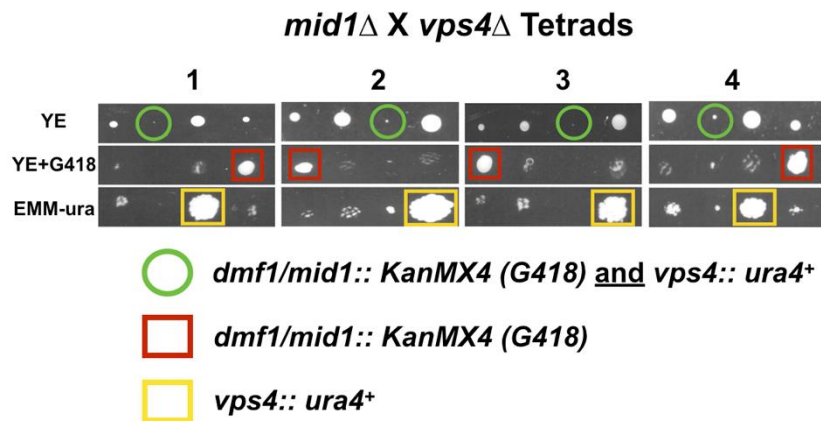


Figure 3-5 A synthetic lethal growth phenotype in the *mid1* Δ *vps4* Δ *S. pombe* double mutant indicates a genetic interaction between the *mid1⁺* and *vps4⁺* genes. Tetrad analysis of h⁻ *vps4* Δ (*vps4⁺::ura4⁺*) mated with h⁺ *mid1* Δ (*dmf1⁺::KanMX4*) to identify *vps4* Δ *mid1* Δ double mutants that show a synthetic lethal growth phenotype. Tetrads were performed by mating the two strains on solid ME medium (25°C) for 2 days. Tetrads were then dissected using Singer MSM Ascus Dissector and spores allowed to grow on solid YE medium (28°C) until colonies formed. Colonies were replicated to solid YE+G418/KanMX4 and EMM -ura media and incubated (28°C) to identify growth phenotypes and double mutants.

The observed impaired growth phenotype in the *vps4* Δ *mid1* Δ double mutants illustrates a strong genetic interaction between *vps4⁺* and *mid1⁺* genes, and further suggests an interaction of the encoded Vps4p and Mid1p proteins required for cell growth.

3.3.4 A physical interaction between Mid1p and Vps4p proteins

3.3.4.1 Design of pull-down experiments

In Section 3.3.3.2, we showed that the *mid1⁺* and *vps4⁺* genes interact in *S. pombe*. To explore the functional relevance of this novel genetic interaction, the physical interaction of the encoded Mid1p and Vps4p proteins was investigated followed by mapping of the interactive domain/s of Mid1p.

Thus, Mid1p protein was expressed in *E. coli* as a fusion protein with glutathione S-transferase (GST) to be purified as three different domains; then, the interaction of each domain with full length Vps4p was tested in "pull-down" experiments. We did not attempt to purify full-length Mid1p since previous studies indicated that the full-length protein is very large that it cannot be expressed in *E. coli* (Anne Paoletti

pers. comm.) Parallel positive and negative control pull-down experiments were also carried out (Figure 3-6).

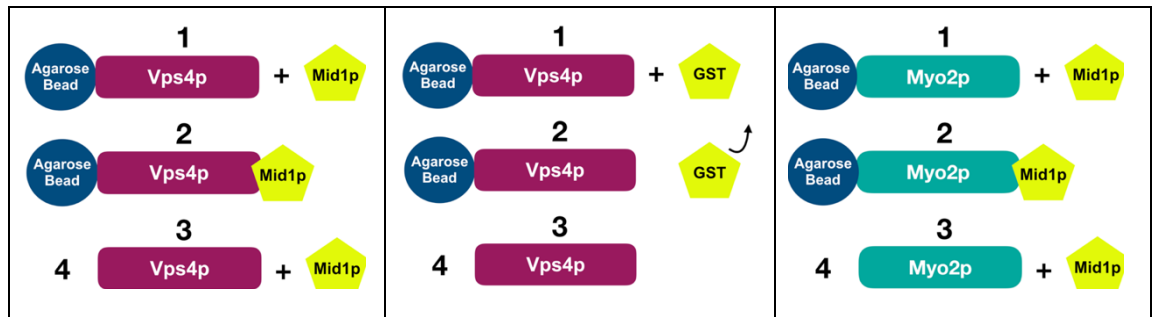


Figure 3-6 Design of *in vitro* pull-down experiments to test for the physical interaction of Mid1p and Vps4p proteins. (Left) His-6-tagged Vps4p bait protein was immobilized to Ni-NTA agarose beads and different domains of prey Mid1p were added separately. (Middle) A negative control was designed by replacing the prey Mid1p domains with purified GST protein, which is predicted not interact with Vps4p. (Right) A positive control was designed by replacing the bait Vps4p by the "C-term" domain of Myo2p, a known interacting partner of Mid1p (Motegi et al., 2004). In all cases (1) the bait protein was immobilized to agarose beads and an equal amount of the prey protein was added, (2) washes were carried out to remove non-specific binding, (3) the bait-prey complex was eluted from the beads, and (4) the eluted bait and/or prey proteins were detected by SDS-PAGE.

3.3.4.2 Purification of prey proteins for the pull-down experiments

Saha and Pollard (2012b) characterized the structural and functional domains of Mid1p. They used complementation experiments in *mid1Δ* cells to identify the biological functions of six putative domains accounting for full-length Mid1p (Table 3-1).

Table 3-1 Description and localization of Mid1p putative domains in *S. pombe* cells (Saha and Pollard, 2012b).

Name	Amino acid residues (aa)	Localization in <i>S. pombe</i>
M1-1	1-149	Localized to the nodes
M1-2	150-308	Partial localization to the nucleus
M1-3	309-452	Partial localization inside the nucleus
M1-4	453-578	Strong localization inside the nucleus
M1-5	579-797	Associated with the nuclear envelope
M1-6	798-920	Partial localization inside the nucleus

Saha and Pollard (2012b) combined the **M1-1**, **M1-2** and **M1-3** domains of Mid1p in a **M1-13** collective domain (aa 1-452). Interestingly, **M1-13** collective domain was able to complete the known functions of the full-length Mid1p, including the assembly of node components in the equatorial cortex. Therefore, we decided to use the **M1-13** domain in pull-down experiments instead of using the **M1-1**, **M1-2** and **M1-3** Mid1p domains separately.

The insoluble domain (aa 579-797: **M1-5**) was found to facilitate the condensation of nodes to the contractile ring (Saha and Pollard, 2012b). However, in our hands, purification of this domain was unsuccessful. Therefore, it was not included in any experiments presented in this Thesis. For simplicity and clarity, we will refer to the domains in this Thesis as the "N-term" (M1-13), "Middle" (M1-4), and "C-term" (M1-6) domains. These three domains of Mid1p were inserted in a pGEX-4T-1 vector and tagged with glutathione S-transferase (GST) (Figure 3-7).

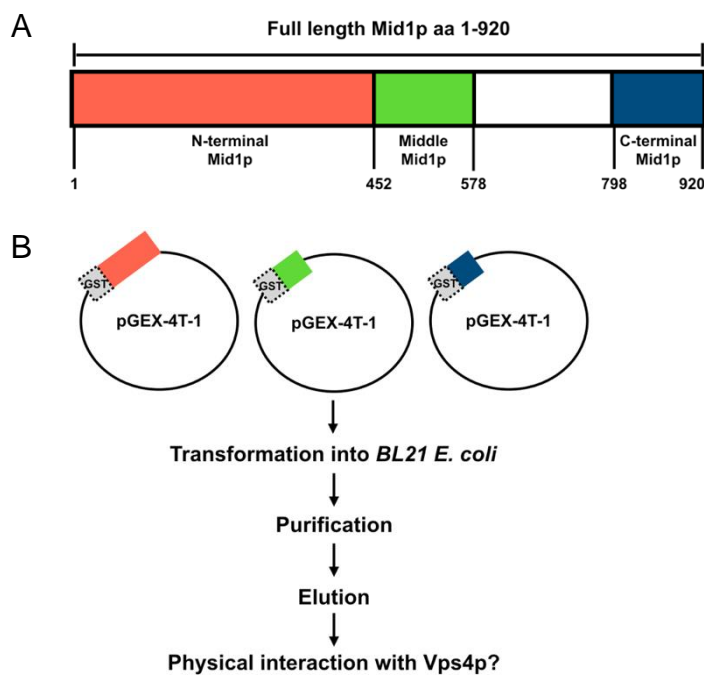


Figure 3-7 Design of Mid1p "N-term", "Middle" and "C-term" domain constructs to test for their physical interaction with Vps4p. (A) The three domains of Mid1p are represented by different colours. **(B)** Recombinant GST-tagged Mid1p domains were expressed in BL21 *E. coli*, followed by purification, elution and quantification of proteins. Recombinant 6His-tagged Vps4p and "C-term" Myo2p proteins were expressed in BL21 *E. coli*, followed by purification and quantification of proteins. The eluted Mid1p domains were subjected to pull-down experiments with Vps4p and Myo2p proteins.

The GST-Mid1p recombinant proteins were expressed in BL21 *E. coli* and their production was induced by the addition of IPTG (this approach is explained in detail in Chapter 2). After expression and induction, the proteins were purified by affinity binding to GST-sepharose beads (Figure 3-8).

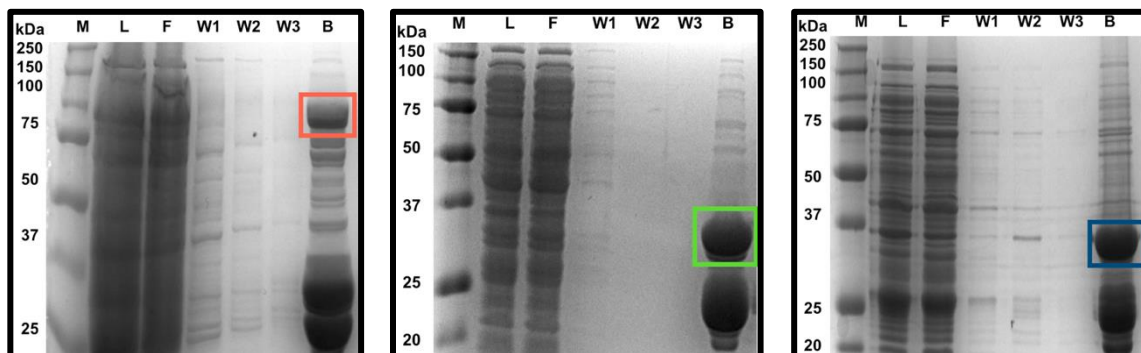


Figure 3-8 Purification of GST-tagged "N-term," "Middle" and "C-term" domains of Mid1p. (Left) Purification of the 76 kDa "N-term" Mid1p domain. (Middle) Purification of the 40 kDa "Middle" Mid1p domain. (Right) Purification of the 39 kDa "C-term" Mid1p domain. Coloured boxes represent the expected protein size; the same colour code is used as in (Figure 3-7). M: Protein marker, L: lysate, F: flow through, W1-3: three washes and B: purified protein bound to GST-sepharose beads. The species at ~25 kDa is likely to be GST.

To examine elution efficiency, samples representing the eluted protein yield (**Sample E**) and the amount of protein that remained attached to the beads after elution (**Sample B-**) were compared (Figure 3-9). At first attempt (data not shown), elution was not efficient as **Sample B-** showed greater protein yield than that in **Sample E**.

Therefore, conditions were optimized to maximize the eluted protein yield. First, the elution buffer pH was increased from pH8 to pH9 (**Elution Condition 1**). Second, a detergent (1% octylglucoside) was added to the elution buffer (**Elution Condition 2**). Here, we show two representative elution experiments using **Elution Condition 1** (Figure 3-9, left) and **Elution Condition 2** (Figure 3-9, right).

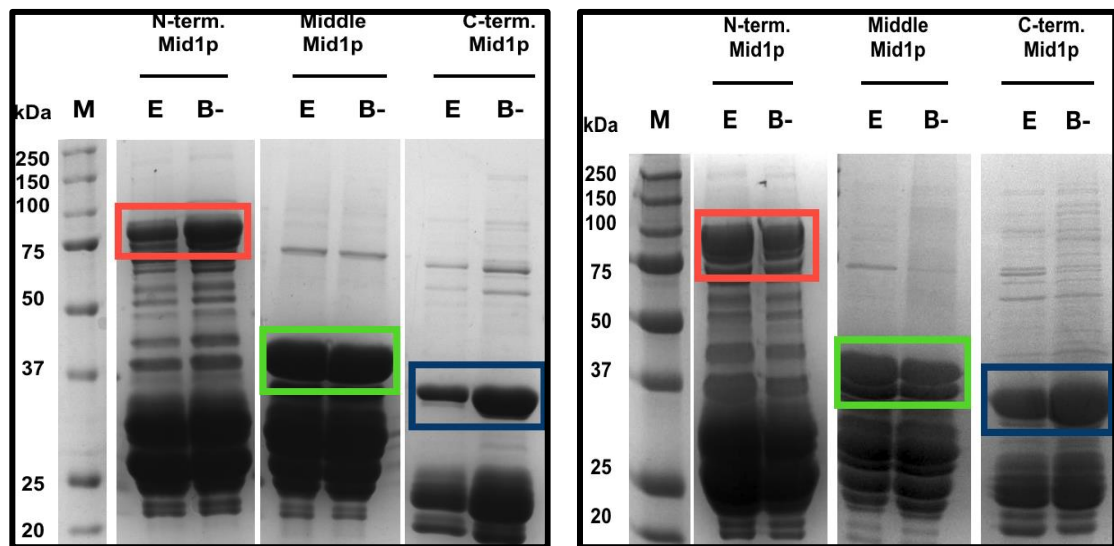


Figure 3-9 Elution of GST-tagged "N-term", "Middle" and "C-term" domains of Mid1p. (Left) The Mid1p domains were eluted from the GST-sepharose beads by the addition of reduced-GST elution buffer PH=9. (Right) The elution experiment with the addition of 1% octylglucoside detergent. Coloured boxes represent the Mid1p domains expected sizes; the same colour code is used as in (Figure 3-7). M: protein marker, E: eluted protein and B-: the beads mixture after elution of the protein.

3.3.4.3 Purification of bait proteins for the pull-down experiments

Biochemical pull-down experiments, as illustrated in Figure 3-6, utilized prey and bait proteins. Prey Mid1p different domain proteins were designed, purified and eluted as shown in Figures 3-7, 3-8, and 3-9 respectively.

To test for the potential interaction between Vps4p and the purified Mid1p domains, the full-length *vps4⁺* gene was designed to encode a 6His-tag by being cloned into a pET-14b vector (explained in detail in Chapter 2).

Myosin 2 protein is known to interact with Mid1p, probably through the "C-term" domain of Myo2p (the aa 1394-1526 region) (Motegi et al., 2004). We took advantage of this published finding to design a positive control parallel pull-down experiment. We replaced the Vps4p bait protein with the "C-term" Myo2p bait protein; the 6His-C-term Myo2p construct was designed similar to 6His-Vps4P construct.

Both 6His-tagged Vps4p and "C-term" Myo2p recombinant proteins were expressed in BL21 *E. coli* and their production was induced by the addition of

IPTG (explained in detail in Chapter 2). After expression, the proteins were purified by binding to Ni-NTA-agarose beads (Figure 3-10).

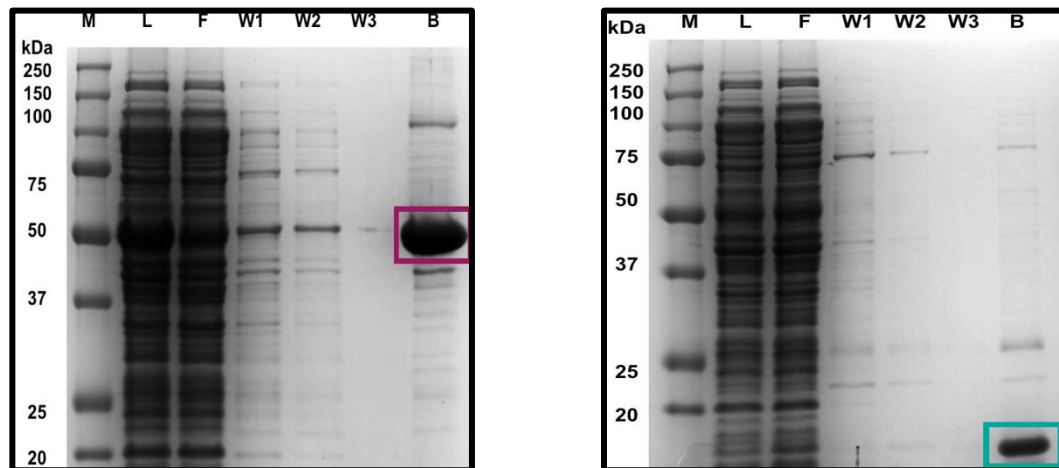


Figure 3-10 Purification of 6His-tagged Vps4p and "C-term" Myo2p proteins. (Left) Purification of the 48 kDa Vps4p (Purple box). (Right) Purification of the 14.5 kDa "C-term" Myo2p (Blue box). M: Protein marker, L: lysate, F: flow through, W1-3: three washes and B: purified protein bound to Ni-NTA agarose beads.

3.3.4.4 Pull-down experiments reveal a physical interaction between Vps4p and the "C-term" domain of Mid1p

In Sections 3.3.4.2 and 3.3.4.3 we illustrated, the design and purification of prey and bait proteins, respectively.

Prior to the pull-down experiments, quantification of the prey and bait proteins was carried out and equal amounts of both prey and bait proteins were added in the pull-down experiments (Figure 3-11), except for the case of "C-term" Myo2p, where smaller amounts were used due to partial degradation of purified protein.

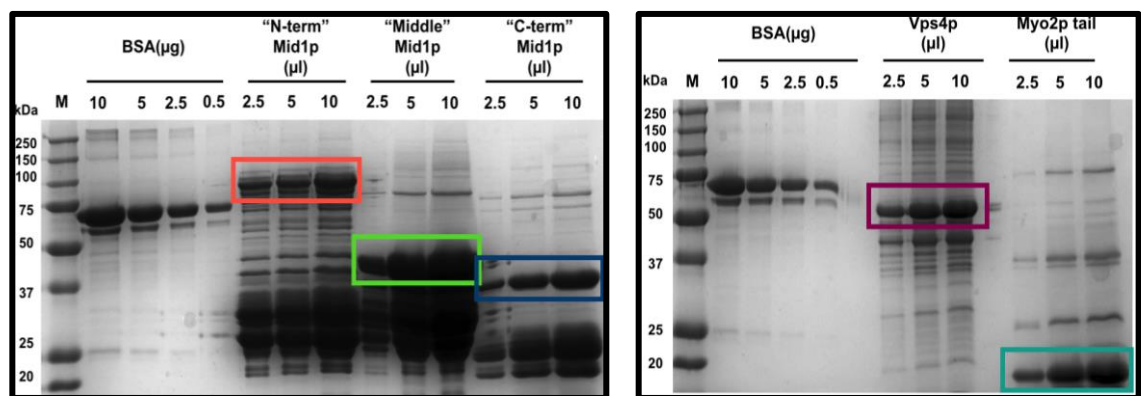


Figure 3-11 Quantification of 6His-tagged: Vps4p, "C-term" Myo2p and GST-tagged: Mid1p "N-term", "Middle" and "C-term" proteins. (Left) Different volumes of prey Mid1p domains were run alongside known concentrations of BSA for quantification; the same colour code is used as in (Figure 3-8). (Right) Different volumes of bait Vps4p and "C-term" Myo2p were run alongside known concentrations of BSA for quantification. Coloured boxes represent the expected sizes of Vps4p (Purple box) and "C-term" Myo2p (Blue box); the same colour code is used as in (Figure 3-10).

The pull-down experiments were performed twice using three batches of purified proteins, and they were divided into two sections (Figure 3-12):

Exp. A. Bait Vps4p pulled-down the "C-term" domain of Mid1p but not the "N-term" or the "Middle" domains. Plain purified GST was used as a prey protein in a negative control pull-down experiment, and as expected it was not pulled down by bait Vps4p.

Exp. B. Positive control experiment. Despite the small amount of bait "C-term" Myo2p used in the pull-down experiment, the bait protein still efficiently pulled down the "N-term" and "Middle" domains of Mid1p.

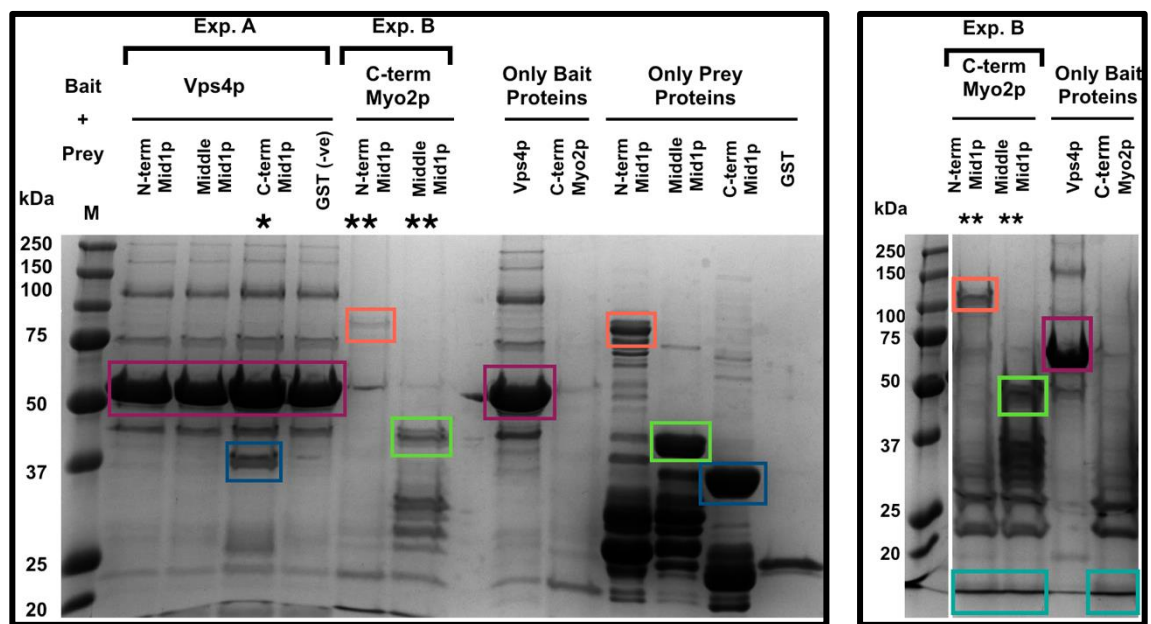


Figure 3-12 A physical interaction between Vps4p and the "C-term" domain of Mid1p. Pull-down experiments and SDS-PAGE analysis were used to test for Mid1p physical *in vitro* interaction with Vps4p. Recombinant GST-tagged (Mid1p domains: "N-term", "Middle" and "C-term") and 6 His-tagged (Vps4p and "C-term" Myo2p) proteins were expressed in BL21 *E. coli* and purified using GST-sepharose beads and Ni-NTA agarose beads, respectively. In Exp. A, the eluted prey Mid1p domains were added to the bait Vps4p that is bound to the Ni-NTA agarose beads, (*) represents the physical interaction of Vps4p and Mid1p "C-term" domain. In Exp. B (Left), the eluted prey Mid1p "N-term" and "Middle" domains were added to "C-term" Myo2p that is bound to the Ni-NTA agarose beads and used as a positive control, however, the 14.5 kDa "C-term" Myo2p was not detected. In a separate experiment Exp. B (Left) shows the detected 14.5 kDa "C-term" Myo2p (Blue box) where (**) represents the physical interaction of Mid1p "N-term" and "Middle" domains with the "C-term" domain of Myo2p.

To further understand the interaction between Vps4p and the "C-term" domain of Mi1p in cells, we sought to determine the localization patterns of Mid1p in *S. pombe* using confocal microscopy.

3.3.5 Localization analysis of GFP-Mid1p in wild-type, *vps4* Δ and PH Δ *mid1* *S. pombe*

3.3.5.1 Investigating the localization of Mid1p in wild-type and *vps4* Δ *S. pombe*

Paoletti and Chang (2000) determined the cellular localization of Mid1p during *S. pombe* cell cycle using a PCR-based recombination approach to construct a strain with four copies of GFP-tagged to the chromosomal locus of the *mid1*⁺ gene (Figure 3-13, Left panel). They characterized Mid1p localization to three different stages based on the cell cycle timing (Paoletti and Chang, 2000). This strain was kindly gifted by Anne Paoletti and was used for two purposes: **first**, to re-characterise the localization of GFP-Mid1p in wild-type *S. pombe* and **second**, to investigate the localization of GFP-Mid1p in *vps4* Δ *S. pombe* strain (Figure 3-13, Right panel).

The rationale of attaching multiple GFP copies to Mid1p is to amplify the GFP signal to allow visualization of Mid1p in cells. Importantly, this approach did not affect the function of Mid1p, as cells containing Mid1p coupled to multiple copies of GFP showed a growth phenotype similar to the wild-type phenotype and maintained the rod shape; in contrast, *mid1* Δ mutant cells showed a dramatic alteration in cell morphology (Figure 3-2, Panel B).

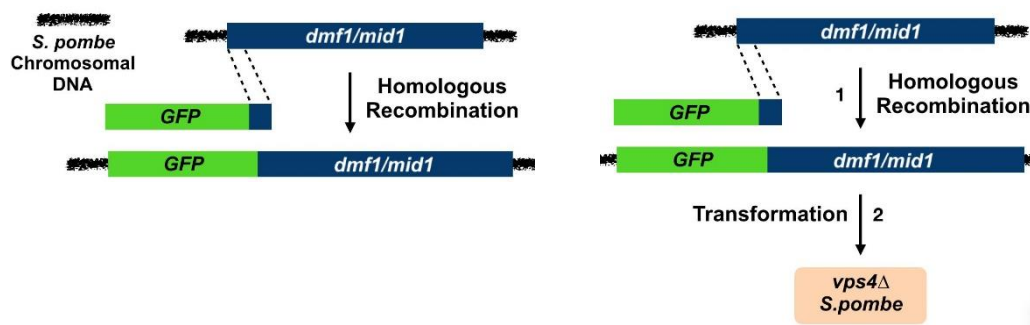
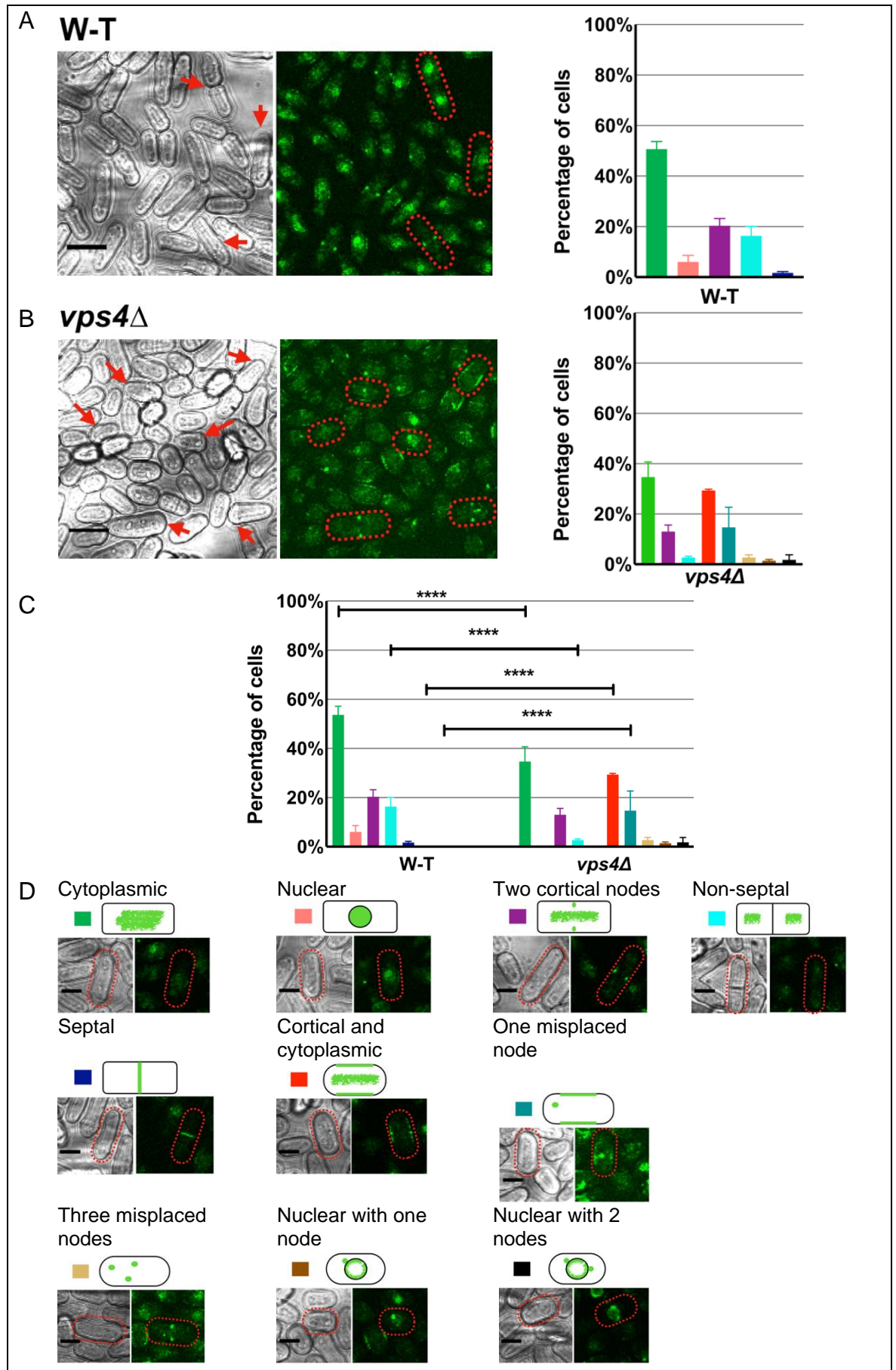


Figure 3-13 Design of GFP-Mid1p wild-type and *vps4* Δ strains. (Left) GFP was tagged to the chromosomal locus of the *mid1*⁺ gene to visualize the GFP-Mid1p localization in wild-type *S. pombe* (Paoletti and Chang, 2000). (Right) The GFP-Mid1p construct was transformed into a *vps4* Δ strain to visualize the GFP-Mid1p localization in *vps4* Δ *S. pombe* strain.



In (Figure 3-14, Panel A), a cell population sample represents the different patterns of GFP-Mid1p localization in **wild-type** *S. pombe*. Five main localization phenotypes were characterized: GFP-Mid1p localization was cytoplasmic in 54% of cells, whereas the localization was restricted to the nucleus in 6% of cells. In 21% of cells, the localization of GFP-Mid1p was in the form of two medial cortical nodes. In 17% of cells, GFP-Mid1p localized between the two dividing cells, whereas septal localization was observed in only 2% of cells.

In (Figure 3-14, Panel B), a cell population sample represents the different patterns of GFP-Mid1p localization in ***vps4Δ*** *S. pombe*. GFP-Mid1p cytoplasmic localization was similar to that of wild-type cells: 35% of cells showed cytoplasmic localization, 13% of cells showed nuclear localization, while only in only 3% of cells GFP-Mid1p localized between the two dividing cells. In this mutant strain, cortical localization was observed in 28% of cells; however interestingly, in 15% of cells GFP-Mid1p localized to the cortex and to only one node or localized to three separate nodes in 3% of cells. A total of 3% percentage of cells showed two additional phenotypes, where GFP-Mid1p nuclear localization was coupled to the node's localization, meaning that nuclear localization was observed with one or two nodes attached to the nuclear envelope. The frequencies of the localization phenotypes characterized in the *vps4Δ* strain was compared with the frequencies in the wild-type cells (Figure 3-14, Panel C). A significant decrease of the cytoplasmic and non-septal phenotypes was observed when compared to wild-type cells. The emergence of cortical localization and the node-displacement phenotypes is probably caused by the *vps4⁺* gene chromosomal deletion.

Overall, GFP-Mid1p localization was altered by the absence of the *vps4⁺* gene. This observation, in addition to our conclusions that the *mid1⁺* and *vps4⁺* genes genetically interact *in vivo* (Sections 3.3.3.2) and that the Mid1p and Vps4p physically interact *in vitro* (Section 3.3.4.4), supports the hypothesis that Mid1p and Vps4p coordinate to regulate *S. pombe* cell cycle.

Given that Mid1p possesses a PH domain in its C-terminal region, and the physical interaction between Vps4p and Mid1p was mapped to Mid1p "C-term" region, we decided to utilize the GFP-Mid1p approach to design another protein localization experiment that further investigates the role of the PH domain in anchoring Mid1p to the plasma membrane.

3.3.5.2 *S. pombe* Mid1p shares structural homology with mammalian anillin

During mammalian and fission yeast cell division, anchorage of the contractile ring at the cell equator involves two scaffold proteins, anillin and Mid1p respectively. The anillin-homology domain (AHD) is one component of the C-terminal domain of anillin (Figure 3-15, Panel A). Structural analysis of AHD revealed a sandwich domain and an anti-parallel coiled-coil domain. The sandwich domain has a C2-like structure that binds lipids (Sun et al., 2015).

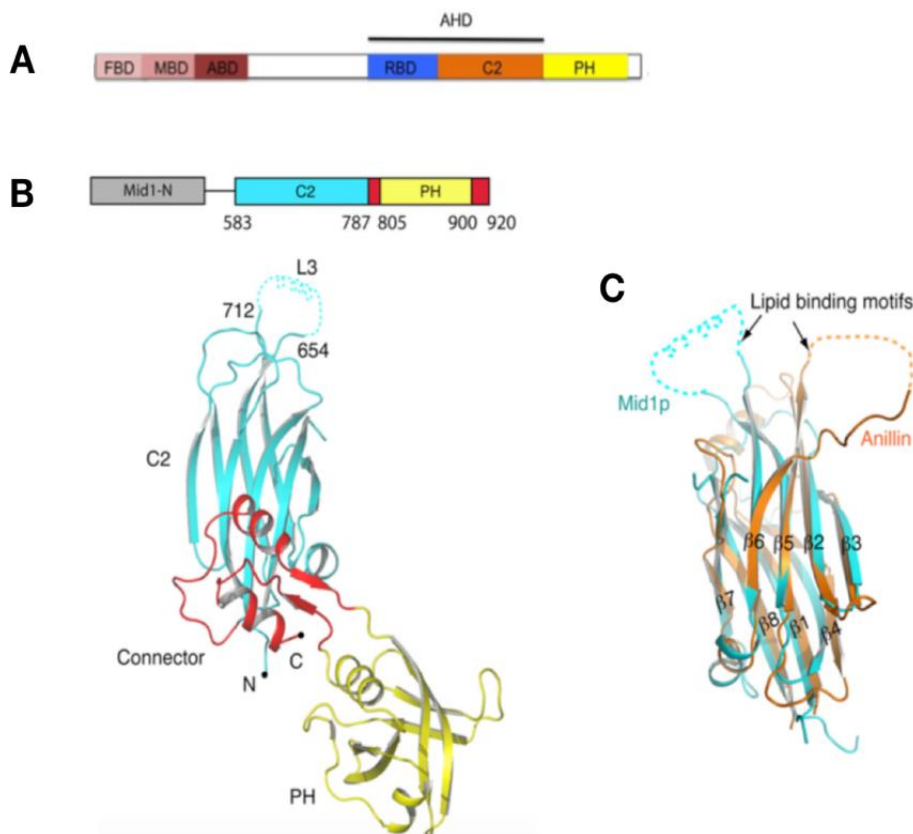


Figure 3-15 Structural lipid-binding domain similarities between anillin and Mid1p. (A) Domain organization of anillin; the N-terminal region (in shaded pink) constitutes: FBD, formin binding domain, MBD, myosin binding domain and ABD, actin binding domain. The N-terminal region is followed by AHD, anillin homology domain, RBD, rho binding domain (in blue), C2 domain (in orange) and the PH domain (in yellow). **(B)** Domain organization of Mid1p and the structure of Mid1p C-terminal region (aa 579-920) with the C2 domain (in cyan), the connector domain (in red) and the PH domain (in yellow); dotted lines represent the lipid binding loop. **(C)** The C2 domain structural alignment of anillin (in orange) and Mid1p (in cyan). Panel (A) is reproduced from Gould (2016), while Panels (B) and (C) are reproduced from Sun et al. (2015).

Sun et al. (2015) indicated that a mutation in the C2 domain leads to disruption of anillin anchorage at the cleavage furrow. In addition, when the C2 lipid-binding loop is deleted and the protein is introduced into cells depleted from endogenous anillin, cytokinesis failed.

The study by Sun and colleagues (2015) revealed a folding pattern of the C-terminal region of the anillin-like Mid1p into three domains: a β -sandwich domain, a connector domain and a PH domain (Figure 3-15, Panel B). Surprisingly, the β -sandwich domain mimics a C2 domain organization and was successfully superimposed with anillin C2 domain (Figure 3-15, Panel C). This C2 domain was found to cause Mid1p dimerization leading to a high affinity for phosphatidylinositol 4,5-bisphosphate (PI4, 5P2). Given that PI4, 5P2 is a component of *S. pombe* plasma membrane (Zhang et al., 2000), Sun et al. (2015) suggested that this mechanism underlies Mid1p anchorage to the plasma membrane during cytokinesis. However, the PH domain role in Mid1p function is still poorly understood.

In their study, a chimera protein composed of both Mid1p (N-terminal domain) and anillin (C-terminal domain) was generated and introduced into cells lacking the endogenous anillin⁺ gene. Interestingly, the chimera protein rescued the defective cytokinesis phenotypes in anillin-depleted cells as in wild-type cells.

Collectively, this evidence suggests a similarity of function between Mid1p and anillin proteins during mitosis.

3.3.5.3 Investigating the localization of Mid1p in PH Δ *mid1* *S. pombe*

The PH domain is known for targeting some proteins to the cell membrane through interactions with membrane phospholipids (Lemmon, Ferguson and Schlessinger, 1996). Paoletti and Chang (2000) tested if Mid1p is targeted to the plasma membrane by its PH domain during the *S. pombe* cell cycle. For that, they used an integrative vector with a mutation in the *mid1*⁺ gene to produce an *S. pombe* strain with a deletion of the Mid1p PH domain (798-920 aa) and called it the PH Δ *mid1* strain (Figure 3-16, Left panel). Surprisingly, when the strain was exposed to anti-*mid1* antibody and examined by fluorescence microscopy, it showed a localization identical to that observed in wild-type cells. They concluded that the PH domain of

Mid1p is not essential for targeting the protein to the cell cortex and nuclear envelope. However, this domain could be indirectly involved in regulating this process.

Our accumulated lines of evidences (Section 3.3.3.2, Section 3.3.4.4 and Section 3.3.5) support the model where an interaction between Vps4p and the "C-term" domain of Mid1p -perhaps the PH domain- regulates nodes attachment to the plasma membrane.

To test this model, we first need to determine the role of the PH domain in Mid1p function. Thus, an experiment investigating the localization of GFP-Mid1p in PH Δ *mid1* cells was designed. The GFP-Mid1p/PH Δ *mid1* was constructed using the same GFP tagging method described in (Figure 3-13, Left panel). The GFP-PH Δ *mid1* strain was grown on solid rich medium alongside with the wild-type *S. pombe* strain to compare colony formation and growth. The strain was able to form viable colonies, similar to wild-type (Figure 3-16, Right panel).

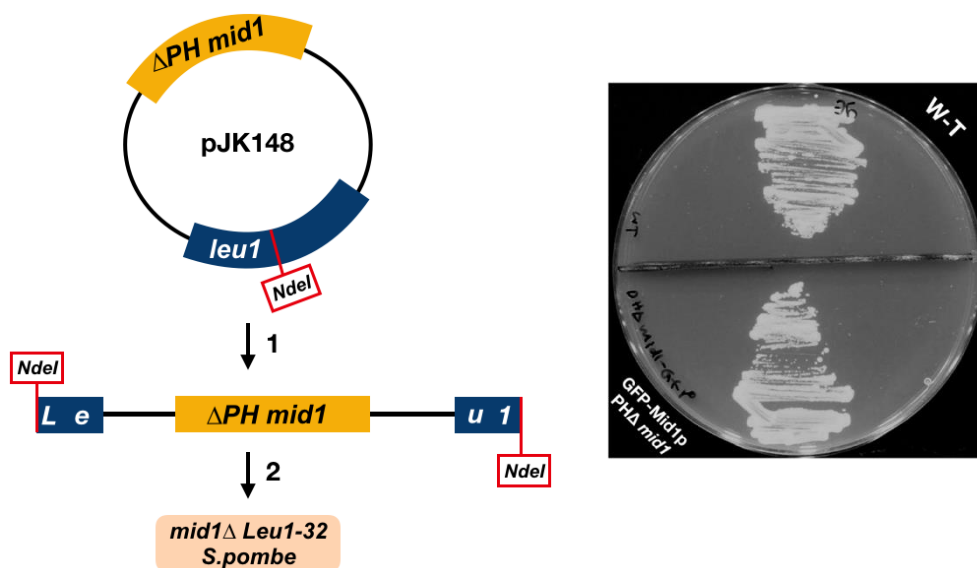


Figure 3-16 Design of the PH Δ *mid1* strain and its growth phenotype. (Left) An integrative plasmid was used to replace the endogenous *mid1*⁺ gene with the PH Δ *mid1* gene (Paoletti and Chang, 2000). **(Right)** The PH Δ *mid1* strain was grown on solid rich YE medium alongside a wild-type *S. pombe* strain to test its growth phenotype.

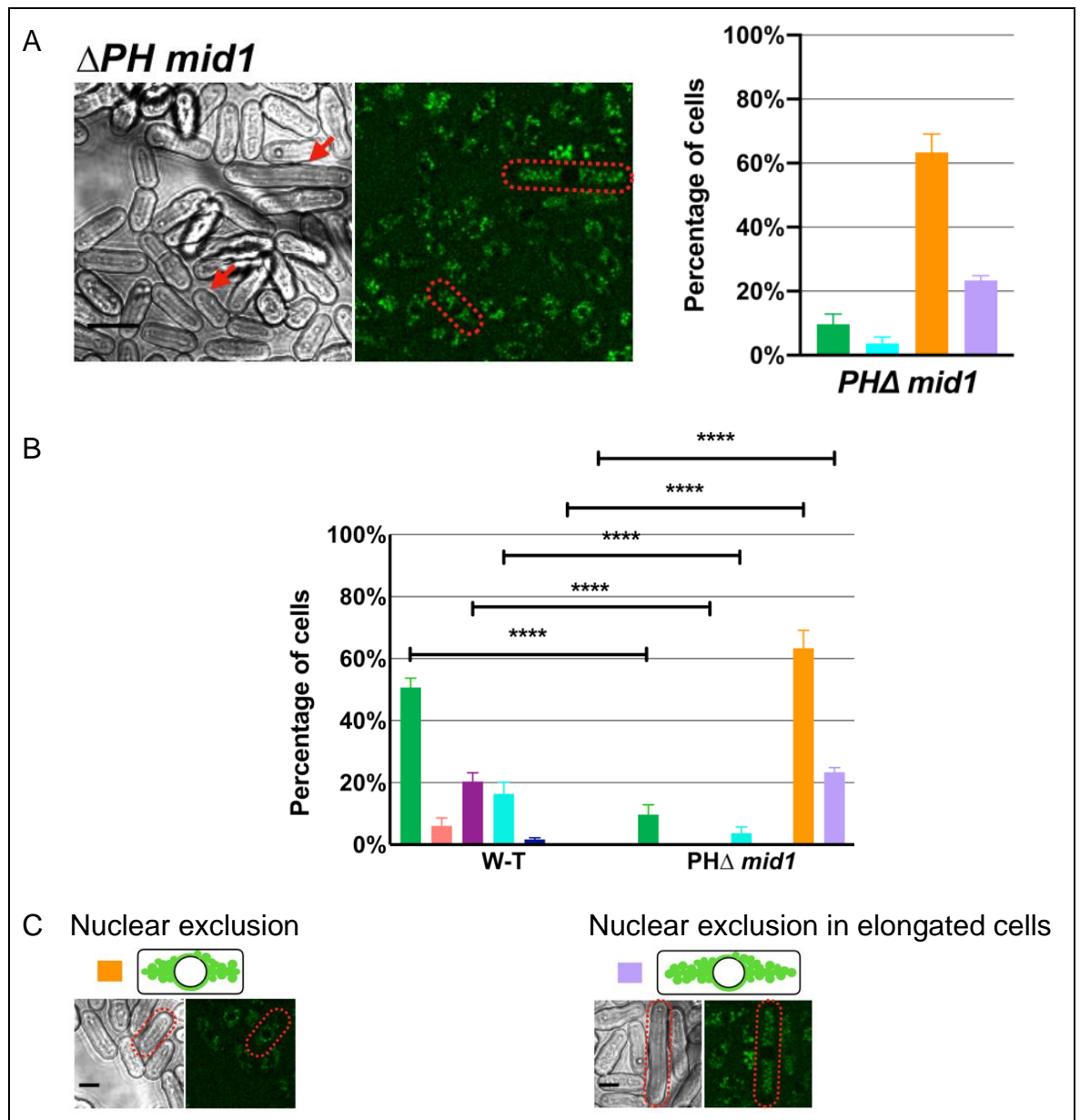


Figure 3-17 Classification and quantification of GFP-Mid1p localization phenotypes in wild-type and $PH\Delta mid1$ *S. pombe*. *S. pombe* strains were grown and visualized as described in Figure 3-14. (A) Population of cells (left) and quantitative analysis of the observed phenotypes (right) are shown in $PH\Delta mid1$ cells. Scale bar 10 μm . 200-250 cells were counted from three independent experiments to produce (A) and (B). In (B), a 2-way ANOVA statistical analysis was used. The frequencies of the localization phenotypes in $PH\Delta mid1$ cells were compared to wild-type frequencies. Asterisks (****) denotes a p value <0.0001 . Error bars represent SEM. (C) Characterized localization phenotypes. Scale bar 5 μm .

In (Figure 3-17, Panel A), a cell population sample represents the different patterns of GFP-Mid1p localization in **PHΔ *mid1*** *S. pombe*. In this strain, two new localization phenotypes were observed. The two localization patterns were similar in terms of GFP-Mid1p localization, but they were both associated with a different cell length: in 63% of cells, GFP-Mid1p localized in the cytoplasm with a clear nuclear exclusion phenotype, while in 23% of cells, this nuclear exclusion phenotype was observed in elongated cells. GFP-Mid1p localization was cytoplasmic in 10% of cells, while in only 4% of cells GFP-Mid1p localized between the two dividing cells (non-septal phenotype). Upon the comparison of the frequencies of these four phenotypes in **PHΔ *mid1*** cells to the frequencies in wild-type cells (Figure 3-17, Panel B), a significant decrease of the cytoplasmic and non-septal localization was observed. In addition to that, the emergence of dominant nuclear exclusion phenotypes observed in **PHΔ *mid1*** strain suggests a novel role of the PH domain in Mid1p nuclear targeting. Interestingly, cortical nodes were not observed, which confirms that the PH domain is needed for nodes cortical anchorage.

3.4 Conclusions

In this Chapter, we combined *in vivo* and biochemical *in vitro* approaches to study the regulation of *S. pombe* septation by the anillin Mid1p and the ESCRT-III regulator Vps4p. Our main five findings are summarized as follows:

First, we confirmed that the *mid1*⁺ gene is required for correct division placement during *S. pombe* septation. We also demonstrated the role of the *vps4*⁺ gene in proper *S. pombe* cells separation after septation.

Second, we illustrated the presence of a striking genetic interaction between the *mid1*⁺ and *vps4*⁺ genes, indicated by a synthetic lethal phenotype in double *mid1*Δ *vps4*Δ mutant cells.

Third, we detected a physical interaction between the "C-term" domain of Mid1p and Vps4p.

Fourth, we characterized localization patterns of GFP-Mid1p in wild-type *S. pombe* cells and demonstrated the requirement of Vps4p for Mid1p correct localization.

Combined, these four findings formulated a model whereby Mid1p and Vps4p coordinate to achieve *S. pombe* correct septation (explained in detail in Chapter 6).

Fifth, we investigated the role of the PH domain in Mid1p function. We concluded that this domain is involved in Mid1p nuclear localization as its deletion resulted in Mid1p nuclear exclusion.

Chapter 4 Investigation into the role of nuclear localization of Mid1p in regulating *S. pombe* septation

4.1 Introduction

4.1.1 Mid1p localization phenotypes regulate its function during *S. pombe* cell cycle

The *mid1⁺* gene is required for *S. pombe* septation, with the Mid1p protein shuttling in and out of the nucleus to regulate *S. pombe* cell cycle (Sohrmann et al., 1996). To understand the role of Mid1p in *S. pombe* cell cycle regulation, Paoletti and Chang (2000) used a GFP-tagged form of Mid1p to monitor its cellular localization. They confirmed that GFP-Mid1p shuttles between the nucleus and the cell surface (Figure 4-1).

The cytoplasmic localization of GFP-Mid1p is in the form of an equatorial band surrounding the nucleus and attached to the cell surface. The position of this band is coupled to the position of the nucleus and depends on close proximity to the nucleus (Paoletti and Chang, 2000).

Daga and Chang (2005) developed an approach to manipulate the nuclear position of *S. pombe* cells to examine the localization of Mid1p after nuclear displacement. Before nuclear displacement, Mid1p was detected in the form of cortical patches near the nucleus, but upon nuclear displacement, these Mid1p patches re-located with the new nuclear position. This observation further confirmed the link between Mid1p nuclear shuttling and cortical localization.

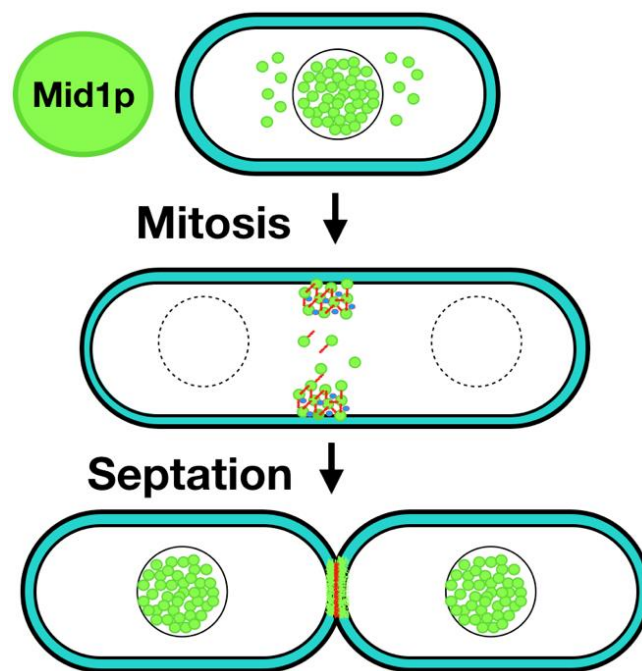


Figure 4-1 The localization of Mid1p throughout *S. pombe* cell cycle. During interphase, Mid1p localizes to the nucleus and cytoplasm. Upon mitotic entry, Mid1p (Green) is exported out of the nucleus. During late mitosis at anaphase, Mid1p localizes to the nodes after which it recruits other proteins (Blue), and myosin2 (Red)-based movement of nodes causes them to constrict forming the contractile ring and the septum. Septation leads to the final separation of the two daughter cells with Mid1p re-localization to the nucleus. Figure derived from Paoletti and Chang (2000) and Almonacid et al. (2009).

4.2 Aims

In Chapter 3, we identified a genetic interaction between the *mid1*⁺ and *vps4*⁺ genes. We then identified a physical interaction between the encoded Vps4p and Mid1p and mapped the interaction to the C-terminal domain of Mid1p, which includes the PH domain that is known to bind membrane lipids. We then characterized GFP-Mid1p localization phenotypes in wild-type, *vps4*Δ and *mid1* PHΔ cells. An increased rate of GFP-Mid1p node mis-localization attachment phenotype was observed in *vps4*Δ cells, while an increased rate of GFP-Mid1p nuclear exclusion localization phenotype was observed in *mid1* PHΔ cells. Both of these phenotypes were not observed in wild-type cells, suggesting that the interaction between Mid1p and Vps4p might require Mid1p nuclear shuttling.

We hypothesized that the interaction between Mid1p and Vps4p requires Mid1p nuclear shuttling. The following specific aims were therefore addressed:

- Generation of the *mid1* NLS* *vps4*Δ and *mid1* 450-506Δ *vps4*Δ double mutants to test for synthetic growth phenotypes.
- Characterization of septation phenotypes in the single (*mid1* NLS* and *mid1* 450-506Δ) and the double (*mid1* NLS* *vps4*Δ and *mid1* 450-506Δ *vps4*Δ) mutants.
- Determination of the cellular localization of GFP-Mid1p in *mid1* NLS* *S. pombe* cells.

4.3 Results

4.3.1 Does the genetic interaction between the *mid1*⁺ and *vps4*⁺ genes require Mid1p nuclear shuttling?

4.3.1.1 The use of Mid1p nuclear localization sequence mutant strains

In Section 3.3.3.2, we tested the genetic interaction between the *mid1*⁺ and *vps4*⁺ genes in *S. pombe*. This was achieved by creating *mid1*Δ *vps4*Δ double mutants by mating of two single chromosomal deletion mutation strains, a deletion of the *mid1*⁺ gene and a deletion of the *vps4*⁺ gene (Section 3.3.3.1). The *mid1*Δ *vps4*Δ double mutants showed an impaired growth phenotype illustrating a genetic interaction between *vps4*⁺ and *mid1*⁺ genes. We then showed a physical interaction of the encoded Vps4p and Mid1p proteins (Section 3.3.4.4), which offers an explanation for the observed genetic interaction between the *mid1*⁺ and *vps4*⁺ genes.

Paoletti and Chang (2000) identified and mutated a basic-rich (aa 691 to 695 RKKRK) nuclear localization sequence (NLS) signal in Mid1p. They produced a substitution mutation in which amino acids 691 to 695 (RKKRK) were replaced with QNSQS to generate a *mid1* NLS* *S. pombe* strain.

In a separate study, Almonacid and colleagues (2009) investigated the spatial control of *S. pombe* septation through Mid1p nuclear export. They identified and mutated a second nuclear localization sequence (aa 450 to 506) in Mid1p and produced a deletion mutation (aa 450-506Δ) to generate a *mid1* 450-506Δ *S.*

pombe strain. Almonacid and colleagues (2009) also combined the Mid1p (aa 450-506 Δ) mutation with the previously characterized Mid1p (NLS*) mutation (Paoletti and Chang, 2000) to produce a (*mid1*^{nsm}) nuclear shuttling mutant. They reported that the *mid1*^{nsm} strain was "completely deficient" in nuclear shuttling. They observed that Mid1p was absent from the nucleus throughout the cell cycle, with its localization detected at the medial cell cortex during interphase, and cells had medial contractile ring assembly similar to wild-type Mid1p mediated assembly (Almonacid et al., 2009). Both *mid1* NLS* and *mid1* 450-506 Δ *S. pombe* strains were kindly gifted by Anne Paoletti for use in this study. The nuclear localization-related mutants are summarized in Table 4-1.

The two *mid1* NLS strains were grown on solid rich medium alongside wild-type *S. pombe* cells to compare colony formation and growth. Both strains were able to form viable colonies similar to wild-type cells (data not shown). As expected, examining cells by light microscopy did not reveal the branched septation phenotype observed in the *mid1* Δ strain. Instead, cells appeared smaller in size compared to wild-type cells, with septa unaffected.

Table 4-1 Mid1p nuclear localization sequences mutations.

Mutant name	Mid1p Sequence alteration
<i>mid1</i> NLS*	Replacement of amino acids 691 to 695 (RKKRK) to amino acids (QNSQS)
<i>mid1</i> 450-506 Δ	Deletion of amino acids 450 to 506
<i>mid1</i> ^{nsm}	Deletion of amino acids 450 to 506, and replacement of amino acids 691 to 695 (RKKRK) to amino acids (QNSQS)

4.3.1.2 Generation of *mid1* NLS *vps4* Δ double mutants

We sought to investigate whether the interaction between Mid1p and Vps4p requires Mid1p nuclear shuttling. To achieve this, the two *mid1* NLS mutant *S. pombe* strains were used in combination with the previously discussed *vps4* Δ mutant *S. pombe* strain (Section 3.3.1). We hypothesized that mutating one or both nuclear localization signal/s in the *mid1*⁺ gene affects its genetic interaction with the *vps4*⁺ gene leading to a synthetic growth phenotype in *S. pombe* cells (Section 3.3.3.2). To explore this, we generated *mid1* NLS *vps4* Δ double mutants by mating the *mid1* NLS single mutants with *vps4* Δ single mutant. Double mutants were identified by tetrad analysis using an ascus dissector microscope and selective media (Figure 4-2).

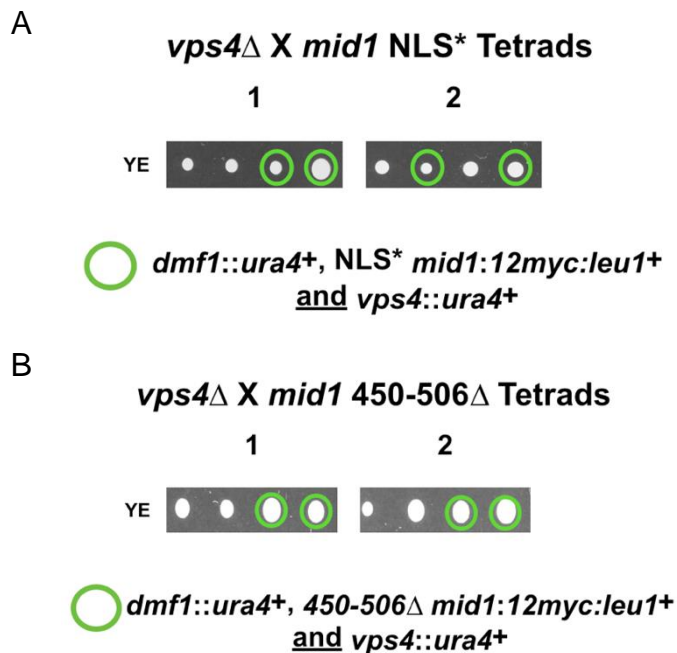


Figure 4-2 Mid1p NLS signals (aa 691-695 and aa 450-506) are not required for the genetic interaction between the *mid1*⁺ and *vps4*⁺ genes. Tetrad analysis of h⁻ *vps4* Δ strain (*vps4*⁺::*ura4*⁺) mated with either (A) h⁺ *mid1* NLS* strain (*dmf1*⁺::*ura4*⁺, NLS* *mid1*:12 *myc*:*leu1*⁺) or with (B) h⁺ *mid1* 450-506 Δ strain (*dmf1*⁺::*ura4*⁺, 450-506 Δ *mid1*:12 *myc*:*leu1*⁺) to identify *mid1* NLS* *vps4* Δ or *mid1* 450-506 Δ *vps4* Δ double mutants that show a normal growth phenotype. Tetrads were performed by mating the two strains on solid ME medium (25°C) for two days. Tetrads were then dissected using Singer MSM ascus dissector and spores allowed to grow on solid YE medium (28°C) until colonies formed and were replicated to solid EMM -ura and EMM -leu media and incubated (28°C) to identify growth phenotypes; two double mutant colonies are indicated for each tetrad.

The synthetic growth phenotype observed in the *mid1* Δ *vps4* Δ double mutant was not observed in *mid1* NLS* *vps4* Δ or *mid1* 450-506 Δ *vps4* Δ double mutants. Both double mutants formed colonies similar to the wild-type and single mutant strains. Therefore, we concluded that the genetic interaction between the *mid1*⁺ and *vps4*⁺ genes was not affected by the absence of the two NLS signals.

Since the *mid1* NLS* *vps4* Δ and *mid1* 450-506 Δ *vps4* Δ double mutants were capable of colony formation, we then sought to characterize the septation phenotypes in the control (wild-type and *vps4* Δ), single mutant (*mid1* NLS* and *mid1* 450-506 Δ) and double mutant (*mid1* NLS* *vps4* Δ and *mid1* 450-506 Δ *vps4* Δ) strains, by calcofluor staining.

4.3.2 Septation analysis of *mid1* NLS *vps4* Δ double mutants

Calcofluor staining was applied to *S. pombe* cells grown in liquid rich medium to visualize newly deposited septa by fluorescence microscopy. In wild-type cells, such analysis yielded two septation phenotypes where most cells had no septa, and some had a single correctly-placed septum. The same analysis was carried out in *vps4* Δ cells to evaluate the effect of *vps4*⁺ gene chromosomal deletion on *S. pombe* septation. A septation defective phenotype, represented in delayed separation after septation, was characterized. The frequency of each septation phenotype was quantified for both strains (Figure 3-2).

Here, the frequencies of the above-mentioned septation phenotypes were determined for the single (*mid1* NLS* and *mid1* 450-506 Δ) and double (*mid1* NLS* *vps4* Δ and *mid1* 450-506 Δ *vps4* Δ) mutant strains. Phenotype frequencies in each single mutant were compared to their respective frequencies in the relevant double mutant as follows: *mid1* NLS* was compared with *mid1* NLS* *vps4* Δ and *mid1* 450-506 Δ was compared with *mid1* 450-506 Δ *vps4* Δ (Figure 4-3).

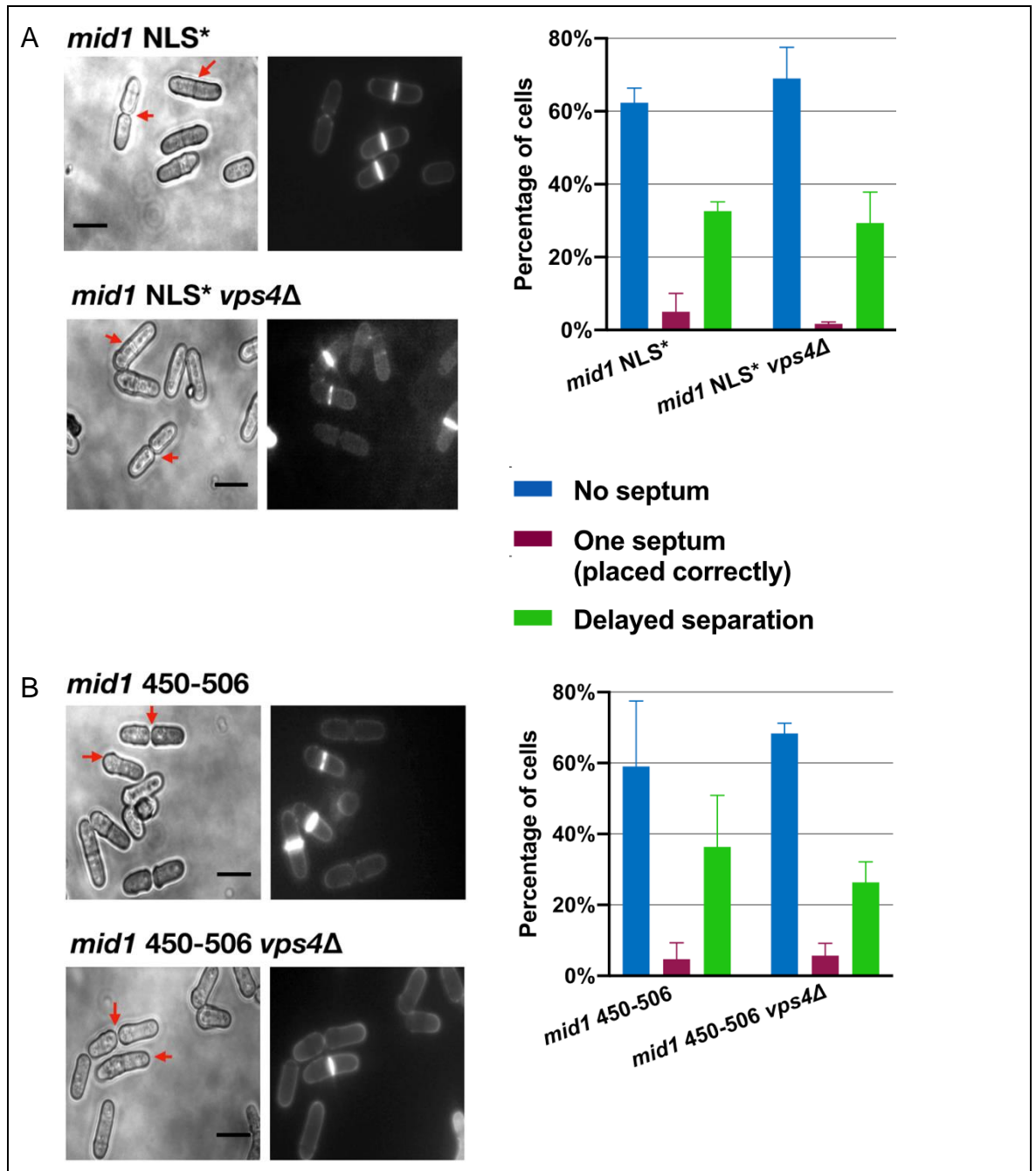


Figure 4-3 Classification and quantification of septation phenotypes in wild-type and NLS* *mid1* *S. pombe*. *S. pombe* strains were grown and visualized as described in Figure 3-14. (A) A population of cells (left) and a quantitative analysis of the observed phenotypes (right) are shown in NLS* *mid1* and NLS* *mid1 vps4*Δ cells. (B) A population of cells (left) and a quantitative analysis of the observed phenotypes (right) are shown in 450-506 *mid1* and 450-506 *mid1 vps4*Δ cells. A 2-way ANOVA statistical analysis was used to compare the frequencies of the localization phenotypes in NLS* *mid1* and 450-506 *mid1* single mutants to the frequencies in NLS* *mid1 vps4*Δ and 450-506 *mid1 vps4*Δ double mutants. Error bars represent SEM.

Comparison of (*mid1* NLS*) with (*mid1* NLS* *vps4*Δ) strain

In the single mutant *mid1* NLS* cells, 62% of cells had no septa, while a single correctly-placed septum was observed in only 5% of cells. 33% of cells showed delayed separation following septation. This phenotype was not observed in wild-type cells, which implicates a role of Mid1p (aa 691-695) nuclear localization signal in *S. pombe* septation regulation, specifically during abscission, to allow for the final separation of the two daughter cells.

In the double mutant *mid1* NLS* *vps4*Δ cells, 69% of cells had no septa, while a single correctly-placed septum was observed in only 2% of cells. 29% of cells showed delayed separation following septation. Comparison of the frequencies of septation phenotypes in *mid1* NLS* cells with those of the *mid1* NLS* *vps4*Δ cells revealed no significant differences (Figure 4-3, Panel A).

Comparison of (*mid1* 450-506Δ) with (*mid1* 450-506Δ *vps4*Δ) strain

In the single mutant *mid1* 450-506Δ cells, 59% of cells had no septa, while a single correctly-placed septum was observed in only 5% of cells. 36% of cells showed delayed separation following septation. This phenotype was not observed in wild-type cells, which implicates a role of Mid1p (aa 450-506) nuclear localization signal in *S. pombe* septation regulation, specifically during abscission, to allow for the final separation of the two daughter cells.

In the double mutant *mid1* 450-506Δ *vps4*Δ cells, 68% of cells had no septa, while a single correctly-placed septum was observed in only 6% of cells. 26% of cells showed delayed separation following septation. Comparison of the frequencies of septation phenotypes in *mid1* 450-506Δ cells with those of the *mid1* 450-506Δ *vps4*Δ cells revealed no significant differences (Figure 4-3, Panel B).

Since the frequencies of septation phenotypes observed in the double mutants *mid1* NLS* *vps4*Δ and *mid1*450-506Δ *vps4*Δ showed no significant differences to those observed in single mutants *mid1* NLS* and *mid1*450-506Δ, it appears that the genetic interaction between the *mid1*⁺ and *vps4*⁺ genes does not require Mid1p nuclear localization.

4.3.3 Localization of GFP-Mid1p in *mid1* NLS* cells

Paoletti and Chang (2000) utilized a PCR-based recombination approach to construct a strain with four copies of GFP tagged to the chromosomal locus of the *mid1*⁺ gene to determine the cellular localization of GFP-Mid1p (Paoletti and Chang, 2000; Section 3.3.5.1). As discussed in Section 4.3.1.1, Paoletti and Chang (2000) generated a *mid1* NLS* strain. When this strain was exposed to anti-*mid1* antibody and examined by fluorescence microscopy, it showed a great reduction in Mid1p nuclear localization.

In this Section, we investigated the cellular localization of GFP-Mid1p in the *mid1* NLS* strain using confocal microscopy. To achieve this, GFP was tagged to the chromosomal locus of the *mid1*⁺ gene to generate GFP-Mid1p NLS* strain. This strain was generated by crossing the GFP-Mid1p *S. pombe* strain (GG 1347; Section 3.3.5.1) with the *mid1* NLS* strain (Section 4.3.1.1).

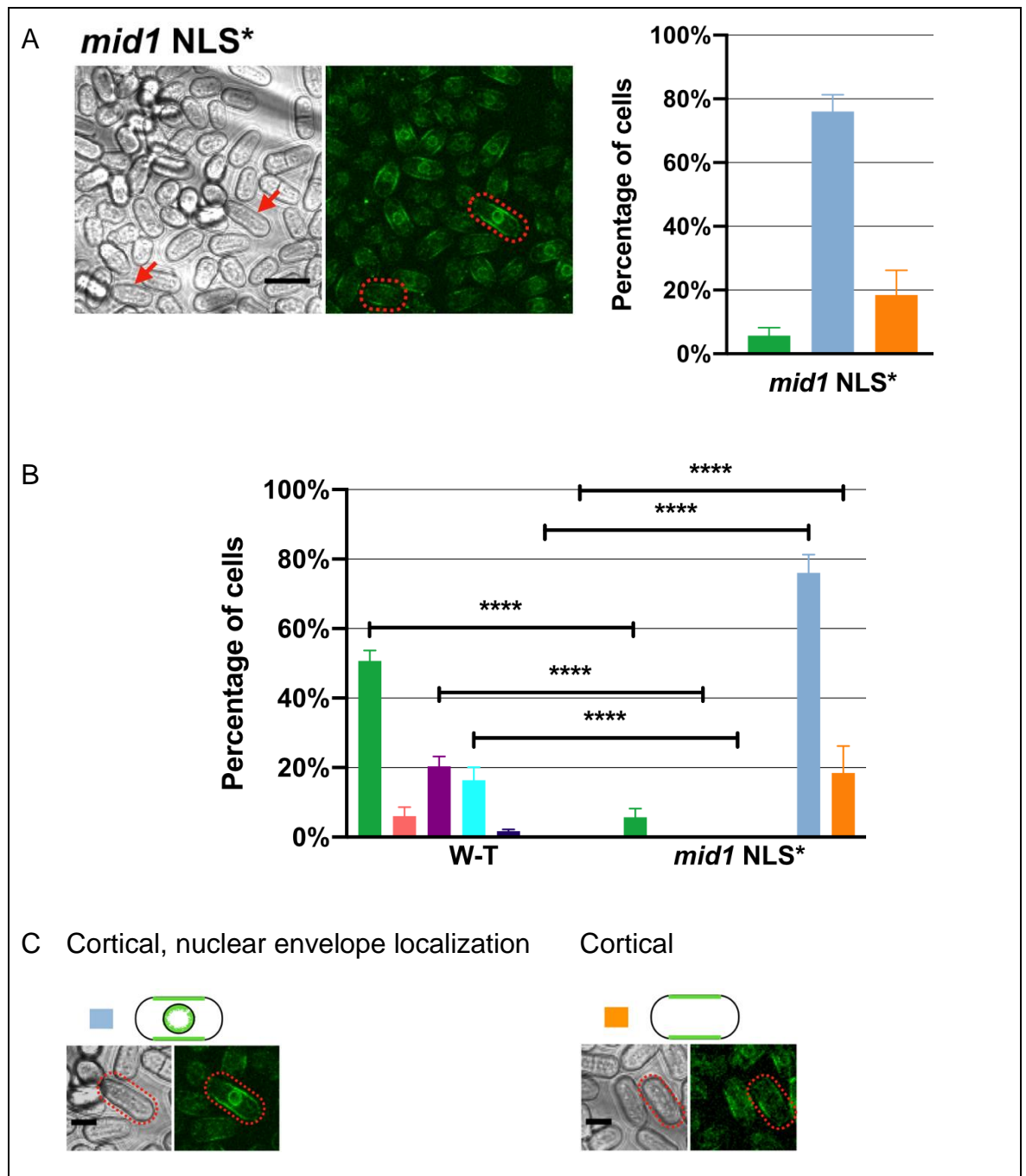


Figure 4-4 Classification and quantification of GFP-Mid1p localization phenotypes in wild-type and *mid1* NLS* *S. pombe*. *S. pombe* strains were grown and visualized as described in Figure 3-14. (A) Population of cells (left) and quantitative analysis of the observed phenotypes (right) are shown in NLS* *mid1* cells. Scale bar 10 μ m. 200-250 cells were counted from three independent experiments to produce (A). In (B), a 2-way ANOVA statistical analysis was used. The frequencies of the localization phenotypes in NLS* *mid1* cells were compared to wild-type frequencies. Asterisks (****) denotes a p value <0.0001. Error bars represent SEM. (C) Characterized localization phenotypes. Scale bar 5 μ m.

In (Figure 4-4, Panel A), a cell population sample represents the different patterns of GFP-Mid1p localization in *mid1 NLS** *S. pombe*. GFP-Mid1p cytoplasmic localization was not similar to that observed in wild-type cells, as only 6% of cells showed cytoplasmic localization, while 18% of cells showed medial cortical localization. In this strain, the majority of cells (76%) acquired medial cortical in addition to unclear envelope localization with GFP-Mid1p excluded from the nucleus. Upon comparison of the frequencies of these three phenotypes with wild-type frequencies (Figure 3-16, Panel A3) cytoplasmic localization frequency showed a significant decrease, additionally, the emergence of the different cortical localization phenotypes indicate that nuclear localization defects in Mid1p alter the distribution of GFP-Mid1p, which is consistent with the known role of Mid1p nuclear shuttling to regulate *S. pombe* cell cycle (Paoletti and Chang, 2000).

Overall, GFP-Mid1p localization was affected by the *mid1 NLS** mutation, and nuclear localization disruption was coupled to cell membrane localization, supporting the hypothesis that Mid1p nuclear shuttling regulates its attachment to the cell membrane during *S. pombe* cell cycle.

In Section 3.3.5, we concluded that Vps4p is involved in the regulation of Mid1p-dependent attachment of nodes to the cell membrane in *S. pombe*. Furthermore, we emphasized the importance of Mid1p PH domain for its localization as the absence of the PH domain (*mid1 PHΔ*) resulted in Mid1p nuclear exclusion localization phenotype.

The *S. pombe* genetic analysis presented here revealed that the interaction between Mid1p and Vps4p may not directly require Mid1p nuclear shuttling (Section 4.3.1.2). However, Mid1p nuclear shuttling might indirectly regulates such an interaction by other mechanisms.

4.4 Conclusions

In Chapter 3, we investigated the regulation of *S. pombe* septation by Mid1p and Vps4p. In this Chapter, we hypothesized that Mid1p nuclear localization signals are involved in its interaction with Vps4p. Our main four findings are:

First, the synthetic growth phenotype observed in the *mid1* Δ *vps4* Δ double mutant was not observed neither in *mid1* NLS* *vps4* Δ nor in *mid1* 450-506 Δ *vps4* Δ double mutants.

Second, we demonstrated a role of the *vps4*⁺ gene in *S. pombe* septation in Section 3.3.2, implicated as a significant increase of the cell septation defects represented in late separation of cells following septation compared to wild-type cells. Here, we detected similar frequencies of this phenotype in the *mid1* NLS* and *mid1* 450-506 Δ single mutants. **Third**, we did not detect a significant increase in the rate of this phenotype between the single (*mid1* NLS* and *mid1* 450-506 Δ) and double mutant (*mid1* NLS* *vps4* Δ and *mid1* 450-506 Δ *vps4* Δ) strains.

Fourth, we characterized the patterns of GFP-Mid1p distribution in *mid1* NLS* *S. pombe* and demonstrated the requirement of the Mid1p nuclear localization signals (aa 691-695) for Mid1p wild-type localization.

Combined, these four findings show that Mid1p nuclear shuttling is required for its function and localization. However, it seems that Mid1p nuclear localization signals (aa 691-695 and aa 450-506) are not directly required for its interaction with Vps4p to regulate *S. pombe* cell cycle.

Instead, mitotic kinases might coordinate Mid1p nuclear shuttling with cell membrane anchorage. The polo-like kinase Plo1p and the aurora kinase Ark1p are known mitotic kinases with important roles in cell cycle regulation. Specifically, Plo1p regulates Mid1p export from the nucleus through phosphorylation. Thus, in the next two Chapters, we investigate the regulation of Mid1p by the mitotic kinases Ark1p and Plo1p.

Chapter 5 Genetic interactions between the *mid1*⁺ and *ark1*⁺ genes, and physical interactions between the Mid1p and aurora A kinase suggest Mid1p regulation by Ark1p in *S. pombe*.

5.1 Introduction

During mammalian cell cycle, plk1 phosphorylates a range of proteins to regulate mitotic events. This is achieved via its specialized phospho-serine and phospho-threonine binding domain, the polo-box domain (PBD). A study by Lowery and colleagues (2007) used this PBD as an affinity capture moiety to characterize plk1 substrates during mitosis; they identified mammalian anillin (*S. pombe* Mid1p) as a substrate for plk1. Additionally, in a separate study, Straight et al. (2005) demonstrated the *in vitro* association of anillin with plk1. To date, only a single version of polo-like kinase was identified in *S. pombe* named Plo1p; this protein was identified as a key regulator of mitotic progression in this organism (Ohkura, Hagan and Glover, 1995). Bähler and colleagues (1998) demonstrated the physical interaction between *S. pombe* Plo1p and Mid1p proteins, where they showed the requirement of this interaction for the correct localization of Mid1p to the contractile ring.

The above lines of evidence confirm the interaction between plk1 and anillin and between Plo1p and Mid1p in mammalian and *S. pombe* cells, respectively. This suggests a conserved pathway for cell cycle regulation through this coordination. In this Thesis in Section 5.3.3, we provide evidence that mammalian plk1 mediates *in vitro* phosphorylation of residues within the "N-term" and "Middle" domains of Mid1p; this further supports the suggested interaction between the two proteins.

The general aim of this research was to investigate the regulation of eukaryotic cytokinesis using *S. pombe* as a model organism; this was achieved by analysis of the cell cycle protein Mid1p. In Chapter 3, we investigated the regulation of Mid1p by Vps4p utilizing *S. pombe* genetics and biochemical approaches. In this Chapter, using similar approaches, we revisit Mid1p regulation by aurora kinase/Ark1p.

5.1.1 Could Plo1p and Ark1p coordinate with Mid1p to regulate *S. pombe* cell cycle?

The role of aurora and polo-like kinases in mammalian cell cycle regulation are well established. Also, the homologue proteins of aurora and Polo-like kinases in *S. pombe* are known to be involved in the regulation of key cell cycle processes. Mid1p was found to be a substrate of Plo1p, but, the interaction between Mid1p and Ark1p was not previously investigated. Therefore, we hypothesized that Ark1p regulates the function of Mid1p, which in turn regulates *S. pombe* cell cycle.

Since the genetic interaction of the *mid1*⁺ and *plo1*⁺ genes were previously demonstrated (Bähler et al., 1998), here we investigated the genetic interaction between the *mid1*⁺ and *ark1*⁺ genes. Using *S. pombe in vivo* tetrad analysis and crossing of a *mid1*Δ strain and an *ark1*⁺ temperature-sensitive (TS) mutant strain, we detected a striking genetic interaction represented in a synthetic lethal growth phenotype of the *mid1*Δ *ark1*-TS double mutants (Sections 5.3.1 and 5.3.2).

The genetic interaction observed between the *mid1*⁺ and *ark1*⁺ genes suggests that the encoded proteins physically interact. To test for this interaction, we carried out *in vitro* phosphorylation experiments utilizing Mid1p different domains and mammalian commercially purified aurora and Polo-like kinases. Successful detection of this *in vitro* phosphorylation interaction was followed by the determination of potential phospho-sites in Mid1p phosphorylated by aurora A (Section 5.3.3).

To confirm the identified potential Mid1p phospho-sites, Mid1p phospho-resistant mutant recombinant proteins were generated to determine the effect of these mutations on the *in vitro* phosphorylation interaction (Sections 5.3.4 and 5.3.5); however, such analysis was inconclusive with regards to confirming the Mid1p phospho-sites. Therefore, an *in vivo S. pombe* integration approach that included the replacement of the endogenous *mid1*⁺ gene by phospho-mimetic/resistant versions of the *mid1*⁺ gene was carried out. These experiments are described in Chapter 6.

5.2 Aims

Previous work has demonstrated that Plo1p regulates Mid1p function during *S. pombe* cell cycle (Bähler et al., 1998). However, to our knowledge, no previous studies investigated the role of Ark1p in Mid1p function to regulate *S. pombe* cell cycle.

The major aim of this Chapter is to investigate the genetic and physical interactions between the *mid1*⁺ and *ark1*⁺ genes, and the Mid1p and aurora kinase proteins, respectively, in an attempt to uncover a novel Mid1p function regulatory pathway. The following specific aims were therefore addressed:

- Investigation of genetic interactions between the *mid1*⁺ and *ark1*⁺ genes using an *in vivo* *S. pombe* genetic approach
- Determination of Mid1p phosphorylation by mammalian plk1 and aurora kinases using an *in vitro* phosphorylation experiment
- Identification of Mid1p potential phospho-sites using an *in vitro* mass spectrometry approach and generation of Mid1p phospho-sites map
- Confirmation of the identified phospho-sites through the generation of Mid1p phospho-resistant mutants to determine the effect of these mutations on the *in vitro* phosphorylation interaction

5.3 Results

5.3.1 *ark1*⁺ *S. pombe* temperature sensitive mutants

A published study was concerned with the identification of Ark1p substrates involved in *S. pombe* chromatin regulation during mitosis, where they generated an Ark1 Temperature Sensitive (TS) mutant, *ark1-T11* (Koch et al., 2011). The *ark1-T11* strain was generated via a PCR-based random mutagenesis approach to replace the endogenous *ark1*⁺ gene with *ark1-T11* (Koch et al., 2011). Another strain, *ark1-T8*, was also used in this Thesis (described in Section 6.3.5.1). Both strains were kindly gifted by Silke Hauf. Theoretically, at a low temperature (i.e. permissive temperature) the TS mutant protein is functional, while a rise in

temperature (i.e. restrictive temperature) ablates the function of the protein (Tan et al., 2009).

To re-examine the growth phenotype of the *ark1*-T11 and *ark1*-T8 (Section 6.3.5.1) strains for this project, the strain was grown on solid rich complete medium alongside with the wild-type *S. pombe* strain at either permissive (25°C) or restrictive (37°C) temperatures, after which colony formation and growth were compared to wild-type cells (Figure 5-1). The strains were able to form viable colonies as in the wild-type strain when grown at 25°C but not at 37°C. When mutant cells were examined by light microscopy, they were found to maintain the rod-shape as in wild-type cells but appeared longer with septa unaffected. This indicates that the *ark1*⁺ gene is not required for proliferation.

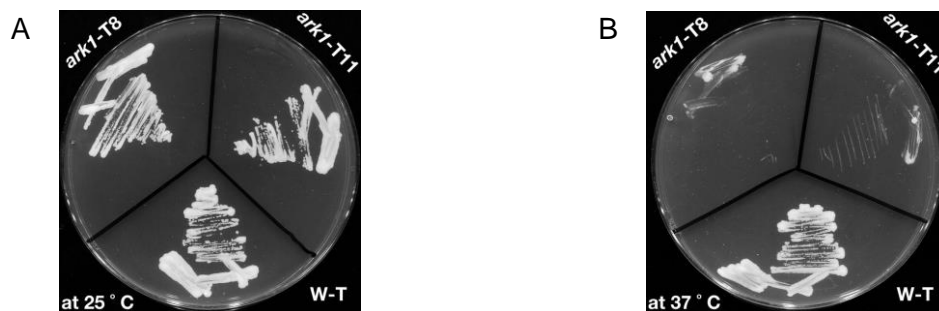


Figure 5-1 Colony growth test of *ark1*-TS mutant strains at permissive and restrictive temperatures. (A) Upon growth at the permissive temperature (25°C), a functional version of the *ark1*⁺ gene that allows growth on a rich medium is produced. (B) Upon growth at the restrictive temperature (37°C), a non-functional version of the *ark1*⁺ gene that does not support growth on a rich medium is produced. In (A) and (B), A sample of the wild-type cells was streaked alongside the *ark1*-TS cells to compare their growth.

5.3.2 A strong genetic interaction between the *mid1*⁺ and *ark1*⁺ genes

Our first aim was to examine the genetic interaction between the *ark1*⁺ and *mid1*⁺ genes. Therefore, we hypothesized that *mid1*⁺ and *ark1*⁺ genes interact to accomplish *S. pombe* cell cycle. To test for this interaction, *S. pombe* strains with either a chromosomal deletion mutation of the *mid1*⁺ gene (*mid1*Δ) as (described in Section 3.3.1) or with an *ark1*-TS mutation were utilized to generate a double mutant strain with both *mid1*Δ and *ark1*-TS mutations; this double mutant strain was, in turn, utilized to detect synthetic growth phenotypes.

To generate the *mid1* Δ *ark1*-TS double mutant strain, the two single mutant strains were crossed using an *in vivo* tetrad analysis approach (as described in Section 3.3.3) and screened for the double mutants in the progeny (Figure 5-2).

The *mid1* Δ *ark1*-TS double mutants were grown on rich media and, interestingly, they failed to form viable colonies unlike the wild-type, single *mid1* Δ and *ark1*-TS mutant strains. This indicates the presence of a striking genetic interaction between the *mid1*⁺ and *ark1*⁺ genes that is required for cell cycle progression.

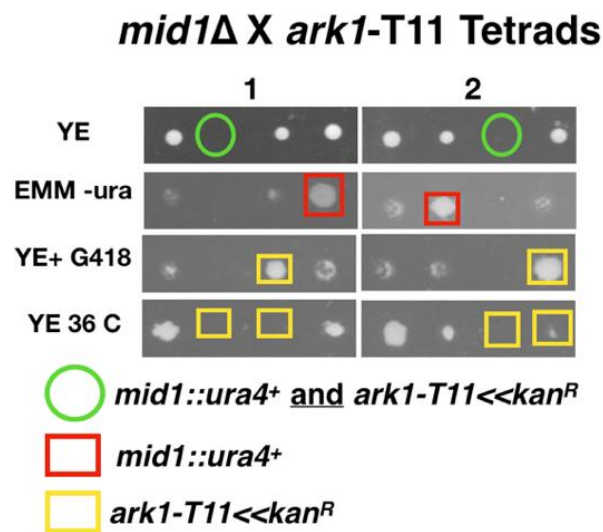


Figure 5-2 A synthetic lethal growth phenotype in the *mid1* Δ *ark1*-T11 *S. pombe* double mutant indicates a potential genetic interaction between the *mid1*⁺ and *ark1*⁺ genes. Tetrad analysis of *h⁺ ark1-T11* (*ark1-T11<<Kan^R*) crossed with *h⁻ mid1* Δ (*mid1⁺::ura⁺*) to identify *mid1* Δ *ark1*-T11 double mutants that show a synthetic lethal growth phenotype. Tetrads were performed by mating the two strains on solid ME medium (25°C) for 2 days. Tetrads were then dissected using Singer MSM Ascus Dissector and spores allowed to grow on solid YE medium (28°C) until colonies formed. Colonies were replicated to solid YE+G418/KanMX4 and EMM -ura media and incubated (28°C) to identify growth phenotypes and double mutants.

This genetic interaction might potentially be explained by a physical interaction between Mid1p and Ark1p proteins. Since Ark1p is a kinase, the resulting interaction may involve the phosphorylation of Mid1p. Therefore, our next aim was to test whether Mid1p is a substrate of Ark1p. *In vitro* phosphorylation experiments were designed to test this hypothesis using recombinant Mid1p domains purified from *E. coli*.

5.3.3 A physical interaction between Mid1p and plk1 and aurora A kinases

5.3.3.1 Design of Mid1p *in vitro* phosphorylation experiments

In Section 5.3.2, we identified an *in vivo* interaction between the *mid1*⁺ and *ark1*⁺ genes that is required for cell cycle progression in *S. pombe*. To investigate the functional relevance of this novel genetic interaction, the physical interaction of the encoded Mid1p and Ark1p proteins was investigated.

In Section 3.3.4.2, we designed *S. pombe* Mid1p recombinant proteins: "N-term", "Middle" and "C-term" domains. However, due to the unavailability of *S. pombe* Ark1p purified recombinant protein, the mammalian homologue aurora kinases were used instead to test whether they phosphorylate Mid1p domains *in vitro*.

As Mid1p is known to be a substrate of *S. pombe* Plo1p (Almonacid et al., 2011), we decided to test if mammalian plk1 is also capable of phosphorylating *S. pombe* Mid1p; therefore, we used a commercially purified recombinant human plk1 in separate *in vitro* phosphorylation experiments.

The chemistry of phospho-transfer reactions that are catalyzed by protein kinases are well understood. In these reactions, magnesium/ATP transfers its gamma (γ)-phosphate group to the active hydroxyl group (a serine, threonine or tyrosine residue) of the substrate protein. The interactions between specific kinases and substrate proteins provide the specificity of the phosphorylation reaction (Haubrich and Swinney, 2016).

In an *in vitro* phosphorylation experiment, a kinase and a potential substrate protein are incubated in the presence of a radiolabeled (γ)-phosphate (³²P-ATP). In the case of phosphorylation, the gamma phosphate is transferred to the substrate by the active kinase, and after resolving the proteins according to their size using SDS-PAGE, an autoradiograph is developed followed by detection of the radiation signal-dependent phosphorylation.

Non-specific substrates could be used to mimic the physiological activity in the phospho-transfer reaction, one such protein is the myelin basic protein (MBP) (Haubrich and Swinney, 2016). Therefore, it was used in a parallel positive control

in vitro phosphorylation experiment to test the activity of the mitotic kinases (plk1, aurora A and aurora B).

In this Chapter, we refer to the Mid1p domains ("N-term", "Middle" and "C-term") and MBP as the "substrate protein" and refer to the plk1, aurora A and B kinases as the "kinase". Three *in vitro* phosphorylation experiments were designed (Figure 5-3).

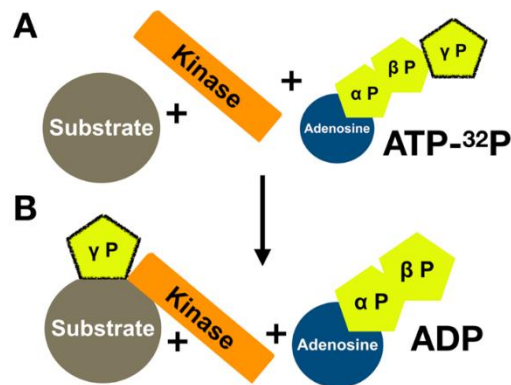


Figure 5-3 Design of *in vitro* phosphorylation experiments to test for interactions between the Mid1p domains with aurora A and B or plk1 kinases. (A) A purified "substrate protein" is incubated with a "kinase" and radiolabelled ATP-³²P. (B) In the case of a phosphorylation interaction, the "kinase" transfers the radiolabelled gamma phosphate (outlined in black) to the "substrate protein". The radiation signal is then detected and developed (discussed in detail in Chapter 2).

5.3.3.2 *In vitro* phosphorylation of the "N-term" and "Middle" domains of Mid1p by plk1 and aurora A kinases

In Section 5.3.3.1, we demonstrated the chemistry of a kinase-mediated phosphorylation reaction; based on this concept, the experiment illustrated in Figure 5-3 was used to test for the *in vitro* phosphorylation of Mid1p by mammalian recombinant purified plk1, aurora A and B kinases.

Prior to these experiments, quantification of the "substrate" proteins was carried out, and the specific activities of the kinase proteins were optimized for each reaction as described in Table 5-1.

Table 5-1 Quantification and optimization of Mid1p *in vitro* phosphorylation experiments using Mid1p "N-term", "Middle" and "C-term" recombinant proteins and plk1, aurora A and aurora B kinases.

	Concentration		Volume used in (μl) per reaction	
"Substrate"	MBP	2.5 μg	MBP	5 μl
	"N-term" Mid1p	2.5 μg	"N-term" Mid1p	5 μl
	"Middle" Mid1p	2.5 μg	"Middle" Mid1p	2.5 μl
	"C-term" Mid1p	2.5 μg	"C-term" Mid1p	5 μl
"Kinase"	plk1 Concentration: 2.32 μg/μl Specific Activity: 60 nmole/min/mg	1:100 μl (0.023 μg/μl)	plk1	1 μl
	aurora A Concentration: 0.1 μg/μl Specific Activity: 62-84 nmole/min/mg	1:10 μl (0.02 μg/2μl)	aurora A	2 μl
	aurora B Concentration: 0.1 μg/μl Specific Activity: 162-219 nmole/min/mg	1:20 μl (0.02 μg/2μl)	aurora B	2 μl
ATP- ³² P cocktail	1μ Ci/μl in kinase assay buffer (Chapter 2)		5 μl	

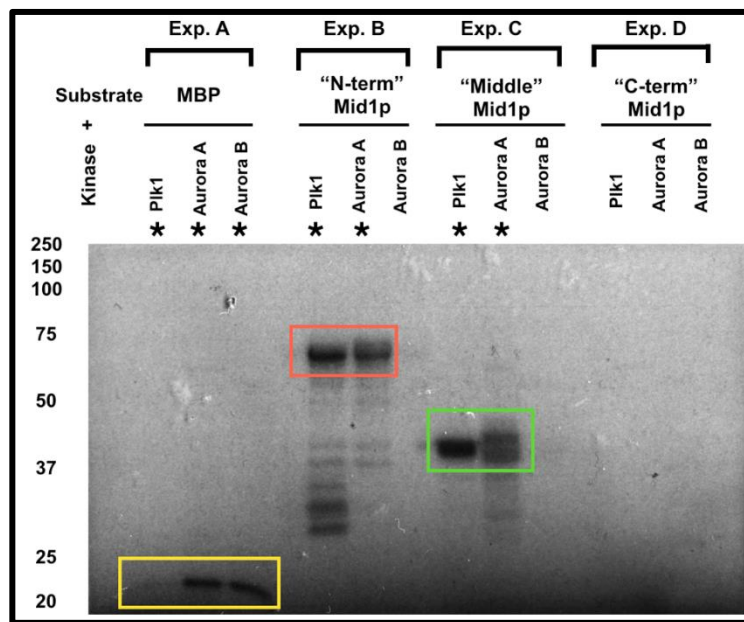


Figure 5-4 *In vitro* phosphorylation of Mid1p "N-term" and "Middle" domains by plk1 and aurora A kinases. *In vitro* phosphorylation was used to test for Mid1p physical interaction with commercially purified active plk1 and aurora kinases A and B. Recombinant GST-tagged (Mid1p domains: "N-term", "Middle" and "C-term") proteins were purified as described in Section 3.3.4.2 and used as "substrate proteins" in the *In vitro* phosphorylation assay. In Exp. A, MBP (yellow box) was used as a positive control, in Exp. B, the "N-term" domain of Mid1p was used, in Exp. C, the "Middle" domain of Mid1p and in Exp. D, the "C-term" domain of Mid1p was used as the substrate in the *in vitro* phosphorylation reactions using the indicated kinase (plk1, aurora A and aurora B). Phosphorylation signals were detected by autoradiography. Coloured boxes represent the expected protein size; the same colour code is used as in Section 3.3.4.2. An asterisk (*) represents detected *in vitro* phosphorylation signals.

The *in vitro* phosphorylation experiments were performed three times with two batches of plk1, aurora A or aurora B kinases as described in (Chapter 2) with similar results in each case; the experiment was divided into four sections (Figure 5-4):

Exp. A. MBP was used in a positive control experiment to test the activity of the kinases. *In vitro* phosphorylation by both aurora A and B kinases was clearly detected, while *in vitro* phosphorylation by Plk1 was barely detectable. **Exp. B.** A strong phosphorylation signal was detected in the "N-term" Mid1p domain by plk1 and aurora A reactions, while no such signal was detected in the "N-term"/aurora B reaction. **Exp. C.** A strong phosphorylation signal was detected in the "Middle"

Mid1p domain by plk1 and aurora A reactions, while no such signal was detected in the "Middle"/aurora B reaction. **Exp. D.** No phosphorylation signal was detected in the "C-term" Mid1p domain by any of the three kinases plk1, aurora A, or aurora B.

The results described in Figure 5-4 indicate the *in vitro* phosphorylation of the "N-term" and "Middle" domains of Mid1p by plk1 and aurora A kinases, while the "C-term" domain of Mid1p was not phosphorylated by any of the three protein kinases (plk1, aurora A and B).

Following detection of the above-mentioned *in vitro* phosphorylation, two experiments described in Sections 5.3.3.3 and 5.3.3.4, respectively, were designed to determine Mid1p potential phospho-sites as follows:

First, stoichiometric quantification of the *in vitro* phosphorylation reactions was carried out to determine the amount of ^{32}P incorporated in each reaction in comparison with the amount of the substrate protein present in each reaction.

Second, an *in vitro* mass spectrometry analysis was carried out to generate a plk1/aurora A phospho-site map of the "N-term" and "Middle" domains of Mid1p.

5.3.3.3 Mid1p "N-term" and "Middle" domains *in vitro* phosphorylation stoichiometric analysis

To determine the stoichiometry of the boxed reactions shown in Figure 5-4, we developed an approach depending on the presence of a known concentration of radioactive ^{32}P . This aimed at determining the number of pmoles of ^{32}P that were incorporated into a known amount of substrate protein (i.e. determining the pmoles of ^{32}P : pmoles of substrate protein ratio). To achieve this, a 1 pmole ^{32}P standard was included in the *in vitro* phosphorylation experiment and was used as a reference for the radiation signal intensity.

It is worth noting that the specific activity of plk1 and aurora A kinases was initially different. To overcome this issue, the *in vitro* phosphorylation experiments were optimized, using an approach similar to the one described in Table 5-1 (data not shown).

The *in vitro* phosphorylation stoichiometric analysis was performed as described in (Chapter 2), and the results are shown in Figure 5-5.

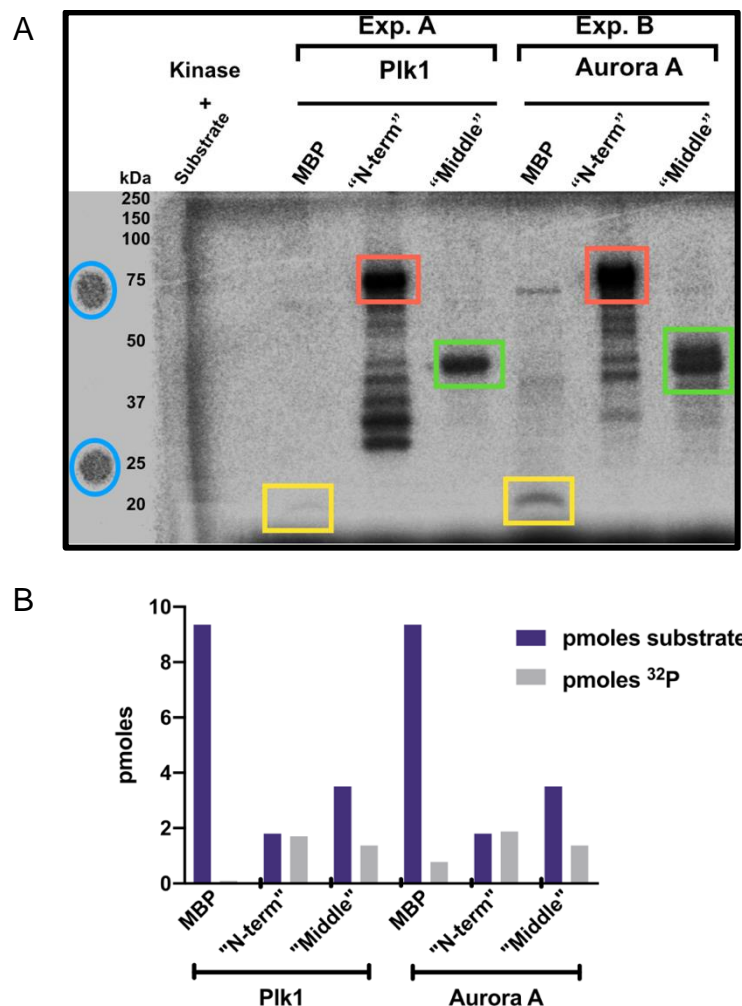


Figure 5-5 Stoichiometric analysis of Mid1p *in vitro* phosphorylation by plk1 and aurora A kinases. (A) An *in vitro* phosphorylation experiment was designed to determine the number of ³²P pmoles incorporated in either MBP or the "N-term" and "Middle" domains of Mid1p by plk1 (In Exp. A) and aurora A (In Exp. B) kinases. Coloured boxes represent the expected protein size; the same colour code is used as in Section 3.3.4.2. The phosphorylation signal detected at ~18 kDa belongs to MBP. Yellow circles represent the 1 pmole ³²P standard at positions 75 and 25 kDa of the protein marker. Phosphorylation signals were detected by phosphor-imaging and quantified using ImageJ software. (B) The stoichiometry of each reaction was quantified using LICOR imaging to determine the number of pmoles of the ³²P incorporated by the kinase into a known amount of the recombinant protein using Image J.

The *in vitro* phosphorylation stoichiometric analysis described in Figure 5-5; Panel B was carried out using Image J software as described in Chapter 2 to yield the ratio of (the number of moles of ³²P incorporated: the number of moles of substrate protein) (Table 5-2).

Table 5-2 Mid1p "N-term", "Middle" and MBP *in vitro* phosphorylation stoichiometric analysis.

"Substrate" + "Kinase"	Conc. of Substrate (μ g)	Conc. of Substrate (pmoles) (A)	Conc. of incorporated 32 P (pmoles) (B)	Ratio (A: B)
MBP+ plk1	2.5	9.35	0.092	1:0.009
"N-term" Mid1p + plk1	2.5	1.8	1.7	1:0.9
"Middle" Mid1p + plk1	2.5	3.5	1.37	1:0.4
MBP+ aurora A	2.5	9.35	0.78	1:0. 009
"N-term" Mid1p + aurora A	2.5	1.8	1.8	1:1
"Middle" Mid1p + aurora A	2.5	3.5	1.37	1:0.4

Four conclusions could be drawn from the statistical analysis represented in Figure 5-5, Panel B and the ratios summarized in Table 5-2, as follows:

First, the "N-term" domain of Mid1p is *in vitro* phosphorylated by plk1 kinase with a ratio of 1:0.9, meaning that for every 1 pmole of protein, 0.9 pmoles of 32 P are incorporated indicating a high efficiency of phosphorylation.

Second, the analysis revealed that the "N-term" domain of Mid1p is *in vitro* phosphorylated by aurora A kinase with a ratio of 1:1, meaning that for every 1 pmole of protein, 1 pmoles of 32 P are incorporated indicating a high efficiency of phosphorylation.

Third, the "Middle" domain of Mid1p is *in vitro* phosphorylated by plk1 kinase with a ratio of 1:0.4, meaning that for every 1 pmole of protein, 0.4 pmoles of 32 P are incorporated indicating a good efficiency of phosphorylation.

Fourth, the "Middle" domain of Mid1p is *in vitro* phosphorylated by aurora A kinase with a ratio of 1:0.4, meaning that for every 1 pmole of protein, 0.4 pmoles of ^{32}P are incorporated indicating a good efficiency of phosphorylation.

All four conclusions suggest that plk1 and aurora A kinases have potential phospho-site/s within the "N-term" and "Middle" domains of Mid1p. Therefore, we decided to identify these potential phospho-sites using an *in vitro* mass spectrophotometry approach.

As mentioned earlier, the source of plk1 and aurora A kinases used in the *in vitro* phosphorylation experiments was mammalian cells, while the Mid1p used in the experiments derived from *S. pombe*. Therefore, the above conclusions do not confirm that Mid1p is a substrate of Ark1p, but rather could be used as an initial indicator if such an interaction occurs; further work involving the use of the endogenous *S. pombe* Ark1p in the *in vitro* phosphorylation experiments with the Mid1p domains is required to confirm this *in vitro* phosphorylation event.

5.3.3.4 Mid1p "N-term" and "Middle" domains phospho-sites determination

In Section 5.3.3, we demonstrated the presence of potential Mid1p phospho-site/s for plk1 and aurora A kinases phosphorylation. To further explore this aspect, an *in vitro* mass spectrophotometry approach was applied to identify the potential phospho-sites. Two experiments were designed to confirm the identified potential phospho-sites as follows:

An *in vitro* phosphorylation experiment was designed by generating phospho-resistant mutants of the Mid1p "N-term" and "Middle" domains and testing the effect of these mutations on their *in vitro* phosphorylation by plk1 and aurora A kinases (Sections 5.3.4 and 5.3.5).

An *in vivo S. pombe* integration experiment was designed by generation phospho-mimetic/resistant versions of the full length *mid1*⁺ gene to replace the endogenous *mid1*⁺ gene; the functional relevance of these phospho-sites on Mid1p was then determined (Chapter 6).

To complete these two experiments, a phospho-protein mapping service offered by the University of Dundee was used to determine the sites of phosphorylation as follows:

First, the full amino acid sequence of Mid1p "N-term" and "Middle" domains, including the GST tag used for purifying the recombinant proteins, was provided to the facility; then the amount of protein was determined through SDS-PAGE resolving both the "N-term" and "Middle" domains of Mid1p.

Second, the "N-term" and "Middle" domains of Mid1p detected gel bands were excised and processed by alkylation, trypsin digestion, and extraction of the peptides. The extracted peptides were then subjected to Nano-scale liquid chromatographic tandem mass spectrometry (nLC-MS/MS).

Third, the database searching for protein identification was applied using the Proteome Discoverer software and the Mascot engine; then the final output was presented as annotated phosphorylation sites. We used this information to generate a Mid1p phospho-site map (Figure 5-6).

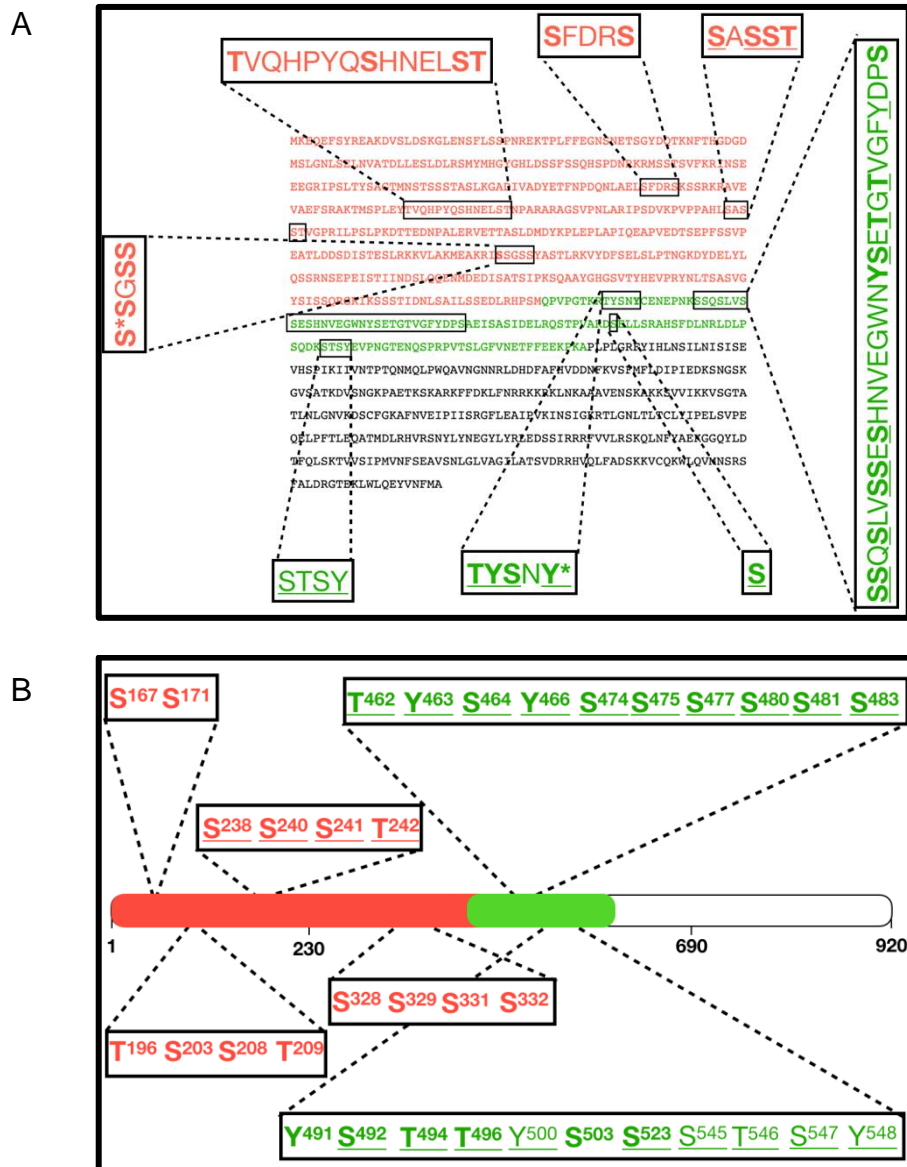


Figure 5-6 Mid1p "N-term" and "Middle" domains have potential plk1 and aurora A kinases phospho-sites. (A) The full-length amino acid sequence of Mid1p with the "N-term" and "Middle" domains showed in different colours. The highlighted peptides include potential phospho-sites for either plk1 kinase (Bold), aurora A kinase (Underlined) or both kinases (Bold and Underlined), which were identified by the mass spectrometry analysis. (B) A phospho-sites map of Mid1p was generated from panel (A) including the 35 residues numbered.

The above analysis resulted in the identification of 35 potential Mid1p phospho-sites of either plk1 and/or aurora A kinases (Figure 5-6). Due to financial and time constraints, confirmation of all of these sites was not possible; therefore, the next step was to narrow down the number of potential sites to allow for further analysis. Between 2011 and 2018, several important research studies concerned with

investigating the fission yeast phospho-proteome have emerged (Carpy et al., 2014). Most of these studies used a st_ab_il_e is_ot_op_e la_be_li_ng by am_in_o ac_id in ce_ll culture (SILAC) approach. We selected four studies which were concerned with studying the *S. pombe* global proteome. These studies presented total *S. pombe* proteome phosphorylation events; furthermore, they all identified several Mid1p specific phospho-sites.

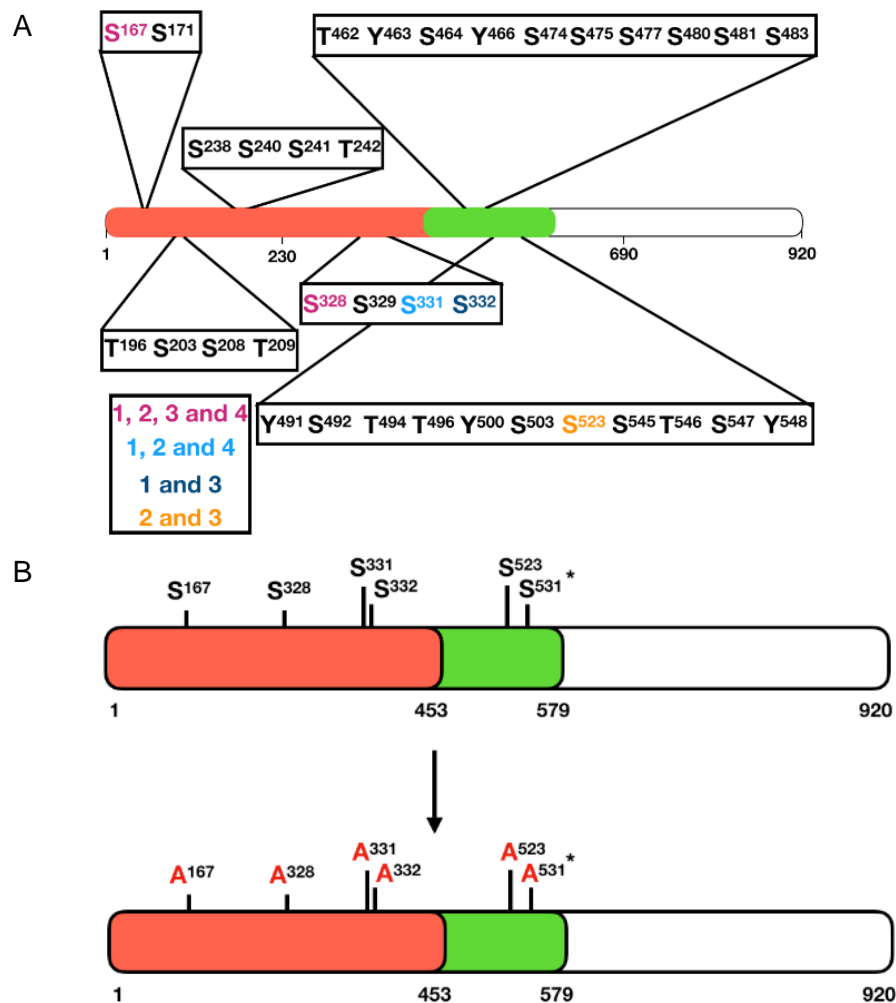


Figure 5-7 Comparison of Mid1p potential phospho-sites from published studies and mass-spectrometry analysis presented in this Thesis. Mass spectrometry analysis identified 35 potential phospho-sites of Mid1p from the *in vitro* phosphorylation reaction of the "N-term" and "Middle" domains of Mid1p by plk1 and aurora A kinases. (A) A Mid1p phospho-sites map was generated from the comparison of the 35 identified phospho-sites in this analysis with the Mid1p phospho-sites identified in four global proteomic studies. (B) To confirm the five phospho-sites of Mid1p described in panel (A), phospho-resistant "N-term" and "Middle" Mid1p domains were designed by the conversion of each (S) serine residue into an (A) alanine residue. An Asterisk (*) shows a sixth phospho-site that was added (discussed in detail in Chapter 7).

The phospho-sites map (Figure 5-7, Panel A) represents a total number of six potential phospho-sites distributed along the "N-term" and "Middle" Mid1p sequence, five of which were identified in this study and the sixth was added.

Four of the phospho-sites were within the Mid1p "N-term" domain and the other two were within the Mid1p "Middle" domain. The six phospho-sites were utilized to confirm the *in vitro* phosphorylation of Mid1p "N-term" and "Middle" domains.

To confirm the phospho-sites shown in (Figure 5-7, Panel B), an *in vitro* phosphorylation experiment involving the generation of phospho-resistant mutants of the "N-term" and "Middle" domains of Mid1p was carried out. These new recombinant proteins were expressed and purified using the same method as described earlier in (Section 3.3.4.2).

In this Chapter, the Mid1p "N-term" domain phospho-sites analysis is described in Section 5.3.4, whereas the Mid1p "Middle" domain phospho-sites analysis is described in Section 5.3.5.

5.3.4 Mid1p "N-term" domain phospho-sites confirmation

5.3.4.1 Design of Mid1p "N-term" domain phospho-resistant mutants

As demonstrated in (Figure 5-7, Panel B), we designed Mid1p "N-term" domain phospho-resistant mutants based on the conversion of the serine residues to alanine residues. Therefore, recombinant proteins of the single mutants ("N-term" A167), ("N-term" A328), ("N-term" A331), ("N-term" A332), and the multiple mutant ("N-term" A167, A328, A331, A332) were designed to be bacterially expressed, then purified and introduced to an *in vitro* phosphorylation experiment with plk1 and aurora A kinases as described in Figure 5-8.

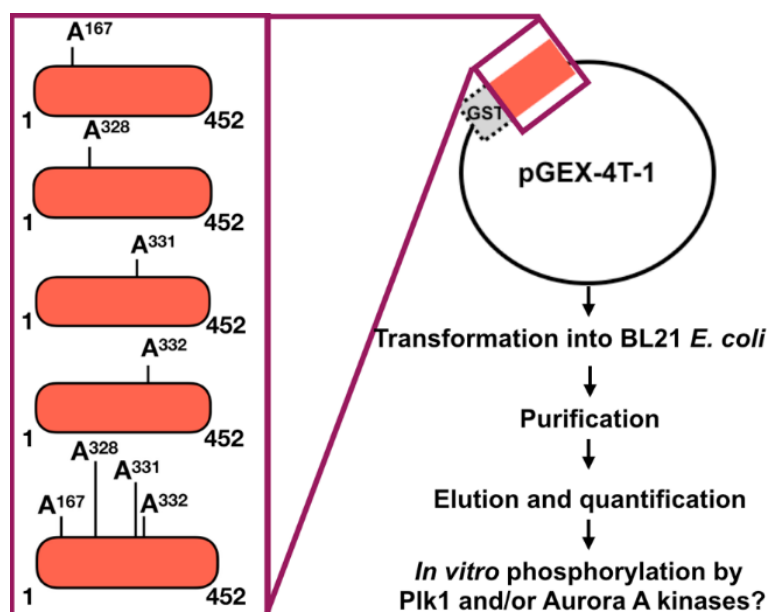


Figure 5-8 Design of Mid1p "N-term" domain phospho-resistant mutants to confirm its *in vitro* phosphorylation. Recombinant GST-tagged Mid1p "N-term" domain phospho-resistant mutants were expressed in BL21 *E. coli*, followed by purification (data shown in Section 5.3.4.2), elution and quantification (data shown in Section 5.3.4.3) of proteins. The eluted proteins were subjected to *in vitro* phosphorylation experiments with plk1 and aurora A kinases (data shown in Figure 5-10).

5.3.4.2 Purification of Mid1p "N-term" domain phospho-resistant mutants

The five GST-tagged Mid1p "N-term" (aa 1-452) phospho-resistant recombinant proteins were expressed in BL21 *E. coli* and their production was induced by the addition of IPTG (discussed in detail in Chapter 2). After expression and induction, the five proteins were purified by affinity binding to GST-sepharose beads as described in Figure 5-9.

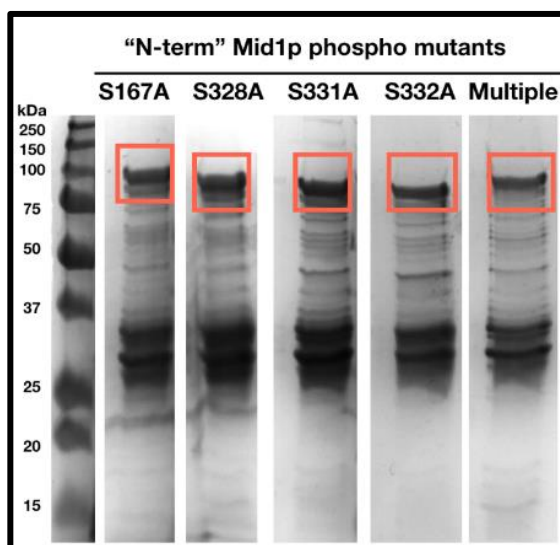


Figure 5-9 Purification of the GST-tagged Mid1p "N-term" domain phospho-resistant mutants. To confirm the *in vitro* phosphorylation of Mid1p "N-term" domain by plk1 and aurora A kinases, phospho-resistant mutants were designed depending on the identified phospho-sites as described in Section 5.3.3.4 resulting in the generation and purification of five recombinant proteins (1) A167, (2) A328, (3) A331, (4) A332 and (5) A167, A328, A331, A332. All five recombinant proteins of 76 kDa were detected by SDS-PAGE and are indicated by coloured boxes; the same colour code is used as in Section 3.3.4.2. The species at ~25 kDa is likely to be GST.

5.3.4.3 *In vitro* phosphorylation of Mid1p "N-term" domain phospho-resistant mutants by plk1 and aurora A kinases

In this Section we describe the *in vitro* phosphorylation experiments of these purified proteins with both plk1 and aurora A kinases. Prior to the *in vitro* phosphorylation experiments, quantification of the substrate proteins was carried out. The five recombinant proteins shown in (Figure 5-9) were eluted from the GST-Sepharose beads (data not shown). A ladder of proteins is observed in each one of the five proteins; this could be due to the degradation of the protein into smaller size fragments. The aim of the *in vitro* phosphorylation experiments described in this Section was to compare the phosphorylation level of the original Mid1p "N-term" domain (boxed in Section 5.3.3.2) by plk1 and aurora A kinases and the phosphorylation level of the Mid1p "N-term" domain phospho-resistant single and multiple mutants.

The *in vitro* phosphorylation experiments were performed and as described in Section 5.3.3.2; the experiment was divided into two sections: the first section aimed to test for *in vitro* phosphorylation by aurora A kinase (Figure 5-10, Exp. A) and the second aimed to test for *in vitro* phosphorylation by plk1 kinase (Figure 5-10, Exp. B). In both experiments MBP was used as a positive control to test the kinase activity.

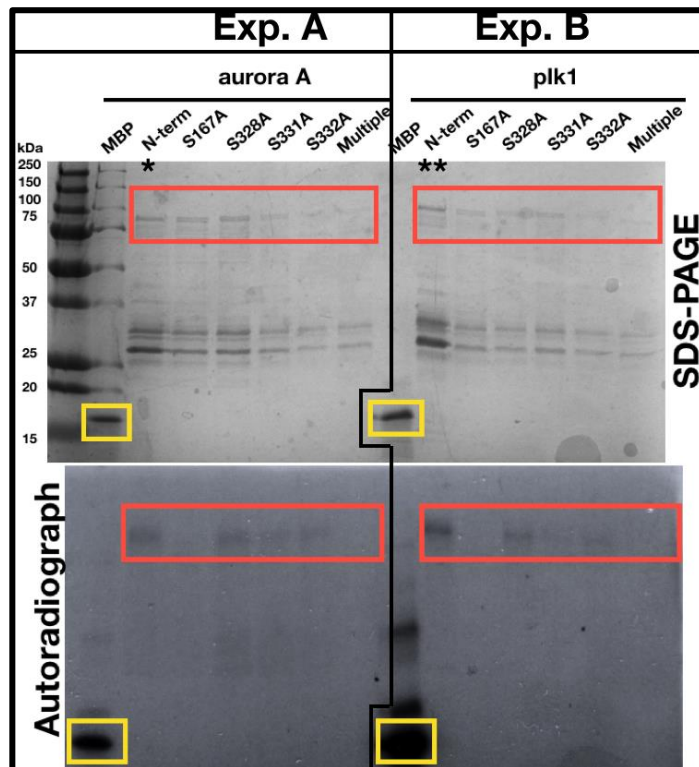


Figure 5-10 *In vitro* phosphorylation of Mid1p "N-term" phospho-resistant mutants by plk1 and aurora A kinases. To confirm the *in vitro* phosphorylation of Mid1p " N-term" domain by plk1 and aurora A kinases, the two potential phospho-sites were mutated and led to designing three GST-tagged recombinant proteins with Mid1p " N-term" domain phospho-resistant mutations. The *in vitro* phosphorylation experiment was carried out as described in Figure 5-4. The original Mid1p " N-term" domain recombinant protein was used as a positive control parallel experiment.

In Exp. A, aurora A kinase was used. The S167A and "N-term" multiple reactions showed a reduced level of phosphorylation when compared to the " N-term" domain phosphorylation (*). In Exp. B, plk1 kinase was used. The S167A and " N-term" multiple reactions showed a reduced level of phosphorylation when compared to the " N-term" domain phosphorylation (**). Detected protein species are colour coded as follows: MBP in yellow and all Mid1p " N-term"-related species in green. " Multiple" indicates a mutation in both four single phospho-sites.

As expected, the original Mid1p "N-term" domain *in vitro* phosphorylation signal detected in the case of plk1 and aurora A kinases was similar to the one detected in Section 5.3.3.2, Figure 5-4. A decrease in phosphorylation signal was expected in the case of all/ or some phospho-resistant "N-term" mutants as a result of having the point mutations of serine residues converted to the non-phosphorylatable alanine residues. S167A, S331A and "N-term Multiple" mutants showed a decreased level of phosphorylation signal by plk1 and aurora A kinases; however, Surprisingly, the level of *in vitro* phosphorylation of S328A generated by both plk1 and aurora A and that of S332A generated by plk1 was similar to that level observed in the original Mid1p "N-term" domain reaction generated by plk1 and aurora A kinases (Section 5.3.3.2).

5.3.5 Mid1p "Middle" domain phospho-sites confirmation

5.3.5.1 Design of Mid1p "Middle" domain phospho-resistant mutants

Following the detection of an *in vitro* phosphorylation interaction of Mid1p "Middle" domain by plk1 and aurora A kinases, we carried out a series of experiments to determine Mid1p potential phospho-sites; this resulted in the determination of four sites within the "N-term" domain of Mid1p (S167, S328, S331 and S332) and two sites within the "Middle" domain of Mid1p (S523 and S531). The two later phospho-sites are potential sites for aurora A kinase phosphorylation.

We designed Mid1p "Middle" domain phospho-resistant mutants based on the conversion of the serine residues to alanine residues. Therefore, recombinant proteins of the single mutants ("Middle" A523), ("Middle" A531) and the multiple mutant ("Middle" A523 and S531) were designed to be bacterially expressed (Figure 5-11), then purified and introduced to an *in vitro* phosphorylation experiment with plk1 and aurora A kinases.

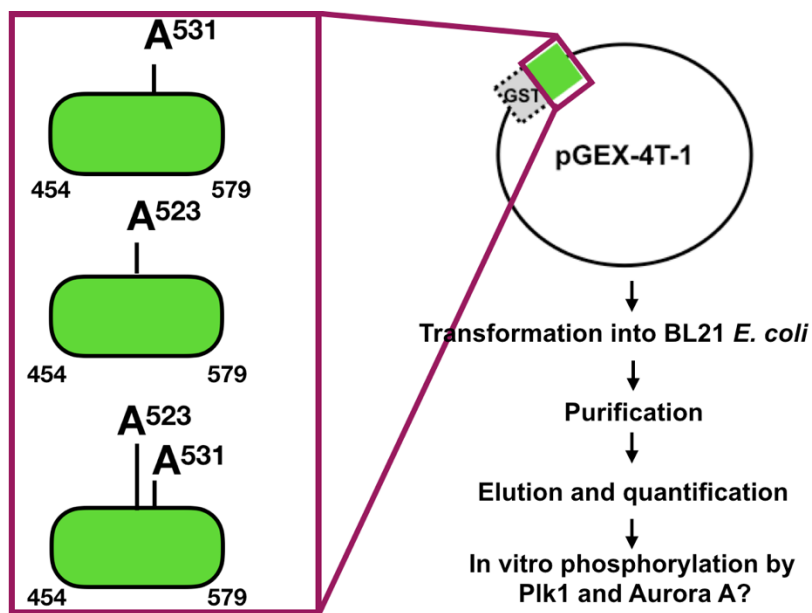


Figure 5-11 Design of Mid1p "Middle" domain phospho-resistant mutants to confirm its *in vitro* phosphorylation. Recombinant GST-tagged Mid1p "Middle" domain phospho-resistant mutants were expressed in BL21 *E. coli*, followed by purification (data shown in Section 5.3.5.2), elution and quantification (data shown in Section 5.3.5.3) of proteins. The eluted proteins were subjected to *in vitro* phosphorylation experiments with plk1 and aurora A kinases.

5.3.5.2 Purification of Mid1p "Middle" domain phospho-resistant mutants

The three GST-tagged Mid1p "Middle" (aa 453-578) phospho-resistant recombinant proteins were expressed in BL21 *E. coli* and their production was induced by the addition of IPTG (Chapter 2). After expression and induction, the proteins were purified by affinity binding to GST-sepharose beads as described in Figure 5-12.

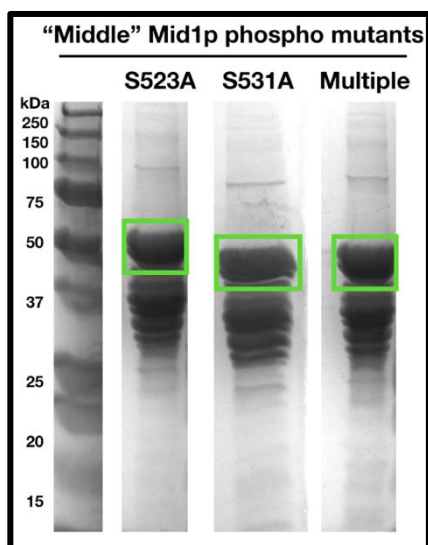


Figure 5-12 Purification of GST-tagged Mid1p "Middle" domain phospho-resistant mutants. To confirm the *in vitro* phosphorylation of Mid1p "Middle" domain by plk1 and aurora A kinases, phospho-resistant mutants were designed depending on the identified phospho-sites as described in Section 5.3.3.4 resulting in the generation and purification of three recombinant proteins (A) A523, (B) A531 and (C) A523 and A531. All three recombinant proteins show a dominant band at 40-60 kDa in panels (A), (B) and (C). Green boxes represent the detected protein size. M: Protein marker, L: lysate, F: flow through, W1-3: three washes and B: purified protein bound to GST-sepharose beads. The species at ~25 kDa is likely to be GST.

The expected size of the three recombinant proteins was 40 kDa; however, a short ladder of bands appeared in the case of each of the three proteins with a predominant protein of 40-60 kDa in size. Thus, the purified protein was not confirmed to be Mid1p "Middle" domain. In Chapter 8, this issue is addressed and discussed in detail.

5.3.5.3 *In vitro* phosphorylation of Mid1p "Middle" domain phospho-resistant mutants

In this Section we describe the *in vitro* phosphorylation experiments of these purified proteins with both plk1 and aurora A kinases. Prior to the *in vitro* phosphorylation experiments, quantification of the "substrate proteins" was carried out as described in Section 5.3.3.2. The three recombinant proteins shown in the Figure above were eluted from the GST-Sepharose beads (data not shown) prior to their quantification. A ladder of bands is observed in each one of the three proteins; this could be due to the degradation of the protein into smaller size

fragments. The aim of the *in vitro* phosphorylation experiments described in this Section was to compare the phosphorylation level of the original Mid1p "Middle" domain (boxed in Section 5.3.3.2) by plk1 and aurora A kinases and the phosphorylation level of the Mid1p "Middle" domain phospho-resistant single and multiple mutants.

The *in vitro* phosphorylation experiments were performed as described in Section 5.3.3.2; the experiment was divided into two Sections: the first Section aimed to test for *in vitro* phosphorylation by aurora A (Figure 5-13, Panel A) and the second aimed to test for *in vitro* phosphorylation by plk1 (Figure 5-13, Panel B).

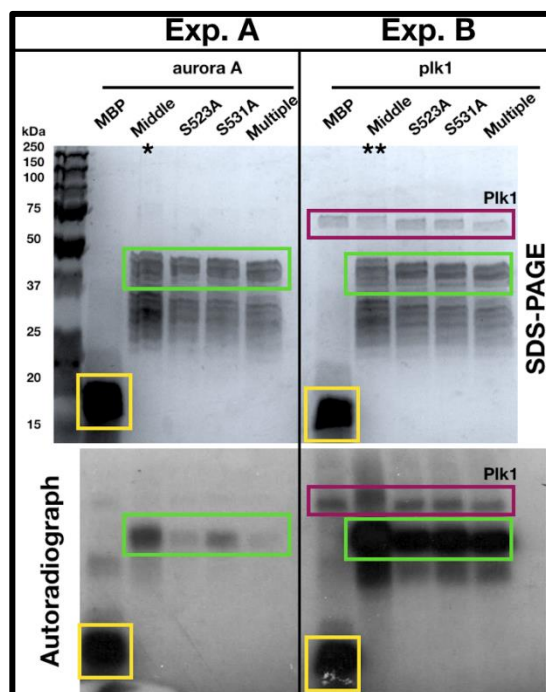


Figure 5-13 *In vitro* phosphorylation of Mid1p "Middle" phospho-resistant mutants by plk1 and aurora A kinases. To confirm the *in vitro* phosphorylation of Mid1p "Middle" domain by plk1 and aurora A kinases, the two potential phospho-sites were mutated and led to designing three GST-tagged recombinant proteins with Mid1p "Middle" domain phospho-resistant mutations. The *in vitro* phosphorylation experiment was carried out as described in Figure 5-4. The original Mid1p "Middle" domain recombinant protein was used as a positive control parallel experiment. In Exp. A, aurora A kinase was used. The S523A and "Middle" multiple reactions showed a reduced level of phosphorylation when compared to the "Middle" domain phosphorylation (*). In Exp. B, plk1 kinase was used. All S523A, S531A and "Middle" multiple reactions showed a high level of phosphorylation when compared to the "Middle" domain phosphorylation (**). Detected protein species are colour coded as follows: plk1 in purple, MBP in yellow and all Mid1p "Middle"-related species in green. "Multiple" indicates a mutation in both two single phospho-sites.

As expected, the Mid1p "Middle" domain *in vitro* phosphorylation signal detected in the case of plk1 and aurora A kinases was similar to the one detected in Section 5.3.3.2, Figure 5-4. However, no such signal was detected in the Mid1p "Middle" domain phospho-resistant mutants "A523", "A531" and "Middle Multiple". This could be due to the low concentration used in the reaction (~0.5 µg) in comparison with the concentration used in the Mid1p "Middle" original reaction (~2.5 µg).

5.4 Conclusions

In this Chapter, we combined an *in vivo S. pombe* genetic approach and *in vitro* phosphorylation experiments to investigate the regulation of Mid1p by the aurora kinase Ark1p. Our main two findings are:

First, we illustrated the presence of a striking genetic interaction between the *mid1⁺* and *ark1⁺* genes, with *mid1Δ ark1-T11* double mutant cells synthetically lethal.

Second, we detected an *in vitro* phosphorylation interaction between Mid1p and both mammalian plk1 and aurora A kinases. Our results could not confirm this interaction; therefore, we designed *in vivo S. pombe* experiments to further investigate this interaction (discussed in detail in the next Chapter).

Combined, these two findings lead to the hypothesis that Mid1p is regulated by Ark1p during *S. pombe* cell cycle. This hypothesis will be further investigated in the next Chapter where the effect of mutations of the potential Mid1p phospho-sites on *S. pombe* cell morphology phenotypes will be examined *in vivo*.

Chapter 6 Investigation into Mid1p regulation by Ark1p through *in vivo* *S. pombe* analyses

6.1 Introduction

6.1.1 Aurora kinases play important roles in mammalian cell cycle regulation

During eukaryotic mitosis, the microtubule organizing centre (MTOC) is divided into two separate MTOCs, with each one generating a microtubule array. Interdigitation of these arrays leads to the assembly of the bipolar mitotic spindle (Wittmann et al., 2001). As this spindle assembles, the chromosomes are condensed and are attached to the spindle through their kinetochores, after which the chromosomes are segregated and located at either pole (Nasmyth et al., 2000). Cytokinesis is established after genome separation leading to the separation of the two daughter cells. Execution of mitosis and cytokinesis requires the action of mitotic kinases including the aurora family of kinases (Nigg, 2001).

Although the function and localization of the aurora kinases differ throughout the cell cycle, the structure of aurora A, B and C is highly conserved (Marumoto, Zhang and Saya, 2005). Aurora A expression and kinase activity are elevated during late G2 to M-phase (Marumoto, Zhang and Saya, 2005). In fact, aurora A was found to have a specific role in centrosome maturation in the model organisms *C.elegans* (Hannak et al., 2001) and *D. melanogaster* (Berdnik and Knoblich, 2002). Additionally, aurora A depletion causes inhibition of the centrosome maturation process in human cells (Hirota et al., 2003).

6.2 Aims

The *in vivo* and *in vitro* analyses described in Sections 5.3.2 and 5.3.3, respectively, suggest the regulation of Mid1p by Ark1p; this encouraged us to further investigate the potential interaction of the encoded Mid1p and Ark1p.

Therefore, we hypothesized that the Mid1p potential s identified by mass spectrometry are required for the function of Mid1p and are important for the regulation of *S. pombe* cell cycle.

The major aim of this Chapter was therefore to investigate the functional relevance of two Mid1p potential phospho-sites and the requirement of Ark1p for the normal localization of Mid1p during *S. pombe* cell cycle. The following specific aims were addressed:

- Generation of *mid1* phospho-resistant/mimetic gene versions by an *in vitro* gene synthesis approach
- Integration of the *mid1* phospho-resistant/mimetic gene versions into *mid1* Δ *S. pombe* cells via an *in vivo* integration approach, and characterization of cell morphology phenotypes of the resultant *S. pombe mid1* phospho-mutant strains
- Crossing of the *mid1* phospho-resistant/mimetic gene versions into *ark1*-T11 *S. pombe* by tetrad analysis, and characterization of cell morphology phenotypes of the resultant *S. pombe* strains
- Determination of the cellular localization of Mid1p in *ark1*-T8 and *ark1*-T11 *S. pombe* cells using an *in vivo* microscopic approach.

6.3 Results

6.3.1 *In vitro* phosphorylation experiments of Mid1p by plk1 and aurora kinases yielded six potential Mid1p phospho-sites

This research was concerned with investigating the regulation of Mid1p throughout the cell cycle of *S. pombe*. In Chapter 5, we investigated the regulation of Mid1p by Plo1p (plk1) and Ark1p (aurora) kinases.

A genetic interaction between the *plo1*⁺ and *mid1*⁺ genes has been previously detected (Bähler et al., 1998); in Section 5.3.2, we detected a similar *in vivo* genetic interaction between the *ark1*⁺ and *mid1*⁺ genes. Therefore, we hypothesized that Ark1p phosphorylates Mid1p to regulate its function during the cell cycle of *S. pombe*.

We successfully detected the *in vitro* phosphorylation of Mid1p "N-term" and "Middle" domains by mammalian plk1 and aurora A kinases. Following this, mass spectrometry analysis was performed on our behalf to determine Mid1p potential phospho-sites, and such analysis identified 35 phospho-sites for potential *in vitro* phosphorylation by plk1 and/or aurora A kinases. Comparison of these 35 phospho-sites with the Mid1p phospho-sites identified in four independent *S. pombe* global proteomic studies yielded six Mid1p phospho-sites as summarized in Table 6-1.

The next step was to confirm the *in vitro* phosphorylation of the six Mid1p phospho-sites by designing the same *in vitro* phosphorylation experiments with Mid1p phospho-resistant mutants replacing the original Mid1p domain. As these experiments were inconclusive, we investigated these potential phospho-sites using a different approach by designing *S. pombe in vivo* integration experiments.

In this Chapter, we describe the *in vivo* analysis of Mid1p potential phospho-sites, and the *in vivo* localization of Mid1p in *ark1* mutant strains.

Table 6-1 A summary of Mid1p phospho-sites for potential *in vitro* phosphorylation by plk1 and/or aurora A kinases

Phospho-site	Mid1p domain	Mutation	relevant kinase	References
S167	"N-term"	S167A	plk1	<ul style="list-style-type: none"> – This analysis – Koch et al., 2011 – Carpy et al., 2014 – Kettenbach et al., 2015 – Swaffer et al., 2018
S328	"N-term"	S328A	plk1	<ul style="list-style-type: none"> – This analysis – Koch et al., 2011 – Carpy et al., 2014 – Kettenbach et al., 2015 – Swaffer et al., 2018
S331	"N-term"	S331A	plk1	<ul style="list-style-type: none"> – This analysis – Koch et al., 2011 – Carpy et al., 2014 – Swaffer et al., 2018
S332	"N-term"	S332A	plk1	<ul style="list-style-type: none"> – This analysis – Koch et al., 2011 – Kettenbach et al., 2015
S523	"Middle"	S523A	plk1 and/or aurora A	<ul style="list-style-type: none"> – This analysis – Carpy et al., 2014 – Kettenbach et al., 2015
S531	"Middle"	S531A	None	<ul style="list-style-type: none"> – Kettenbach et al., 2015 – Swaffer et al., 2018

6.3.2 Investigating the functional relevance of the Mid1p S523 and S531 potential phospho-sites

6.3.2.1 An *in vivo* *S. pombe* integration approach

The integration experiments mentioned in Section 6.3.1 involved introducing single or combination mutations of the six potential phospho-sites on the *mid1* gene to yield either phospho-mimetic - by converting serine (S) to aspartic acid (D)- or phospho-resistant -by converting serine (S) to alanine (A)- versions of the gene.

pJK148 is a popular *S. pombe* integrative plasmid that can be used to integrate DNA sequences into the *leu1*⁺ chromosome locus. The plasmid is first linearized and then transformed into an *S. pombe* strain with a point mutation in the *leu1*⁺ gene, followed by prototrophy selection (Siam, Dolan and Forsburg., 2004). We used this approach to produce *S. pombe* strains with phospho-mimetic/resistant versions of the *mid1* gene to test the effect of such mutations on Mid1p function through examining cell morphology.

All 19 versions (1-13: single mutants; 14-19: mutants in combination) of the *mid1*⁺ gene were designed to have the *mid1*⁺ endogenous promoter and 1 kbp upstream of *mid1*⁺ reading frame and were synthesized by GenScript.

Following the successful integration of all the *mid1* mutant genes (1-19) - summarized in Table 6-2- into *mid1* Δ *S. pombe* (GG 1129) as schematically described in Figure 6-1, the strains were subjected to an *in vivo* microscopy analysis (Chapter 2).

Due to time constricts, the results presented throughout this Chapter describe the functional analysis of only two Mid1p potential phospho-sites, S523 and S531.

Table 6-2 A summary of the phospho-mimetic/resistant mutant versions of the *mid1* gene integrated into *mid1* Δ *S. pombe* for the *in vivo* microscopy analysis presented in Section 6.3.2.3. The *S. pombe* strains were generated by Christopher McInerny and given a yeast collection (GG) number. S: serine, A: alanine, D: aspartic acid.

Strain/ GG No.	1	2	3	4	5	6	7	8	9	10	11	12	13	14	15	16	17	18	19
	3181	3267	3271	3275	3279	3283	3287	3291	3295	3185	3189	3193	3197	3299	3303	3201	3205	3307	3311
Mid1p 167	S	A	D	S	S	S	S	S	S	S	S	S	S	A	D	S	S	A	D
Mid1p 328	S	S	S	A	D	S	S	S	S	S	S	S	S	A	D	S	S	A	D
Mid1p 331	S	S	S	S	S	A	D	S	S	S	S	S	S	A	D	S	S	A	D
Mid1p 332	S	S	S	S	S	S	S	A	D	S	S	S	S	A	D	S	S	A	D
Mid1p 523	S	S	S	S	S	S	S	S	S	A	D	S	S	S	S	A	D	A	D
Mid1p 531	S	S	S	S	S	S	S	S	S	S	S	A	D	S	S	A	D	A	D

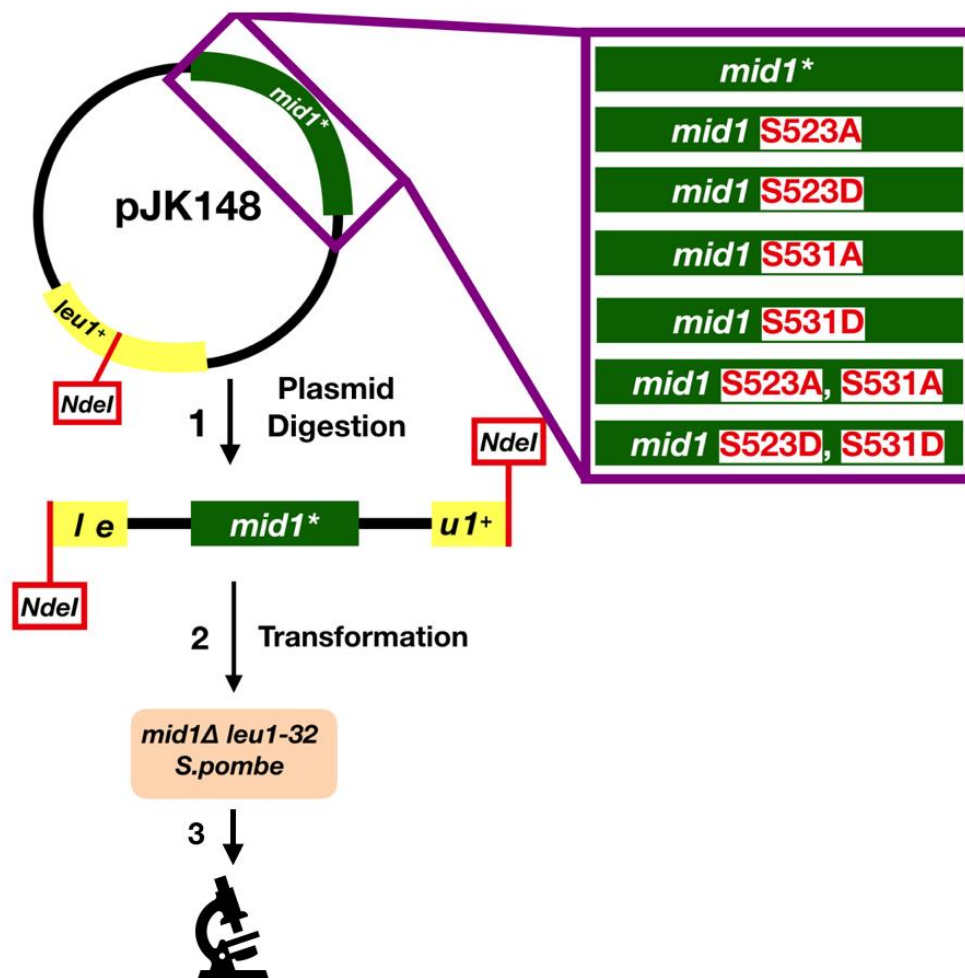


Figure 6-1 An integrative vector is used to replace the endogenous *mid1*⁺ gene with phospho-resistant/mimetic mutant versions of the gene. An *S. pombe* *in vivo* integration experiment was designed to test for the functional relevance of Mid1p potential phospho-sites. A pJK148 integrative vector with a *leu1*⁺ selective marker that includes a *Nde* I restriction site harbours the Mid1p phospho-mimetic/resistant mutant versions of the gene. *mid1*⁺ represent the wild-type *mid1*⁺ gene, and the *mid1* gene mutants are described in detail in Table 6-2. (1) The plasmid is digested with *Nde* I to linearize in *leu1*⁺, and then (2) transformed into a *mid1*Δ *S. pombe* strain with a *leu1*-32-point mutation, where it integrates at the *leu1*⁺ locus. The resulting *S. pombe* strain is subjected to (3) cell morphology analysis through microscopy.

6.3.2.2 Integration of *mid1* phospho-mimetic/resistant genes into the *mid1* Δ *S. pombe* strain

The seven highlighted *S. pombe* strains in Table 6-2 (**1**, **10**, **11**, **12**, **13**, **16** and **17**) were examined microscopically to characterize *S. pombe* cell morphology phenotypes.

Two control experiments that utilized two previously described *S. pombe* strains, wild type (W-T) and *mid1* Δ (Section 3.3.1), were included in this analysis: **firstly**, to characterize the wild-type cell morphology phenotypes; and **secondly**, to investigate the effect of the complete absence of the *mid1*⁺ gene on the characterized phenotypes.

A third control experiment was designed by generating Strain **1** (Section 6.3.2.1) that included the wild-type *mid1*⁺ gene integrated into a *mid1* Δ *S. pombe* strain. This strain was expected to exhibit similar cell morphology phenotypes to those observed in the wild-type strain, which confirms that the integration process did not affect cell morphology.

Strains **10**, **12** and **16** contained phospho-resistant mutations of S523A and/or S531A residues on Mid1p. While Strains **11**, **13** and **17** contained phospho-mimetic mutations of S523D and/or S531D residues on Mid1p as described in Table 6-2.

For simplicity and clarity, the seven strains used to generate the results in Figures 6-2 and Section 8.1.4, Figure 8-1 were re-named as follows:

Strain **1**: *mid1* Δ pJK148:*mid1*⁺, Strain **10**: *mid1* Δ pJK148:*mid1***S523A**, Strain **11**: *mid1* Δ pJK148:*mid1***S523D**, Strain **12**: *mid1* Δ pJK148:*mid1***S531A**, Strain **13**: *mid1* Δ pJK148:*mid1***S531D**, Strain **16**: *mid1* Δ pJK148:*mid1***S523A S531A** and Strain **17**: *mid1* Δ pJK148:*mid1***S523D S531D**.

S. pombe cells were grown in liquid rich medium to mid-logarithmic phase and visualized under bright field using confocal microscopy; representative population images are presented in Figure 6-2.

The cell morphology phenotypes of each strain described above were characterized and a detailed statistical analysis of the phenotypes is presented in Section 8.1.4, Figure 8-1.

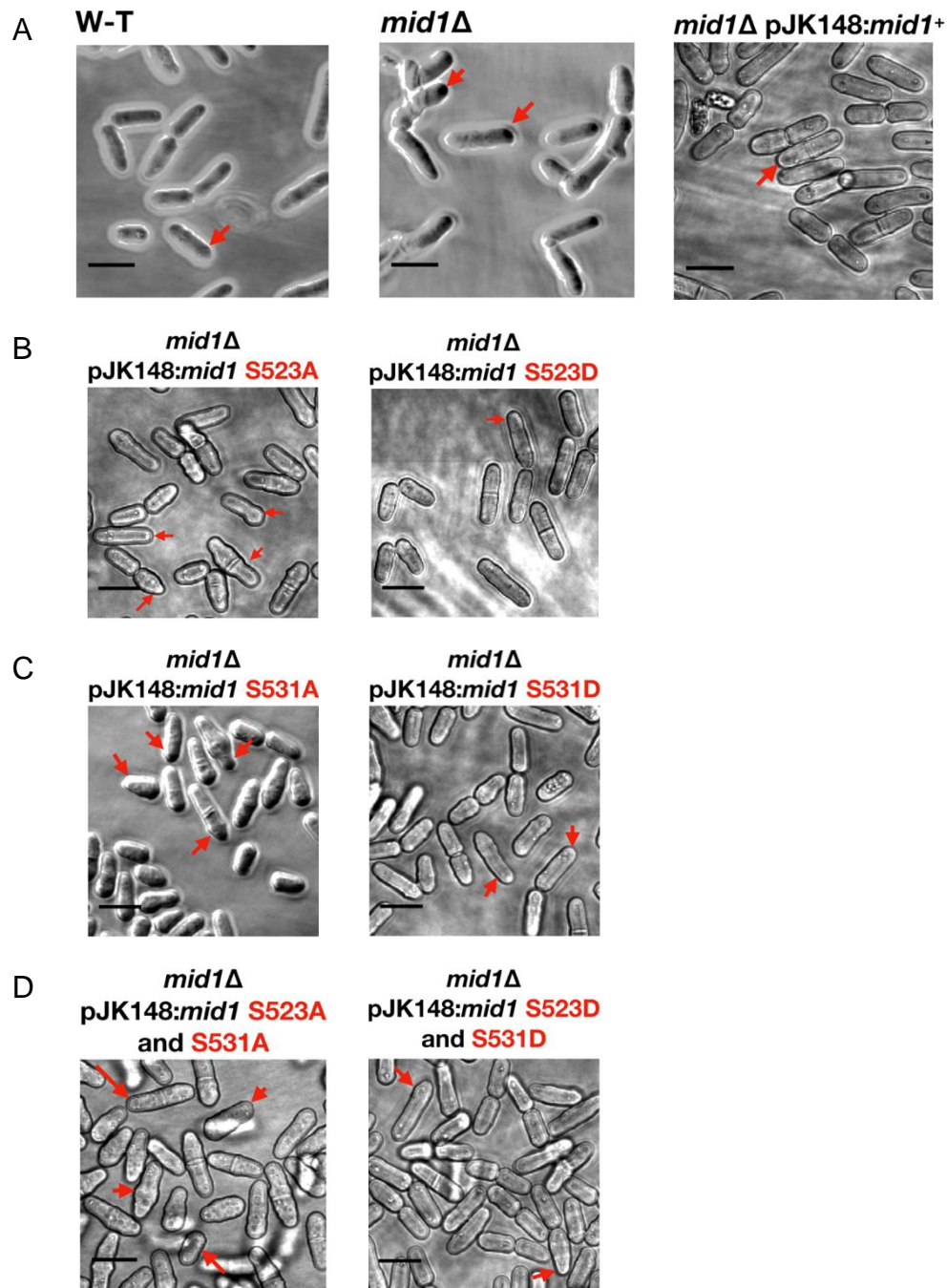


Figure 6-2 Microscopic analysis of *mid1* phospho-resistant/mimetic mutant *mid1*Δ *S. pombe*. W-T, *mid1*Δ, *mid1*Δ pJK148:*mid1*⁺, *mid1*Δ pJK148:*mid1*S523A, *mid1*Δ pJK148:*mid1*S523D, *mid1*Δ pJK148:*mid1*S531A, *mid1*Δ pJK148:*mid1*S531D, *mid1*Δ pJK148:*mid1*S523A S531A and *mid1*Δ pJK148:*mid1*S523D S531D strains were grown at (25°C) in liquid YE medium to mid-exponential phase. Cells were visualized by confocal microscopy under bright field. Scale bar 10 μm. The characterized cell morphology phenotypes (detailed statistical analysis is shown in Section 8.1.4, Figure 8-1) are indicated by red arrows.

Following the characterization of the *S. pombe* cell morphology phenotypes in the three control strains (wild-type, *mid1* Δ and *mid1* Δ pJK148:*mid1*⁺), and in the six phospho-resistant/mimetic strains, the frequency of each phenotype was quantified for each strain. Then, cell morphology phenotype frequencies of the phospho-resistant and phospho-mimetic mutants were compared to the frequencies of the *mid1* Δ pJK148:*mid1*⁺ phenotypes and the results were tested for statistical significance as described in Section 8.1.4, Figure 8-1.

All **wild-type (W-T)** *S. pombe* cells had a rod shape, similarly all ***mid1* Δ pJK148:*mid1*⁺** cells retained the rod shape. As this strain was generated by integrating the wild-type *mid1*⁺ gene into a *mid1* Δ strain under the control of endogenous *mid1* promoter, the similar frequencies of the rod shape phenotype of ***mid1* Δ pJK148:*mid1*⁺** and **W-T** cells confirms the success of the integration experiment. As expectedly, in ***mid1* Δ** cells, the frequency of rod shape cells showed a significant decrease when compared to that in **W-T** cells with only 28% of cells having a rod shape, while the majority of cells, 72%, were branched.

41% of the ***mid1* Δ pJK148:*mid1***S523A**** cells had a rod shape. Additionally, four defective morphology phenotypes were observed in this strain but not in the ***mid1* Δ pJK148:*mid1*⁺** strain, these phenotypes included cells with medial bulges (25% of cells), cells with a "capping" shape in one cell tip (26% of cells), cells with a "pointy" shape in one cell tip (5% of cells) and cells with misplaced septa (3% of cells).

95% of ***mid1* Δ pJK148:*mid1***S523D**** cells had a rod shape, while only 5% of cells showed a "capping" shape in one cell tip. This indicates a partial rescue of the defective cell morphology phenotypes observed in the ***mid1* Δ pJK148:*mid1***S523A**** strain.

32% of the ***mid1* Δ pJK148:*mid1***S531A**** cells were rod in shape. Additionally, three defective morphology phenotypes were observed in this strain but not in the ***mid1* Δ pJK148:*mid1*⁺** strain, these phenotypes included cells with medial bulges (21% of cells), cells with a "capping" shape in one cell tip (12% of cells) and cells with a "pointy" shape in one cell tip (35% of cells).

84% of ***mid1* Δ pJK148:*mid1***S531D**** cells had a rod shape, while 16% of cells showed a "capping" shape in one cell tip. This indicates a partial rescue of the

defective cell morphology phenotypes observed in the *mid1* Δ **pJK148:*mid1*S531A** strain.

33% of the *mid1* Δ **pJK148:*mid1*S523A S531A** cells had a rod shape. Additionally, three morphology defective phenotypes were observed in this strain but not in the *mid1* Δ **pJK148:*mid1*⁺** strain, these phenotypes included cells with medial bulges (31% of cells), cells with a "capping" shape in one cell tip (11% of cells) and cells with a "pointy" shape in one cell tip (25% of cells).

82% of *mid1* Δ **pJK148:*mid1*S523D S531D** cells had a rod shape, while 18% of cells showed a "pointy" shape in one cell tip. This indicates a partial rescue of the defective cell morphology phenotypes observed in the *mid1* Δ **pJK148:*mid1*S523A S531A** strain.

The results of the above experiments suggest that the two S523 and S531 phospho-sites are required for the function of Mid1p.

6.3.2.3 *In vivo* integration of *mid1* phospho-mimetic/resistant genes into the *mid1* Δ *ark1*-T11 *S. pombe* strain

Central to this research was investigating the potential interaction between Mid1p and Ark1p. In Section 6.3.2.2, we explored this interaction by generating phospho-mimetic/resistant versions of the *mid1* gene in cells corresponding to Mid1p potential phospho-sites identified in Section 5.3.3.4.

Two Mid1p potential phospho-sites, S523 and S531, were investigated to characterise cell morphology phenotypes. Such analysis resulted in the characterization of five cell morphology defective phenotypes that are not observed in the wild-type cells. We therefore concluded that the two S523 and S531 phospho-sites are required for the function of Mid1p (Section 6.3.2.2).

As demonstrated in Section 5.3.2, a synthetic lethal growth phenotype was observed in the *ark1*-T11 mutant. This suggests that the genetic interaction detected between the *mid1*⁺ and *ark1*⁺ genes is required for *S. pombe* cell cycle establishment. We decided to test the involvement of Mid1p S523 and S531 phospho-sites with the interaction of Ark1p by investigating the effect of Mid1p S523 and S531 phospho-mimetic/resistant mutations on the cell morphology of *ark1*-T11 *S. pombe*. The individual 19 phospho-mimetic/resistant strains

generated in Section 6.3.2.2 and summarized in Table 6-2 were each crossed with an *ark1*-T11 *S. pombe* strain (GG 2417). This yielded 19 new *mid1* Δ *ark1*-T11 *S. pombe* triple mutant strains. These new strains are summarized in Table 6-3.

Table 6-3 A summary of the phospho-mimetic/resistant mutant versions of the *mid1* gene integrated into *ark1*-T11 *S. pombe* for the *in vivo* microscopy analysis presented in Section 6.3.2.3. The *S. pombe* strains were generated by Christopher McInerny and given a yeast collection (GG) number. S: serine, A: alanine, D: aspartic acid.

Strain/ GG No.	20	21	22	23	24	25	26	27	28	29	30	31	32	33	34	35	36	37	38
	3205	3321	3324	3327	3330	3333	3336	3339	3342	3218	3230	3235	3239	3242	3246	3345	3349	3352	3355
Mid1p 167	S	A	D	S	S	S	S	S	S	S	S	S	S	A	D	S	S	A	D
Mid1p 328	S	S	S	A	D	S	S	S	S	S	S	S	S	A	D	S	S	A	D
Mid1p 331	S	S	S	S	S	A	D	S	S	S	S	S	S	A	D	S	S	A	D
Mid1p 332	S	S	S	S	S	S	S	A	D	S	S	S	S	A	D	S	S	A	D
Mid1p 523	S	S	S	S	S	S	S	S	S	A	D	S	S	S	S	A	D	A	D
Mid1p 531	S	S	S	S	S	S	S	S	S	S	S	A	D	S	S	A	D	A	D

The seven highlighted *S. pombe* strains in Table 6-3 (**20**, **29**, **30**, **31**, **32**, **35** and **36**) were used in the *in vivo* microscopy experiments described in this Section to characterize *S. pombe* cell morphology phenotypes. A positive control experiment was designed utilizing the previously described *ark1*-T11 strain (Section 5.3.1) to characterize its cell morphology phenotypes. A second control experiment was designed by generating Strain **20**, as described in Section 6.3.2.1, that included the wild-type *mid1*⁺ gene integrated into a *mid1* Δ *ark1*-T11 *S. pombe* strain (GG 1129). This strain was expected to exhibit similar cell morphology phenotypes to the ones observed in the *ark1*-T11 strain.

Strains **29**, **31** and **35** contained phospho-resistant mutations of **S523A** and/or **S531A** residues on Mid1p, while Strains **30**, **32** and **36** contained phospho-mimetic mutations of **S523D** and/or **S531D** residues on Mid1p as described in Table 6-3.

For simplicity and clarity, the seven strains used to generate the results in Figures 6-3, Section 8.1.5, Figure 8-2 were re-named as follows:

Strain **20**: *mid1* Δ *ark1*-T11, Strain **29**: *mid1* Δ pJK148:*mid1* **S523A** *ark1*-T11, Strain **30**: *mid1* Δ pJK148:*mid1* **S523D** *ark1*-T11, Strain **31**: *mid1* Δ pJK148:*mid1* **S531A**

ark1-T11, Strain **32**: *mid1* Δ pJK148:*mid1* **S531D** *ark1-T11*, Strain **35**: *mid1* Δ pJK148:*mid1* **S523A S531A** *ark1-T11* and Strain **36**: *mid1* Δ pJK148:*mid1* **S523D S531D** *ark1-T11*. The *S. pombe* cells were grown in liquid rich medium to visualize them under bright field using confocal microscopy; representative population images are presented in Figure 6-3.

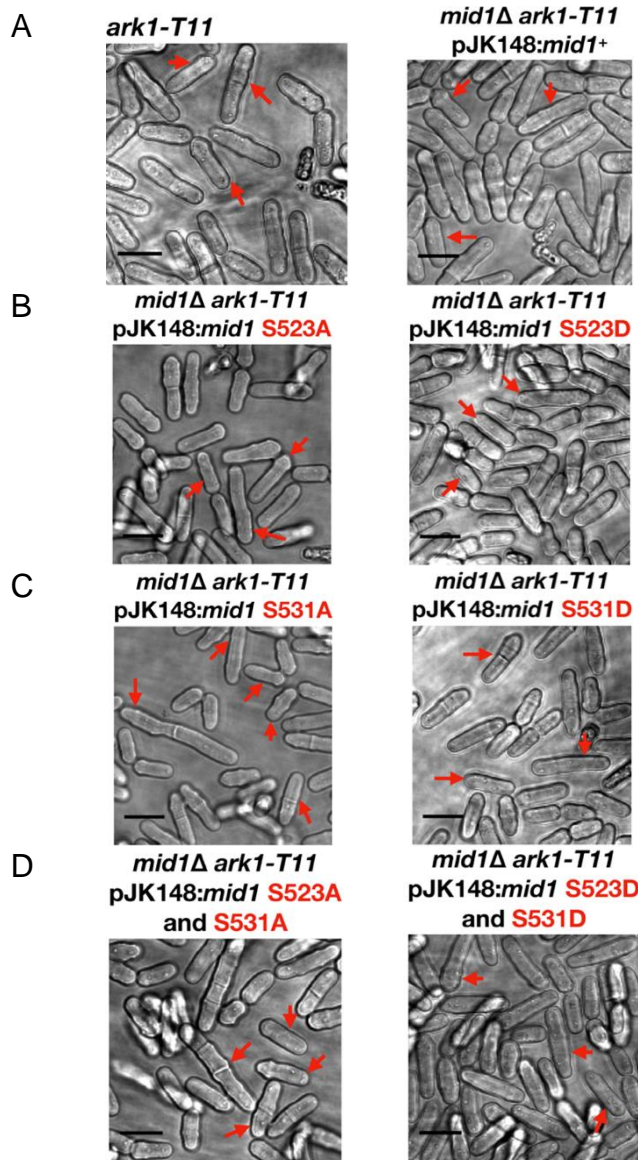


Figure 6-3 Microscopic analysis of *mid1* phospho-resistant/mimetic mutant *mid1* Δ *ark1-T11* *S. pombe*. *ark1-T11*, *mid1* Δ *ark1-T11* pJK148:*mid1*⁺, *mid1* Δ *ark1-T11* pJK148:*mid1***S523A**, *mid1* Δ *ark1-T11* pJK148:*mid1***S523D**, *mid1* Δ *ark1-T11* pJK148:*mid1***S531A**, *mid1* Δ *ark1-T11* pJK148:*mid1***S531D**, *mid1* Δ *ark1-T11* pJK148:*mid1***S523A S531A** and *mid1* Δ *ark1-T11* pJK148:*mid1***S523D S531D** strains were grown at (25°C) in liquid YE medium to mid-exponential phase. Cells were visualized by confocal microscopy under bright field. Scale bar 10 μ m. The characterized cell morphology phenotypes (detailed statistical analysis is shown in Section 8.2.1, Figure 8-2) are indicated by red arrows.

Following the characterization of the *S. pombe* cell morphology phenotypes in the two control strains (*ark1-T11* and *ark1-T11 mid1Δ pJK148:mid1⁺*), and in the six phospho-resistant/mimetic strains, the frequency of each phenotype was quantified for each strain. Then, cell morphology phenotype frequencies all mutant strains were compared to the frequencies of the and ***ark1-T11 mid1Δ pJK148:mid1⁺*** phenotypes and the results were tested for statistical significance as described in Section 8.1.5, Figure 8-2. In the ***ark1-T11*** strain, 72% of cells had a rod shape, while 4% of cells appeared with a "capping" shape in one cell tip. Interestingly, 24% of cells appeared to be elongated. This reflects the important role of Ark1p in *S. pombe* cell cycle regulation, particularly in cytokinesis.

Frequencies of the cell morphology phenotypes in ***ark1-T11 mid1Δ pJK148:mid1⁺*** strain were very similar to those observed in ***ark1-T11*** cells, as in in ***ark1-T11 mid1Δ pJK148:mid1⁺*** cells, 68% of cells had a rod shape, while 7% of cells appeared with a "capping" shape in one cell tip. Interestingly, 25% of cells appeared to be elongated. As this strain was generated by integrating the wild-type *mid1⁺* gene into a ***mid1Δ ark1-T11*** strain under the control of an endogenous *mid1⁺* promoter, the similarity of the characterized phenotypes frequencies compared to those of the ***ark1-T11*** cells confirms the success of the integration experiment. Elongated cell morphology phenotype was observed in both ***ark1-T11*** and ***mid1Δ ark1-T11*** cells but not **wild-type** *S. pombe*.

In the ***ark1-T11 mid1Δ pJK148:mid1S523A*** strain, 82% of cells had a rod shape. 10% of cells showed a "capping" shape in one cell tip. Additionally, 8% of cells appeared to be elongated with a bending angle.

In the ***ark1-T11 mid1Δ pJK148:mid1S523D*** strain, 92% of cells had a rod shape, while 8% of cells appeared to be elongated. This indicates a partial rescue of the defective cell morphology phenotypes observed in the ***ark1-T11 mid1Δ pJK148:mid1S523A*** strain.

In the ***ark1-T11 mid1Δ pJK148:mid1S531A*** strain, 59% of cells had a rod shape. 13% of cells showed a "capping" shape in one cell tip. Cells with medial bulges (11% of cells) and cells with a "pointy" shape in one cell tip (4% of cells), were also observed. Additionally, 8% of cells appeared to be elongated and 5% of cells appeared to be elongated with a bending angle.

In the *ark1-T11 mid1Δ pJK148:mid1S531D* strain, 78% of cells had a rod shape, 11% of cells showed a "capping" shape in one cell tip, and 11% of cells appeared to be elongated. This indicates a partial rescue of the defective cell morphology phenotypes observed in the *ark1-T11 mid1Δ pJK148:mid1S531A* strain.

In the *ark1-T11 mid1Δ pJK148:mid1S523A S531A* strain, 54% of cells had a rod shape, 14% of cells showed a "capping" shape in one cell tip, 6% of cells showed a "pointy" shape in one cell tip, and 6% of cells had a mis-placed septum. Interestingly, in this strain the frequency of elongated cells showed a significant decrease (only 3% of cells) when compared to that of *ark1-T11 mid1Δ* (25%) cells. Additionally, 17% of cells appeared to be elongated with a bending angle and multiple septa. This phenotype is observed in the *mid1Δ* cells.

In the *ark1-T11 mid1Δ pJK148:mid1S523D S531D* strain, 75% of cells had a rod shape, 12% of cells showed a "capping" shape in one cell tip, while 13% of cells appeared to be elongated. This indicates a partial rescue of the defective cell morphology phenotypes observed in the *ark1-T11 mid1Δ pJK148:mid1S523A S531A* strain.

The results of the above experiments suggest that the two S523 and S531 phospho-sites are required for the function of Mid1p.

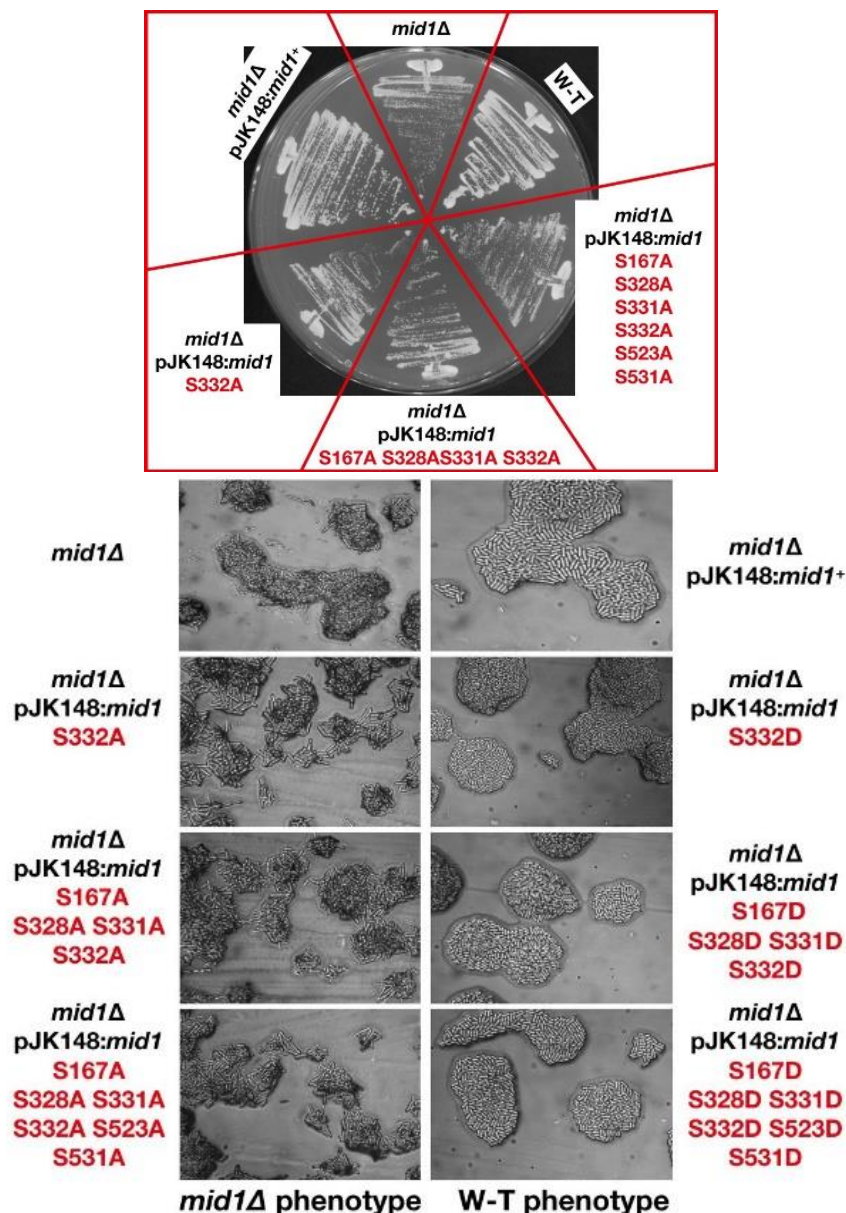
6.3.3 *In vivo* analysis of the role of S167, S328, S331 and S332 phospho-sites for the function of Mid1p during *S. pombe* cell cycle

We also completed some preliminary analysis of mutations in the other potential phospho-sites mapped in Mid1p, the serine residues S167, S328, S331 and S332. As described previously, strains were created by integrating in single copy versions of Mid1p mutated in these residues to either a phospho-mimetic or a phospho-resistant point mutation(s), either singly or in combination (Table 6-2).

Initial experiments grew the strains with either the phospho-mimetic or a phospho-resistant point mutation(s) of Mid1p potential phospho-sites (S167, S328, S331 and S332) on solid YE media, with the successful formation of colonies observed

in all strains. In *mid1* Δ pJK148:*mid1* S167A, S167D, S328A, S328D, S331A, S332D S331D cells appeared similar in shape to wild-type cells (data not shown).

However interestingly, only in *mid1* Δ pJK148:*mid1* S332A mutant, cells had defects in morphology similar to the defects observed in *mid1* Δ cells, with slower growth at 25°C (Top Panel, Figure 6-4), and altered morphology defined as branched cells with multiple septa (Lower Panel, Figure 6-4). Encouragingly, these preliminary data indicate the requirement of S332 for the function of Mid1p. However, *S. pombe* liquid culture microscopic analysis is required to provide statistical evidence of cell morphology phenotypes. This approach would advance our current knowledge of Mid1p phospho-regulation during *S. pombe* cell cycle.



6.3.4 Potential coordination between Mid1p, Ark1p and Vps4p to regulate *S. pombe* cell cycle

We identified a genetic interaction between the *mid1*⁺ and *ark1*⁺ genes (Chapter 5). We also identified the interaction between the *mid1*⁺ and the *vps4*⁺ genes (Chapter 3). Similarly, Bhutta et al., (2014) observed genetic interactions between the ESCRT genes and *ark1*⁺ genes. They generated *ark1*-T8 *vps4*Δ and *ark1*-T11 *vps4*Δ double mutants and examined their septation phenotypes. Comparison of septation phenotypes between *ark1*-T8 and *ark1*-T11 single mutants with *ark1*-T8 *vps4*Δ and *ark1*-T11 *vps4*Δ double mutants showed a significant increase in the proportion of cells with a mis-aligned septum and cells with an increase in length. Therefore, they proposed that Ark1p regulates the function of Vps4p during *S. pombe* septation.

To examine the role of Mid1p phosphorylation on its interaction with Vps4p, we crossed phospho-mimetic/resistant versions of Mid1p with *vps4*Δ *S. pombe* cells and searched for phenotypes.

Initial experiments attempted to cross the double *mid1* S523 and S531 phospho-mimetic/resistant versions of the gene with *vps4*Δ *S. pombe* cells and grow them on solid YE media; successful formation of colonies was observed in all strains. However, colony formation was slower in the case of the Mid1p phospho-mimetic *mid1*Δ pJK148:*mid1* S523D S531D *vps4*Δ double mutants. Importantly, cells had defects in morphology similar to the defects observed in *mid1*Δ cells and defined branched cells with multiple septa (Figure 6-5).

These preliminary results indicate the presence of a link between the regulation of Mid1p by Vps4p and the regulation of Mid1p by Ark1p. However, *S. pombe* microscopic analysis of all *mid1* phospho-mimetic/resistant *vps4*Δ strains is required to provide statistical evidence of cell morphology phenotypes. Future work should focus on investigating the common pathway integrating Mid1p, Vps4p and Ark1p functions to regulate *S. pombe* cell cycle.

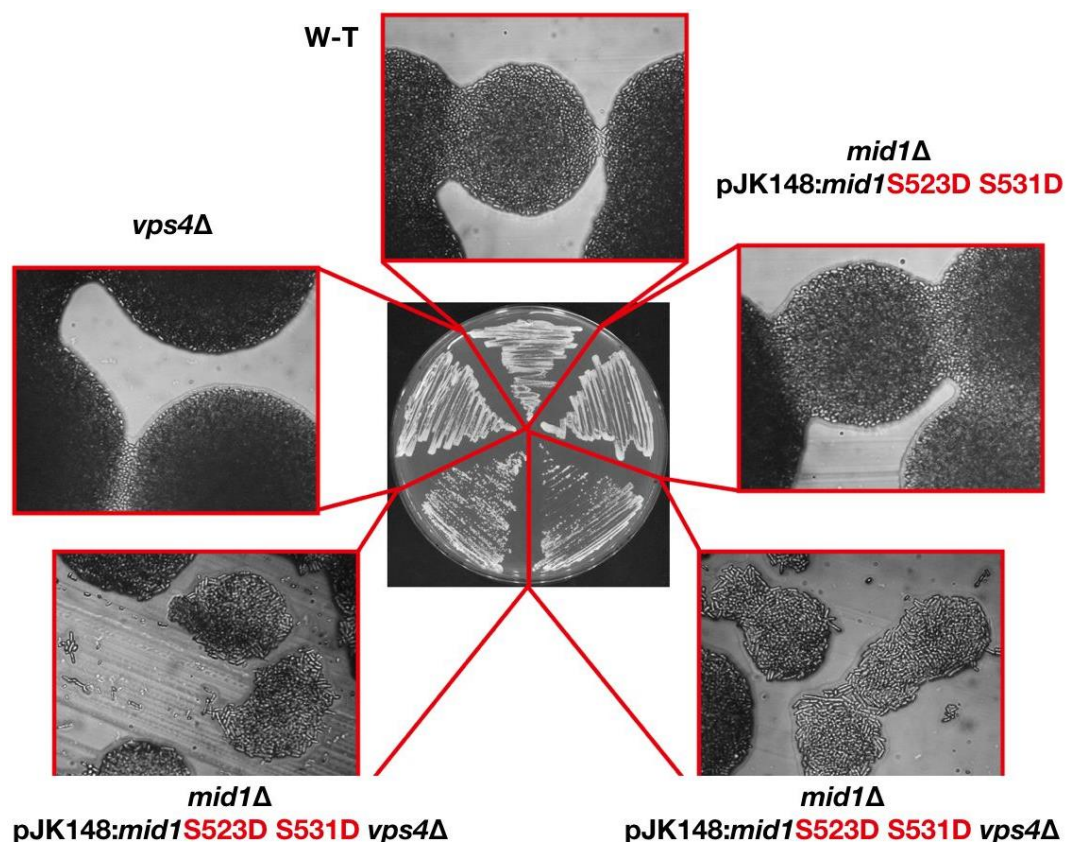


Figure 6-5 Mid1p S523 and S531 potential phospho-sites might regulate its interaction with Vps4p during *S. pombe* cell cycle. *mid1* Δ pJK148:*mid1*S523D S531D phospho-mimetic mutant was crossed with *vps4* Δ strain. In the *mid1* Δ pJK148:*mid1*S523D S531D cells, colonies showed wild-type growth phenotype similar to that observed in wild-type and *vps4* Δ *S. pombe* cells when grown at 25 °C. In the *mid1* Δ pJK148:*mid1*S523D S531D *vps4* Δ cells, colonies from two different isolates showed the *mid1* Δ phenotype indicating a role of Mid1p S523 and S531 potential phospho-sites in the interaction with Vps4p. Colonies were imaged using a Sony DSC-75 camera and Zeiss Axioscope microscope.

6.3.5 Investigation of the localization of GFP-Mid1p in *ark1*-TS cells

6.3.5.1 Generation of GFP-Mid1p *ark1*-TS *S. pombe* strains

A study investigated the role of Ark1p in sister kinetochore mono-orientation during *S. pombe* meiosis, where they generated an *ark1*-TS mutant, *ark1-T8* (Koch et al., 2011). The *ark1-T8* strain was generated via a PCR-based random mutagenesis approach to replace the endogenous *ark1*⁺ gene with *ark1-T8* (Koch et al., 2011). This strain was kindly gifted by Silke Hauf.

Upon re-examination of the growth phenotype of the *ark1-T8 S. pombe* for this project, the strains were grown on solid rich complete medium alongside with the wild-type *S. pombe* strain at either permissive (25°C) or restrictive (37°C) temperatures, after which colony formation and growth were compared to wild-type strain. The strain was able to form viable colonies as in the wild-type strain when grown at 25°C but not at 37°C.

When mutant cells were examined by light microscopy, they were found to maintain the rod-shape as in wild-type cells but appeared longer with septa unaffected. This indicates that the *ark1⁺* gene is not required for proliferation (data not shown).

In Section 5.3.1, we discussed the *ark1-T11 S. pombe* strain. Here, we used both *ark1-T11* and *ark1-T8* (we will refer to both strains as *ark1-TS*) to obtain GFP-Mid1p *ark1-T11* and GFP-Mid1p *ark1-T8 S. pombe* strains.

Throughout this Thesis, we provide several lines of evidence directly and indirectly supporting the interaction between the *mid1⁺* and *ark1⁺* genes and the Mid1p and Ark1p proteins, respectively. We therefore hypothesized that Ark1p is required for the localization of Mid1p in *S. pombe*.

To test the above hypothesis, we utilized the two *ark1-TS* strains and a GFP-Mid1p strain, where GFP was tagged to the chromosomal locus of the *mid1⁺* gene to generate GFP-Mid1p *ark1-T11* and GFP-Mid1p *ark1-T8* strains. These strains were generated by crossing the GFP-Mid1p *S. pombe* strain (GG 1347) described in Section 3.3.5 with either *ark1-T11* (described in Section 5.3.1) or *ark1-T8 S. pombe* strains.

6.3.5.2 Ark1p is required for the localization of GFP-Mid1p in *S. pombe*

In Section 3.3.5, we investigated the localization of GFP-Mid1p in wild-type *S. pombe* living cells. Such experiment yielded the characterization of five localization phenotypes (Figure 3-14).

We sought to investigate the localization of GFP-Mid1p in *ark1-TS* cells to test the effect of these TS mutations on the GFP-Mid1p wild-type localization.

The growth temperature of these two strains affects not only the activity of the *ark1⁺* gene but also causes cell cycle arrest; therefore, any phenotypes observed from growing the strains at a restrictive temperature cannot not be solely attributed

to the total absence/inactivation (disturbance) of the *ark1*⁺ gene. To avoid this confusion, the cells were grown at a permissive temperature so that any phenotypes observed are considered results of at least a "partial" absence (disturbance) of the Ark1p protein.

In this Section, we describe experiments of the localization of GFP-Mid1p in *ark1*-T11 (Figure 6-6) and *ark1*-T8 (Figure 6-7) cells and characterize the different localization phenotypes.

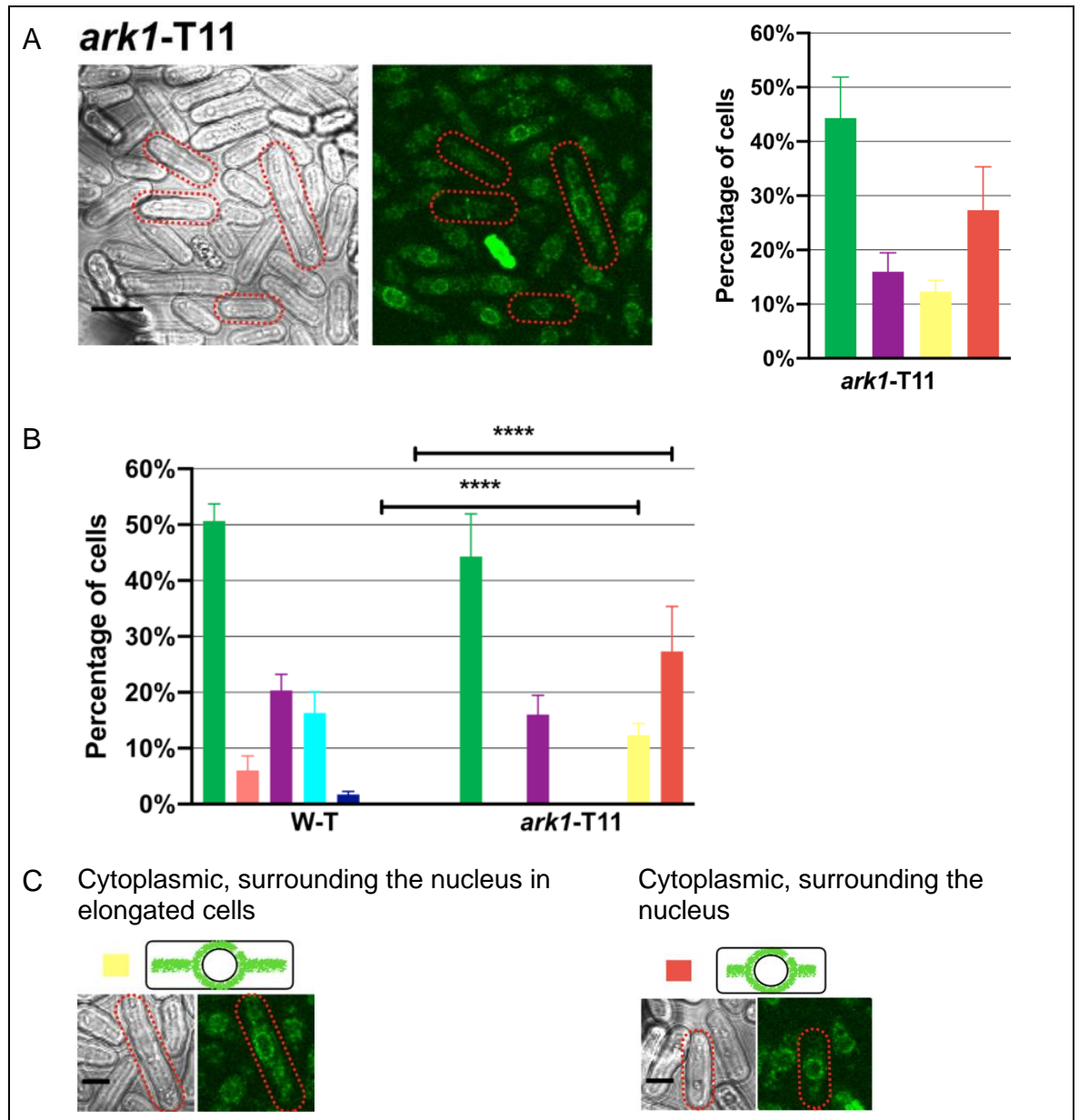


Figure 6-6 Classification and quantification of GFP-Mid1p localization phenotypes in W-T and *ark1-T11* *S. pombe*. *S. pombe* strains were grown and visualized as described in Figure 3-14. (A) Population of cells (left) and quantitative analysis of the observed phenotypes (right) are shown in *ark1-T11* cells. Scale bar 10 μ m. 200-250 cells were counted from three independent experiments to produce (A). In (B), a 2-way ANOVA statistical analysis was used. The frequencies of the localization phenotypes in *ark1-T11* cells were compared to wild-type frequencies. Asterisks (****) denotes a p value <0.0001 . Error bars represent SEM. (C) Characterized localization phenotypes. Scale bar 5 μ m.

GFP-Mid1p localization in *ark1-T11 S. pombe*

In (Figure 6-6, Panel A), a cell population sample represents the different patterns of GFP-Mid1p localization in ***ark1-T11 S. pombe***. In this mutant strain, 45% of cells showed cytoplasmic localization, while in 16% of cells GFP-Mid1p localized to two cortical nodes. However, unlike in wild-type cells nuclear and septal localization were not observed. Interestingly, GFP-Mid1p showed nuclear exclusion and appeared to be wrapping the nucleus in 27% of cells. In addition to that, the same phenotype was observed in 12% of cells which appeared elongated.

The frequencies of these four phenotypes observed in ***ark1-T11 S. pombe*** were measured and compared to the frequencies of the phenotypes in wild-type cells (Figure 6-6, Panel B). No significant differences were observed in the cytoplasmic and nodal localization phenotypes upon such comparison. However, since the nuclear exclusion phenotypes were not observed in wild-type cells, they are probably caused by the partial absence of Ark1p function in *S. pombe*.

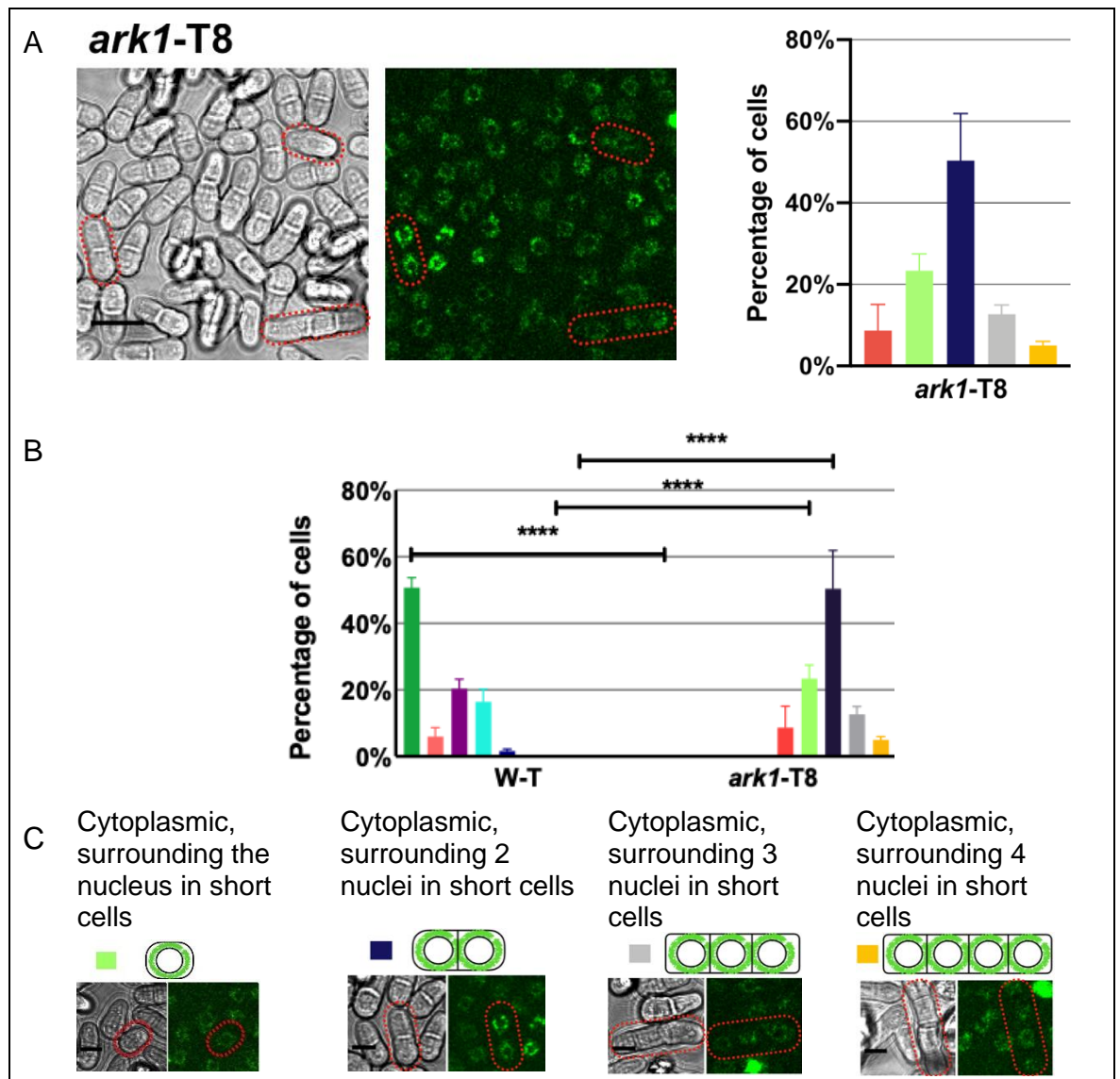


Figure 6-7 Classification and quantification of GFP-Mid1p localization phenotypes in W-T and *ark1-T8* *S. pombe*. *S. pombe* strains were grown and visualized as described in Figure 3-14. (A) Population of cells (left) and quantitative analysis of the observed phenotypes (right) are shown in *ark1-T11* cells. Scale bar 10 μ m. 200-250 cells were counted from three independent experiments to produce (A). In (B), a 2-way ANOVA statistical analysis was used. The frequencies of the localization phenotypes in *ark1-T11* cells were compared to wild-type frequencies. Asterisks (****) denotes a p value <0.0001 . Error bars represent SEM. (C) Characterized localization phenotypes. Scale bar 5 μ m.

GFP-Mid1p localization in *ark1-T8 S. pombe*

In (Figure 6-7, Panel A), a cell population sample represents the different patterns of GFP-Mid1p localization in ***ark1-T8 S. pombe***. In this mutant strain, cytoplasmic localization was observed in only 2% of cells. In addition to that, GFP-Mid1p showed nuclear exclusion and appeared to be wrapping the nucleus in 30% of cells (specifically, 7% of cells had a rod shape and 23% of cells were round in shape). Interestingly, the same localization phenotype was observed in cells with: two nuclei (in 50% of cells), three nuclei (in 13% of cells) or four nuclei (in 5% of cells).

The frequencies of these four phenotypes observed in ***ark1-T8 S. pombe*** were measured and compared to the frequencies of the phenotypes in wild-type cells (Figure 6-7, Panel B). Such comparison indicated a significant decrease of GFP-Mid1p cytoplasmic localization. Since the nuclear exclusion phenotypes were not observed in wild-type cells, they are probably caused by the partial absence of Ark1p function in *S. pombe*.

Thus, GFP-Mid1p localization was affected by the partial absence of Ark1p function. This observation in addition to our conclusions from (Sections 5.3.2: that the *mid1*⁺ and *ark1*⁺ genes genetically interact *in vivo*, and 5.3.3: that the Mid1p has potential phospho-sites for phosphorylation by aurora A kinase, and 6.3.2: that the Mid1p potential phospho-sites are important for the function of Mid1p in *S. pombe*) supports the hypothesis that Mid1p and Ark1p coordinate to regulate *S. pombe* cell cycle.

6.4 Conclusions

In this Chapter, we described *in vivo* *S. pombe* microscopy experiments to investigate the regulation of Mid1p by Ark1p. Our main findings are:

First, we detected an increased rate of cell morphology defects represented in the formation of medial bulges in the *mid1* Δ pJK148:*mid1*S523A, *mid1* Δ pJK148:*mid1*S531A and *mid1* Δ pJK148:*mid1*S523A S531A cells. *In vitro* experiments suggest that these serine residues are phosphorylated by aurora A (Section 5.3.3).

Second, the medial bulges phenotype was not observed in the *mid1* Δ pJK148:*mid1*S523D, *mid1* Δ pJK148:*mid1*S531D and *mid1* Δ pJK148:*mid1*S523D S531D cells.

Third, we detected an increased rate of cell morphology defects represented in the formation of long bended cells with multiple septa in *ark1*-T11 *mid1* Δ pJK148:*mid1*S523D S531A cells.

Fourth, the of long bended cells were not observed *ark1*-T11 *mid1* Δ pJK148:*mid1*S523D S531A cells.

These four findings emphasize the importance of S523 and S531 for the function of Mid1p supporting the hypothesis of Mid1p regulation by Ark1p.

Fifth, we characterized the patterns of GFP-Mid1p distribution in two *ark1*-TS *S. pombe* strains and found a requirement of Ark1p for Mid1p localization, further supporting the interaction of Mid1p and Ark1p to regulate *S. pombe* cell cycle.

Combined, these observations support a role for the interaction of Ark1p and Mid1p in controlling cytokinesis in fission yeast. Also, preliminary results Suggest the requirement of S332 for the function of Mid1p and indicate the presence of a link between the regulation of Mid1p by Vps4p and the regulation of Mid1p by Ark1p.

Chapter 7 Discussion

7.1 Control of the anillin Mid1p by the ESCRT regulator Vps4p in *S. pombe* cell cycle.

7.1.1 The *mid1*⁺ and *vps4*⁺ genes are involved in *S. pombe* cell cycle regulation

During *S. pombe* cell cycle, a sequence of events, starting with placement of the division plane and ending with septation and midbody resolution, are regulated by the anillin protein Mid1p (Paoletti and Chang, 2000) and the ESCRT proteins (Bhutta et al., 2014), respectively. As preliminary data suggested an interaction between these two classes of proteins (Bhutta, 2014), we hypothesized that Mid1p might coordinate with the ESCRT proteins to ensure correct septation in *S. pombe* and sought to further analyze this interaction.

A chromosomal deletion of the *mid1*⁺ gene (in *mid1*Δ cells) caused dramatic defects in *S. pombe* septation phenotypes (Section 3.3.2). These phenotypes were characterized and defined as: mis-placed single septa, , multi septa, branched cells with multiple septa, and delayed separation after septation, with none of these phenotypes observed in wild-type cells. These observations are consistent with the similar septation defects observed in *mid1*Δ cells by four independent published studies: Paoletti and Chang (2000), Celton-Morizur et al. (2004), Almonacid et al. (2009) and Saha and Pollard (2012a). Together they confirm the requirement of Mid1p function for correct division plane positioning in *S. pombe*.

The ESCRT family of proteins is required to establish cell division in eukaryotic cells (Morita et al., 2007). In particular, Bhutta et al. (2014) demonstrated the requirement of the ESCRT proteins, including Vps4p, for septation in *S. pombe* cells. In Section 3.3.5.1, we illustrate the effect of a chromosomal deletion of the *vps4*⁺ gene (in *vps4* Δ cells), where daughter cells remain connected even after septation and septum degradation initiation. This phenotype was observed in approximately 33% of *vps4* Δ cells but not in wild-type cells. These observations are consistent with the increased frequency of the same septation phenotype described by Bhutta et al. (2014) in *vps4*Δ cells. An increased frequency of this

phenotype was also observed in cells with single chromosomal deletions of the ESCRT-0 *sst4⁺* gene (*sst4Δ*) and the two ESCRT-III *vps20⁺* (*vps20Δ*) and *vps24⁺* (*vps24Δ*) genes, which further confirms the important role of the ESCRT proteins in resolving the midbody during *S. pombe* septation (Bhutta et al., 2014).

To test our hypothesis that Mid1p might coordinate with ESCRT proteins to ensure correct septation in *S. pombe*, we first examined the genetic interaction between the *mid1⁺* gene and each of the *S. pombe* ESCRT-0, I, II and III and *vps4⁺* genes (C. McInerny pers. comm.). Apart from the *vps4⁺* gene which showed synthetic lethality, no genetic interactions were detected. Data presented in this Thesis (Section 3.3.3.2) confirmed this novel genetic interaction, and experiments were carried out to explore how the potential physical interaction between Mid1p and Vps4p proteins regulates *S. pombe* cell cycle.

7.1.2 A model for the interaction between Mid1p and Vps4p to regulate *S. pombe* cortical nodes localization

An explanation for the genetic interaction between the *mid1⁺* and *vps4⁺* genes is a physical interaction of the encoded proteins, Mid1p and Vps4p; therefore, this potential physical interaction was investigated by designing *in vitro* pull-down experiments utilizing bacterially expressed Vps4p and Mid1p "N-term", "Middle" and "C-term" Mid1p domains. These experiments mapped the physical interaction with Vps4p to Mid1p "C-term" domain (Section 3.3.4.4).

Structural analysis of Mid1p by SUPERFAMILY database (superfam.org) revealed the presence of a PH domain in the 803-900 region (i.e. within the "C-term" domain of Mid1p recombinant protein). Since the PH domain is known to facilitate protein attachment to lipid membranes (Lemmon, Ferguson and Schlessinger, 1996), this suggested that Vps4p physically interacts with the PH domain of Mid1p to facilitate Mid1p binding to the cell cortex.

We demonstrated that a chromosomal deletion of the *vps4⁺* gene caused defects in the cellular localization of GFP-Mid1p in *S. pombe* (in *vps4Δ* cells) compared to wild-type *S. pombe* (Section 3.3.5.1). These defects were defined as mis-localization of nodes and represented in GFP-Mid1p localization to one node randomly positioned and localization to three nodes. Interestingly, in this *vps4Δ*

strain, nuclear localization was coupled to the node's localization, where GFP-Mid1p localization was observed in the nucleus and in one or two nodes attached to the nucleus. During cell division the spindle pole bodies (SPB) structure duplicates and represent two poles for the assembly of the spindle in the nucleus, as the spindle elongates the two SPBs segregate and move to the two opposite ends (Ding et al., 1997). Therefore, the observed GFP-Mid1p localization phenotype defined as nuclear localization coupled to the node's localization might be that nuclear localization was coupled to the SPB/s instead of nodes.

Since none of the above-mentioned phenotypes were observed in wild-type cells, this suggests a role of Vps4p in the Mid1p-dependent node localization pathway, which led us to hypothesize that the function of Mid1p is regulated by Vps4p specifically during nodes attachment to the plasma membrane.

As discussed in Chapter 1, two types of nodes are involved in *S. pombe* ARC assembly and contraction. Mid1p cortical anchorage drives the recruitment of cytokinesis proteins, then interactions with myosin filaments drives the condensation of nodes into the ACR (Figure 1-3). Mid1p cortical anchorage depends on the PH domain (Sun et al., 2015) and its potential interaction with Vps4p might stabilize this interaction. Since Vps4p physically interacts with residues within the C-terminal domain of Mid1p, which contains membrane binding motifs, Vps4p might facilitate Mid1p cortical anchorage to promote *S. pombe* medial division.

Here we suggest that a physical interaction between Vps4p and Mid1p, probably via Mid1p PH domain, regulates Mid1p-dependent node attachment to the plasma membrane to determine the division plane in *S. pombe*, and that this interaction directly or indirectly involves Mid1p PH domain cell cortex anchorage (Figure 7-1).

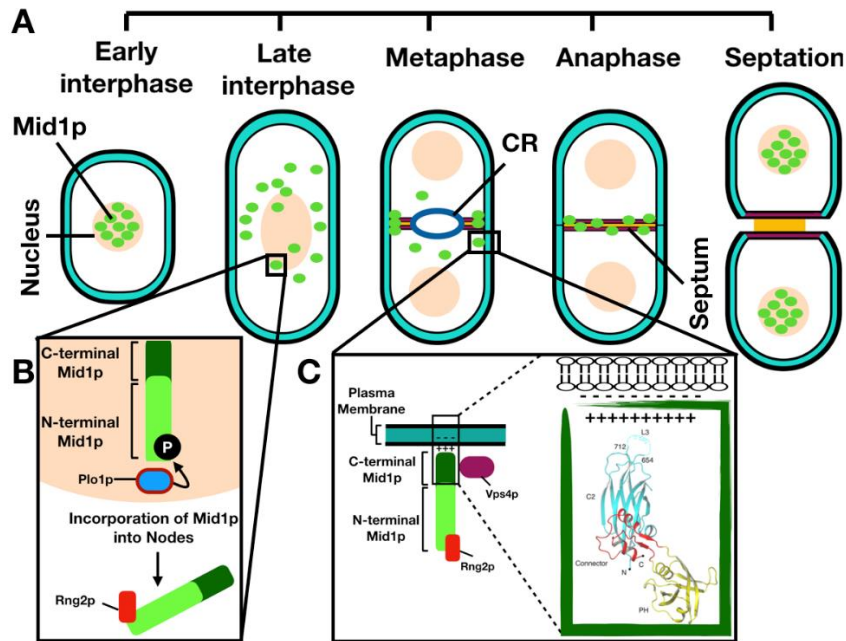


Figure 7-1 A model for the interaction between Mid1p and Vps4p to regulate *S. pombe* septation. Following the detection of the genetic and physical interactions between the *mid1*⁺ and *vps4*⁺ genes and the Mid1p and Vps4p proteins, respectively, GFP-Mid1p *S. pombe* localization analysis revealed a mechanism for the interaction between the two proteins. (A) A schematic representation of Mid1p localization during the different *S. pombe* cell cycle stages derived from Paoletti and Chang (2000) in addition to the experimental results presented in this Thesis (Section 3.3.5.1). (B) Mid1p is phosphorylated by Plo1p to promote mitotic entry, during which Rng2p and other proteins interact with the N-terminal domain of Mid1p. (C) During mitosis, Mid1p forms nodes; these nodes are attached to the plasma membrane via Mid1p C-terminal domain, which contain lipid binding motifs (Blue: cryptic domain and an amphipathic sequence, Yellow: PH domain). Vps4p might catalyse the interaction between Mid1p C-terminal domain and the plasma membrane.

As shown in Sections 3.3.5.3 and 4.3.3, the localization of GFP-Mid1p was examined in *S. pombe* cells lacking either the PH domain (*mid1* PHΔ cells) or a nuclear localization sequence (*mid1* NLS⁺ cells), respectively, by confocal microscopy. In both cases, mis-localization of Mid1p was observed. In *mid1* PHΔ cells, nuclear exclusion was observed, whereas an increased plasma membrane localization in addition to nuclear exclusion were observed in *mid1* NLS⁺ cells.

Experiments by Paoletti and Chang (2000) investigated the localization of Mid1p in *mid1* PHΔ cells and *mid1* NLS⁺ cells through their exposure to anti-*mid1* antibody and subsequent examination by fluorescence microscopy. The reported localization of GFP-Mid1p in *mid1* NLS⁺ cells was consistent with the data presented in this Thesis (Section 4.3.3). By contrast, the reported localization of

GFP-Mid1p in *mid1* PH Δ cells was similar to that observed in wild-type cells, which was not consistent with the data presented in this Thesis (Section 3.3.5.3). Paoletti and Chang's (2000) work yielded several conclusions on the importance of NLS and PH sequences for the function of Mid1p during *S. pombe* cell cycle: First, they asked a question "why should a cytokinesis factor be present in the nucleus?". They hypothesized a possible mode of action for Mid1p, where Mid1p localization to the cell surface may depend on its nuclear shuttling; and second, they generated a large C-terminal deletion in Mid1p (*mid1* 507-920 Δ cells) which removes both the NLS and PH sequences; localization of Mid1p in these cells was solely cytoplasmic with the absence of nodal, nuclear or septal localization. These data suggested that the C-terminal domain of Mid1p included determinants for Mid1p cortical association.

Combined, the data reported in this Thesis, alongside the data reported by Paoletti and Chang (2000), suggest the presence of a common pathway to regulate Mid1p nuclear and cortical localization through the NLS and the PH sequences.

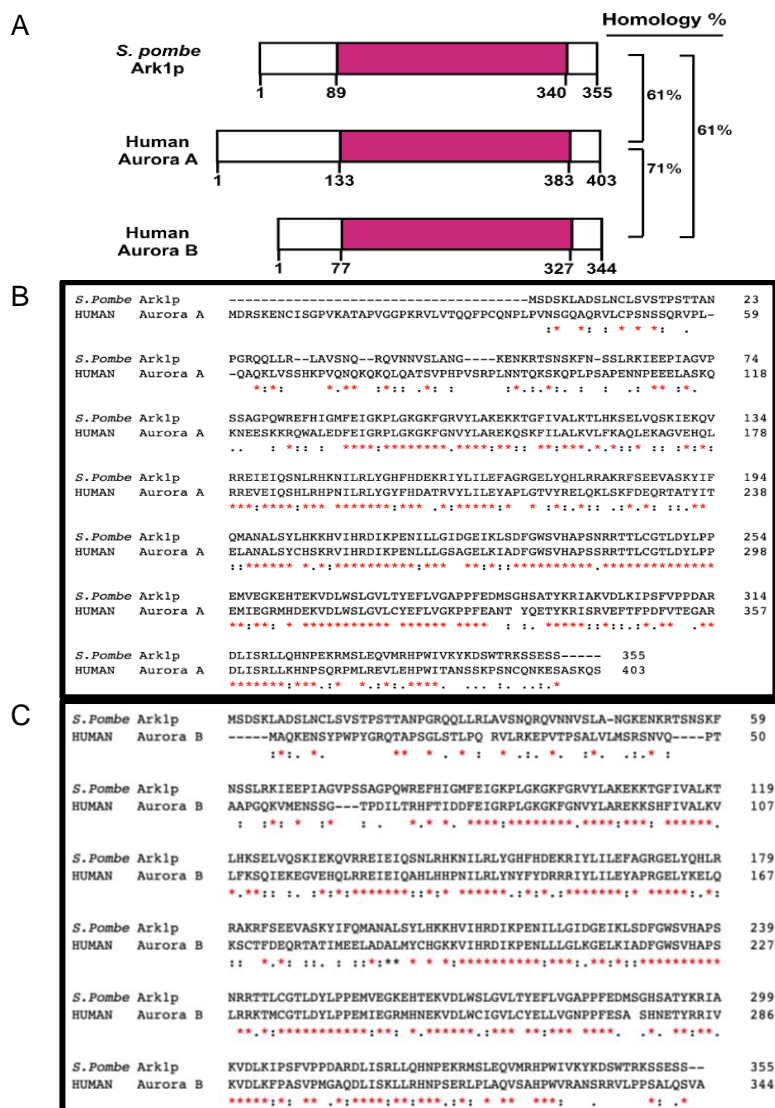
7.2 Regulation of anillin/Mid1p by the aurora kinase

Ark1p in *S. pombe* cell cycle.

7.2.1 *mid1*⁺ genetic interaction with the *ark1*⁺ gene suggests the phosphorylation of Mid1p by Ark1p to regulate *S. pombe* cell cycle

During the *S. pombe* cell cycle, Mid1p is phosphorylated by Plo1p kinase to promote mitotic entry (Almonacid et al., 2011). Similarly, the aurora Ark1p kinase is involved in regulating key events in *S. pombe* cell cycle (Leverson et al., 2002). Therefore, Mid1p could be a candidate substrate for Ark1p to regulate its function. To test for this regulation, we first investigated the genetic interaction between the *mid1*⁺ and *ark1*⁺ genes. Data presented in this Thesis demonstrated a novel genetic interaction (Section 5.3.2). To understand this genetic interaction, experiments were carried out to explore how the potential phosphorylation of Mid1p by Ark1p regulates *S. pombe* cell cycle.

We examined the *in vitro* phosphorylation of Mid1p "N-term", "Middle" and "C-term" recombinant proteins utilizing the mammalian homologue recombinant proteins of Ark1p (aurora A and B kinases) and Plo1p (plk1). The *in vitro* phosphorylation of the "N-term" and "Middle" domains of Mid1p by aurora A and plk1 kinases was detected. However, data generated from experiments had two main limitations: First, these experiments utilized purified mammalian aurora A and B kinases instead of *S. pombe* Ark1p due to the commercial unavailability of purified Ark1p. Therefore, the *in vitro* phosphorylation results could be misleading due the potential presence of different phospho-acceptor sites in Mid1p that could be phosphorylated by Ark1p. However, despite the difference in sequence between aurora kinases and Ark1p, both kinases have sequence homology and share a similar kinase domain sequence (Figure 7-2).



Second, the detected phosphorylation signals were generated from *in vitro* reactions, where in each case the substrate protein and the kinase were placed in close proximity, which might not mimic the physiological state in *S. pombe* cells. Although this is often cited as a limitation, there are many examples in which *in vitro* phosphorylation reactions identify phospho-acceptor sites which correspond to those observed *in vivo* (Aran, Bryant and Gould, 2011) and (Collins et al., 2012). Our *in vitro* phosphorylation experiment results showed that phosphorylation signals were detected by both mammalian recombinant kinases, aurora and plk1, suggesting that the aurora and plk1 mapped phospho-sites on Mid1p might be also recognized by *S. pombe* Ark1p and Plo1p, respectively.

7.2.1.1 Investigation of Mid1p potential plk1 and aurora A phospho-sites (S167, S328, S331, S332, S523 and S531)

Phospho-mapping of Mid1p "N-term" and "Middle" domains yielded a total of 35 potential phospho-sites, including phospho-sites S167, S328, S331, S332 and S523, where some/all of these five sites were identified not only in this analysis but also in some/all of four independent *S. pombe* global proteomic studies. Such comparison analysis allowed us to narrow down the number of Mid1p potential phospho-sites from 35 to 5 (Figure 5-7, Panel A) for further study.

In a different analysis, we used a Group-based prediction system (GPS) software to predict potential phospho-sites in Mid1p, which yielded one additional potential phospho-site, S531. In addition, S531 was identified as a Mid1p phospho-site by (Kettenbach et al., 2015), further supporting the possibility that it might represent a Mid1p phospho-site in our case. Therefore, it was added to the five Mid1p potential phospho-sites (S167, S328, S331, S332 and S523). To confirm these potential phospho-sites, Mid1p phospho-resistant mutants were designed for bacterial expression and purification then introduced to *in vitro* phosphorylation experiments with plk1 and aurora A kinases following by assessment of the phosphorylation signal status. Theoretically, the conversion from a serine (S) residue to an alanine (A) residue inhibits the phosphorylation event (if present). Therefore, the Mid1p phospho-resistant mutants were expected to show a reduced level of phosphorylation signals.

Data from the Mid1p "N-term" phospho-mutants' experiments (Section 5.3.4.3) showed a reduction in the phosphorylation signal of the "N-term" **S167A** and "N-term" **multiple** mutants (by both aurora A and plk1 kinases), and "N-term" **S331A** (by plk1 kinase) when compared to the phosphorylation signal of the original Mid1p "N-term" domain by aurora A and plk1. This suggests that the Serine (S) to Alanine (A) point mutation caused such reduction. This confirms the *in vitro* phosphorylation of S167 and S331 phospho-sites of the Mid1p "N-term" domain by aurora A and/or plk1 kinases.

Data from the Mid1p "Middle" phospho-mutants' experiments (Section 5.3.5.3) showed a reduction in the phosphorylation signal of the "Middle" **S523A** and "Middle" **multiple** mutants (by aurora A kinases) when compared to the phosphorylation signal of the original Mid1p "Middle" domain by aurora A and plk1. This suggests that the Serine (S) to Alanine (A) point mutation caused such reduction. Such reduction of the phosphorylation signal was not observed in the case of plk1 kinase reactions, where all "Middle" **S523A**, "Middle" **S531A** and "Middle" **multiple** mutants showed a strong phosphorylation signal similar to that observed in the original Mid1p "Middle" domain by plk1. This confirms the *in vitro* phosphorylation of S523 phospho-site of the Mid1p "Middle" domain by aurora A kinases.

The *in vitro* phosphorylation approach used to confirm Mid1p potential phospho-sites has limitations, as they may be not relevant in cells. To overcome these limitations, a complementary *in vivo* approach was used to confirm the relevance of the Mid1p S167, S328, S331, S332, S523 and S531 potential phospho-sites.

7.2.2 *In vivo* analysis of the role of S523 and S531 phospho-sites for the function of Mid1p during *S. pombe* cell cycle

S. pombe cells exhibit severe morphology defects in the absence of Mid1p function. Therefore, we tested the effect of mutations of Mid1p potential phospho-sites on cell morphology. Versions of the *mid1* gene containing phospho-site mutations were generated and integrated in a single copy into chromosomal DNA of in *S. pombe mid1Δ* cells whereby it was the sole *mid1* gene and expressed at endogenous levels. Such *mid1* phospho-sites mutations were subsequently

crossed into *ark1*-T11 cells to test their effect in the presence of defective Ark1p. Each version of the *mid1* gene had either a phospho-mimetic (serine to aspartic acid) or a phospho-resistant (serine to alanine) point mutation(s), to yield either single or multiple phospho-site(s) mutant *S. pombe* strains. Due to time constraints, data shown in this Thesis represents the functional analysis of two Mid1p potential phospho-sites, S523 and S531.

Upon integrating the wild-type *mid1*⁺ gene into *mid1*Δ cells and crossing into the *mid1*Δ *ark1*-T11 strains, similar cell morphology phenotype frequencies were observed in cells grown in liquid culture to those observed in wild-type and *ark1*-T11 strains, respectively. This confirmed that the *mid1*⁺ gene integrated in single copy at the *leu1*⁺ locus expressed at the endogenous level and fully complemented *mid1*Δ.

Upon integrating the phospho-mimetic mutants *mid1*Δ pJK148:*mid1*S523D or *mid1*Δ pJK148:*mid1*S531D genes into a *mid1*Δ strain, no cell morphology defects were observed in cells grown in liquid culture; moreover, they showed morphology phenotypes similar to those observed in wild-type cells. In contrast, upon integrating the phospho-resistant mutants *mid1*Δ pJK148:*mid1*S523A or *mid1*Δ pJK148:*mid1*S531A genes into a *mid1*Δ strain, cell morphology defects were observed in cells grown in liquid culture. These phenotypes were characterized and defined as cells with medial bulges, cells having a "capping" shape in one cell tip, cells having a "pointy" shape in one cell tip), and with diagonal septa instead of being perpendicular to the growth axis. Interestingly, no such cell morphology defects were observed in cells grown in solid YE media, instead the phospho-resistant mutants looked like wild-type cells (data not shown). Similarly, upon crossing the *mid1*Δ pJK148:*mid1*S523A or *mid1*Δ pJK148:*mid1*S531A genes into a *mid1*Δ *ark1*-T11 strain, cell morphology defects were observed. These phenotypes were characterized and defined as elongated cells, elongated cells with a bending angle, and elongated cells with a bending angle and multiple septa. Such cell morphology defects were not observed in *ark1*-T11 cells.

Overall, the cell morphology defects observed upon introducing a phospho-resistant mutation on the single or multiple S523A or S531A into either *mid1*Δ or *mid1*Δ *ark1*-T11 strains were defined in loss of the rod-like shape of cells. This indicated the importance of these two phospho-sites in Mid1p function during *S.*

pombe cell cycle to ensure medial division plane placement, and consequently equal sized and rod-shaped daughter cells. This suggests that the two potential phospho-sites, S523 and S531, are important for the function of Mid1p in *S. pombe* cell cycle regulation. Additionally, in Section 6.3.5, we illustrated that two different temperature-sensitive mutations in *ark1*⁺ gene, *ark1*-T8 and *ark1*-T11, caused defects in the cellular localization of GFP-Mid1p. These defects were mainly defined in *ark1*-T8 cells represented in GFP-Mid1p showing nuclear exclusion and appearing to be wrapping the nucleus. Overall, these cell separation defects suggest that the potential phosphorylation of Mid1p by Ark1p is involved in *S. pombe* septation regulation.

7.3 Overall conclusions

In this research, for the first time, we detected genetic interactions between both the *vps4*⁺ and *ark1*⁺ genes with the *mid1*⁺ gene. Combinatorial mutants revealed a synthetic growth phenotype indicating their requirement for *S. pombe* survival. Therefore, this research investigated two important aspects of Mid1p regulation to achieve *S. pombe* cell cycle regulation:

First: we tested Mid1p potential regulation by the ESCRT regulator Vps4p (Chapters 3 and 4). Initially, a physical interaction between Vps4p and Mid1p recombinant proteins was detected and mapped to the "C-term" domain of Mid1p.

Next, the effects of the absence of this interaction on the cellular localization of Mid1p were determined; this analysis revealed mis-localization of Mid1p and suggested a potential mechanism whereby Vps4p interacts with Mid1p through the PH domain to regulate Mid1p localization to cortical nodes. Then, this hypothetical mechanism was investigated by determining effects of the absence of Mid1p PH domain on its localization in *S. pombe*. Such analysis revealed mis-localization of Mid1p, but it was inconclusive in confirming the interaction between Mid1p-PH domain and Vps4p. Interestingly, the absence of the PH domain caused a Mid1p nuclear exclusion phenotype, suggesting that Mid1p PH domain is involved not only in its known role in Mid1p cortical anchorage but also in Mid1p nuclear localization. Therefore, it is possible that Mid1p nuclear localization regulates its interaction with Vps4p. To test this hypothesis, the well-characterized NLS regions

in Mid1p were utilized, and their requirement for the interaction with Vps4p was tested. Such analysis revealed that the interaction between Vps4p and Mid1p does not depend on Mid1p nuclear localization.

Second: we tested Mid1p potential regulation by the aurora kinase Ark1p (Chapters 5 and 6). Initially, *in vitro* phosphorylation of recombinant Mid1p by mammalian recombinant aurora A and plk1 kinases was tested; such analysis confirmed this interaction and mapped it to the "N-term" and "Middle" domains of Mid1p.

Next, Mid1p "N-term" and "Middle" domains were mapped to yield six potential phospho-sites (S167, S328, S331, S332, S523 and S531), which were utilized to confirm the *in vitro* phosphorylation. The results were inconclusive, so an *in vivo* integration *S. pombe* approach was utilized to confirm the phospho-sites. This approach involved the production of several versions of the *mid1* gene, each bearing a single or multiple phospho-mimetic or phospho-resistant mutation/s. These *mid1* gene versions were integrated into the chromosomal DNA of *mid1* Δ or a *mid1* Δ *ark1-T11* *S. pombe* strain at the endogenous *mid1*⁺ locus. Cell morphology phenotypes were then characterized for two selected Mid1p potential phospho-sites, S523 and S531. Defects in cell morphology were observed in the case of all phospho-resistant mutants but were not observed in the case of all phospho-mimetic mutants. Therefore, we concluded that the two Mid1p sites, S523 and S531, are important for its function.

Overall, the work reported in this Thesis provides insights into *S. pombe* cell cycle regulation. Using *in vivo* *S. pombe* genetic and microscopic approaches, in addition to *in vitro* pull-down and phosphorylation experiments we discovered novel Mid1p-dependent pathways for *S. pombe* cell cycle regulation.

7.4 Future directions

Does the Mid1p and Vps4p interaction involve the ATPase activity of Vps4p?

Vps4p is an AAA-type ATPase. During cytokinesis, it uses its ATPase activity to de-polymerize ESCRT-III filaments (Davies, Azmi and Katzmann, 2009); this

allows for the recycling of ESCRT-III subunits promoting further membrane scission events to yield the final separation of the two daughter cells (Chapter 1). Similarly, the interaction between Vps4p and the C-terminal domain of Mid1p might involve the ATPase activity of Vps4p.

We have attempted to measure the ATPase activity of Vps4p using an *in vitro* calorimetric approach, Malachite green assay, in which ATP hydrolysis can be quantified by increased green colour intensity. Our initial experimental design aimed at determining Vps4p original ATPase activity and comparing it to the activity upon addition of the Mid1p "N-term", "Middle" and "C-term" domains. However, we encountered difficulties in the elution of 6His-tagged Vps4p from Ni-NTA sepharose beads used for its purification, and therefore we could not obtain a sufficient amount of Vps4p to carry out the experiments.

Such experiments produced preliminary results on the activity of Vps4p (data not shown). Examining effects of the addition of each Mid1p domain separately on the ATPase activity of Vps4p could help in understanding and dissecting the nature of the interaction between Vps4p and Mid1p. Similarly, mutation of Vps4p to make so-called dominant negative versions which lack ATPase activity and the subsequent consideration of the impact of ATPase activity on these interactions would represent interesting avenues to explore.

Do Mid1p and Vps4p co-localize during *S. pombe* cell cycle?

The model we presented in Figure 7-1 claims that Vps4p regulates the function of Mid1p by facilitating its cortical anchorage to determine the division plane; this suggests that Mid1p and Vps4p might co-localize in the nodes and/or cell cortex during *S. pombe* cell cycle. Thus, *S. pombe* microscopy experiments were designed to investigate this potential co-localization.

In these experiments, an mCherry cassette that contains the antibiotic resistant marker KanR for selection in addition to a *nmt41* promoter to control overexpression of mCherry-Vps4p was generated and amplified by a PCR-based approach. This cassette was integrated into the chromosomal locus of the *vps4⁺* gene through homologous recombination to yield mCherry-Vps4p *S. pombe* strain.

The mCherry-Vps4p strain was crossed with the GFP-Mid1p (Section 3.3.5.1) using tetrad analysis and double mutants of *mcherry-vps4 gfp-mid1* were isolated; however unfortunately, due to time constraints and technical difficulties the co-localization of mCherry-Vps4p and GFP-Mid1p was not examined by confocal microscopy. The results of this experiment could yield valuable information on the spatial co-localization of Mid1p and Vps4p throughout *S. pombe* cell cycle.

Do Mid1p phospho-resistant mutants show a reduced level of *in vitro* phosphorylation by aurora A and plk1 kinases?

In vitro phosphorylation experiments we designed to confirm Mid1p S167, S328, S331, S332, S523 and S531 potential phospho-sites, where Mid1p phospho-resistant mutant recombinant proteins were generated (Section 5.3.3). Due to the lack of a stop codon at the end of Mid1p sequence, these proteins were re-designed to have the complete correct sequence including the stop codon.

Following bacterial expression and purification of these recombinant proteins, they will be introduced to new *in vitro* phosphorylation experiments by aurora A and plk1 kinases, to test the level of their *in vitro* phosphorylation. Data from the *in vivo* integration experiments confirmed the functional relevance of S523 and S531 (Section 6.3.2), Therefore, it was concluded that Ark1p is involved in regulating Mid1p function; encouragingly, data from the new *in vitro* phosphorylation experiments could support this conclusion.

Do Mid1p phospho-resistant mutations affect its localization in *S. pombe* cell cycle?

This Thesis provided a detailed analysis of the localization of GFP-Mid1p in wild-type *S. pombe* (Section 3.3.5.1). Strains similar to the GFP-Mid1p strain could be obtained by tagging GFP into the chromosomal locus of the phospho-mimetic/resistant *mid1* gene. Such confocal microscopy experiments could give valuable information regarding the effect of these mutations on the localization of Mid1p during *S. pombe* cell cycle. Tagging the *ark1*⁺ gene with mCherry in the GFP-Mid1p *S. pombe* strain might provide a clue of whether the two proteins co-localize or exist in close proximity to confirm their interaction to regulate *S. pombe*

cell cycle. To our knowledge, no such co-localization experiment was performed; this could be a promising future direction to further understand the regulation of *S. pombe* septation by Mid1p and Ark1p.

A potential coordination between Mid1p, Vps4p and Ark1p to regulate *S. pombe* cell cycle

Preliminary data from tetrad analysis experiments of aurora-related Mid1p S523 and S531 potential phospho-sites crossed with *vps4* Δ cells, indicated a defective cell morphology phenotype similar to that found in *mid1* Δ cells upon the introduction of a phospho-mimetic mutation of both Mid1p S523 and S531 residues. Several experimental approaches could build up based on this observation:

First, since the cell morphology defects observed in strains with both *ark1*-T11 and Mid1p S523 and S531 phospho-resistant mutations, detailed septation analysis is required to confirm any septation defects to compare them (if any) with the septation defect of *mid1* Δ (Section 3.3.2). **Second**, measurement of Vps4p ATPase activity upon the addition of the Mid1p original "N-term" and "Middle" domain versus Mid1p "N-term" and "Middle" phospho-mimetic/resistant mutant domains will provide information on the effect of these mutation on Vps4p ATPase activity (if any). However, crucial to these experiments is to first determine whether Vps4p ATPase activity is involved in the interaction with Mid1p.

Investigating anillin/VPS4 interaction during Extracellular Vesicle (EV) biogenesis in HEK293 human cells

Extracellular vesicle (EV) biogenesis is known to play a role in many important cellular processes such as, intercellular communication and membrane proteins release. EVs are grouped based on their intracellular origin to either ectosomes, which bud directly from the plasma membrane, or to exosomes, which are generated within endosomes and are released when fused to the plasma membrane (discussed in Chapter 1). Release of the extracellular vesicles involves members of the ESCRT machinery including VPS4, which plays a role in regulating ESCRT-III dynamics (discussed in Chapter 1).

A recent study by Jackson and colleagues investigated the role of ESCRTs in (EV) biogenesis by studying the effect of VPS4 inhibition on EVs release; they showed that VPS4 inhibition decreases the amount of released EVs, confirming the role of the ESCRT machinery in EV biogenesis (Jackson et al., 2017). From their conclusion we reasoned that ectosome EV releasing mechanism involves membrane fission events that might be similar to those carried out by ESCRT-III/VPS4 in abscission during cytokinesis (Discussed in Chapter 1).

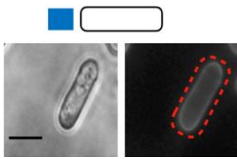
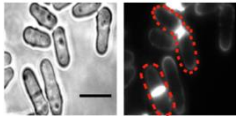
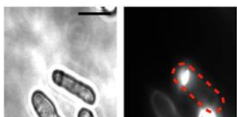
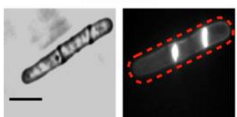
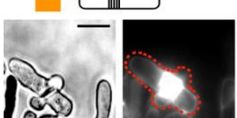
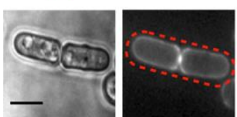
Data reported in this Thesis demonstrated the genetic and physical interactions between Mid1p and Vps4p; therefore, anillin might interact with VPS4 in mammalian cells. If this is the case during ectosome EV release, inhibition of anillin will affect EV release. An approach that involves the use of siRNA to inhibit anillin and ultracentrifugation to recover EVs from HEK293 human cells could give us a clue if anillin interacts with VPS4 to regulate such a process.

Chapter 8 Appendices

8.1 Appendix 1: *S. pombe* characterized phenotypes

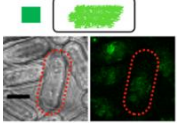
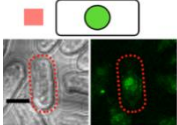
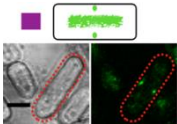
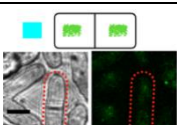
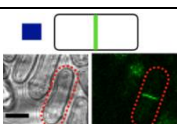
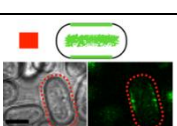
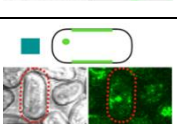
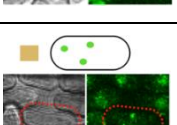
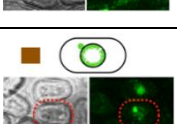
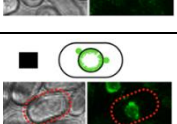
8.1.1 A summary of *S. pombe* septation phenotypes

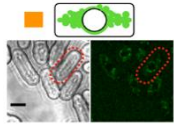
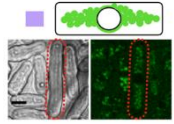
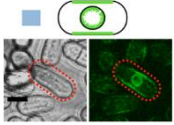
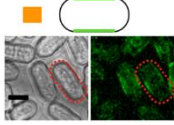
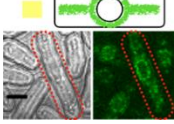
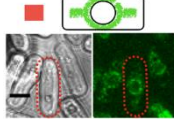
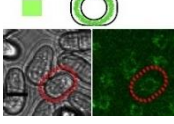
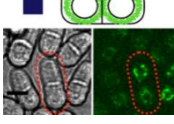
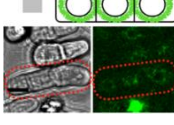
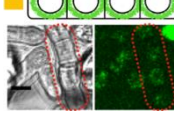
Table 8-1 *S. pombe* septation phenotypes characterized in this study.

No.	Septation phenotype	Description	Reference
1		Cells had a single septum medially positioned perpendicular to the growth axis (wild-type phenotype)	Section 3.3.2
2		Cells with septa not positioned at the centre of the cell but are instead displaced	Section 3.3.2
3		Cells with septa placed at the centre of the cell but are diagonal instead of being perpendicular to the growth axis	Section 3.3.2
4		Cells with two septa positioned at random sites of the cell	Section 3.3.2
5		Cells with branched and multiple septa	Section 3.3.2
6		Cells showed delayed separation after septation	Section 3.3.2

8.1.2 A summary of *S. pombe* GFP-Mid1p localization phenotypes

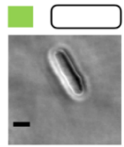
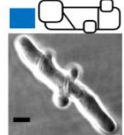

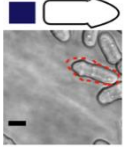


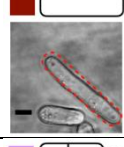
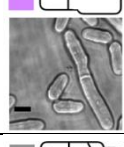
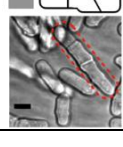
Table 8-2 *S. pombe* GFP-Mid1p localization phenotypes characterized in this study.

No.	GFP-Mid1p localization phenotype	Description	Reference
1		Cytoplasmic GFP-Mid1p localization	Section 3.3.5.1
2		Nuclear GFP-Mid1p localization	Section 3.3.5.1
3		GFP-Mid1p localized to two cortical nodes and the cytoplasm	Section 3.3.5.1
4		GFP-Mid1p was localized to the cytoplasm of two dividing cells	Section 3.3.5.1
5		GFP-Mid1p localization was septal	Section 3.3.5.1
6		GFP-Mid1p had a partial localization to the cytoplasm and medial cortex	Section 3.3.5.1
7		GFP-Mid1p localized to the medial cortex and one node randomly positioned	Section 3.3.5.1
8		GFP-Mid1p localized to three randomly positioned nodes	Section 3.3.5.1
9		Nuclear localization was coupled to the node's localization, (node attached to the nucleus)	Section 3.3.5.1
10		Nuclear localization was coupled to the node's localization, (two nodes attached to the nucleus)	Section 3.3.5.1

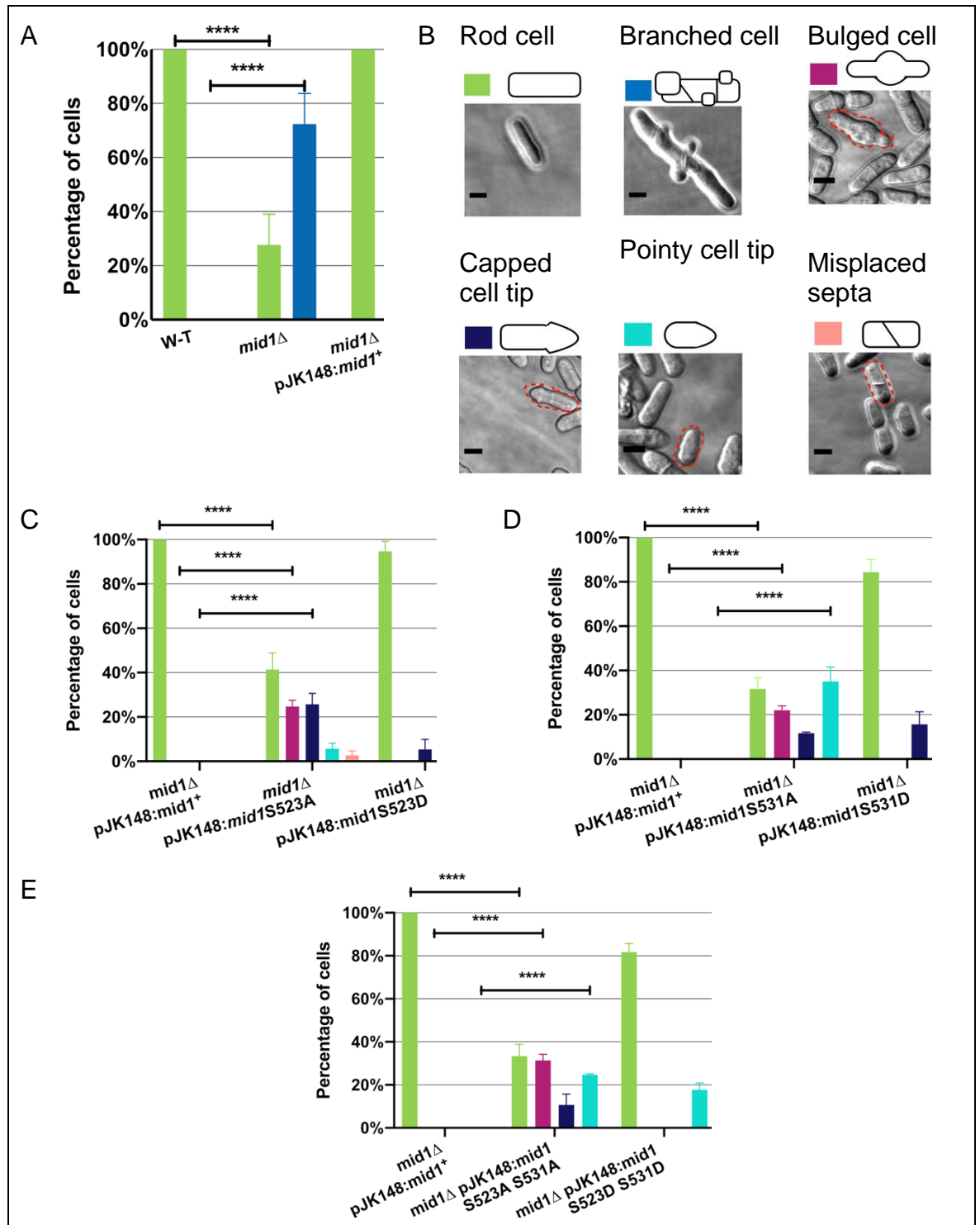
11		GFP-Mid1p localization cytoplasmic with a clear nuclear exclusion phenotype	Section 3.3.5.3
12		GFP-Mid1p localization cytoplasmic with a clear nuclear exclusion phenotype in elongated cells	Section 3.3.5.3
13		GFP-Mid1p showed medial cortex and nuclear exclusion localization	Section 4.3.3
14		GFP-Mid1p localized to the medial cortex	Section 4.3.3
15		GFP-Mid1p localization showed nuclear exclusion and appeared to be wrapping the nucleus in elongated cells	Section 6.3.5
16		GFP-Mid1p localization showed nuclear exclusion and appeared to be wrapping the nucleus	Section 6.3.5
17		GFP-Mid1p localization showed nuclear exclusion and appeared to be wrapping the nucleus in round cells	Section 6.3.5
18		GFP-Mid1p localization showed nuclear exclusion and appeared to be wrapping two nuclei	Section 6.3.5
19		GFP-Mid1p localization showed nuclear exclusion and appeared to be wrapping three nuclei	Section 6.3.5
20		GFP-Mid1p localization showed nuclear exclusion and appeared to be wrapping four nuclei	Section 6.3.5

8.1.3 A summary of *S. pombe* cell morphology phenotypes

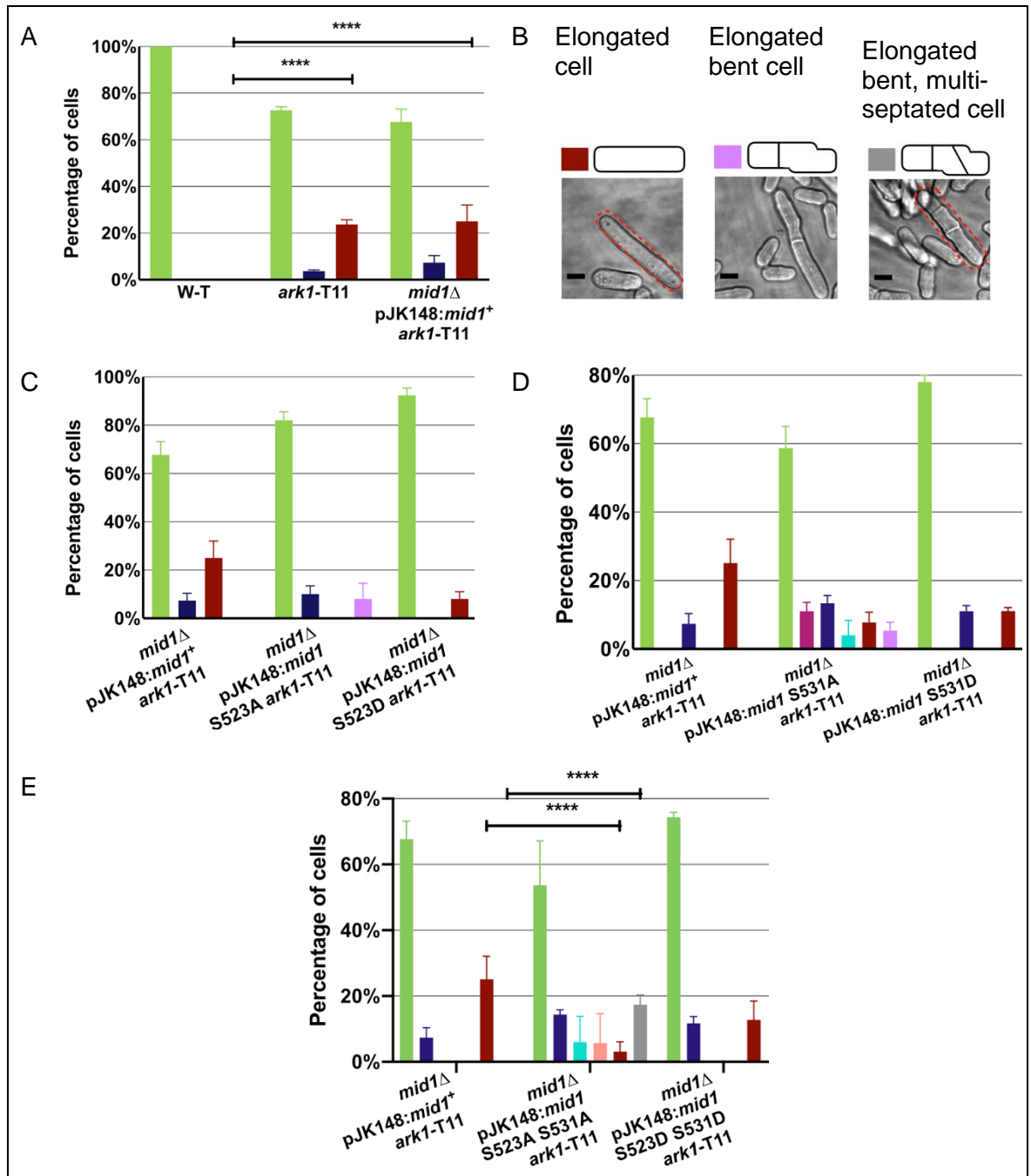
Table 8-3 *S. pombe* cell morphology phenotypes characterized in this study.

No.	Cell morphology phenotype	Description	Reference
1		Cells had a rod shape	Section 6.3.2.2
2		Cells acquired severe defects in shape as they appeared branched with multiple septa	Section 6.3.2.2
3		Medial bulges were observed	Section 6.3.2.2
4		Cells were not rod in shape but had a "capping" shape in one cell tip	Section 6.3.2.2
5		Cells were not rod in shape but had a "pointy" shape in one cell tip	Section 6.3.2.2
6		Septa were placed at the centre of the cell but are diagonal instead of being perpendicular to the growth axis	Section 6.3.2.2
7		Cells had a rod shape but appeared elongated	Section 6.3.2.3
8		Cells appeared long with a bending angle	Section 6.3.2.3
9		Cells appeared long with bending angles and multiple septa	Section 6.3.2.3

8.1.4 Classification and quantification of cell morphology phenotypes in *mid1* phospho-mimetic/resistant mutant *S. pombe* strains



8.1.5 Classification and quantification of cell morphology phenotypes in *mid1* phospho-mimetic/resistant mutant *S. pombe* strains



List of References

- Adams, R., Maiato, H., Earnshaw, W. and Carmena, M. (2001). Essential Roles of Drosophila Inner Centromere Protein (Incenp) and Aurora B in Histone H3 Phosphorylation, Metaphase Chromosome Alignment, Kinetochore Disjunction, and Chromosome Segregation. *The Journal of Cell Biology*, 153(4), pp.865-880.
- Akamatsu, M., Berro, J., Pu, K. M., Tebbs, I. R. and Pollard, T. D. (2014). Cytokinetic nodes in fission yeast arise from two distinct types of nodes that merge during interphase. *The Journal of Cell Biology*, 204(6), pp.977-988.
- Almonacid, M., Celton-Morizur, S., Jakubowski, J. L., Dingli, F., Loew, D., Mayeux, A., Chen, J. S., Gould, K. L., Clifford, D. M. and Paoletti, A. (2011). Temporal control of contractile ring assembly by Plo1 regulation of Myosin II recruitment by Mid1/Anillin. *Current Biology*, 21(6), pp.473-479.
- Almonacid, M., Moseley, J. B., Janvore, J., Mayeux, A., Fraissier, V., Nurse, P. and Paoletti, A. (2009). Spatial control of cytokinesis by Cdr2 kinase and Mid1/Anillin nuclear export. *Current Biology*, 19(11), pp.961-966.
- Anand, S., Penrhyn-Lowe, S. and Venkitaraman, A. R. (2003). AURORA-A amplification overrides the mitotic spindle assembly checkpoint, inducing resistance to Taxol. *Cancer Cell*, 3(1), pp.51-62.
- Anderson, B., Boldogh, I., Evangelista, M., Boone, C., Greene, L., and Pon, L. (1998). The Src Homology Domain 3 (SH3) of a Yeast Type I Myosin, Myo5p, Binds to Verprolin and Is Required for Targeting to Sites of Actin Polarization. *The Journal Of Cell Biology*, 141(6), pp.1357-1370.
- Arai, R. and Mabuchi, I. (2002). F-actin ring formation and the role of F-actin cables in the fission yeast *Schizosaccharomyces pombe*. *The Journal of Cell Science*. 115(5). pp, 887-98.
- Aran, V., Bryant, N. J. and Gould, G. W. (2011). Tyrosine phosphorylation of Munc18c on residue 521 abrogates binding to Syntaxin 4. *BMC Biochemistry*, 12(1), p.19.

- Babst, M., Davies, B. A. and Katzmman, D. J. (2011). Regulation of Vps4 during MVB sorting and cytokinesis. *Traffic*, 12(10), pp.1298-1305.
- Babst, M., Katzmman, D. J., Estepa-Sabal, E. J., Meerloo, T. and Emr, S. D. (2002). ESCRT-III: an endosome-associated heterooligomeric protein complex required for MVB sorting. *Developmental Cell*, 3(2), pp.271-282.
- Bähler, J., Wu, J. Q., Longtine, M. S., Shah, N. G., McKenzie III, A., Steever, A., B. Wach, A., Philippsen, P. and Pringle, J. R. (1998). Heterologous modules for efficient and versatile PCR-based gene targeting in *Schizosaccharomyces pombe*. *Yeast*, 14(10), pp.943-951.
- Balasubramanian, M. K., McCollum, D., Chang, L., Wong, K. C., Naqvi, N. I., He, X., Sazer, S. and Gould, K. L. (1998). Isolation and characterization of new fission yeast cytokinesis mutants. *Genetics*, 149(3), pp.1265–1275.
- Bathe, M. and Chang, F. (2010). Cytokinesis and the contractile ring in fission yeast: towards a systems-level understanding. *Trends in Microbiology*, 18(1), pp.38-45.
- Berdnik, D. and Knoblich, J. A. (2002). *Drosophila* Aurora-A is required for centrosome maturation and Actin-dependent asymmetric protein localization during mitosis. *Current Biology*, 12(8), pp.640-647.
- Bhola, N. E., Jansen, V. M., Bafna, S., Giltane, J. M., Balko, J. M., Estrada, M. V., Meszoely, I., Mayer, I., Abramson, V., Ye, F., Sanders, M., Dugger, T. C., Allen, E. V. and Arteaga, C. L. (2015). Kinome-wide functional screen identifies role of PLK1 in hormone-independent, ER-positive breast cancer. *Cancer Research*, 75(2), pp.405-414.
- Bhutta, M.S. (2014). *Investigating the Role of the ESCRT Proteins in Cytokinesis*. PhD Thesis submitted to the University of Glasgow.
- Bhutta, M.S., Roy, B., Gould, G.W. and McNerny, C.J. (2014). A complex network of interactions between mitotic kinases, phosphatases and ESCRT proteins regulates septation and membrane trafficking in *S. pombe*. *PLoS ONE*, 9(10), p.e111789.
- Bostock, C. J. (1970). DNA synthesis in the fission yeast *Schizosaccharomyces pombe*. *Experimental Cell Research*, 60(1), pp.16-26.

Caballe, A. and Martin-Serrano, J. (2011). ESCRT machinery and cytokinesis: the road to daughter cell separation. *Traffic*, 12(10), pp.1318-1326.

Carpy, A., Krug, K., Graf, S., Koch, A., Popic, S., Hauf, S. and Macek, B. (2014). Absolute proteome and phosphoproteome dynamics during the cell cycle of *Schizosaccharomyces pombe* (fission yeast). *Molecular & Cellular Proteomics*, 13(8), pp.1925-1936.

Castro, A., Bernis, C., Vigneron, S., Labbé, J. C. and Lorca, T. (2005). The anaphase-promoting complex: a key factor in the regulation of cell cycle. *Oncogene*, 24(3), pp.314-325.

Celton-Morizur, S., Bordes, N., Fraissier, V., Tran, P. T. and Paoletti, A. (2004). C-terminal anchoring of Mid1p to membranes stabilizes cytokinetic ring position in early mitosis in fission yeast. *Molecular and Cellular Biology*, 24(24), pp.10621-10635.

Chan, C. S., and Botstein, D. (1993). Isolation and characterization of chromosome-gain and increase-in-ploidy mutants in yeast. *Genetics*, 135(3), pp.677–691.

Chang, F. and Nurse, P. (1996). How fission yeast fission in the middle. *Cell*, 84(2), pp.191-194.

Chang, F., Woollard, A. and Nurse, P. (1996). Isolation and characterization of fission yeast mutants defective in the assembly and placement of the contractile actin ring. *Journal of Cell Science*, 109(Pt1), pp.131-142.

Chieffi, P., Cozzolino, L., Kisslinger, A., Libertini, S., Staibano, S., Mansueto, G., De Rosa, G., Villacci, A., Vitale, M., Linardopoulos, S., Portella, G. and Tramontano, D. (2006). Aurora B expression directly correlates with prostate cancer malignancy and influence prostate cell proliferation. *The Prostate*, 66(3), pp.326-333.

Coffman, V., Nile, A., Lee, I., Liu, H., and Wu, J. (2009). Roles of Formin Nodes and Myosin Motor Activity in Mid1p-dependent Contractile-Ring Assembly during Fission Yeast Cytokinesis. *Molecular Biology Of The Cell*, 20(24), pp. 5195-5210.

Collins, L. L., Simon, G., Matheson, J., Wu, C., Miller, M. C., Otani, T., Yu, X., Hayashi, S., Prekeris, R. and Gould, G. W. (2012). Rab11-FIP3 is a cell cycle-regulated phosphoprotein. *BMC Cell Biology*, 13(1), p.4.

Cueille, N., Salimova, E., Esteban, V., Blanco, M., Moreno, S., Bueno, A. and Simanis, V. (2001). Flp1, a fission yeast orthologue of the *S. cerevisiae* CDC14 gene, is not required for cyclin degradation or rum1p stabilisation at the end of mitosis. *Journal of Cell Science*, 114(14), pp. 2649-64.

Daga, R. R. and Chang, F. (2005). Dynamic positioning of the fission yeast cell division plane. *Proceedings of the National Academy of Sciences*, 102(23), pp.8228-8232.

Davies, B. A., Azmi, I. F. and Katzmann, D. J. (2009). Regulation of Vps4 ATPase activity by ESCRT-III. *Biochemical Society Transactions*, 37(1), pp.143-145.

D'Avino, P. P. (2009). How to scaffold the contractile ring for a safe cytokinesis - lessons from Anillin-related proteins. *Journal of Cell Science*, 122(8), pp.1071-1079.

D'Avino, P. P., Takeda, T., Capalbo, L., Zhang, W., Lilley, K. S., Laue, E. D. and Glover, D. M. (2008). Interaction between Anillin and RacGAP50C connects the actomyosin contractile ring with spindle microtubules at the cell division site. *Journal of Cell Science*, 121(8), pp.1151-1158.

Duijf, P. H., Schultz, N. and Benezra, R. (2012). Cancer cells preferentially lose small chromosomes. *International Journal of Cancer*, 132(10), pp.2316-2326.

Elia, N., Fabrikant, G., Kozlov, M. M. and Lippincott-Schwartz, J. (2012). Computational model of cytokinetic abscission driven by ESCRT-III polymerization and remodeling. *Biophysical Journal*, 102(10), pp.2309-2320.

Elia, N., Sougrat, R., Spurlin, T. A., Hurley, J. H. and Lippincott-Schwartz, J. (2011). Dynamics of endosomal sorting complex required for transport (ESCRT) machinery during cytokinesis and its role in abscission. *Proceedings of the National Academy of Sciences*, 108(12), pp.4846-4851.

- Evans, T., Rosenthal, E. T., Youngblom, J., Distel, D. and Hunt, T. (1983). Cyclin: a protein specified by maternal mRNA in sea urchin eggs that is destroyed at each cleavage division. *Cell*, 33(2), pp.389-396.
- Fields, A. P. and Justilien, V. (2010). The guanine nucleotide exchange factor (GEF) Ect2 is an oncogene in human cancer. *Advances in Enzyme Regulation*, 50(1), pp.190-200.
- Fujiwara, K. and Pollard, T. D. (1976). Fluorescent antibody localization of myosin in the cytoplasm, cleavage furrow, and mitotic spindle of human cells. *The Journal of Cell Biology*, 71(3), pp.848-875.
- Gassmann, R., Carvalho, A., Henzing, A., Ruchaud, S., Hudson, D., Honda, R., Nigg, E., Gerloff, D. and Earnshaw, W. (2004). Borealin. *The Journal of Cell Biology*, 166(2), pp.179-191.
- Ghazi-Tabatabai, S., Saksena, S., Short, J. M., Pobbati, A. V., Veprintsev, D. B., Crowther, R. A., Emr, S. D., Egelman, E. H. and Williams, R. L. (2008). Structure and disassembly of filaments formed by the ESCRT-III subunit Vps24. *Structure*, 16(9), pp.1345-1356.
- Glover, D. M., Leibowitz, M. H., McLean D. A. and Parry, H. (1995). Mutations in aurora prevent centrosome separation leading to the formation of monopolar spindles. *Cell*, 81(1), pp.95-105.
- Goliand, I., Adar-Levor, S., Segal, I., Nachmias, D., Dadosh, T., Kozlov, M. M. and Elia, N. (2018). Resolving ESCRT-III spirals at the intercellular bridge of dividing cells using 3D STORM. *Cell Reports*, 24(7), pp.1756-1764.
- Gopalan, G., Chan, C. and Donovan, P. (1997). A Novel Mammalian, Mitotic Spindle-associated Kinase Is Related to Yeast and Fly Chromosome Segregation Regulators. *The Journal of Cell Biology*, 138(3), pp.643-656.
- Gould, G.W. (2016). Animal cell cytokinesis: the role of dynamic changes in the plasma membrane proteome and lipidome. *Seminars in Cell & Developmental Biology*, 53, pp.64-73.
- Grallert, A., Grallert, B., Ribar, B., and Sipiczki, M. (1998). Coordination of initiation of nuclear division and initiation of cell division in

- Schizosaccharomyces pombe*: genetic interactions of mutations. *Journal of bacteriology*, 180(4), pp.892–900.
- Gruneberg, U., Glotzer, M., Gartner, A. and Nigg, E. (2002). The CeCDC-14 phosphatase is required for cytokinesis in the *Caenorhabditis elegans* embryo. *The Journal of Cell Biology*, 158(5), pp.901-914.
- Guizetti, J., Schermelleh, L., Mäntler, J., Maar, S., Poser, I., Leonhardt, H., Müller-Reichert, T., and Gerlich, D. W. (2011). Cortical constriction during abscission involves helices of ESCRT-III-dependent filaments. *Science*, 331(6024), pp. 1616-1620.
- Gutteridge, R. E., Ndiaye, M. A., Liu, X. and Ahmad, N. (2016). Plk1 inhibitors in cancer therapy: from laboratory to clinics. *Molecular Cancer Therapeutics*, 15(7), pp.1427-1435.
- Guzman-Vendrell, M., Baldissard, S., Almonacid, M., Mayeux, A., Paoletti, A. and Moseley, J. B. (2013). Blt1 and Mid1 provide overlapping membrane anchors to position the division plane in fission yeast. *Molecular and Cellular Biology*, 33(2), pp.418-428.
- Hachet, O. and Simanis, V. (2008). Mid1p/anillin and the septation initiation network orchestrate contractile ring assembly for cytokinesis. *Genes & Development*, 22(22), pp.3205-3216.
- Hagting, A., Den Elzen, N., Vodermaier, H. C., Waizenegger, I. C., Peters, J. M. and Pines, J. (2002). Human securin proteolysis is controlled by the spindle checkpoint and reveals when the APC/C switches from activation by Cdc20 to Cdh1. *Journal of Cell Biology*, 157(7), pp.1125–1137.
- Hannak, E., Kirkham, M., Hyman, A. A., and Oegema, K. (2001). Aurora-A kinase is required for centrosome maturation in *Caenorhabditis elegans*. *The Journal of Cell Biology*, 155(7), pp.1109-1115.
- Hanson, P. I. and Cashikar, A. (2012). Multivesicular body morphogenesis. *Annual Review of Cell and Developmental Biology*, 28(1), pp.337-362.
- Hartwell, L. H., Culotti, J., Pringle, J. R. and Reid, B. J. (1974). Genetic control of the cell division cycle in yeast. *Science*, 183(4120), pp.46-51.

- Haubrich, B. A. and Swinney, D. C. (2016). Enzyme activity assays for protein kinases: strategies to identify active substrates. *Current Drug Discovery Technologies*, 13(1), pp.2–15.
- Hauf, S., Cole, R. W., LaTerra, S., Zimmer, C., Schnapp, G., Walter, R., Heckel, A., van Meel, J., Rieder, C. L. and Peters, J. M. (2003). The small molecule Hesperadin reveals a role for Aurora B in correcting kinetochore–microtubule attachment and in maintaining the spindle assembly checkpoint. *The Journal of Cell Biology*, 161(2), pp.281-294.
- Hickson, G. R. and O'Farrell, P. H. (2008). Rho-dependent control of anillin behavior during cytokinesis. *The Journal of Cell Biology*, 180(2), pp.285-294.
- Hirota, T., Kunitoku, N., Sasayama, T., Marumoto, T., Zhang, D., Nitta, M., Hatakeyama, K. and Saya, H. (2003). Aurora-A and an interacting activator, the LIM protein Ajuba, are required for mitotic commitment in human cells. *Cell*, 114(5), pp.585-598.
- Hunt, T., Nasmyth, K., and Novák, B. (2011). The cell cycle. *Philosophical transactions of the Royal Society of London. Series B, Biological sciences*, 366(1584), pp. 3494–3497.
- Hussey, P., Allwood, E., and Smertenko, A. (2002). Actin–binding proteins in the Arabidopsis genome database: properties of functionally distinct plant actin–depolymerizing factors/cofilins. *Philosophical Transactions Of The Royal Society Of London. Series B: Biological Sciences*, 357(1422), pp. 791-798.
- Iwaki, T., Onishi, M., Ikeuchi, M., Kita, A., Sugiura, R., Giga-Hama, Y., Fukui, Y. and Takegawa, K. (2007). Essential roles of class E Vps proteins for sorting into multivesicular bodies in *Schizosaccharomyces pombe*. *Microbiology*, 153(8), pp.2753-2764.
- Jackson, C. E., Scruggs, B. S., Schaffer, J. E. and Hanson, P. I. (2017). Effects of inhibiting VPS4 support a general role for ESCRTs in extracellular vesicle biogenesis. *Biophysical Journal*, 113(6), pp.1342-1352.
- Johnson, V. L., Scott, M. I., Hussein, D. and Taylor, S. S. (2004). Bub1 is required for kinetochore localization of BubR1, Cenp-E, Cenp-F and Mad2, and chromosome congression. *Journal of Cell Science*, 117(8), pp.1577-1589.

- Johnson, A. E., McCollum, D. and Gould, K. L. (2012). Polar opposites: fine-tuning cytokinesis through SIN asymmetry. *Cytoskeleton*, 69(10), pp.686-699.
- Kamasaki, T., Osumi, M., and Mabuchi, I. (2007). Three-dimensional arrangement of F-actin in the contractile ring of fission yeast. *The Journal Of Cell Biology*, 178(5), pp. 765-771.
- Kettenbach, A. N., Deng, L., Wu, Y., Baldissard, S., Adamo, M. E., Gerber, S. A. and Moseley, J. B. (2015). Quantitative phosphoproteomics reveals pathways for coordination of cell growth and division by the conserved fission yeast kinase Pom1. *Molecular & Cellular Proteomics*, 14(5), pp.1275-1287.
- Kim, H., Johnson, J. M., Lera, R. F., Brahma, S. and Burkard, M. E. (2017). Anillin phosphorylation controls timely membrane association and successful cytokinesis. *PLoS Genetics*, 13(1), p.e1006511.
- Koch, A., Krug, K., Pengelley, S., Macek, B. and Hauf, S. (2011). Mitotic substrates of the kinase Aurora with roles in chromatin regulation identified through quantitative phosphoproteomics of fission yeast. *Science Signaling*, 4(179), pp.rs6-rs6.
- Krapp, A., Collin, P., Cokoja, A., Dischinger, S., Cano, E. and Simanis, V. (2006). The *Schizosaccharomyces pombe* septation initiation network (SIN) is required for spore formation in meiosis. *Journal of Cell Science*, 119(14), pp.2882-2891.
- Laplante, C., Huang, F., Tebbs, I. R., Bewersdorf, J. and Pollard, T. D. (2016). Molecular organization of cytokinesis nodes and contractile rings by super-resolution fluorescence microscopy of live fission yeast. *Proceedings of the National Academy of Sciences*, 113(40), pp.E5876-E5885.
- Laporte, D., Coffman, V. C., Lee, I. J. and Wu, J. Q. (2011). Assembly and architecture of precursor nodes during fission yeast cytokinesis. *The Journal of Cell Biology*, 192(6), pp.1005-1021.
- Lara-Gonzalez, P., Westhorpe, F., G, and Taylor, S., S. (2012). The spindle assembly checkpoint. *Current Biology*. 22(22), Pp. R966-80.

- Le Goff, X., Utzig, S. and Simanis, V. (1999). Controlling septation in fission yeast: finding the middle, and timing it right. *Current Genetics*, 35(6), pp.571-584.
- Lemmon, M. A., Ferguson, K. M. and Schlessinger, J. (1996). PH domains: diverse sequences with a common fold recruit signaling molecules to the cell surface. *Cell*, 85(5), pp.621-624.
- Lens, S. M. A. and Medema, R. H. (2019). Cytokinesis defects and cancer. *Nature Reviews Cancer*, 19(1), pp.32-45.
- Leverson, J. D., Huang, H. K., Forsburg, S. L. and Hunter, T. (2002). The *Schizosaccharomyces pombe* Aurora-related kinase Ark1 interacts with the inner centromere protein Pic1 and mediates chromosome segregation and cytokinesis. *Molecular Biology of the Cell*, 13(4), pp.1132-1143.
- Lian, Y. F., Huang, Y. L., Wang, J. L., Deng, M. H., Xia, T. L., Zeng, M. S., Chen, M. S., Wang, H. B. and Huang, Y. H. (2018). Anillin is required for tumor growth and regulated by miR-15a/miR-16-1 in HBV-related hepatocellular carcinoma. *Aging*, 10(8), pp.1884-1901.
- Lowery, D. M., Clauser, K. R., Hjerrild, M., Lim, D., Alexander, J., Kishi, K., Ong, S. E., Gammeltoft, S., Carr, S. A. and Yaffe, M. B. (2007). Proteomic screen defines the Polo-box domain interactome and identifies Rock2 as a Plk1 substrate. *The EMBO journal*, 26(9), pp. 2262–2273.
- Mabuchi, I. and Okuno, M. (1977). The effect of myosin antibody on the division of starfish blastomeres. *The Journal of Cell Biology*, 74(1), pp.251-263.
- Maddox, A. S., Desai, A., Oegema, K. and Habermann, B. (2005). Distinct roles for two *C. elegans* anillins in the gonad and early embryo. *Development*, 132(12), pp.2837-2848.
- Maity, S., Caillat, C., Miguet, N., Sulbaran, G., Effantin, G., Schoehn, G., Roos, W. H. and Weissenhorn, W. (2019). VPS4 triggers constriction and cleavage of ESCRT-III helical filaments. *Science Advances*, 5(4), p.eaau7198.
- Marks, J., and Hyams, J. S. (1985). Localization of F-actin through the cell division cycle of *Schizosaccharomyces pombe*. *European Journal of Cell Biology*. (39), pp. 27–32.

- Marumoto, T., Zhang, D. and Saya, H. (2005). Aurora-A — a guardian of poles. *Nature Reviews Cancer*, 5(1), pp.42-50.
- McCollum, D. and Gould, K. (2001). Timing is everything: regulation of mitotic exit and cytokinesis by the MEN and SIN. *Trends in Cell Biology*, 11(2), pp.89-95.
- Melichar, B., Adenis, A., Lockhart, A. C., Bennouna, J., Dees, E. C., Kayaleh, O., Obermannova, R., DeMichele, A., Zatloukal, P., Zhang, B., Ullmann, C. D. and Schusterbauer, C. (2015). Safety and activity of alisertib, an investigational aurora kinase A inhibitor, in patients with breast cancer, small-cell lung cancer, non-small-cell lung cancer, head and neck squamous-cell carcinoma, and gastro-oesophageal adenocarcinoma: a five-arm phase 2 study. *The Lancet Oncology*, 16(4), pp.395-405.
- Mertins, P., and Gallwitz, D. (1987). A single intronless actin gene in the fission yeast *Schizosaccharomyces pombe*: nucleotide sequence and transcripts formed in homologous and heterologous yeast. *Nucleic Acids Research*, 15(18), pp. 7369-7379.
- Miller, K. G., Field, C. M. and Alberts, B. M. (1989). Actin-binding proteins from *Drosophila* embryos: a complex network of interacting proteins detected by F-actin affinity chromatography. *The Journal of Cell Biology*, 109(6), pp.2963-2975.
- Mishima, M., Kaitna, S. and Glotzer, M. (2002). Central spindle assembly and cytokinesis require a kinesin-like protein/RhoGAP complex with microtubule bundling activity. *Developmental Cell*, 2(1), pp.41-54.
- Moreno, S., Klar, A. and Nurse, P. (1991). Molecular genetic analysis of fission yeast *Schizosaccharomyces pombe*. *Methods in Enzymology*, 194, pp.795-823.
- Morgan, D. O. (1995). Principles of CDK regulation. *Nature*, 374(6518), pp.131-134.
- Morgan, D. O. (1999). Regulation of the APC and the exit from mitosis. *Nature Cell Biology*. 1(2), E47-E53.

- Morita, E., Colf, L. A., Karren, M. A., Sandrin, V., Rodesch, C. K. and Sundquist, W. I. (2010). Human ESCRT-III and VPS4 proteins are required for centrosome and spindle maintenance. *Proceedings of the National Academy of Sciences*, 107(29), pp.12889-12894.
- Morita, E., Sandrin, V., Chung, H. Y., Morham, S. G., Gygi, S. P., Rodesch, C. K. and Sundquist, W. I. (2007). Human ESCRT and ALIX proteins interact with proteins of the midbody and function in cytokinesis. *The EMBO Journal*, 26(19), pp.4215-4227.
- Motegi, F., Mishra, M., Balasubramanian, M. K. and Mabuchi, I. (2004). Myosin-II reorganization during mitosis is controlled temporally by its dephosphorylation and spatially by Mid1 in fission yeast. *The Journal of Cell Biology*, 165(5), pp.685-695.
- Musacchio, A. and Salmon, E. (2007). The spindle-assembly checkpoint in space and time. *Nature Reviews Molecular Cell Biology*, 8(5), pp.379-393.
- Nasmyth, K. (2001). Disseminating the genome: joining, resolving, and separating sister chromatids during mitosis and meiosis. *Annual Review of Genetics*, 35, pp.673–745.
- Nezi, L. and Musacchio, A. (2009). Sister chromatid tension and the spindle assembly checkpoint. *Current Opinion in Cell Biology*, 21(6), pp.785-795.
- Nigg, E. A. (2001). Mitotic kinases as regulators of cell division and its checkpoints. *Nature Reviews Molecular Cell Biology*, 2(1), pp.21-32.
- Niiya, F., Xie, X., Lee, K. S., Inoue, H. and Miki, T. (2005). Inhibition of cyclin-dependent kinase 1 induces cytokinesis without chromosome segregation in an ECT2 and MgcRacGAP-dependent manner. *Journal of Biological Chemistry*, 280(43), pp.36502-36509.
- Nurse, P., Thuriaux, P., and Nasmyth, K. (1976). Genetic control of the cell division cycle in the fission yeast *Schizosaccharomyces pombe*. *Molecular and General Genetics*, 146(2), pp. 167-178.
- Obita, T., Saksena, S., Ghazi-Tabatabai, S., Gill, D. J., Perisic, O., Emr, S. D. and Williams, R. L. (2007). Structural basis for selective recognition of ESCRT-III by the AAA ATPase Vps4. *Nature*, 449(7163), pp.735-739.

- Oegema, K., Savoian, M. S., Mitchison, T. J. and Field, C. M. (2000). Functional analysis of a human homologue of the *Drosophila* Actin binding protein Anillin suggests a role in cytokinesis. *The Journal of Cell Biology*, 150(3), pp.539-552.
- Ohkura, H., Hagan, I. M. and Glover, D. M. (1995). The conserved *Schizosaccharomyces pombe* kinase plo1, required to form a bipolar spindle, the actin ring, and septum, can drive septum formation in G1 and G2 cells. *Genes & Development*, 9(9), pp.1059-1073.
- Paavilainen, V., Bertling, E., Falck, S., and Lappalainen, P. (2004). Regulation of cytoskeletal dynamics by actin-monomer-binding proteins. *Trends In Cell Biology*, 14(7), pp.386-394.
- Pantaloni, D. (2001). Mechanism of Actin-Based Motility. *Science*, 292(5521), pp.1502-1506.
- Paoletti, A., and Chang, F. (2000). Analysis of mid1p, a protein required for placement of the cell division site, reveals a link between the nucleus and the cell surface in fission yeast. *Molecular biology of the cell*, 11(8), pp.2757–2773.
- Pelham, R., and Chang, F. (2002). Actin dynamics in the contractile ring during cytokinesis in fission yeast. *Nature*, 419(6902), pp. 82-86.
- Petersen, J. and Hagan, I. M. (2003). *S. pombe* Aurora kinase/survivin Is required for chromosome condensation and the spindle checkpoint attachment response. *Current Biology*, 13(7), pp.590-597.
- Petersen, J., Paris, J., Willer, M., Philippe, M. and Hagan, I. M. (2001). The *S. pombe* aurora-related kinase Ark1 associates with mitotic structures in a stage dependent manner and is required for chromosome segregation. *Journal of Cell Science*, 114(24), pp.4371-4384.
- Pollard, T., D. and Korn, E., D. (1973). Acanthamoeba myosin. I. Isolation from Acanthamoeba castellanii of an enzyme similar to muscle myosin. *The Journal of Biological Chemistry*. 248(13). pp, 4682-90.
- Pollard, T., Blanchoin, L., and Mullins, R. (2000). Molecular Mechanisms Controlling Actin Filament Dynamics in Nonmuscle Cells. *Annual Review Of Biophysics And Biomolecular Structure*, 29(1), pp.545-576.

- Rechsteiner, M. and Rogers, S. W. (1996). PEST sequences and regulation by proteolysis. *Trends in Biochemical Sciences*, 21(7), pp.267-271.
- Rezig, I., Bremner, S., Bhutta, M., Salt, I., Gould, G.W. and McInerny, C.J. (2019). Genetic and cytological methods to study ESCRT cell cycle function in fission yeast. Culetto E, and Legouis R, (eds.). In: *Lab Protocol Series Methods in Molecular Biology*. Springer Nature Edition. In Press.
- Russell, P. and Nurse, P. (1986). *Schizosaccharomyces pombe* and *Saccharomyces cerevisiae*: a look at yeasts divided. *Cell*, 45(6), pp.781-782.
- Saha, S. and Pollard, T. D. (2012a). Anillin-related protein Mid1p coordinates the assembly of the cytokinetic contractile ring in fission yeast. *Molecular Biology of the Cell*, 23(20), pp.3982-3992.
- Saha, S., & Pollard, T. D. (2012b). Characterization of structural and functional domains of the anillin-related protein Mid1p that contribute to cytokinesis in fission yeast. *Molecular biology of the cell*, 23(20), pp.3993–4007.
- Sambrook, J. and Green, M. (2012). *Molecular Cloning*. 4th ed. New York: Cold Spring Harbor Laboratory Press, USA.
- Schlüter, K., Jockusch, B., and Rothkegel, M. (1997). Profilins as regulators of actin dynamics. *Biochimica et Biophysica Acta - Molecular Cell Research*, 1359(2), pp. 97-109.
- Schroeder, T. E. (1972). The contractile ring. II. Determining its brief existence, volumetric changes, and vital role in cleaving *Arbacia* eggs. *The Journal of Cell Biology*, 53(2), pp.419-434.
- Schroeder, T. E. (1973). Actin in dividing cells: contractile ring filaments bind heavy meromyosin. *Proceedings of the National Academy of Sciences*, 70(6), pp.1688-1692.
- Schuh, A. L. and Audhya, A. (2014). The ESCRT machinery: from the plasma membrane to endosomes and back again. *Critical Reviews in Biochemistry and Molecular Biology*, 49(3), pp.242-261.
- Shimoda, C. (2004). Forespore membrane assembly in yeast: coordinating SPBs and membrane trafficking. *Journal of Cell Science*, 117(3), pp.389-396.

- Siam, R., Dolan, W. P. and Forsburg, S. L. (2004). Choosing and using *Schizosaccharomyces pombe* plasmids. *Methods*, 33(3), pp.189-198.
- Sohrmann, M., Fankhauser, C., Brodbeck, C. and Simanis, V. (1996). The *dmf1/mid1* gene is essential for correct positioning of the division septum in fission yeast. *Genes & Development*, 10(21), pp.2707-2719.
- Sorrentino, R., Libertini, S., Pallante, P. L., Troncone, G., Palombini, L., Bavetsias, V., Spalletti-Cernia, D., Laccetti, P., Linardopoulos, S., Chieffi, P., Fusco, A. and Portella, G. (2005). Aurora B overexpression associates with the thyroid carcinoma undifferentiated phenotype and is required for thyroid carcinoma cell proliferation. *The Journal of Clinical Endocrinology & Metabolism*, 90(2), pp.928-935.
- Sparks, C. A., Morpew, M. and McCollum, D. (1999). Sid2p, a spindle pole body kinase that regulates the onset of cytokinesis. *The Journal of Cell Biology*, 146(4), pp.777-790.
- Straight, A. F., Field, C. M. and Mitchison, T. J. (2005). Anillin binds nonmuscle Myosin II and regulates the contractile ring. *Molecular Biology of the Cell*, 16(1), pp.193-201.
- Stuchell-Brereton, M. D., Skalicky, J. J., Kieffer, C., Karren, M. A., Ghaffarian, S. and Sundquist, W. I. (2007). ESCRT-III recognition by VPS4 ATPases. *Nature*, 449(7163), pp.740-744.
- Sun, L., Guan, R., Lee, I. J., Liu, Y., Chen, M., Wang, J., Wu, J. Q. and Chen, Z. (2015). Mechanistic Insights into the anchorage of the contractile ring by Anillin and Mid1. *Developmental Cell*, 33(4), pp.413-426.
- Swaffer, M. P., Jones, A. W., Flynn, H. R., Snijders, A. P. and Nurse, P. (2018). Quantitative phosphoproteomics reveals the signaling dynamics of cell-cycle kinases in the fission yeast *Schizosaccharomyces pombe*. *Cell Reports*, 24(2), pp.503-514.
- Tan, G., Chen, M., Foote, C. and Tan, C. (2009). Temperature-sensitive mutations made easy: generating conditional mutations by using temperature-sensitive inteins that function within different temperature ranges. *Genetics*, 183(1), pp.13-22.

- Tanaka, K., Petersen, J., MacIver, F., Mulvihill, D., Glover, D. and Hagan, I. (2001). The role of Plo1 kinase in mitotic commitment and septation in *Schizosaccharomyces pombe*. *The EMBO Journal*, 20(6), pp.1259-1270.
- Terada, Y., Otsu, M., Fujita, S., Yasuda, Y., Suzuki, F. and Tatsuka, M. (1998). AIM-1: a mammalian midbody-associated protein required for cytokinesis. *The EMBO Journal*, 17(3), pp.667-676.
- Touré, A., Dorseuil, O., Morin, L., Timmons, P., Jégou, B., Reibel, L. and Gacon, G. (1998). MgcRacGAP, a new human GTPase-activating protein for Rac and Cdc42 similar to *Drosophila* rotund RacGAP gene product, is expressed in male germ cells. *Journal of Biological Chemistry*, 273(11), pp.6019-6023.
- Tuncel, H., Shimamoto, F., Kaneko Guangying Qi, H., Aoki, E., Jikihara, H., Nakai, S., Takata, T. and Tatsuka, M. (2012). Nuclear Aurora B and cytoplasmic Survivin expression is involved in lymph node metastasis of colorectal cancer. *Oncology Letters*, 3(5), pp.1109-1114.
- Umesono, K., Hiraoka, Y., Toda, T. and Yanagida, M. (1983). Visualization of chromosomes in mitotically arrested cells of the fission yeast *Schizosaccharomyces pombe*. *Current Genetics*, 7(2), pp.123-128.
- Vagnarelli, P., and Earnshaw, W. (2004). Chromosomal passengers: the four-dimensional regulation of mitotic events. *Chromosoma*, 113(5), pp.211-222.
- Vavylonis, D., Wu, J. Q., Hao, S., O'Shaughnessy, B. and Pollard, T. D. (2008). Assembly mechanism of the contractile ring for cytokinesis by fission yeast. *Science*, 319(5859), pp.97-100.
- Visintin, R., Craig, K., Hwang, E., Prinz, S., Tyers, M., and Amon, A. (1998). The Phosphatase Cdc14 Triggers Mitotic Exit by Reversal of Cdk-Dependent Phosphorylation. *Molecular Cell*, 2(6), pp.709-718.
- Willet, A. H., DeWitt, A. K., Beckley, J. R., Clifford, D. M. and Gould, K. L. (2019). NDR kinase Sid2 drives Anillin-like Mid1 from the membrane to promote cytokinesis and medial division site placement. *Current Biology*, 29(6), pp.1055-1063.e2.

- Willet, A. H., McDonald, N. A. and Gould, K. L. (2015). Regulation of contractile ring formation and septation in *Schizosaccharomyces pombe*. *Current Opinion in Microbiology*, 28, pp.46-52.
- Wilson, E. (1900). *The Cell in Development and Heredity, Chapter 2: Cell Division*. 2nd ed. New York: Macmillan., pp.64-67
- Wittmann, T., Hyman, A. and Desai, A. (2001). The spindle: a dynamic assembly of microtubules and motors. *Nature Cell Biology*, 3(1), pp.E28-E34.
- Wolfe, B. A. and Gould, K. L. (2005). Split decisions: coordinating cytokinesis in yeast. *Trends in Cell Biology*, 15(1), pp.10-18.
- Wollert, T. and Hurley, J. H. (2010). Molecular mechanism of multivesicular body biogenesis by ESCRT complexes. *Nature*, 464(7290), pp.864-869.
- Wu, J. Q., Kuhn, J. R., Kovar, D. R. and Pollard, T. D. (2003). Spatial and temporal pathway for assembly and constriction of the contractile ring in fission yeast cytokinesis. *Developmental Cell*, 5(5), pp.723-734.
- Wu, J. Q. and Pollard, T. D. (2005). Counting cytokinesis proteins globally and locally in fission yeast. *Science*, 310(5746), pp.310-314.
- Wu, J. Q., Sirotkin, V., Kovar, D. R., Lord, M., Beltzner, C. C., Kuhn, J. R. and Pollard, T. D. (2006). Assembly of the cytokinetic contractile ring from a broad band of nodes in fission yeast. *The Journal of Cell Biology*, 174(3), pp.391-402.
- Yang, B., Stjepanovic, G., Shen, Q., Martin, A. and Hurley, J. H. (2015). Vps4 disassembles an ESCRT-III filament by global unfolding and processive translocation. *Nature Structural & Molecular Biology*, 22(6), pp.492-498.
- Zhang, Z., Hou, X., Shao, C., Li, J., Cheng, J. X., Kuang, S., Ahmad, N., Ratliff, T. and Liu, X. (2014). Plk1 inhibition enhances the efficacy of androgen signaling blockade in castration-resistant prostate cancer. *Cancer Research*, 74(22), pp.6635-6647.
- Zhang, S., Nguyen, L. H., Zhou, K., Tu, H. C., Sehgal, A., Nassour, I., Li, L., Gopal, P., Goodman, J., Singal, A. G., Yopp, A., Zhang, Y., Siegwart, D. J. and Zhu, H. (2018). Knockdown of Anillin Actin binding protein blocks cytokinesis in hepatocytes and reduces liver tumor development in mice without affecting regeneration. *Gastroenterology*, 154(5), pp.1421-1434.

Zhang, Y., Sugiura, R., Lu, Y., Asami, M., Maeda, T., Itoh, T., Takenawa, T., Shuntoh, H. and Kuno, T. (2000). Phosphatidylinositol 4-phosphate 5-kinase Its3 and calcineurin Ppb1 coordinately regulate cytokinesis in fission yeast. *Journal of Biological Chemistry*, 275(45), pp.35600-35606.

Zhao, Y. and Lieberman, H. B. (1995). *Schizosaccharomyces pombe*: a model for molecular studies of eukaryotic genes. *DNA and Cell Biology*, 14(5), pp.359-371.

